THE VISUO-OCULOMOTOR SYSTEM AS A BIOLOGICAL MODEL OF DECISION MAKING

Doctor of Philosophy

Cardiff University

2016

MEGARDON Geoffrey

Summary

Animals, wild or civilized, are permanently in interaction with their environment through a perception-action loop. Their brains are experts in transforming the continuous flow of perceived information into action – continuously deciding the next action and seamlessly executing it. The present work addresses the mechanisms forming the stream from perception to action, which embody the interaction between signals driven by the environment and signals driven by the goals and expectations of the animal. In the case of the visuo-oculomotor system, which we take as a biological model, those signals converge in the intermediate layers of the Superior Colliculus (SCi), which serves as an interface spatially representing the possible eye movements. Interestingly, action execution can start while the selection is not completed, allowing us to infer the signals present in the SCi from the eye movements. In Chapter 2, using a computational model, we addressed the spatial interactions possibly occurring upstream the SCi and discuss their effects on behaviour. In Chapter 3, we inferred the presence of a spatiotopic signal in the SCi and refute current models of the visuo-oculomotor system. In Chapter 4, we introduced a new way to infer activity of the SCi, and we used it to distinguish the effects of goal-driven and expectation-related signals on the SC map. In Chapter 5, modelling separately the superficial and the intermediate layers of the SC based on recent neurophysiological recordings, we explored how neural properties and connectivity affect signal interactions. Finally, we discussed how we could implement the theories developed in this thesis, how our view of the visuo-oculomotor system could be refined, and whether this system could become a general model of decision making.

1

Acknowledgements

I am authorized to only put my name as author of this thesis, but this thesis is also the one of my supervisor, Petroc Sumner, who listened to me, guided me, and advised me all the way through to submission day. He would always add value to my work and always encourage me to publish it. He was always keen to spend hours discussing science with me and to let me draw all over the white board of his office. My thesis was probably not the simplest one for him to direct as I was exploring domains in which he was not an expert. However, this was compensated by the incredible ability of Petroc to -- since the first day I met him and despite my French accent -- remember or understand exactly and in a second anything I said or explained to him. Because of this surprising and unlimited capacity of understanding, I found in him my favourite interlocutor and I hope we will continue to fill white boards with our ideas.

I would also like to thank Aline Bompas and Rafal Bogacz to have accepted to be, respectively, my internal and external examiners.

I want to express my gratitude to Alain Guillaume who incited me to apply for this PhD in Cardiff with Petroc Sumner and without whom Chapter 2 of this thesis never would have existed. For more than a year, he spent a considerable amount of his time giving me feedback and helping me make this work publishable. This joint writing effort has been an initiatory route toward a good academic communication. Although my communication can still be improved, that journey has definitely made the writing of this thesis easier.

I am also grateful to:

- Casimir Ludwig who advises me on Chapter 3 and who is helping us to publish this work; he particularly introduced the idea of testing for the effect of residual activity from the previous saccade.

- Douglas Munoz, Brian White and colleagues for having hosted me in their laboratory for one month and a half. They particularly gave me feedback on Chapter 2. Douglas helped me to create the models in Chapter 5. Finally, Brian showed me the different aspects of extra-cellular recording in monkeys (I need to thank Indie who was the monkey we worked with). Brian also became a valuable friend who was here when I needed encouragement.

- Richard Morey who helped me to apply Bayes Factor analyses, especially for Chapter 3;

- Tom Freeman who gave us access to his 1000 Hz Eye tracker for Chapter 3 and 4. I would also like to thank the Psychology Band, of which Tom and Petroc are a part, for their amazing music to which PhD students have danced and relaxed on more than one occasion

- Michelle Symonds for the feedback that she gave me on my English. She invested a lot of her time in helping me make this thesis consistent with academic and English standards. Her thousands of comments and corrections have definitively changed and improved my written communication.

- Cardiff University, which have funded this thesis and some of my expenses to go to conferences.

- The IT managers for their work and help in keeping our working place practicable.

I also want to thank my friends and people that I have met in UK. Brice, Katie and Robert for their amazing support during my first year of PhD. Brice, again, for always being here to discuss and relax and whose way of speaking will always make me laugh and smile. Lukas, for being an amazing housemate, always here to play video games and relax, and for being an inspiring example of how to complete a PhD with simplicity and elegance. Paul, Lins, Sarah, Katia, Luke, Adrián and all the people I met, for offering me a rich social environment that kept me happy all the way to the submission deadline.

Of course, I want to thank my family – close and extended -- who have been supportive during this PhD (and during all my life in general). Most importantly, they have always been here to kindly mock me and to make jokes about researchers and academia. It helped me to always relativize the importance of research, to always put in perspective the pretentiousness of academia, and to relax. They, as usual, provided me with joy, pride, and modesty.

A special thank you to Atanaska Nikolova who is undoubtedly the most significant discovery that I made during this PhD, and represents a real breakthrough in my life. She probably does not realise how much she is of importance in keeping me proactive and working with passion and determination. If it was not for the stability that she provided me, and for my obstinate will to keep her proud, I probably would never have found in myself the energy to write this thesis as it is written today.

Finally, a very special thank you to my childhood friend, Dr. Maxime Robillart. This thesis, and thus the last 3 and a half years of my life, were dedicated solely to the kids we were and to the naïve dream we had of becoming doctors.

Table of Contents

Chapter One: General Introduction

1

1

1 A Biological Model to understand Decision-Making?

1.1 General Questions

As detailed in **Figure 1-1**, most decisions are based on the interaction between two main sources of information: the current environment (forming exogenous stimuli) and your current state (forming endogenous stimuli). Your current state is the product of what you memorized from your past and current interactions with the environment. It defines both your current goals, and your current expectations.

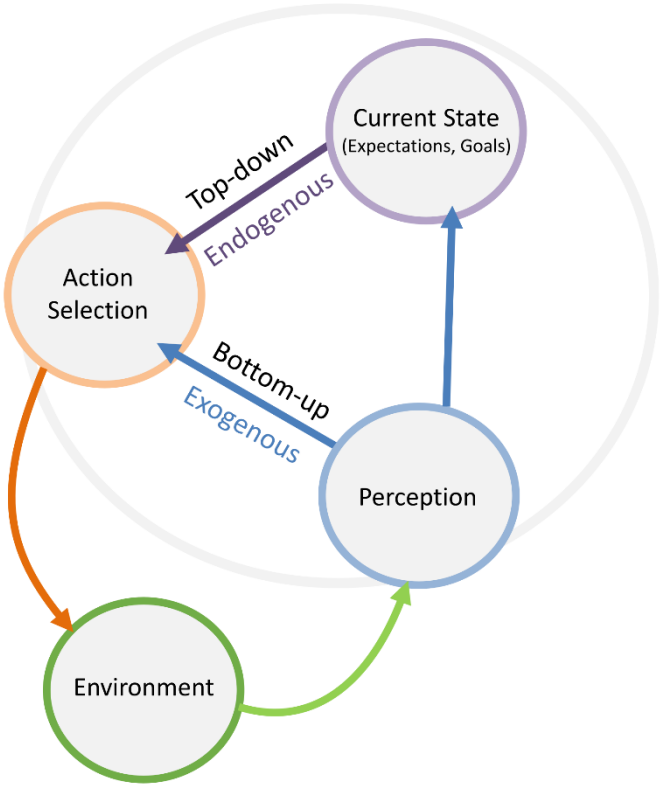

Figure 1-1: Simple Interaction Loop between an Animal and its Environment. *Animals need to act in a coherent manner in their environment to survive. The environment is perceived by the organism. The resulting perceptive signals participate more or less directly in the selection of action. The most direct paths between perception and action – treating the perceptive signals as potential actions -- are named Bottom-up paths. These are reflexive and rather rigid. The most indirect paths – treating the perceptive signals in relation to the animal´s current expectations and goals – are named Top-Down paths. These goals and expectations are adapted throughout the animal's interaction with the environment. It is usual to say that Bottom paths send exogenous signals (predominantly driven by the environment) while the Top-Down path represents endogenous signals (predominantly driven by internal processes).*

A hunter is strongly engaged in aiming at a deer 500m away though the scope of his rifle. An unexpected flash occurs in his peripheral vision. The hunter automatically "decides"[1] to shift his sight to the unexpected event: something has crashed a few kilometres from him. Now, you are speaking with a friend during a firework display, and lots of flashes occur in your peripheral vision. These flashes are expected events in the context of being around fireworks. You therefore "decide" to ignore them and continue to look at your friend while speaking. In a final example, you are looking for a gift for your nephew. Your partner shows you two cuddly toys and asks, "which one would he prefer?" You look at both toys alternately, thinking "what does my nephew like?" After some reflection, you "decide" to look at one of them and say "this one". In the first of the situations just described, our brain needs to prioritize an exogenous event – i.e., a flash -- over our endogenous goal – i.e., killing a deer. In the second situation, the brain needs to do to the exact opposite: it prioritizes an endogenous goal over a multitude of flashes. In the third situation, the brain needs to compare exogenous information with endogenous information held in memory in order to prioritize one of the exogenous stimuli: it is a discrimination task. These types of decisions for an orienting response are occurring all the time, in all species. One could, for instance, imagine a frog that is hunting flies and "decides" to stop his hunt in order to prioritize a leap away from a predator.

These examples attempt to highlight the notion that decision-making processes are driven by the modulations (such as prioritization) and the interactions (such as comparison) between exogenous and endogenous stimuli. This is the focus of interest in the current thesis. In particular, we aim to pose the following questions: "What kind of interactions and modulations are possible? And what are the mechanisms ruling those interactions and modulations?

1.2 Introduction to the Visuo-Oculomotor System

One way of approaching decision-making problems is through action selection. This approach assumes that decisions are coupled with actions and that they can be observed through the perception-action or sensori-motor loop. In fact, it has been argued that decision making can hardly be understood if not integrated into a body (embodied cognition, Adams, 2010; M. L. Anderson, 2003; Sandamirskaya, Zibner, Schneegans, & Schöner, 2013; Spencer, Perone, & Johnson, 2009). One of the most accessible and widely studied sensori-motor loops is the *orienting response system*. This system essentially decides where - and when - to orient the

[1] Note that the verb "decide" is put in parentheses as the subject is probably not aware of making a decision.

body, head, or eyes of the animal according to the current exogenous and endogenous signals that it receives. To select "where to look next?" shapes how sighted individuals extract information from their environment and how they interact with it. Ultimately, it bestows social or evolutionary advantages to the species. Therefore, this system undoubtedly plays an essential role in survival.

The central part of the *orienting response system* is embodied in the optic tectum that is present in all clades of vertebrates or near-precursors (Butler & Hodos, 2005; Northcutt, 2002; Vanegas, 1984). In primates, there are cortical structures that share the work with the optic tectum (we will return to this in the General Discussion) but it remains the predominant path to trigger orienting responses (Hanes & Wurtz, 2001) and a good model for understanding action selection.

In Anuran amphibians (toads and frogs) for instance, the *optic tectum* is able to initiate an orienting response accompanied by a reaching response of the tongue when detecting a prey-like stimulus (i.e. small stimulus) or can initiate an avoidance response - typically a leap away - when detecting a predator-like stimulus (i.e. large stimulus) (Ewert, 1970). In rodents, which are more evolved[2] vertebrates than frogs and which, unlike frogs, are not predators, the optic tectum still initiates orienting responses (typically for floor level stimuli), avoidance responses (typically for overhead stimuli)– and *fear* responses such as freezing or backward shuffling movements (Ellard & Goodale, 1986; Northmore, Levine, & Schneider, 1988). Finally, in lampreys, which can be seen as an early lineage of vertebrates (they are characterized by a primitive spine made of cartilage), it has recently been shown that the optic tectum can control eye movements, steering, and locomotion toward a goal (Saitoh, Ménard, & Grillner, 2007). This fascinating brain structure, whose organisation and role have been conserved through evolution (more details below), is also known as the *Superior Colliculus* in mammals.

In our work, we will focus specifically on a subsystem of the orienting response system - the pathway linking visual stimuli to eye orienting response – i.e. the visuo-oculomotor pathway. Eye orienting responses – i.e. saccades -- to visual stimuli are of prime importance to mammals with fovea, such as primates, as they aim at rapidly aligning a target with the centre of their fovea: this retina region has the highest cone density and allows sharp colour vision of the aligned target. There are several reasons for which the visuo-oculomotor system is the system

[2] It seems that the term "less/more evolved" is a controversial term in the parlance of evolutionary theorists. Here, more evolved is taken to refer to more modern and more complex, and it should not be confused with more adapted to survival. Any sustainable species is *de facto* adapted to survival.

of choice to explore action selections in both humans and primates: 1) the ease with which its input can be controlled (i.e. requires only a monitor), 2) the simplicity with which its output can be recorded and analysed (i.e. requires only an eye tracker, eye traces require only two dimensional analysis), and 3) its relatively well studied and accessible neural pathways. It is a cost-effective and easy way to study how interactions between perceived stimuli and memorized information influence the selection of an action from the various orienting responses that are available to an organism.

During the next sections, we will be presenting the visual pathways (Section 2), the selection of where-to-look-next (section 3) and its related oculomotor pathways (Section 4) in order to introduce our own understanding of the visuo-oculomotor system (Section 5). But before that, we shall finish this section with a brief description of the internal organization of the optic tectum.

1.3 Internal Organisation of the Optic Tectum

Figure 1-2A is a top view of the dorsal part of the midbrain. The Superior Colliculus forms the two upper bumps (*colliculus* means "small hill") on the dorsal surface of the midbrain's roof, just above the Inferior Colliculus. Its surface has a rostral-caudal axis (**Figure 1-2**A, green axis) and a lateral-medial axis (**Figure 1-2**A, red axis). If a needle pierces the SC's surface orthogonally to its tangent, the tip of that needle will be moving along the dorsal-ventral axis (**Figure 1-2**B, blue axis), or superficial-deep axis. Possibly because it has continued to play the same kind of role throughout evolution, the SC has also kept the same general organisation – although each clade has its own unique features (Butler & Hodos, 2005; Northcutt, 2002; Vanegas, 1984). In particular, we can note four features that have been strongly conserved in the optic tectum throughout the course of evolution.

First, the optic tectum is a layered structure (**Figure 1-2**B). The different layers are distributed over the ventro-dorsal axis and principally formed by an alternation of cellular and fibre strata. The reported number of layers differs between vertebrates. For instance, there are 4 for the Hagfish, 15 for the House sparrow or 5-7 for the Domestic cat (Northcutt, 2002). These differences can be attributed either to naming / method variations between investigators or to actual biological differences. However, it appears that there are always three major groups of layers: superficial, central and periventricular zones (Butler & Hodos, 2005). Moreover, in mammals, investigators divide the layers into only two groups: the superficial layers (SCs) and

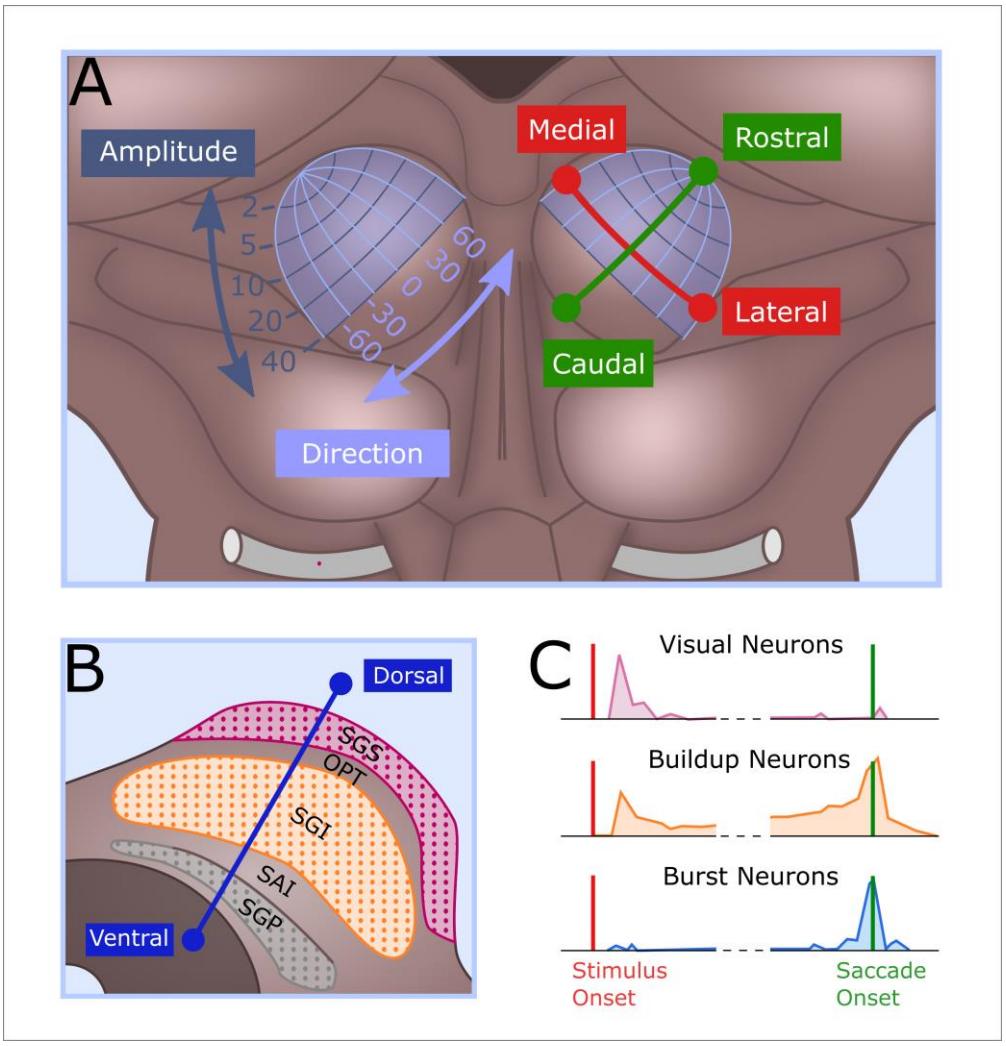

Figure 1-2: Organisation of the Superior Colliculus. A, *Top view of the Midbrain Roof. To apply a strong electrical stimulation in the SCi triggers consistent saccades: their amplitude and direction depends on the stimulation location and are given in degrees. The saccade amplitudes increase along the rostro-caudal axis – in green – whilst the saccade directions change along the medio-lateral axis – in red. The most rostral part is sometimes called the fixation zone as its activation helps to maintain the eyes in a still position.* ***B,*** *Coronal section of the Superior Colliculus. Different layers of alternating cells and fibres can be observed throughout the dorso-ventral axis of the Superior Colliculus – in blue. They consist of the* SGS*, stratum griseum superficiale, which is sometimes divided into three sublayers; the* OPT*, stratum opticum; the* SGI*, stratum griseum intermedium; the* SAI*, stratum album intermedium; the* SGP*, stratum griseum profundum. Cell layers are represented with a dotted pattern. Note that some nomenclatures also distinguish the SZ: stratum zonal, which is a very thin layer on top of the SGS and the SAI: stratum album profundum which is a thin fibre layer just below the SGP.* ***C,*** *Classical neural activity types observed in the Superior Colliculus. The three graphs represent the firing rate of the different neuron types during a saccade task. On the left part of the graphs, the activity of the neuron is aligned on the stimulus onset. On the right part, the activity of the neuron is aligned on the saccade onset. The different neuron types are discussed in the main text.*

the intermediate/deep layers (SCi); the latter contain both central and periventricular zones (Sparks & Hartwich-Young, 1989). The SCs consist mainly of the *stratum griseum superficiale* (SGS, purple layer in **Figure 1-2**B) while the SCi consists mainly of the *stratum griseum intermedium* (SGI, orange layer in **Figure 1-2**B) and the *stratum griseum profundum* (SGP, grey layer in **Figure 1-2**B). Note that the other strata are fibre/axons strata (M. F. Huerta, 1984). Importantly, the SCs and SCi are thought to be functionally distinct. Indeed, according to their main afferent and efferent projections (see section 2.2 and 4.1), the SCs is primarily a visual treatment centre while the SCi is an interface for integrating multimodal and cognitive information into motor control (for behavioural evidence see Casagrande, Harting, Hall, Diamond, & Martin, 1972; Harting, Hall, Diamond, & Martin, 1973). Nonetheless, SCs and SCi are not independent: there are direct projections of the SCs to the SCi (Isa, Endo, & Saito, 1998; Saito & Isa, 2003, 2005) and from the SCi to SCs (Ghitani et al., 2014).

Second, its efferent neurons and afferent input projections are primarily organised in a topographic manner (find more details in Appendix A, section 7) and are in register with each other. The surface of one colliculus functionally represents a map of the orienting movements that can be made toward the contralateral hemifield (Adamuk, 1872; Apter, 1946; Ottes, Van Gisbergen, & Eggermont, 1986; D. A. Robinson, 1972). This organisation makes it easy to request, facilitate, and inhibit orienting movements for external brain regions. The ease of this is such that an experimenter can operate the orienting response system of any vertebrate (du Lac & Knudsen, 1990; Herrero, Rodriguez, Salas, & Torres, 1998; McHaffie & Stein, 1982; Saitoh et al., 2007). In monkeys, when applying sufficiently high electrical stimulation in the SCi, the amplitude and direction of the triggered orienting responses depend only on the location of this stimulation over the SCi surface (Robinson, 1972). From this, a topography of the saccadic vectors represented over the SCi map can be drawn (see **Figure 1-2**A, left side). In more naturalistic conditions, most of the neurons have a receptive/movement field: a neuron receiving visual input will respond preferentially – but not exclusively -- to a specific stimulus position (Goldberg & Wurtz, 1972), and saccade-related neurons will spike preferentially for a specific saccade vector (Sparks, Holland, & Guthrie, 1976)[3]. Importantly, the topography of the saccadic vectors on the SCi map matches with the topography used for visual information on the SCs map: visual stimuli are coded at map locations that are in register with the saccadic vectors that would trigger an orienting response towards them (Schiller & Stryker, 1972). The

[3] In fact, the receptive/movement field can be open-ended: a saccade-related neuron can respond preferentially to all saccade vectors larger than a specific one.

other modalities (e.g. auditory, somatosensory) projecting to the SCi follow the same organizational principle; this allows coherent multimodal competition for an orienting response (Amlôt, Walker, Driver, & Spence, 2003; Frens & Van Opstal, 1998; Meredith & Stein, 1986).

Third, there are (except for cartilaginous fishes and some others) small piriform cells (*piriform* means "shaped like a pear") in the optic tectum which often have long centrifugal dendrites passing through several layers of the optic tectum (Butler & Hodos, 2005). These are likely to be essential in order to combine and conduct the sensory information to the motor layers. In addition to this, neurophysiology studies on monkeys have revealed the distinction between visual, burst, and build up neurons (see **Figure 1-2**C), which is thought to apply to other mammals such as cats (A. Grantyn & Berthoz, 1985; Munoz & Guitton, 1986). The first type belongs to the SCs and the two other types to the SCi (Mays & Sparks, 1980; Munoz & Wurtz, 1995a). Build up neurons are usually recorded at a deeper location than burst neurons, and their movement fields are larger than those of the burst neurons – i.e., less selective for their preferred saccade vector. During paradigms where a monkey needs to make a saccade to a visual stimulus, the typical *visual neurons* emit a strong discharge locked on to the stimulus onset (**Figure 1-2**C, first row), while the typical *burst neurons* emit a strong discharge (a burst of action potentials) that is locked on to the saccade onset (**Figure 1-2**C, third row). On their side, the *build-up neurons* emit a visual discharge in response to the onset of a stimulus, and a motor discharge locked on to the onset of a saccade. If the saccades are voluntarily delayed after stimulus onset then the *build-up neurons* maintain a small but tonic activity between its visual and motor discharges. This activity builds up as the saccade time approaches (**Figure 1-2**C, second row). These build up neurons appear to respond to extra-retinal information related to the expectations of the animal such as: the target location probability (Dorris & Munoz, 1998) or the predicted locations of the stimuli after a saccade (quasivisual cells, Mays & Sparks, 1980). Interestingly, there is a continuum of neural behaviours throughout the three types (McPeek & Keller, 2002a, fig. 1).

We will return to the quasi-visual cells in Chapter 3, and we will describe the less-known details of the SC's organisation in the General Discussion. We will now turn to the visual inputs that are received by the SC.

2 Input Streams of the Visuo-Oculomotor system: from divergence to convergence.

2.1 Ascending Visual pathways

To understand the visuo-oculomotor pathway of the orienting system, one needs to form an overview of the different visual pathways existing in the brain, identifying their connections to the optic tectum – or Superior Colliculus. Here, we distinguish three streams of visual information treatment that have either developed or regressed in importance throughout evolution but still have a major impact on primate behaviour.

From the retina, an anatomical and ultimately functional dichotomy is made: the visual stream is distributed between the *retino-tecto-pulvinar* pathway and the *retino-geniculo-striate* pathway (this terminology is primarily used for mammals) -- respectively represented in orange and blue in **Figure 1-3**. The former pathway is characterized by direct projections from the retina to one of the superficial layers of the optic tectum that, in turn, projects indirectly to some visual areas of the telencephalon[4] via the Lateral Posterior – pulvinar (LP/pulvinar) complex in mammals, or via the rotundus nucleus in birds/reptiles. Ultimately, the visual areas served by the *retino-tecto-pulvinar* pathways are the entopallium (note that the pallium is the ancestor of the cortex) in birds/reptiles, and the extrastriate cortex (visual cortex V3, V4, V5, in light red in **Figure 1-3**) in mammals (Butler & Hodos, 2005, Chapter 18 for a comprehensive review across vertebrates); it also reaches the lateral intraparietal region (LIP) and the Inferior Temporal area (Michael F. Huerta & Harting, 1984). Note that although the entopallium and extrastriate cortex are not evolutionary equivalent, they share anatomical features and both play a role in motion and pattern discriminations (Lazareva, Shimizu, & Wasserman, 2012, p. 476). On its side, the *retino-geniculo-striate* pathway is characterized by direct projections from the retina to the dorsal lateral geniculate nucleus (dLGN, sometimes called nucleus anterior) that, in turn, projects to some visual areas of the telencephalon. It reaches the visual pallium in birds/reptiles and the primary visual cortex in mammals. Interestingly, Schneider (1969), in a seminal paper, addressed the question of why, with the same brain lesion, an animal can appear to be blind in one task and sighted in another. His work suggests that the role of the *retinotectal*

[4] The telencephalon is part of forebrain: the dorsal telencephalon develops into the pallium in birds and reptiles and into the cortex in mammals; the ventral telencephalon develops into the subpallium in birds and reptile and into the basal ganglia – mostly the striatum -- in mammals.

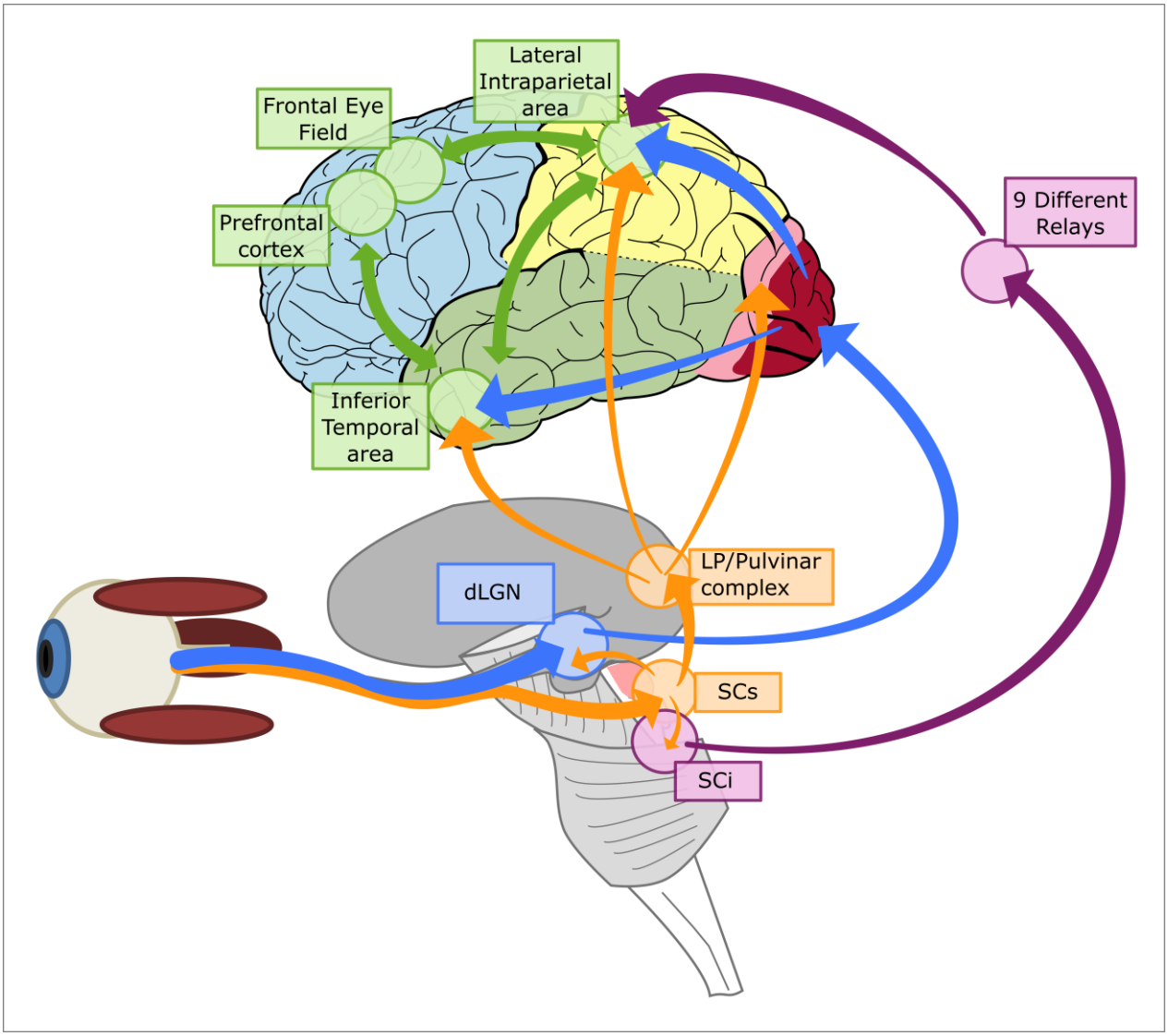

Figure 1-3: Summary of the Ascending Visual Pathways. **Anatomy.** *In the bottom part,* ***in grey:*** *the brainstem topped by the thalamus: dLGN and the LP/pulvinar complex are both in the thalamus while the SC – consisting of the SCs and SCi -- is on the roof of the brainstem. In the top half, the human brain is represented. Each coloured area corresponds to a cerebral lobe:* ***in green,*** *the temporal lobe;* ***in yellow,*** *the parietal lobe;* ***in dark red,*** *the striate visual cortex;* ***in light red,*** *the extrastriate visual cortex;* ***in blue,*** *the frontal lobe.* **Arrow.** *The different groups of coloured arrows represent pathways that are addressed in the main text:* ***in blue,*** *the classical visual streams: the blue arrow to the inferior temporal lobe represents the What stream while the blue arrow going to the lateral intraparietal area represents the Where/How stream;* ***in orange,*** *the retino-tecto-pulvinar pathway which passes through the SCs and ultimately projects to different regions of the cortex;* ***in purple,*** *an alternative tecto-cortical pathway which passes through the SCi; note that this pathway could send motor-related rather than visual-related feedback;* ***in green,*** *the interconnections between visual streams and frontal regions.* Image of the cerebrum extracted from Figure 728 of Gray's Anatomy *(1918)*, which is in the public domain.

pathways (part of the *retino-tecto-pulvinar* pathways) is to *locate objects* for orienting response while the *retino-geniculo-striate* pathways are more involved in the *identification of objects* followed by an operant response. Finally, note here that in amniotes[5], a minor stream exists from the optic tectum and the dLGN; this stream was predominant and was a substitute for the *retino-geniculo-striate* pathway in older vertebrates (such as teleost fishes, Ebbesson, 1980). Also, on its side, the *retino-tectal* pathway is less predominant in primates in comparison with other mammals (in monkeys, 20% of retinal ganglions cells project to the optic tectum, Weller & Kaas, 1989). In sum, it appears that the optic tectum was the main hub of visual streams in old vertebrates and that this function has migrated slowly to the visual cortex V1. Nevertheless, the *retino-tecto-pulvinar* pathway in higher mammals should not be overlooked, since clinical cases of pulvinar lesions have demonstrated that it still plays an important role in human vision (Karnath, Himmelbach, & Rorden, 2002; Zihl & Cramon, 1979). Such a lesion notably causes hemi-spatial neglect and slower orienting responses to contralateral visual stimuli.

In addition to the dichotomy between the *retino-tecto-pulvinar* and the *retino-geniculo-striate* pathways -- which both ultimately project to the visual cortex -- it has been thought for some time that there are, at least in primates, two cortical visual pathways (Goodale & Milner, 1992; Livingstone & Hubel, 1988; Mishkin, Ungerleider, & Macko, 1983; Ungerleider & Haxby, 1994). The *ventral stream* runs from the striate cortex to the inferior temporal cortex, whilst the *dorsal stream* runs from the striate cortex to the posterior parietal region. The *ventral stream* plays a role in the identification of visual objects (also known as the *what* stream); the *dorsal stream* plays a role in the sensori-motor transformation for visually guided interaction with objects (also known as the *how* stream, or the *where* stream). The *dorsal* stream is also considered to operate more rapidly than the *ventral* stream. As seen before, the visual cortex receives its input from the dLGN. Interestingly, in mammals, three different types of retinal ganglion cells are distinguished and named after their targets in the dLGN. In particular, the P-cells project to the Parvocellular layer of the dLGN, the M-cells to the Magnocellular layer, and the K-cells to the Koniocellular layer. Note that the role of the Koniocellular layer is not well established (Hendry & Reid, 2000 for a review); and we will not consider it further in the frame of this thesis. The P-cells are typically sensitive to contrast, colours, and fine details, while the M-cells are typically more sensitive to low contrasts and rapid changes (Derrington & Lennie, 1984; Ehud Kaplan & Shapley, 1986; E. Kaplan & Shapley, 1982; Lennie & Movshon, 2005). It was

[5] Amniotes: birds, reptiles, mammals

initially suggested that the parvocellular layer was the major input to the *ventral* stream while the magnocellular layer of the dLGN was the major input to the *dorsal* stream (Livingstone & Hubel, 1988). This parallelism was essentially intuitive: the *ventral* stream would have privileged access to colour and fine detail information, which is particularly useful to identify objects, whilst the *dorsal* stream would have privileged access to contrast and movement information, which is sufficient and relevant for interacting with an object. However, this parallelism is not as clear as initially thought. In particular, parvo- and magnocellular pathways often combine, such as in V1, V2 (Sawatari & Callaway, 1996; Sincich & Horton, 2005, p. 2; Vidyasagar, Kulikowski, Lipnicki, & Dreher, 2002), V4 (Ferrera, Nealey, & Maunsell, 1992) and MT (Maunsell, Nealey, & DePriest, 1990). Although the two-stream theory is very popular, it is important to note that both streams – ventral and dorsal – are highly interconnected and share reciprocal connections with the frontal cortex (Andersen, Asanuma, Essick, & Siegel, 1990; Blatt, Andersen, & Stoner, 1990; Merigan & Maunsell, 1993; Webster, Bachevalier, & Ungerleider, 1994) – the green arrows in **Figure 1-3** represent some of those interconnections.

Finally, it would seem logical that the *retino-tecto-pulvinar* pathways has a privileged relation with the cortical *dorsal* stream, as they both localise objects for motor interaction. Indeed, Huerta and Harting's review (1984) reveals the predominance of indirect projections of the SCi to cortical area 7 (part of parietal cortex and of the *dorsal* visual pathway) via 9 different relays -- **Figure 1-3**, purple arrows. As the SCi is involved in the motor execution of orienting responses, these pathways may send motor feedback rather than visual information.

2.2 Descending Pathways: to the Superior Colliculus

In addition to the direct input from the retina (see above), the optic tectum in amniotes receives projections from the striatum (part of the basal ganglia) through two major relays: the posterior pretectal nucleus (or equivalent) and the substantia nigra pars reticulata (SNr). The latter pathway is predominant in mammals in comparison with birds and reptiles (Reiner, Medina, & Veenman, 1998, fig. 15). Note that several regions from the cortical visual streams project on the striatum (Saint-Cyr, Ungerleider, & Desimone, 1990) – blue arrows in **Figure 1-4**. Moreover, the visual pallium of birds and reptiles projects directly to the optic tectum, while several cortical areas project to the optic tectum – Superior Colliculus -- of mammals. Finally, in most vertebrates, the superficial layers of the optic tectum (i.e. SCs) are reciprocally

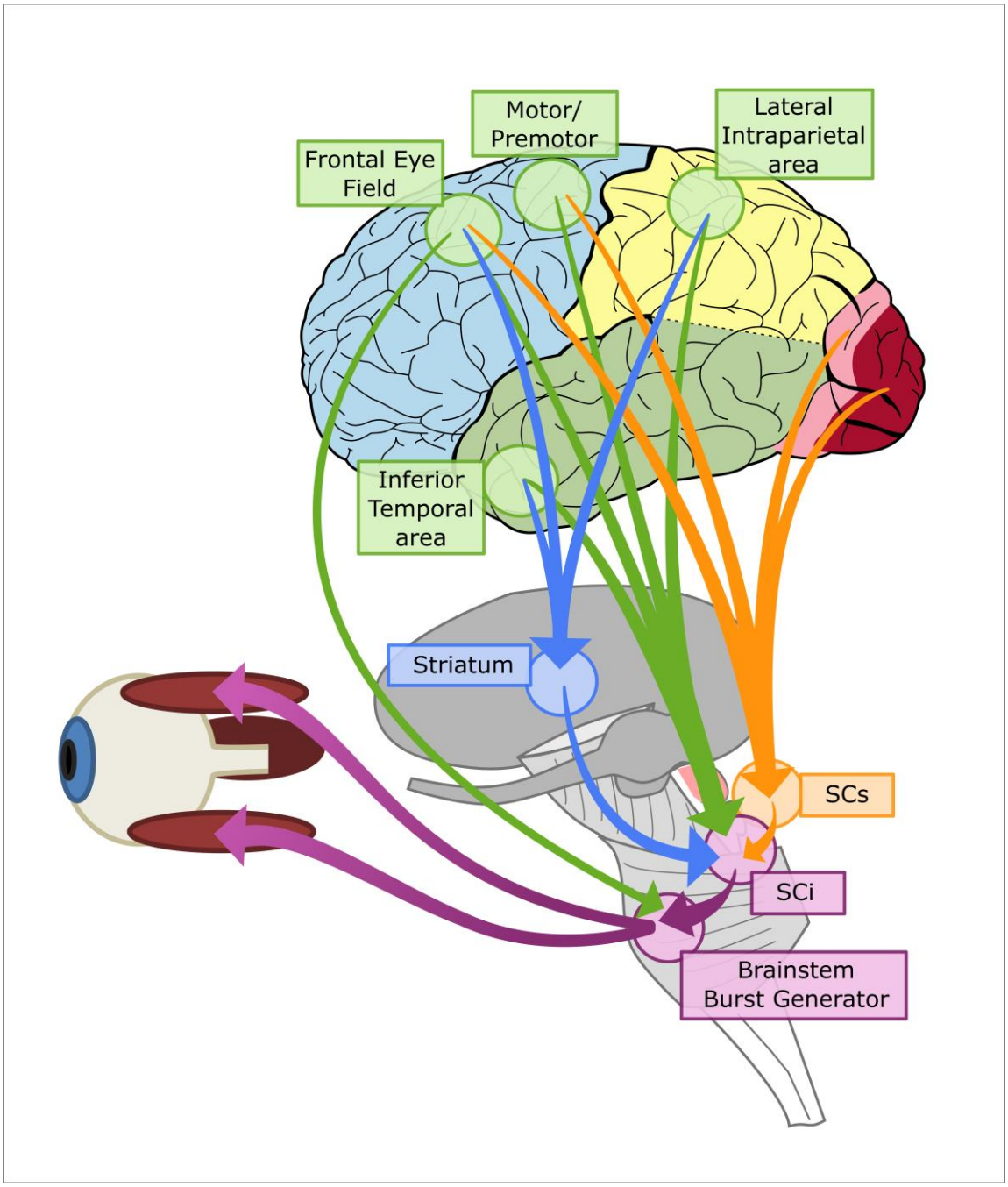

Figure 1-4: Summary of the Descending Visuo-Oculomotor Pathways. **Anatomy.** *Same description as in Figure 1-3.* **Arrow.** *The different groups of coloured arrows represent pathways that are addressed in the main text.* ***In blue,*** *the striatum project inhibitory projection to the SCi, whilst receiving information from the cortex.* ***In orange,*** *the SCs projects is the main source of visual information to the SCi; the visual information of the SCs can be modulated by prefrontal and motor information.* ***In green,*** *the SCi receives information from all cortical regions seen in Figure 1-3, and from the premotor/motor regions. Only one cortical region, the Frontal Eye Field, projects directly to the Brainstem Burst Generator, by-passing the SCi.* ***In purple,*** *the SCi is projecting to the Brainstem Burst Generator so that it can control eye movements. It is important to note that we represented only the FEF (Frontal Eye Field) from the prefrontal cortex and only the LIP (Lateral Intraparietal area) from the posterior parietal cortex – i.e. area 7.*

and topographically connected to nucleus isthmi – or parabigeminal nucleus (see Butler & Hodos, 2005, Chapter 18 for a comprehensive review of ascending projections to the optic tectum across vertebrates; see Hunt, Streit, Künzle, & Cuénod, 1977 for the isthmo-tectal loop). The mammals' afferent connections are to be described in more detail next.

As described in Section 1.3, the Superior Colliculus is divided into two layers: the superficial layer (SCs) and the intermediate/deep layer (SCi). The SCs receives topographic input from the retina, the visual cortices V1, V2, V3, V4, MT (Fries, 1984; Lock, Baizer, & Bender, 2003; Tigges & Tigges, 1981), the premotor cortex (area 6) and the frontal eye field (area 8) (Fries, 1984, 1985) – orange arrows in **Figure 1-4**. The SCi receives projections from the posterior parietal cortex (area 7, convergence between vision and proprioception), part of the somatosensory cortex (area 2), and the motor, premotor, and prefrontal cortex – green arrows in **Figure 1-4**. In fact, it can be noted that some of these areas – particularly area 7, which includes LIP – are part of the *how/dorsal* visual pathways linking vision to action seen in Section 2.1 (**Figure 1-3**). Furthermore, the SCi receives input from the inferior temporal gyrus (areas 20 and 21), which is part of the *what/ventral* visual pathway seen in Section 2.1. Finally, the SCi receives input from the auditory cortex (area 22), the SCs (involved in visual localisation) and the inferior colliculi (involved in sound localisation). This, with its connections to the somatosensory cortex, highlights that the SCi is an interface for multiple modalities. Note, finally, that some studies report that the frontal eye field projects to the SCi and not to the SCs (Leichnetz, Spencer, Hardy, & Astruc, 1981). Rather, it appears that the frontal eye field projects to several layers of the SC (Shipp, 2004). It should be noted that most of these projections are organised in a topographic fashion, in register with each other (more details in Appendix A, section 7).

To finish with non-cortical structures, the SCi notably receives input from the cerebellum via the caudal fastigial nucleus (Katoh, Arai, & Benedek, 2000; Person, Andrezik, Dormer, & Foreman, 1986), which has encouraged the development of models (Quaia, Lefèvre, & Optican, 1999), and from the Locus Coeruleus (Appell & Behan, 1990; S. B. Edwards, Ginsburgh, Henkel, & Stein, 1979) which is thought to play an important role in the sleep-wake cycle, arousal/vigilance and in decision making (Aston-Jones & Bloom, 1981; Aston-Jones & Cohen, 2005; Aston-Jones, Rajkowski, Kubiak, & Alexinsky, 1994; Foote, Aston-Jones, & Bloom, 1980). Indeed, this potential interaction between the SC and the Locus Coeruleus formed, in part, the basis of the work described in Chapter 4. Finally, the SNr is known to tonically inhibit the SCi (Hikosaka & Wurtz, 1983, 1985), and to release its inhibition to allow orienting responses. Interestingly, the SNr and the SCi share reciprocal and topographic connections (Peter

Redgrave et al., 2010); that presages a complex role of the SNr (to which we return in General Discussion). Before ending this section, we should note that there are more than 40 sources of subcortical projections to the SC, which we will not overview here (for a more comprehensive list, see Edwards et al., 1979).

2.3 Distinction between Saliency map and Priority Map

Wherever an orienting response is voluntary or reflexive, it is usually directed towards or away from a stimulus. Thus, selecting an orienting response usually involves selecting which stimulus most deserves to trigger an action. In their seminal theory, Koch and Ullman (1985) suggested that potential points of interest are extracted in parallel by several feature maps, each evaluating (and/or filtering) a specific feature such as colour, luminance, or direction contrast from the visual input. The points of interest obtained from all the feature maps converge to a saliency map. The saliency of a position is often defined as a normalized sum of the output of the feature maps for this position. Therefore a high degree of salience at a given position would be defined by a high average score across all the feature maps. The winning position to trigger an orienting response would be that with the highest salience on the saliency map. In this sense, a saliency map can drive or may act as an action selection map.

First, the fact that 1) the SCs receives projections from multiple visual areas of the brain, 2) its responses to visual stimuli are not feature-driven (orientation, colour, luminance) but rather contrast-driven (e.g. contrast in colour, in luminance, in orientation), 3) its contrast detection covers a large range of features, and 4) it projects directly to the SCi that triggers orienting responses, leads us to assume that the SCs is an instance of a *visual* saliency map (it is near to the stereotype introduced by Koch and Ullman). Second, the fact that the SCi receives visual, auditory, and tactile input (see Section 2.2) in register with each other, and in a topographic organisation, suggests that the SCi is a *multimodal* saliency map. In particular, it is very likely that it gathers saliency maps from different modalities. However, the SCi also receives projections from the frontal, parietal, and temporal cortices (see section 2.2) that potentially modulate and bias the input of the saliency maps according to the current goals and the current history of the animal. Due to this possibility, more than a *multimodal* saliency map, the SCi has been suggested to be a *priority* map (Fecteau & Munoz, 2006; Serences & Yantis, 2006; White & Munoz, 2011). However, it should be noted that the SCs itself receives projections from the frontal eye field (Fries, 1984) that render it potentially sensitive to goal-related feedback. In fact, all the cortical visual areas, and even the LGN, receive goal-related feedback that biases

their responses to visual stimulation (reviewed in Serences & Yantis, 2006 for human and monkey data). Hence, the frontier between saliency maps and priority maps may be blurred. However, given the density of projections from the frontal, parietal and temporal cortices, it appears that the SCi is more of a priority map than the SCs.

In conclusion, the SC can be depicted as a *unimodal saliency map* (SCs) projecting to a *multimodal priority map* (SCi). We will return to these points in Chapters 2 and 5. The SCi is a very special priority map, as it is at the same time the main and ultimate action selection map of the orienting response system (discussed further in section 4.1). We will next try to understand how an action is selected from all the signals converging to the SCi.

3 Mechanisms of Action Selection of the Visuo-oculomotor System or the Art of Deciding When but not Where to go

3.1 A Model of Priority Map: Endogenous and Exogenous signals converging on a Dynamic Neural Field.

Current models of action selection in the visuo-oculomotor system are based on the convergence of, and on the interaction between, endogenous and exogenous signals on a dynamic neural field – i.e. a neural network organised in a 1-D line or 2-D map. This dynamic neural field, because of its inputs, is *de facto* a model of a priority map. Given that it is also used to trigger saccades, the analogy with the SCi is quite attractive. In Appendix B (section 8), we introduce dynamic neural fields, along with a description of how they work and how they came to figure centrally in modelling the visuo-oculomotor system. Here, we will focus on one of the modern and widely used models of the SCi.

The models of Kopecz (1995) and Kopecz & Schöner (1995), based on the work of Amari (1977) caught the attention of the eye movement community by the simplicity of their approach and the intuitiveness of their inputs. First, they suggest that there are only three levels that are functionally needed to explain target selections for eye movements: 1) a transfer level, that is an input/initiation map on which potential targets are represented; 2) a planning level, that is a dynamic neural field set to drive a winner-take-all system, selecting one saccadic vector and suppressing the others; 3) a motor control plan, that is a mechanism to read out the winning position from the planning level. Second, they proposed that the input sources converging to the planning level can be reduced to two streams: the *visual information* from

the transfer level and the *pre-information* streams. The pre-information is information present in the brain before the decision making process begins, which could be acquired from previous learning or instruction. It was introduced in their model to explain that, when asking participants to saccade to a designated target, the history of the target position through the trials can bias the landing positions of eye movements (He & Kowler, 1989). In short, the planning level is a combination of an action selection map and priority map.

Later, Trappenberg, Dorris, Munoz and Klein (2001) reintroduced Kopecz and Schöner's model. First, they reduced it to its planning level – i.e., a winner-take-all dynamic neural field. Second, they identified the SCi as a good biological instance of the planning level using neurophysiological recordings in monkeys. Third, they applied the model to a large set of experimental paradigms, focusing particularly on fitting *reaction times* – i.e., focusing on when saccades go whilst ignoring where saccades go. Finally, they introduced the term *exogenous* signals (replacing "visual information") to refer to "only marginally processed sensory inputs" and *endogenous* signals (replacing "pre-information") to refer to "voluntary inputs, which are dependent on task-related instructions or expectancies" (p. 257). Note that one could question the voluntary aspect of *endogenous* signal. Interestingly, this is the work of Trappenberg et al. (2001) that is the most widely cited and used today. This is possibly due to the fact that it succeeds in combining the simplicity of Kopecz and Schöner's model with a very experimentalist ground.

Until recently, a large number of models of the visuo-oculomotor system have followed the assumptions of Trappenberg et al. (2001) and Schöner and Kopecz (1995). In particular, they adopt the following assumptions: 1) a long range inhibition/winner-take-all mechanism to select the saccade, and 2) an activity threshold mechanism to trigger saccades (Bompas & Sumner, 2011; Marino, Trappenberg, Dorris, & Munoz, 2012; Meeter, Stigchel, & Theeuwes, 2010; Satel, Fard, Wang, Trappenberg, & others, 2014; Taouali, Goffart, Alexandre, & Rougier, 2015; Z. Wang & Theeuwes, 2014; Wilimzig, Schneider, & Schöner, 2006). We will see throughout the next sections that the two mechanisms are redundant. For now, we will argue that the winner-take-all mechanism is not only unnecessary, but also fails to receive strong support from the literature.

3.2 No experimental support for a Winner-take-all Decision

The first assumption of Trappenberg et al. (2001) emerged from neurophysiological data suggesting that there is global inhibition serving a winner-take-all mechanism in the SCi at saccade onset (Munoz & Istvan, 1998) along with other pharmacological evidence of horizontally spreading inhibitory neurons in the SCi (Meredith & Ramoa, 1998). In fact, the occurrence of a winner-take-all to select only one action makes perfect sense: when one speaks about decision making, he/she often has in mind a system for choosing only one option among several. It is for precisely this reason that Schöner and colleagues introduced the planning level: in order to provide the motor control level with only one, unambiguous, target. With this approach, one could simply read the position of the unique winner on the SCi map to know where the triggered saccade is directed (as is done in Wang & Theeuwes, 2014). Interestingly, this is not what Schöner and colleagues employed (see below). One could also readily estimate the time needed to make a decision in different experimental situations by detecting when the activity on the map passed a certain threshold; this threshold would be chosen to be reachable only by the winner (as in Bompas & Sumner, 2011; Marino et al., 2012; Trappenberg et al., 2001).

However, Phongphanphanee et al. (2014)'s recent results (which are detailed further in Chapters 2 and 5) do not support Trappenberg et al. (2001)'s assumptions. In particular, they did not find long-range inhibition in the SCi in their *in vitro* study. Furthermore, they observed that the interaction between several inputs is quite opposed to what would be expected on the basis of a winner-take-all system. Indeed, when they applied an input current simultaneously at two different locations, they observed that the resulting activity over the map is supportive of a linear combination (i.e. an addition) of two bumps of activity. Interestingly, 10 years before Phongphanphanee et al.'s results were published, Arai and Keller (2004) had already constructed a model of the SCi, which dispensed with the assumptions of Trappenberg et al. (2001). Their choice was made in light of neurophysiological data that are particularly hard to access for consultation (to consult in printed books: Özen, Helms, & Hall, 2004) along with SC recording studies in monkeys (Edelman & Keller, 1998; McPeek, Han, & Keller, 2003; McPeek & Keller, 2002b; Port & Wurtz, 2003). In McPeek, Han and Keller (2003)'s experiment, for instance, the monkey had to make a saccade to a target that was presented among distractors. They clearly showed that when the saccade was triggered toward the target, there was some activity at the locations of the distractors. Importantly, they observed that having activity at

one of the distractors' locations was accompanied by a curvature of the saccade deviating toward this distractor. A second example is the Global Effect (or saccade averaging, that we will address in detail in Section 4 and Chapter 4). Edelman and Keller (1998) found evidence to suggest that when a monkey is presented with two stimuli at the same time to initiate a saccade, there can be two bumps of activity on the SCi at saccade onset. This seems to be particularly true for saccades with very fast reaction times that will finally land in between the two stimuli (this is saccade averaging, or the Global Effect). Also worthy of note is the large and diffuse activation of the build up neuron population during saccades (R. W. Anderson, Keller, Gandhi, & Das, 1998; Sparks et al., 1976), which makes this population incompatible with a winner-take-all system.

It therefore appears that *if* there is a competition mechanism, it does *not* systematically lead to a winner-take-all scenario. The visuo-oculomotor system is not an ideal decision-making system that chooses exactly one option. Rather, it is able to trigger a saccade before the selection process has been completed. We will see in Section 4 that the mechanism used by default in the work of Schöner and Kopecz (1995) to transform the activity at the planning level/SCi into a command for the control level is – ironically -- a viable solution for obtaining a saccade vector even when the decision of where-to-go is not complete. For now, the next section focuses on the relevance of a threshold mechanism to trigger a saccade.

3.3 A Race to Threshold for Triggering a Saccade

With regard to the second assumption of Trappenberg et al. (2001), a threshold mechanism has been reported since the first electrical stimulation of the monkey SCi (D. A. Robinson, 1972). There is an electrical intensity threshold under which no eye movements are triggered, whilst there is also a threshold under which saccades are triggered with a lesser eccentricity than normal. Furthermore, in more natural situations (saccade to visual stimuli), several studies have claimed that there is a fixed activity level above which saccades are triggered and cannot be withdrawn (J. W. Brown, Hanes, Schall, & Stuphorn, 2008; Hanes & Schall, 1996; M. Paré & Hanes, 2003). Further investigations have shown that even if it seems that there is a threshold effect, this threshold is not fixed – rather, it varies according to the task - and is likely to be modulated by endogenous/pre-information signals (Jantz, Watanabe, Everling, & Munoz, 2013).

In notorious and general decision making models such as the Drift-Diffusion model (Ratcliff & McKoon, 2008 for a review) or the Accumulator/Race model (S. D. Brown & Heathcote, 2008; Gold & Shadlen, 2007 for a review), a threshold (referred to as boundary in that literature) is used to end and complete the process of decision. For instance, in the case of a two-alternative choice, the race model would consist of two accumulators that respectively integrate incoming "evidence" for each alternative over time. It is the first accumulator to reach a sufficient amount of evidence – i.e., an arbitrary threshold -- that wins. Importantly, these more general models demand flexible thresholds to explain behavioural data. The distance of the threshold from the baseline activity is often linked to the "cautiousness" of the subject/model – which can be seen as an *endogenous signal*. Manipulation of the threshold plays an important role in replicating the behavioural speed/accuracy trade-off observed in two-alternative forced-choice tasks; to favour accuracy, one puts the threshold far from baseline, whilst to favour speed, one places the threshold closer to the baseline (Ratcliff & Rouder, 1998). Further, accumulator models have been shown to fit very well with FEF/LIP neuronal responses to visual input as well as the performance of the visuo-oculomotor system (Purcell et al., 2010; Schall, Purcell, Heitz, Logan, & Palmeri, 2011). Interestingly, these studies claim that two features were necessary to obtain a good fit: 1) an input gating system, such that insufficient levels of visual input are not integrated; 2) no inhibition/competition. This last point echoes our suggestion of an absence of winner-take-all mechanisms. Interestingly, the burst neurons of the SCi, because of their all-or-nothing (also refer to as switch-like) response before a saccade, have been proposed as the actual threshold detectors of FEF/LIP activity, while the striatum, via the SNr, could modulate this threshold (Lo & Wang, 2006; J. Zhang & Bogacz, 2008).

Although there is evidence for both the presence and functional necessity of a threshold effect in SCi and FEF, its underlying mechanism is still a matter of debate. Our opinion (we will address it in more detail in the General Discussion) is that low activity in the SC could not trigger a saccade, but once a region of the SCi passes the threshold (i.e. the race-winner), a saccade is triggered and *all* activity present in the SC would drive the saccade through the Brainstem Burst Generator. We also propose that the inhibitory release from the SNr and the dynamic of the burst neurons *enhance the race-winner signal*, giving it an advantage over the other regions. Next, we will focus on how the activity in the SCi is transformed into a motor command.

4 Output Stream of the Visuo-Oculomotor Pathways or the Art of Acting without a Clear Decision

4.1 Descending Pathway: From the Superior Colliculus to Eye Muscles

As described previously, the SCs projects back to the cortical areas via the LGN and the LP/pulvinar complex and it has reciprocal connections with the parabigeminal nucleus. The SCi, on its side, has direct projections to many subcortical regions along with an abundance of indirect projections to cortical areas (Graham, 1977; J. K. Harting et al., 1973; John K. Harting, 1977; for a brief review, see Michael F. Huerta & Harting, 1984). Interestingly, the SCi has reciprocal projections with the SNr (Substantia Nigra pars reticulata).

Here, we will focus only on the descending projections involved in controlling orienting responses toward a stimulus - namely the projections of the SC to the Saccadic Brainstem Burst Generator via the contralateral predorsal bundle (or tecto spinal tract/crossed pathways). We will ignore its projections to the ipsilateral tectopontine pathway (or uncrossed pathway) which is thought to control defensive movement, such as orienting responses away from a stimulus (Dean, Redgrave, & Westby, 1989). It can also be noted that the FEF is the only cortical structure to send direct projections to the Brainstem Burst Generator, bypassing the SC. However, it has been shown that electrical stimulation of the FEF while the SC is deactivated is not sufficient to trigger saccades (Hanes & Wurtz, 2001).

The network downstream the SC that shapes the motor signal for the extra-ocular muscles during a saccade, is routinely referred to as the Saccadic Brainstem Burst Generator (or Burst Generator). It is thought that the Burst Generator treats the vertical and horizontal components of a saccade in two different regions: the rostral interstitial nucleus of the medial longitudinal fasciculus (riMLF) for the vertical component (Büttner-Ennever & Büttner, 1978; Büttner, Büttner-Ennever, Henn, & others, 1977), and the paramedian pontine reticular formation (PPRF) for the horizontal component (Büttner-Ennever & Henn, 1976; Bernard Cohen & Komatsuzaki, 1972). In general, the horizontal component pathway appears to be more established (Scudder, Kaneko, & Fuchs, 2002; Sparks, 2002, for a review) and it consists of different groups of neurons, which are described in **Figure 1-5**. First, the motoneurons contact the extra-ocular muscle and produce a pulse-step signal during the saccade. This pulse-step is

similar to a linear combination of a velocity signal and a trajectory signal (Fuchs & Luschei, 1970; D. A. Robinson, 1970; Schiller, 1970). Second, there are Excitatory/Inhibitory Burst Neurons (EBNs/IBNs): the EBNs stay in the PPRF, while the IBNs stay in the medullary reticular formation (medRF). During a saccade, the ipsilateral EBNs discharge and excite the ipsilateral motoneurons while the ipsilateral IBNs discharge and inhibit the contralateral motoneurons, IBNs, EBNs and nucleus prepositus hypoglossi (Strassman, Highstein, & McCrea, 1986a, 1986b). Both EBNs and IBNs are discharging a velocity related signal. Third, the Long-Lead Burst neurons (LLBNs) were first found in the PPRF, and begin to fire long before the saccade. Some of these behave in a similar way to the SCi neurons, discharging for a specific saccadic vector (Hepp & Henn, 1983; Raybourn & Keller, 1977), whilst others discharge for a specific saccade direction, similar to the EBNs. They project to the EBNs and to the omnidirectional pause neurons (OPNs, Kamogawa, Ohki, Shimazu, Suzuki, & Yamashita, 1996). Fourth, the OPNs are found in a region of the PPRF known as the raphe interpositus (RIP, Büttner-Ennever, Cohen, Pause, & Fries, 1988). They maintain a constant level of activity when the eyes are fixating and pause during a saccade (Evinger, Kaneko, & Fuchs, 1982). They inhibit both the EBNs/IBNs (Strassman, Evinger, McCrea, Baker, & Highstein, 1987). Finally, the nucleus prepositus hypoglossi (NPH) is thought to be involved in creating the trajectory signal needed by the motoneurons by integrating the velocity signal of the EBNs (Cannon & Robinson, 1987; McFarland & Fuchs, 1992).

The SCi sends direct and excitatory projections to the LLBNs, EBNS, MN, and OPNs (Büttner-Ennever, Horn, Henn, & Cohen, 1999; S. B. Edwards & Henkel, 1978). Interestingly, its rostral part (linked to gaze fixation) is predominantly connected to the OPNs, while its caudal part projects more connections to the LLBNs/MN. In addition to these direct projections, the SCi has reciprocal projections with the central mesencephalic reticular formation (cMRF, Chen & May, 2000) that, in turn, sends projections to the OPNs. The rostral part of the SC contacts cMRF cells that excite the OPN whilst the caudal part of the SC contacts cMRF cells that inhibit the OPN. This distinction is thought to be involved in saccade triggering (N. Wang, Perkins, Zhou, Warren, & May, 2013).

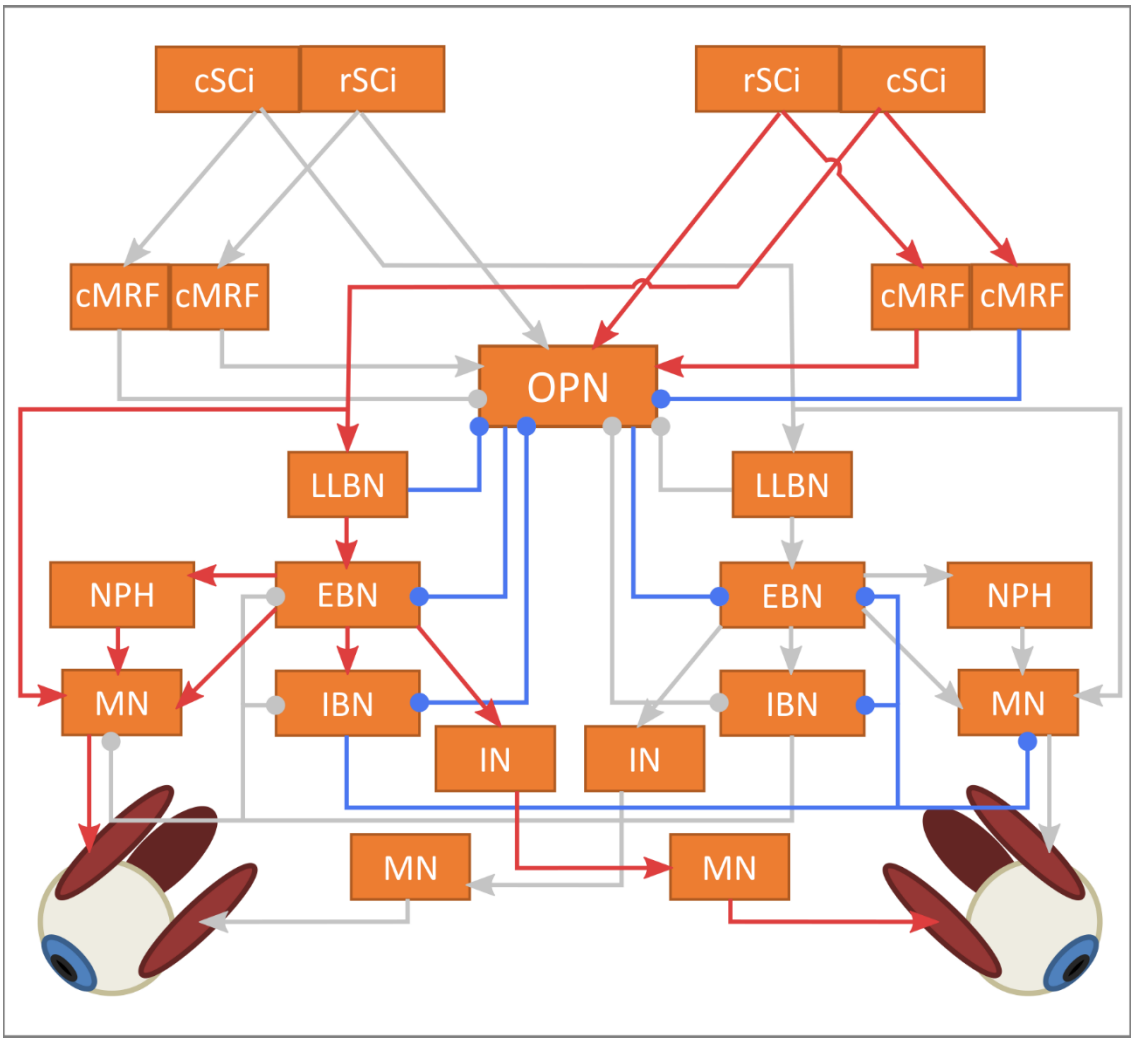

Figure 1-5: Summary of the Descending Pathways From the Superior Colliculus to the Extra-ocular Muscles. *The circuit is detailed in the main text. Here, we highlight the excitatory (red lines, arrow head) and inhibitory (blue lines, circle head) circuit activated during a horizontal saccade to the right (relying on the pathway originating from the cSCi), followed and preceded by a fixation state (relying on the pathway originating from the rSCi). Note: cSCi, caudal part of the intermediate layers of the Superior Colliculus; rSCi, rostral part of the intermediate layers of the Superior Colliculus; cMRF, central mesencephalic reticular formation; OPN, omni-pause neurons; LLBN, long-lead burst neurons; EBN, excitatory burst neurons; IBN, inhibitory burst neurons; NPH, nucleus prepositus hypoglossi; IN, intermediate neurons; MN, motoneurons.*

4.2 How to Extract an Action from No Selection? The Easy Way

The most straightforward (and almost correct) answer is: the centre of gravity of the SCi activity gives the saccadic vector of the current saccade – note that the SC is organised as a *saccadic vector map* (see section 1.3). This theory – saccadic vector averaging, **Figure 1-6**A -- was originally proposed by Sparks, Holland and Guthrie (1976) and it has generated successful

predictions in many circumstances. It is famously supported by an elegant study deactivating a small region of the SCi (C. Lee, Rohrer, & Sparks, 1988) (1988). In this study, the authors show that the subject (a monkey) can still make a precise saccade to the location coded by the small, deactivated area. The explanation of the *saccadic vector averaging* is that the deactivated region represents a hole in the centre of the activated region coding for this specific saccade. Because this hole is well centred, it does not affect the centre of gravity of the activated region. Moreover, the theory can explain Edelman and Keller´s (1998) Global Effect (introduced earlier). They showed that when presented with two closed visual stimuli, the monkey's SC presents two corresponding bumps of activity at the onset of the saccade. In this case, the saccade lands in between the two stimuli as if there was an averaging of the saccadic vector.

However, it is important to clarify that the *saccadic vector map* is an abstraction: the single spike of a single neuron at one location on the SC map does not trigger any saccade. When an experimenter applies electrical stimulation to the SCi at one *precise* location, it is a *large and diffuse* population of neurons in the SCi that is activated. This activation leads, somehow, to a *precise* saccadic vector. Thus it is the experimenter who ultimately maps the *precise* location of his electrode to the *precise* saccadic vector: he deduces a relationship but does not provide an explanation. Based on these considerations, the *saccadic vector averaging theory* is a circular explanation. More specifically, it explains how *large and diffuse* activation of the SC leads to a *precise* saccadic vector based on an unexplained map of *saccadic vectors.* In short, it explains the saccadic vector map by using the saccadic vector map. Alongside this successful but circular theory, the minivector summation theory was developed, which attempted to be pragmatic but had difficulties in replicating data.

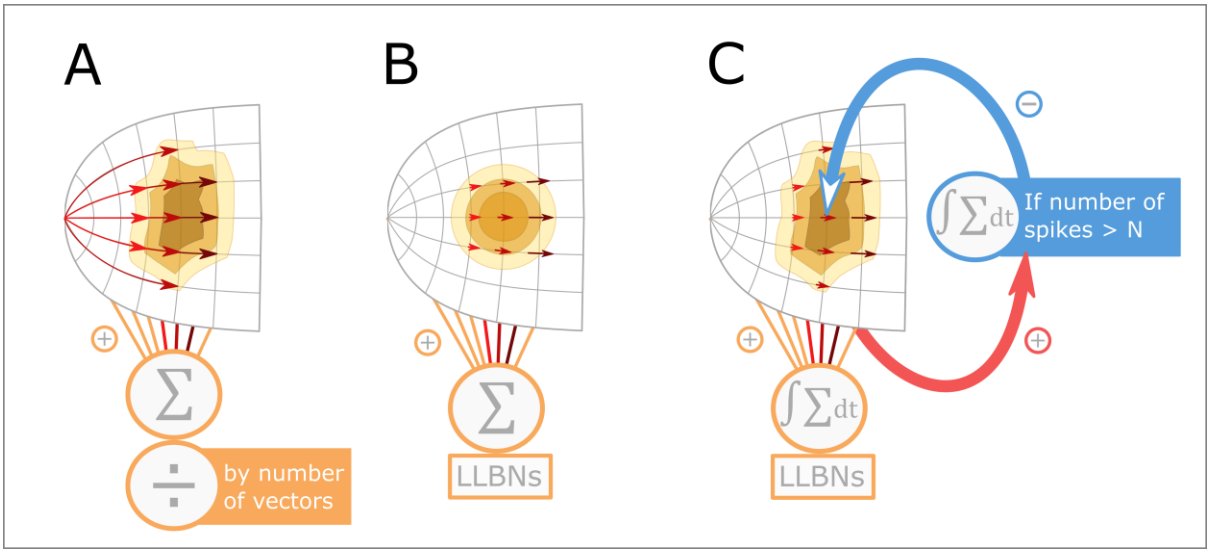

Figure 1-6: Summary of the Different Models Suggested for Transforming SC Activity into a Saccade. A, *the Saccadic Vector Averaging, see section 4.2.* ***B,*** *the Minivector Summation, see section 4.3.* ***C,*** *the Dynamic Minivector Summation, see Section 4.4.*

4.3 How to Extract an Action from No Selection? The Hard Way

In the initial minivector summation model – or linear ensemble coding model, **Figure 1-6**B (Van Gisbergen, Van Opstal, & Tax, 1987), the authors adopted the following assumptions. First, each neuron in the SCi codes for a minivector -- i.e. a very small vector when compared with the vectors found in the *saccadic vector map*. Second, and importantly, the size and direction of these minivectors depend on the neurons' location over the SC map. Third, the saccade-related burst of activity in the SCi has roughly the same spatial radius, the same peak, and the same duration for all saccades (i.e. the same spatio-temporal profile). Fourth, it is the summation of all the minivectors coded by each neuron of the activated population that makes the current saccadic vector. To simplify, any saccade is driven by a very similar "circle" of activated neurons; it guarantees that we are summing the same amount of minivectors over space and time for any saccade. Thus, it is only the *location* of the circle of activated neurons that controls the saccade metric.

One may now ask the question of how the minivectors are actually represented. Van Gisbergen, Van Opstal and Tax (1987) assumed that the Brainstem Burst Generator maintains a Cartesian representation of saccadic movements such that there are LLBNs specialized in each of the relative directions: left, right, up, and down. Thus, the minivectors coded by each SC neuron are simply defined by the strength of the connections that each SC neuron has with each of the LLBN directional groups. This assumption is supported by the fact that the caudal part of the SC – coding for large saccades -- projects more densely to the LLBN than the rostral part of the SC – coding for small saccades (S. B. Edwards & Henkel, 1978).

Whilst it has a number of strengths, the model of Van Gisbergen et al. (1987) has a major flaw: it requires a fixed spatio-temporal profile of activity to work properly[6]. This makes it unable to explain the results of Lee et al. (1988) and of Edelman & Keller (1998) described previously. Furthermore, we have argued that there is no perfect winner-take-all system and no fixed spatio-temporal profile of activity in the SCi. This therefore raises the question of how the

[6] Interestingly, Amari neural fields (particularly the winner-take-all setting) are ideal for creating a fixed spatio-temporal profile of activity, regardless of the winner's location (see Chapter 2). That coincidence is a strong call for combining this kind of neural field with the vector summation theory - precisely what was carried out by Schöner and Kopecz (1995).

minivector summation theory can be improved to accommodate all of the previously discussed findings. This will be taken up in the next section.

4.4 How to Extract an Action from No Selection: The Modern Way

Ironically, the solution is hidden in the motivation for using a fixed spatio-temporal profile. In particular, Van Gisbergen et al. (1987) adopted this approach in order to always integrate the same number of minivectors. However, when the spatial profile is obviously not fixed one needs to change the temporal profile accordingly in order to keep the number of integrated minivectors constant. Goossens and Van Opstal (2005) therefore aimed to solve this issue with a *dynamic* linear ensemble coding model (see also Van Opstal & Goossens, 2008) -- **Figure 1-6**C. Now, in this model, the authors considered the spikes of the neurons in the SC, by assuming that it is when a neuron spikes that its minivector is added to the sum of vectors. The claim defended by Goossens and Van Opstal is that, whatever the circumstances, once the gating mechanism (discussed in Section 3.3) has opened the communication from the SCi to the Brainstem Burst Generator, the latter will not stop transforming the SCi activity into an eye movement until the overall SCi population has emitted a *certain quota of spikes*. They supported this claim by actually counting the number of spikes emitted by the neurons in the SCi for 1) saccades to a single visual stimulus, and 2) saccades perturbed by a blink reflex. Furthermore, their model produces normal amplitude saccades when the activated population is centred on a small deactivated region of the SCi – replicating Lee et al. (1988)'s experiment. Moreover, they reported that the resulting saccades were slower due to less neurons being involved in firing. This is compatible with behavioural data (Aizawa & Wurtz, 1998; C. Lee et al., 1988; Quaia, Aizawa, Optican, & Wurtz, 1998) and with the dual-coding hypothesis suggesting that the firing rate of the SC population codes for velocity (Sparks & Mays, 1990). Finally --although they did not test this directly-- in mathematical terms, the spike quota also resolves the Global Effect/two bumps issue – without the need for long-range inhibition. In fact, the quota assumption makes *the vector summation theory producing exactly equivalent endpoints as the saccadic vector averaging theory*.

The idea behind the quota theory is that there is a system that sends inhibitory feedback to the SCi so that the quota is met. This could come from downstream feedback from the Burst Generator (Soetedjo, Kaneko, & Fuchs, 2002). Interestingly, the cerebellum has been suggested to control when/how to stop the burst of activity in the SCi (Quaia et al., 1999).

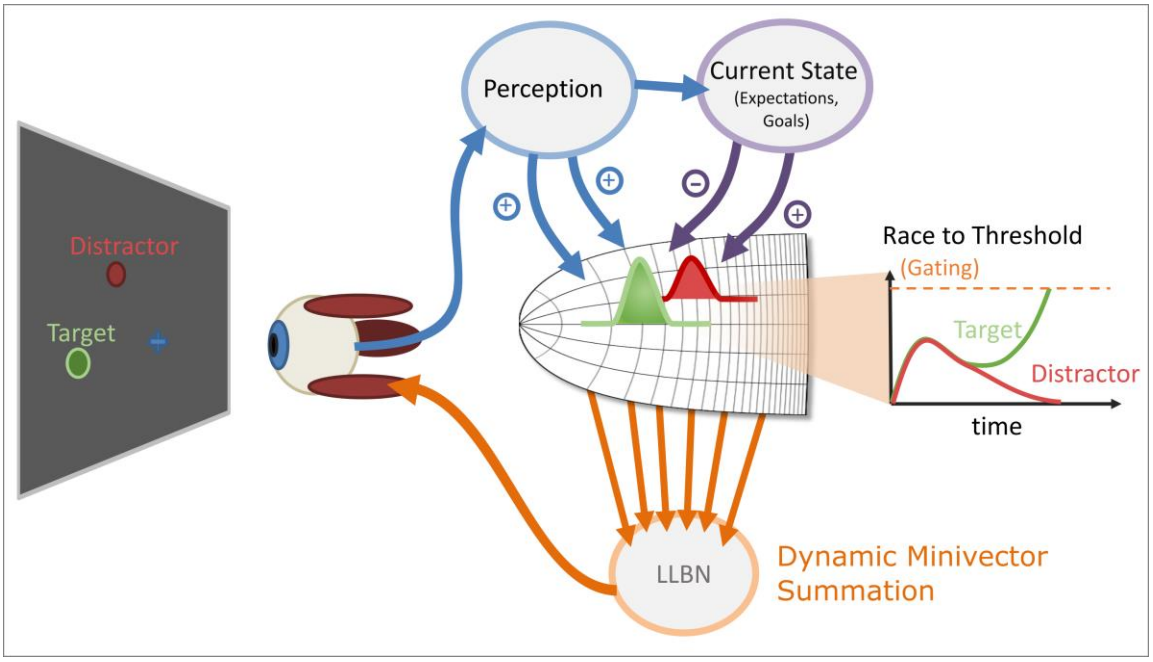

Figure 1-7: Summary of the Action Selection Processes for Saccadic Eye Movement. *Endogenous signals – carrying goal-related and history-related information -- and exogenous signals – mainly driven by the environment – converge on a neural field accumulator – the SCi. On this neural field the different signals accumulate spatially and temporally. The remote signals, such as the distractor in red and the target in green here, compete in the sense that they are racing to a threshold that will trigger a saccade and that will enhance the race-winner activity. However, once the threshold is reached, it is all the activity in the SC that will be fed to the LLBN and guide the saccade. It is important to note that the bifurcation of the target and distractor signals observable on the left graph (Race to Threshold) are considered to be mainly driven by cortical structures such as FEF or LIP involved in the selection of a target from distractors.*

5 Conclusion: Separation of When and Where to go

We saw throughout this introduction that the optic tectum represents a manifold interface; it is 1) an *interface between perceptive modalities*, 2) an *interface between cognitive and perceptive signals* and finally, 3) a *simple, abstract and shared interface to control the motor system* downstream. It represents a clear and ideal model of action selection (a summary can be found in **Figure 1-7**).

Furthermore, the theoretical framework on saccade selection and execution that has unfolded throughout this introduction suggests that the decisions of *when* and *where* to go are separate – which is reminiscent of the theoretical framework[7] of Findlay and Walker (1999). In Findlay and Walker's framework, while still using winner-take-all systems, they separated the saccade

[7] Theoretical framework is used here to express the idea that it is not an implemented model

triggering from the saccade selection. They proposed two winner-take-all systems and a dynamic saliency/priority map. A simple winner-take-all was used to select between the *fixate* state and the *move* state. Importantly, the saliency map was updated independently of these states. When the system switched to *move* state, a spatially distributed winner-take-all was used to read-out the maximum of the saliency map at that time: a saccade was triggered according to the corresponding saccadic vector. As opposed to this framework, in single winner-take-all models (Trappenberg et al., 2001, amongst others), the same winner-take-all system defines both the when-to-go and the where-to-go decisions, making them particularly coupled and synchronised.

In our framework, as far as the SCi is concerned, 1) the when-to-go decision is based on a threshold effect – which is similar to the fixate/move switch introduced by Findlay and Walker (1999); 2) the where-to-go decision is based on the spatial distribution of the SCi activity once the threshold is passed; 3) the SCi can *always* transform its current activity into a saccade – the last two points make our read-out system very similar to that of Findlay and Walker (1999). These small tricks represent, in fact, a remarkable twist: from the perspective of the SCi, the where-to-go is *always* defined. However, its activity – as a priority map -- depends on many other brain regions relaying endogenous and exogenous signals. From the perspective of these brain regions, the where-to-go may depend on questions such as “is this salient?”, “is this red or green?”, “where was the last target?”, “is red the most reinforcing colour?”. Thus, on the one hand, there are *several* where-to-go decision processes that project to the SCi and these processes progress independently of the when-to-go decision. On the other hand, the final decision of where-to-go made by the SCi (i.e., the actual saccade execution) depends on the decision of when-to-go. Indeed, the SCi will execute a saccade that reflects the state of the where-to-go decision processes projecting to it at the time at which the when-to-go decision triggered the saccade. A read-out system of this sort can explain, for instance, the time course of the Global Effect over reaction times (Wilimzig et al., 2006).

However, our theoretical framework distinguished itself from the framework of Findlay and Walker (1999) on some aspects, and we will highlight two of them. First, in Findlay and Walker’s framework, the *saccade triggering* (when-to-go) is controlled by a one-variable fixate system, while the *saccade metric* (where-to-go) is controlled by a spatially distributed move system. A saccade is triggered when the activity of the fixate system falls under a specific threshold. At the time of their paper, this view was justified by neurophysiological data that suggested a separation of the Superior Colliculus into fixation and saccadic zones (Munoz &

Guitton, 1991; Munoz & Wurtz, 1993). It was also thought that the pause of the OPN – and thus triggering of the saccade -- was caused by a decrease of activity in the fixation zone (Munoz & Wurtz, 1995b, fig. 13) because it was observed that the fixation zone has excitatory projections to the OPN (Gandhi & Keller, 1997; M. Paré & Guitton, 1994). From that, Findlay and Walker separated the where and when decisions into two physical pathways. However, this view is now questioned, since 1) it was observed that the so-called fixation zone of the SC is involved in small and micro saccades (Hafed & Krauzlis, 2012), and 2) the pause of the omnipause neurons was shown to be caused by glycinergic inhibition (Kanda, Iwamoto, Yoshida, & Shimazu, 2007; see also General Discussion). In our theoretical framework, we have only a spatially distributed move system, and we assumed a threshold/gating system to trigger saccades (we will discuss the possible mechanisms underlying this gating system in the General Discussion, Section 3.2). Second, the most important difference with Findlay and Walker's framework is that they considered the saccade execution to be mostly ballistic and they do not consider saccade curvatures: once the *when-to-go* is decided, the *where-to-go* is selected and frozen. In our framework, there is no clear sequential separation between action selection and action execution: the *where-to-go* decision processes and other signals projecting to the SCi continue to progress during and after execution of the movement. Due to this, saccadic eye movements and their curvature can be used to detect signals projecting to the SCi, and possibly represent a window opened on general decision making processes.

6 Thesis Organisation

In Chapter 2, we will study the properties of a winner-take-all neural field as a model of the SCs. In particular, we will argue that surround inhibition effects and deviation effects of visual stimuli can be expected in the SC map – and that these effects may have an impact on the saccades. A study reported in the appendix will also address whether a single winner-take-all neural field can be used to model the where-to-go decision when there are interactions between the Global Effect and Surround Inhibition.

In Chapter 3, we will be measuring the curvature of saccades to make inferences regarding the activity in the SCi during the saccade. By means of a differential paradigm, we will reveal that the SCi receives endogenous updates concerning the position of previously fixated stimuli. The spatial frame of this update is incompatible with recent models of saccade curvature. We discuss how those models could be modified in order to explain our results.

In Chapter 4, we will introduce a new measure – the Bimodal Global Effect – to examine the activity of the SCi during the saccade. This will allow us to understand what happened on the side of the stimulus that did not trigger the saccade. We use the measure to draw the spatial profile of a goal/discrimination-related signal and a history-related signal projected to the SCi.

Simple architectures of DNFs can readily explain saccadic behaviours. In Chapter 5, we address whether complex neurophysiological data from the SC neurons can be connected to saccadic behaviours via these simple architectures. This opens a discussion regarding the possible neural heterogeneity in SCs and the data needed to parametrize neuronal network models.

In the General Discussion, we will discuss about a possible implementation of the different concepts developed in the present thesis. We will also introduce the different aspects of the visuo-oculomotor system that deserve more attention in order to improve the current models. Finally, we conclude by considering the possibility of applying the visuo-oculomotor framework to the study of general decision-making.

7 APPENDIX A: Note on Topography of Afferent Projections and Efferent Neurons in the Superior Colliculus

Most of the afferent fibres to the colliculus - regardless of their origin - appear to be organised in a topographic fashion and to be in register with each other. For instance, the retina, the frontal eye field, and the visual cortices project their visually related information so that the rostral part of the SC corresponds to central vision (with a magnification of the foveal region) and the caudal part corresponds to peripheral vision (Drager & Hubel, 1976; Feldon, Feldon, & Kruger, 1970; Finlay, Schneps, Wilson, & Schneider, 1978; Sommer & Wurtz, 2000 for FEF). A similar topography is found for auditory signals: sound sources in front of the animal activate the rostral part, whilst sound sources from the side activate more caudal zones (King, 1999, fig. 2). The somatosensory signals are organised such that the nose/muzzle is represented on the rostral part (with a magnification of the whisker zone, or of the nose for respectively the mouse or star-nose mole), and the rear of the animal on the caudal part (Catania & Remple, 2004; Crish, Comer, Marasco, & Catania, 2003; Drager & Hubel, 1976). Finally, a topographic organisation of the afferent fibres is also found for the premotor and motor areas : the finger-arm-shoulder representation projects to the rostral part of the SCi whilst the arm-trunk representation projects to the caudal part of the SCi (Fries, 1985). Interestingly, around 28% of the neurons in the SCi receive multimodal input (Wallace, Wilkinson, & Stein, 1996), and these multimodal neurons are part of the tecto-reticulo-spinal pathway -- i.e. they can produce motor responses (Wallace, Meredith, & Stein, 1993). Note that the projections of the SC with the substantia nigra, the parabigeminal nucleus and the central mesencephalic reticular formation appear also to be organised in a topographic fashion (B. Cohen & Büttner-Ennever, 1984; Graybiel, 1978; Hikosaka & Wurtz, 1983; P. Redgrave, Marrow, & Dean, 1992). As stated in Section 1.3, this topographic organisation is an important and robust feature of the optic tectum/SC through evolution.

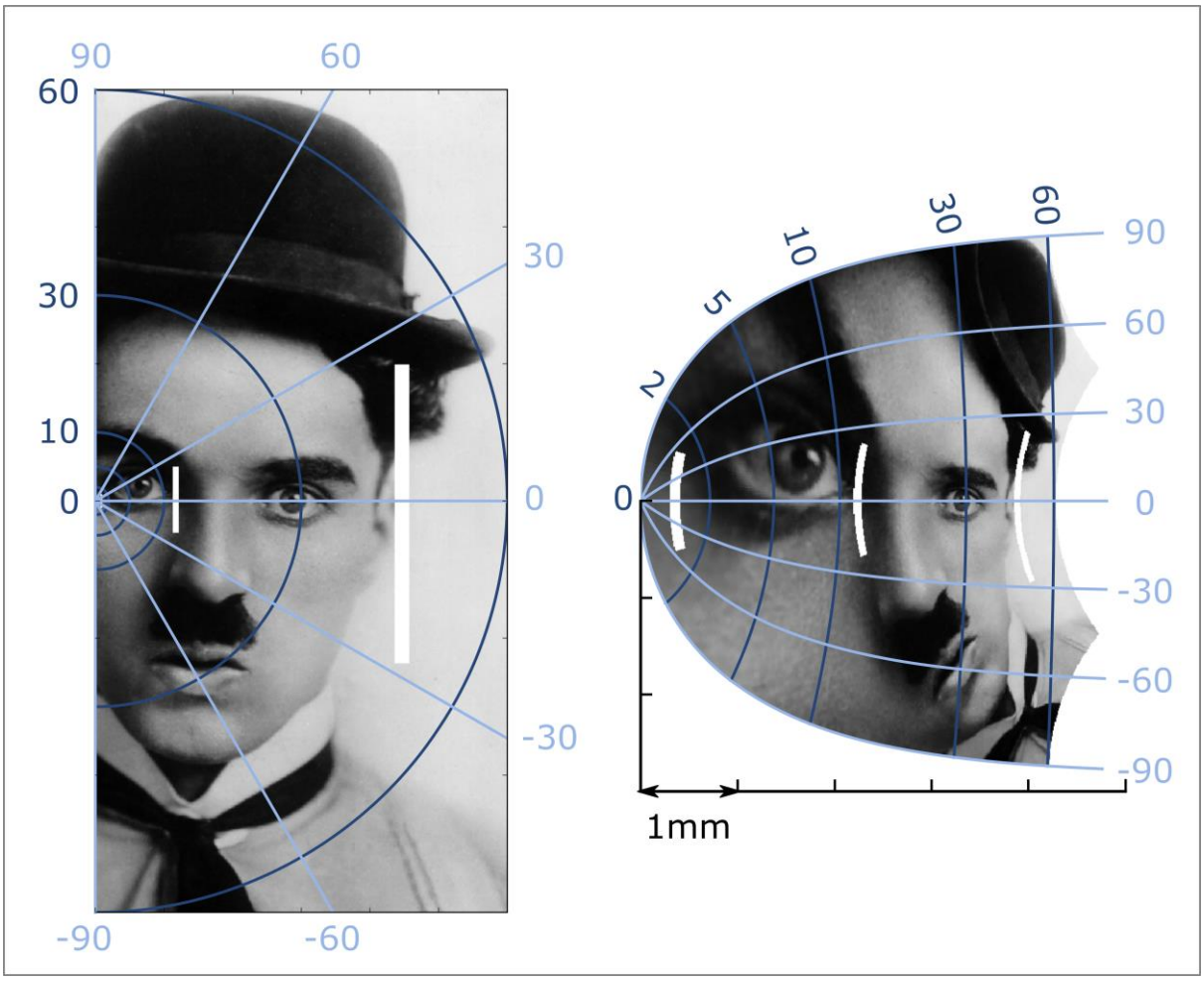

Figure 1-8: Illustration of the Projection of the Visual Space of the Right Hemifield of the Retina to the Left Superior Colliculus. On the left side, *we display the visual space of the right hemifield – the subject is looking at Charlie Chaplin, fixating particularly on the bottom left corner of Chaplin's right eye. The white bars drawn on the visual space are used as markers.* ***On the right side,*** *we display the projection of the visual space of the right hemifield on the space of the left superior colliculus. The white markers correspond to the markers represented in the visual space.* ***On both sides,*** *blue lines denote the visual space in polar coordinates. The dark blue lines and numbers represent the eccentricity angles whilst the light blue lines and numbers indicate the directional angles.*

8 APPENDIX B: Note on Dynamic Neural Fields and their application to the Visuo-oculomotor System

The seminal idea of describing the dynamics of neural populations instead of a single neuron dates back to the 50s and 60s with the work of Beurle (1956) and Griffith (1963; 1965). It leads to the so-called Cowan-Wilson population rate model (H. R. Wilson & Cowan, 1972)

considering an homogenous population of interconnected inhibitory and excitatory neurons. For our concerns, these *dynamic* models describe the evolution over time of two variables: 1) the average rate of action potentials within a neural population – i.e. the firing rate or population rate -- which is considered as the main output signal underlying neural interactions; and 2) the average membrane potential, which is computed as a leaky accumulation and summation of the inputs to the population. The term *leaky* means that the membrane potential has a tendency to return to a certain state of equilibrium. Finally, the population rate is computed as following a saturated function of the average membrane potential (the function used is often a sigmoid). By 1973, Wilson and Cowan had already begun to model *spatially organised neural tissues* – inspired by cortical and thalamic tissue -- introducing a model that will later be called the *dynamic neural field*. Dynamic neural fields are continuous spaces (usually a 1D line or 2D map) where each point in space is considered a neural population that follows the Wilson-Cowan model – or derivative.

Following this, Amari (1977), extended the Wilson-Cowan model, by exploring and formalizing the dynamics of a neural field with *short range* excitatory and *long range* inhibitory connections. Note that "long range inhibition" only means "longer than the excitation range". The main characteristic of Amari's type of dynamic neural fields is that – for a specific parameter region -- an input signal can initiate a self-stabilized bump of activity in the field at the input's maximum peak location. When there are several input peaks, they may compete – if they are within inhibition range of each other -- or merge into one central peak of activity – if they are proximal from each other. If the degree of inhibition/excitation is strong enough and the inhibition range relatively long, competition may lead to a single self-stabilized bump of activity in the field – i.e. we obtain a *winner-take-all* mechanism (see Chapter 1 for more details on dynamic neural fields). Thus winner-take-all neural fields are a subtype of Amari's neural fields. Finally, depending on the strength of the recurrent excitation, the self-stabilized bumps of activity may or may not survive the removal of the input. When they do, such bumps are referred to as self-sustained, rather than self-stabilized, bumps (see Spencer et al., 2009 for a more detailed discussion on the properties of self-sustained and self-stabilized bumps).

From that, Schöner, Spencer and colleagues have elaborated a Dynamic Field Theory. In particular, they proposed that Amari's model is a central and ubiquitous mechanism in the brain that can explain a multitude of behavioural phenomena going beyond the scope of this introduction (the theory led to a recent book, Schoner, Spencer, Group DFT Research, & others, 2015). Interestingly, Schöner and colleagues began to construct their theory by applying it to

the visuo-oculomotor system (Kopecz, 1995; Kopecz, Engels, & Schöner, 1993; Kopecz & Schöner, 1995). At this time, the idea of using dynamic neural fields to model the visuo-oculomotor system had already been introduced by Dominey and Arbib (1992), Lefèvre and Galiana (1992) or Arai et al. (1993, 1994) although they did not use the same terminology (e.g. "two-dimensional neural surfaces" instead of neural fields). The use of dynamic neural fields was a logical step: the majority of the brain regions involved in the visuo-oculomotor system, such as the LIP, FEF, SCs, SCi, are spatially organised neural tissue i.e., saccadic vectors, visual stimuli that are represented in register with each other over the two spatial dimensions of the neural tissue surface (a saccadic vector determine an amplitude and a direction). These pioneering researchers, by introducing a *dynamic* aspect to SC models, have highlighted new possibilities to explain old issues (more details to find in the discussion of Chapter 2). This approach has also allowed for a better integration of SC models with the brainstem burst generator models (situated downstream) which were, at the time, already dynamic (D. A. Robinson, 1975; see also Scudder, 1988).

1

2

Chapter Two: Limitations of Short Mexican Hat Connection for Target Selection

Activity Suppression and Deviation from Input Stimuli.

Abstract[8]:

Dynamic Neural Field models (DNF) often use a kernel of connection with short range excitation and long range inhibition. This organization has been suggested as a model for brain structures or for artificial systems involved in winner-take-all processes such as saliency localisation, perceptual decision or target/action selection. A good example of such a DNF is the superior colliculus (SC), a key structure for eye movements. Recent results suggest that the superficial layers of the SC (SCs) exhibit relatively short range inhibition with a longer time constant than excitation. The aim of the present study was to further examine the properties of a DNF with such an inhibition pattern in the context of target selection. First we tested the effects of stimulus size and shape on when and where self-maintained clusters of firing neurons appeared, using three variants of the model. In each model variant, small stimuli led to rapid formation of a spiking cluster, a range of medium sizes led to the suppression of any activity on the network and hence to no target selection, while larger sizes led to delayed selection of multiple loci. Second, we tested the model with two stimuli separated by a varying distance. Again single, none, or multiple spiking clusters could occur, depending on distance and relative stimulus strength. For short distances, activity attracted towards the strongest stimulus, reminiscent of well-known behavioural data for saccadic eye movements, while for larger distances repulsion away from the second stimulus occurred. All these properties predicted by the model suggest that the SCs, or any other neural structure thought to implement a short range MH, is an imperfect winner-take-all system. Although those properties call for systematic testing, the discussion gathers neurophysiological and behavioural data suggesting that such properties are indeed present in target selection for saccadic eye movements.

[8] Note that the present Chapter is adapted from Mégardon et al. (2015).

1

1 Introduction

The SCi was recognised as the main action selection map of the visuo-oculomotor system in General Introduction. This Chapter will assess the spatial interactions between exogenous signals that are likely to happen even before that exogenous signals reach the SCi – so that perceptive levels are already shaping decisions. It will also be the opportunity to introduce the framework of Dynamic Neural Field models and spiking neuron models that will be used through this thesis.

It has been suggested for a long time that a connectivity pattern of short range excitation and long range inhibition in topographically organized visual structures could achieve *saliency localization* - see blob detection models for computer vision (Bretzner & Lindeberg, 1998; Kong, Akakin, & Sarma, 2013; Lowe, 1999) but also models of V1/LGN (Kang, Shelley, & Sompolinsky, 2003; Schwabe, Obermayer, Angelucci, & Bressloff, 2006; Spratling, 2010; Zeng, Li, & Li, 2011) - and *target selection* (Arai et al., 1994; Kopecz, 1995; Kopecz & Schöner, 1995; Trappenberg et al., 2001). This connectivity pattern is often referred as a Mexican hat (MH) or centre-surround inhibition, and was already implemented in early Dynamic Neural Field (DNF) models (e.g. Amari 1977). Recently the relevance of such organization has also been underlined for action selection in artificial cognition (Erlhagen & Bicho, 2006; Richter, Sandamirskaya, & Schoner, 2012; Sandamirskaya, 2014); hardware implementations have emerged (Millner, Grübl, Meier, Schemmel, & Schwartz, 2010) and are suggested to be an important milestone for developing complex cognition (Indiveri, Chicca, & Douglas, 2009).

Among neural structures often modelled using a DNF with MH connectivity (which we will refer to as DNF-MH), a prominent example is the superior colliculus (SC). While both SCi and SCs have been assumed to have MH connectivity, most modelling has focused on the SCi (and hence on target/action selection rather than saliency). Results of SCi studies (electrophysiology: McIlwain 1982,Munoz and Istvan 1998; and anatomy: Behan and Kime 1996; Meredith and Ramoa 1998) were in favour of MH connectivity and also suggested that inhibition from a given site can concern very distant areas of the map. Hence, without more precise measures, it was assumed that the inhibitory influence was very large. Numerous models implementing long range inhibition (Arai et al., 1993; Bompas & Sumner, 2011; Kopecz, 1995; Kopecz & Schöner, 1995; Marino et al., 2012; Meeter et al., 2010; Trappenberg et al., 2001; Wilimzig et al., 2006) showed that it was successful for winner-take-all selection of a saccade target among several options.

However, the idea of long range inhibition in the SC has been challenged (Isa & Hall, 2009; P. Lee & Hall, 2006). Very recently, a clearer picture has been obtained. Phongphanphanee et al. (2014) using multi-electrode arrays on slice preparations of rodent SC evaluated the local connectivity in SCs and SCi. This study found MH connectivity only in SCs and that, in this case, the range of inhibition is relatively short (see below for details). In SCi, the excitation zone was at least as large as the area of inhibitory influence. The second main difference between the SCs and the SCi revealed by the study concerned the time course of their excitatory and inhibitory responses to a sustained stimulation: where the SCi was behaving as an accumulator, the SCs showed transient responses. Globally these results led the authors to conclude that the winner-take-all phenomenon is observed in the SCs and that it enables saliency detection. Phongphanphanee et al. (2014) wrote "The sensory layer (SCs) is optimized to localize the single most salient stimulus" (p. 2342). The SCi, in turn, would cascade activity from the SCs and integrate it with its other inputs to perform target selection. Importantly, the saliency selected and localised by the SCs can be translated into the winner of the SCi target selection when other target candidates are negligible. As stated above, numerous models of the SC were implementing long range inhibition to perform selection. The results of Phongphanphanee et al. (2014) call for an exploration of properties of map integrating MH with short range inhibition and temporal dynamics based on the SCs.

The aims of the present study were: 1) to test the capacity of such a DNF-MH with short range inhibition to perform reliable target selection and 2) to highlight its noticeable properties and its potential limitations in such a context. Importantly, those properties could represent testable predictions to address if the SCs – or any brain structure – performances are indeed driven by a short range MH. We implemented this type of DNF-MH in two dimensions with spiking neurons. We fed it with various types of input stimulation to assess the emergence of localized and stable clusters of firing neurons (a “spiking cluster”) that would represent saliency and/or target selection. We first explore the effect of stimulus size on the performance of the model. Second, we tested the model while two stimuli were presented at the same time and we measured their interaction while varying their weights and the distance between them.

As a final note, although our rationale is largely based on results obtained in the SC, especially the superficial layers, our results describe a set of phenomena possible for any DNF-MH implementation and usage.

2 Material and Methods

2.1 Overview of the Model

The model is a simple network of neurons organized as one 2D layer of 100x100 cells (**Figure 2-1**A) and connected according to a 2D Mexican hat kernel (**Figure 2-1**B). Our model is close to those of K. Arai, Keller, and Edelman 1993; Marino et al. 2012; Trappenberg et al. 2001; Wilimzig, Schneider, and Schöner 2006. Nevertheless the critical differences are that we implemented a MH with a short range of inhibition and spiking neurons (**Figure 2-1**C) which allow to set up different synaptic decay times for inhibition and excitation (see section 2.2). Finally, we did not implement the logarithmic compression of space that is observed in the SC to remain general.

The model is implemented in Python 2.7 (http://www.python.org/) and using the library BRIAN, a spiking neuron network simulator (D. Goodman & Brette, 2008; D. F. Goodman & Brette, 2009). The code source for all the following simulations can be found at: https://github.com/Nodragem/SuppData-MHLimitations-Selection. We used the libraries numpy and matplotlib for our computations and figures (see respectively Walt, Colbert, and Varoquaux 2011 and Hunter 2007).

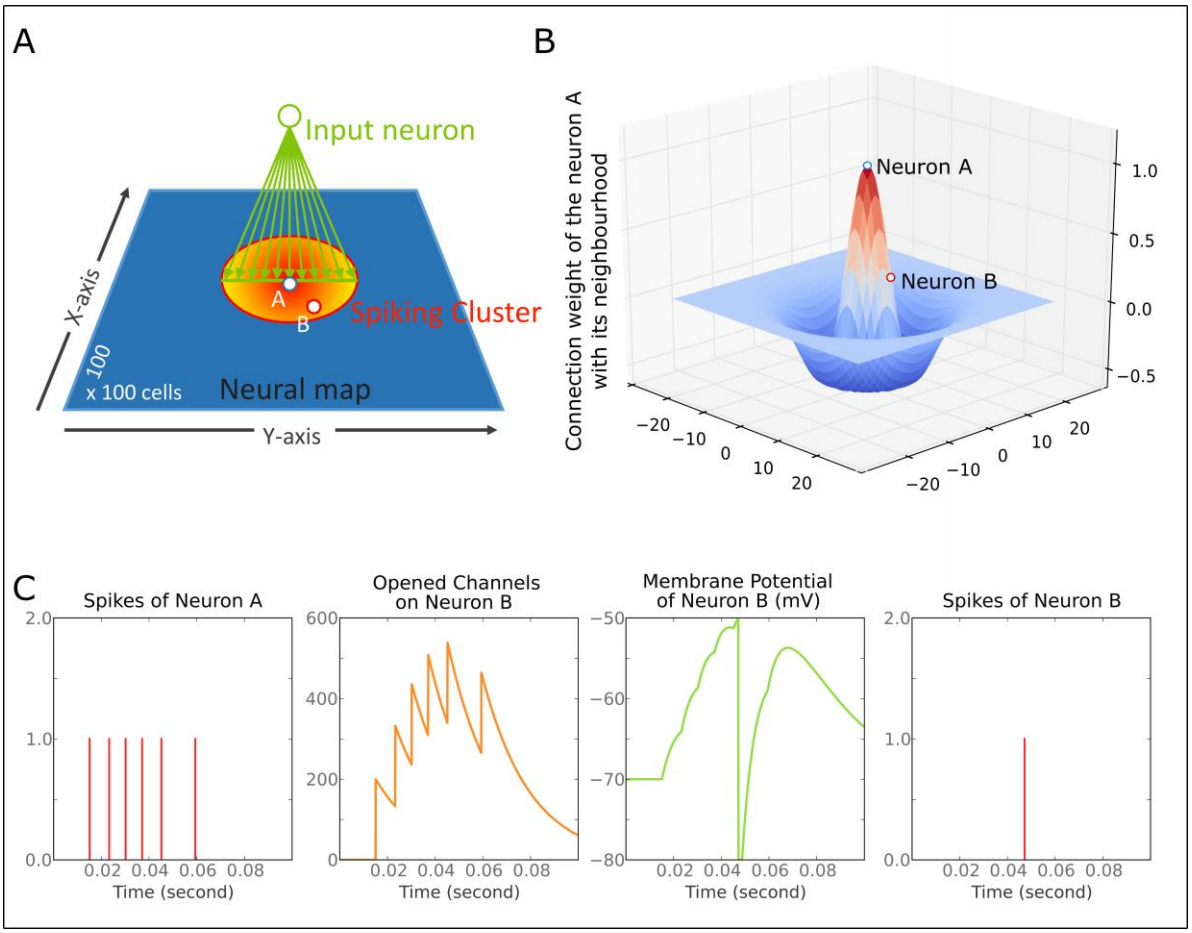

Figure 2-1: Overview of the model. Subplot A: *The model is a dynamic neural field (DNF) of 100x100 cells. The red to yellow circle represents the cluster of spiking neurons after stimulation of the neurons on the green line fed by the input neuron (green circle). This cluster forms a circle centred on neuron A. Neurons A (blue-white dot) and B (red-white dot) are marked in reference to subplots B and C.* ***Subplot B:*** *Illustration of the reference Mexican hat kernel (K = 1.2; β = 6.0; σ_y = σ_x = 5; see main text). The graph shows the connection weight of neuron A with its neighbourhood. The X- and Y-axis represent the distance from neuron A in number of cells; The Z-axis represents the weight of connection, a positive number is excitatory while a negative number is inhibitory (arbitrary unit).* ***Subplot C:*** *illustration of equation 1. Each spike of neuron A (panel 1, red bars) opens excitatory channels on the membrane of neuron B that close by themselves according to time constant τe (panel 2, orange curve). These opened excitatory channels raise the membrane potential of neuron B (panel 3, green curve). When a threshold (-50 mV here) is reached, a spike is triggered in the neuron B (panel 4, red bar).*

The spiking neuron model (Lapicque, 1907; Brunel & van Rossum, 2007 for translation) used here is a simplification of conductance-based integrate-and-fire (Hodgkin & Huxley, 1952; Shadlen & Newsome, 1998). Activity of each neuron (unit) of this network can be described with the following equations:

$$\begin{cases} \tau_m \dfrac{\partial V(n,t)}{\partial t} = -(V - V_0) - g_e(V - V_e) - g_i(V - V_i) & \text{(a)} \\ \dfrac{\partial g_e(n,t)}{\partial t} = -\dfrac{g_e}{\tau_e} + \alpha_e \sum_{n'} \sum_{f} \delta\left(t_{n'}^{f} - t\right) w_e(n', n) + \alpha_s w_s F_s & \text{(b)} \\ \dfrac{\partial g_i(n,t)}{\partial t} = -\dfrac{g_i}{\tau_i} + \alpha_i \sum_{n'} \sum_{f} \delta\left(t_{n'}^{f} - t\right) w_i(n', n) & \text{(c)} \end{cases} \quad (1)$$

$$\text{with } V = V_r \text{ if } V > V_t$$

Equation (a) describes the time course of the membrane potential *V* for all neuron n (**Figure 2-1**C, column 3). It goes toward its equilibrium V_0 with a time constant τ_m when at rest while it goes toward *Ve* or *Vi* when *ge* or *gi* are different from zero. When *V* reaches a threshold *Vt* for a neuron n, a spike is emitted and *V* is reset to *Vr* for that neuron n. After it emits a spike, a neuron will be unaffected by any input during a refractory period of 1.5 ms. This refractory period limits the maximum firing rate to 600 Hz which is consistent with SC cell recordings for instance (R. W. Anderson et al., 1998; Sparks et al., 1976).

Equations (b) and (c) describe the time course of the opening of excitatory and inhibitory gates – *ge* and *gi* -- on neuron *n*'s membrane (**Figure 2-1**C, column 2). By default, *ge* (respectively *gi*) goes to zero with a time constant of τe (respectively τi) – the synapse decay time. For each time $t_{n'}^{f}$ -- corresponding to a spike *f* of a neuron *n'* in the network -- *ge* (respectively *gi*) gets an immediate increase (from the Dirac function) which corresponds to the weight connecting *n* to *n'* defined by *we* (respectively *wi*). Finally, one or more experimenter-controlled spiking neurons can be connected to the model through *ge* (see **Figure 2-1**A). Their firing rate over time is controlled by a curve *Fs*; in that sense, they resemble electric stimulations used in neurophysiology and do not follow a Poison process.

The connections to the network are defined within the unit interval with a matrix *ws* and are modulated with *αs*.

The matrices of connections *we* and *wi* are of size 10000x10000 (the number of neurons in the network is 100x100 = 10000). Each row defines the connections of one neuron *n* with the other neurons *n'*. The matrices *wi* and *we* are computed from a difference of Gaussians equation:

$$f(x, y \mid \theta_x, \theta_y, K, \beta) =$$

$$(1+\beta)\exp\left(-\frac{(x-\mu_x)^2}{2\sigma_x^2}-\frac{(y-\mu_y)^2}{2\sigma_y^2}\right)-\beta\exp\left(-\frac{(x-\mu_x)^2}{2K^2\sigma_x^2}-\frac{(y-\mu_y)^2}{2K^2\sigma_y^2}\right)$$

(2)

Where the positive part of *f* is used to define *we,* while the negative part is used for *wi*. It is important to note that *f* describes a 2D Mexican hat curve (as in **Figure 2-1**B), and so it returns a 2D map of connections for one neuron. In order to populate *we* and *wi* with *f*, we used the following relation:

$$x-\mu_x = c \bmod 100 - r \bmod 100$$
$$y-\mu_y = \text{Quotient}(c, 100) - \text{Quotient}(r, 100)$$

Where *c* and *r* denote the column and row index of the matrices, respectively. This operation simply centres and slices the map of connections returned by *f* for each neuron so that it can be written as a row of *we* (or *wi*).

Finally, the variables *σx*/*σy* and *Kσx*/*Kσy* define the standard deviation of the Gaussians. Thus, *K* is used to set up the inhibitory/excitatory extent ratio while the parameter *β* controls the depth of the inhibition. It can be noted that the values of *f* are constrained not to exceed the range -1 to 1: *αe* and *αi* are used to scale them to a relevant dimension for the network, its unit being millivolt.

2.2 Parameter Choice

All the parameters of the model are summarized in Table 1. Parameters for which values are not given in the table have values varying in the different simulations and these values are to be found in the description of each specific simulation. The neuron parameters were taken from recent spiking neuron models of the SC (Lo, Boucher, Paré, Schall, & Wang, 2009; Morén, Shibata, & Doya, 2010, 2013) and adapted to obtain clusters that maintain a stable activity on the map for the range of stimulations we used. Concerning synaptic decay times, *τi* is longer to

τe which is coherent with the observation of Phongphanphanee et al. (2014) during a sustained stimulation of the SC (see their figure 7): indeed, **Figure 2-4**E of the present report shows that our model was able to reproduce a transient response of the membrane potential to a sustained input. However, to our knowledge the time constants τi and τe of actual SC neurons have never been specifically measured, which explains large differences in parameters values between the work of the two previous teams. By default, no noise will be introduced in the model. If a noise source is used, it will be stated in the text.

Concerning the lateral connection parameters, we used values for K and β that were chosen based on previous physiological or modelling studies. The parameter K, corresponding to the ratio inhibition range/excitation range, was set to 1.2 to limit lateral inhibitory influence to a relatively small range consistent with recent results (see Isa and Hall 2009 for a review). This ratio is similar to the value suggested by the SCs in-vitro study of Phongphanphanee et al. (2014). Indeed, they reported an EPSC half-width area of 130 μm^2 and IPSC half-width area of 145 μm^2 (see their figure 4D and their text page 5; note also that Lee and Hall's (2006) *in vitro* study on rat SCi reported ratios of 500µm/300µm = 1.6 or 500µm/400µm = 1.25). The parameter β corresponds to the strength of inhibition; it was set at 6.0 in order to set the maximum inhibition weight at roughly the half of the excitation maximum weight to fit with the results of Arai et al. (1994) (see the black curve of our **Figure 2-2** -- the minimum weight of the reference MH is at -100 mV for a maximum of 200 mV). Note that we test variations in K and β values below.

Lastly, our parameters are chosen for the neural field to be bistable between the all-off state and a spiking cluster state. When a bump in the membrane potential reaches the threshold, the model generates systematically a stable and well-defined group of spiking neurons around the point which passed the threshold. We name this group a "spiking cluster" to distinguish it from bumps in the membrane potential. This spiking cluster is similar to a bump of activity in a population rate model, and being stable, it survives after we stop stimulating the neural field.

Table 1: Model parameters and variables:

General parameters	**Symbol**	**Value and unit**
simulation time	None	200 ms
map size	None	100x100 neurons
simulation clock precision	None	0.01 ms
recording clock precision	None	1 ms
Neuron parameters	**Symbol**	**Value and unit**
membrane time constant	τm	10 ms
excitation time constant	τe	3 ms
inhibition time constant	τi	10 ms
potential threshold	Vt	-50 mV
reset potential	Vr	-80 mV
resting potential	V_0	-70 mV
Nernst potential of excitation ions	Ve	0 mV
Nernst potential of inhibition ions	Vi	-80 mV
Neuron variables	**Symbol**	**Unit**
membrane potential	V	mV
number of opened excitatory channels	ge	no unit
number of opened inhibitory channels	gi	no unit
Mexican hat parameters	**Symbol**	**Unit**
depth of inhibition controller	β	no unit
inhibition/excitation extent ratio	K	no unit
standard deviation on Y-axis	σy	cells
standard deviation on X-axis	σx	cells
centre position on X-axis	Mx	cells
center position on Y-axis	My	cells
matrix of positive connections	We	no unit
weight factor for positive connection	Ae	200 mV
matrix of negative connections	Wi	no unit
weight factor for negative connection	Ai	200 mV
External stimulus parameters	**Symbol**	**Unit**
spikes train	Fs	no unit
matrix of connections with the model	Ws	no unit
weight factor	As	mV

2.3 Simulation Set 1: Size Variation of a Single Stimulus

In a first set of simulations we want to characterize the response of the selection map to stimuli of different sizes. We iterate the exploration for three different instances of the MH to test for the effect of slight variations in the inhibition strength and extent.

A range of stimulus lines of varying size (see below) was tested with the model. We ran three different sub-simulations (S1, S2, S3): one testing the reference MH (see section 2.2) and two testing variations of it in order to make sure that the results are robust to moderate changes in the connectivity profile. More specifically, the first sub-simulation (S1) implemented the reference MH (K = 1.2 and β = 6.0; see Model parameters). The second sub-simulation (S2) was conducted to test a larger extent of inhibition. K was fixed to 2.0, which covers the upper end suggested by data of Phongphanphanee et al. (2014). In order to only address the extent of inhibition, β was set to 1.43 with an optimization algorithm to keep the minimum of MH function (depth of the inhibition) similar to S1. The third sub-simulation (S3) was conducted with K = 1.2 and β = 8.0 to observe the effect of a stronger inhibition while keeping its extent constant. For the whole set of simulations in this part, σx and σy were fixed to 5 neurons, this was chosen to get relatively small MH lateral connections compared to the dimension of the model map. Given that the determinant factor is the relative size of the stimuli compared to the MH's size, having small connections allowed us to increase the range of tested stimulus sizes.

The map was stimulated with line-shaped stimuli with twenty sizes (2 neurons up to 42 neurons in steps of 2 neurons along the Y-axis). These line-shaped stimuli were defined by $Is = \alpha s * ws * Fs$ as explained in the equation (1.b). The maximum size of 42 neurons represents less than 50% of the Y-axis size of the model map in order to limit border effects (map size = 100x100 neurons, see table 1). The firing rate pattern over time of the external input, Fs, was a Gaussian centred on 25 ms with a standard deviation of 80 ms and a maximum frequency of 400 Hz. The strength of the stimulus was αs = 4000mV. Finally, the duration of each simulation was 200 ms.

The results will be split in two parts. The first part focuses on the spatial pattern of spikes obtained on the map while the second part focus the temporal pattern happening before the spikes, at subthreshold level. Further explorations are presented in Appendix B where we extend our results to 2D shapes and Appendix C where we investigate whether our results are similar when using a sustained input (section 8). In Appendix A, we used our model in

combination with behavioural data to address a recent hypothesis linking the SCs to saccadic behaviours.

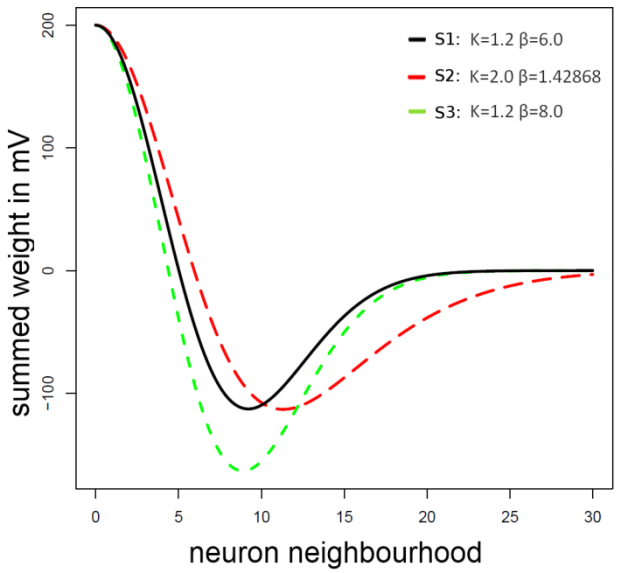

Figure 2-2: The three Mexican hats tested in Simulation 1. *They correspond to the connection of a neuron n with its neighbourhood (i.e. αe.we + αi.wi). They are only plotted on the X-axis and for one direction.*

2.4 Simulation Set 2: Interaction of Two Stimuli

Our first set of simulations addresses the effect of stimulus size in a simple DNF-MH used as a target selection map. However, such a map is prone to receive many candidate points of interest from satellite structures feeding it. Our second set of simulations tests the behaviour of our DNF-MH model when stimulated at two points with varying the distance and relative strength. In a comparison of our model with the SCs, this simulation is analogous to the in-vitro experiments conducted by Phongphanphanee et al. (2014) and by Vokoun et al. (2014) in which these two teams stimulated two points in the SCs varying the distance and the strength of stimulations injected in each point.

Two stimulation points, A and B, of size 2x2, are considered. Stimulation A is kept at a fixed location (x= 31; y= 51), while stimulation B is tested for distances from 2 to 40 cells with a step of 2. Stimulation A and B both have the same firing rate pattern as used in simulation 1. While the stimulation B is always connected with a weight of 4000 mV to the model, stimulation A is tested for 3 different weights: 1333 mV, 2000 mV and 4000 mV. We used the reference MH

configuration (K = 1.2; β = 6.0) but in a larger implementation (σx = σy = 8.5 cells, compared to 5 cells in Simulation 1, to increase the MH size and hence virtually increase the granularity of our probing). The result we report here is the position of the spiking cluster nearest to stimulation B on the map. Its localization is defined by the centre of gravity of its spike count over all the simulation. To control that border effects was not at the origin of the following observations, a control condition was run that tested the spiking cluster position for the different location of the stimulation B alone. The spiking cluster positions were then well aligned with the stimulation B and suggest there is not border effect at those locations.

The results for the simulation set 2 will be split in two parts. The first part presents the results without including noise in the model. The second part tests if the results obtained for the condition 4000mV-4000mV are robust to the addition of noise in the model and if they extend to a slight inequality in A and B intensity (3500mV-4000mV). Precisely, the noise was added to the membrane potential and was following a normal distribution of standard deviation 4 mV.

3 Results

3.1 Simulation Set 1: Spatial Patterns

Figure 2-3 shows membrane potential and firing rate for all neurons of the neural field for a subset of stimulus sizes for the 3 MH variants (S1, S2, S3, depicted in **Figure 2-2**). These values of membrane potential and firing rate were averaged over all the simulation time (200ms). The represented line sizes illustrate the different activity patterns that we observed. Panel D shows the number of spiking clusters (see parameter section for definition) as a function of the stimulus size for the three MH variants, as further explained below.

For the first MH (S1, K = 1.2 and β = 6.0, **Figure 2-3**A and black line in 3D), a unique circular spiking cluster located on the centre of the stimulus line was observed from the smallest size up to the size of 18. Despite the transient nature of the stimulation, the spike cluster persists during the whole duration of the simulation. On the contrary, from size 20 to the largest tested size (size 42), no spiking clusters appeared on the firing rate map: a complete activity suppression was observed. It can be noticed that on the membrane potential map, the activity appears equally spread for size 20 while the activity is stronger on the extremities for size 42. This sub-threshold activity distribution suggests that the extremities could win the competition if the spiking threshold was decreased.

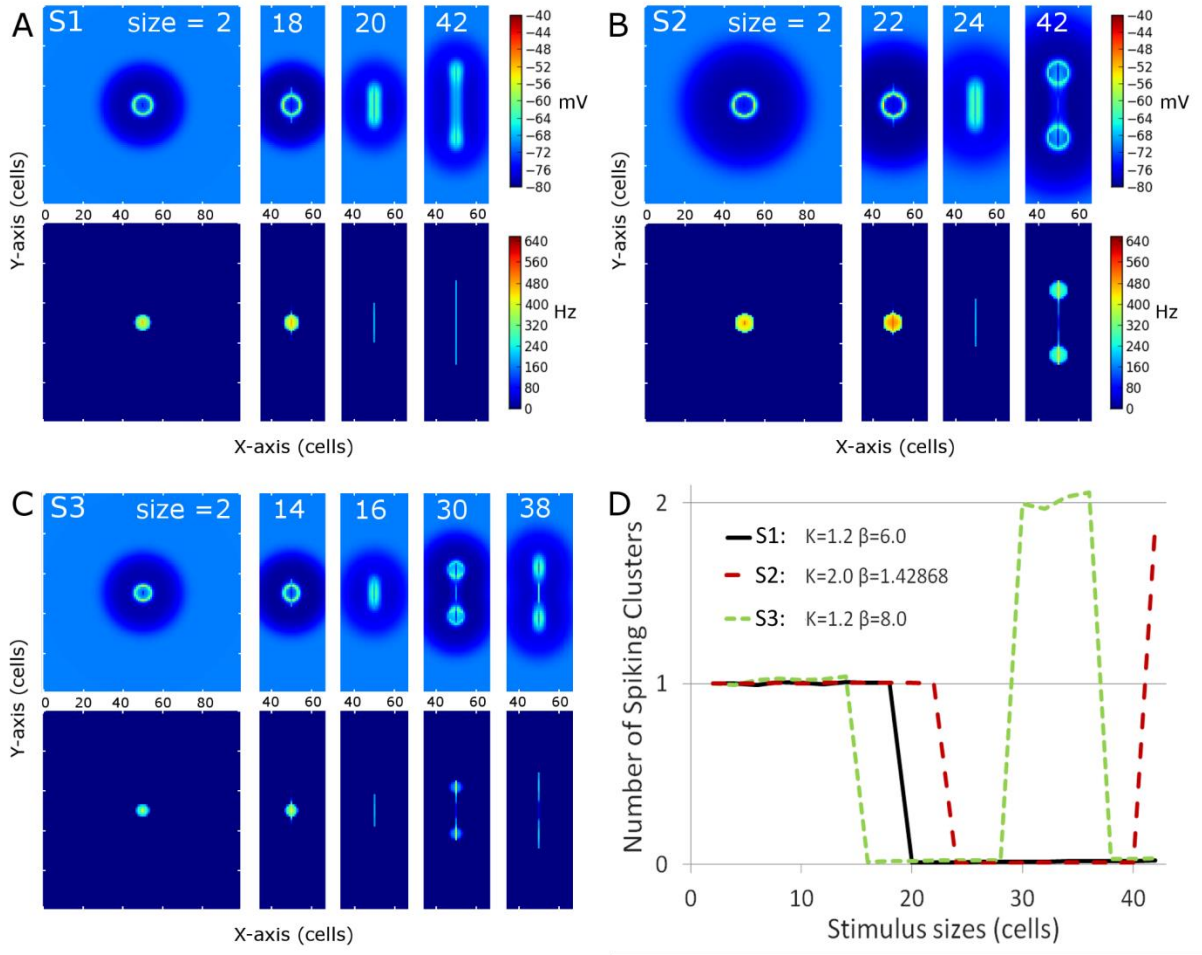

Figure 2-3: Overview of the spiking clusters spatial distribution during S1, S2 and S3 *(respectively subplot A, B and C). The results are shown for the most informative stimulus sizes, which are different according to the set of simulations and are indicated on each column of the graphs.* ***Subplot A, B, C:*** *On each picture, the top part shows average membrane potential during the simulation; the lower part shows average firing rate during the simulation.* ***Subplot D*** *summarizes the result: the number of spike clusters is computed as the sum of spikes on the map divided by the sum of spikes occurring for the first distractor size (each first distractor size gave rise to one spike cluster that is used as reference).*

In the second sub-simulation (S2, K = 2.0 and β = 1.43, **Figure 2-3**B and red line in D), we observed similar results but the spiking cluster for small line sizes was larger and the complete activity suppression starts at a larger stimulus size. These two observations are to be related to the slightly larger excitation influence in S2 with respect to S1 (**Figure 2-2**). The main difference with S1 appears at size 42: the activity on the extremities was strong enough to give rise to two spiking clusters. Those two spiking clusters have a weaker average firing rate than the one observed for previous sizes. Below (section 3.2), we show this is due to a larger latency before the first spike rather than a lower firing rate once initiated.

In the third sub-simulation (S3, K = 1.2 and β = 8.0, **Figure 2-3**C and green line in D), similar results as in S2 and S1 are found but with a smaller radius of the spiking cluster for small line sizes and a suppression that starts at a smaller stimulus size (size 16). Here, two spiking clusters were observed, as in S2, for stimulus size 30 to 36. However, S3 differs from S2 as a complete suppression was again observed for larger sizes than 36. When present, the two spiking clusters were on average weaker than the unique spiking cluster observed for smaller sizes. Once more, below (section 3.2), we explain that this is due to a larger latency before that the spiking clusters arise.

Thus complete activity suppression occurred for at least one range of sizes for each set of simulations. The stimulus size for which it appears is positively correlated with the size of the positive area of the MH used for these simulations.

Lastly, note that the stimuli tested were spatially homogenous: each point of the stimulus gave the same input to the map. This type of stimulation may favour complete suppression, and if noise were present in the network, it is conceivable that it could randomly favour the selection of a spiking cluster and hence eliminate the phenomenon of complete suppression. To test this hypothesis we added normally distributed noise in the membrane potential of all the units of the 2D network, using K = 1.2 and β = 6.0 (S1). The standard deviation of the noise was of 4mV, which corresponds to a fifth of the distance between the resting potential and the threshold. The results were similar to those presented above. Hence, even with noise in the network, the phenomenon of complete suppression could be observed.

3.2 Simulation Set 1: Temporal Dynamics

In simulations S2 and S3 larger stimuli could lead to two spiking clusters, which show a lower firing rate average than for the unique cluster appearing for smaller sizes. **Figure 2-4**A, B, C shows the evolution of the membrane potential for neurons just next to the stimulus line (see caption for more details) for the same sizes addressed in **Figure 2-3**A, B and C. It can be observed that the threshold to the first spike is reached much later for sizes giving rise to two spiking clusters (size 42 in SA2 and size 30 in SA3) when compared to sizes leading to one spiking cluster. In addition we have estimated the firing rate of the spiking clusters for the last 50 ms of each simulation: their firing rate does not change between stimulus size (550-600Hz for S2, 350-400Hz for S3,). Hence the change in firing rate average observed in S2 and S3 was the result of the change in latency for the membrane potential to reach the threshold.

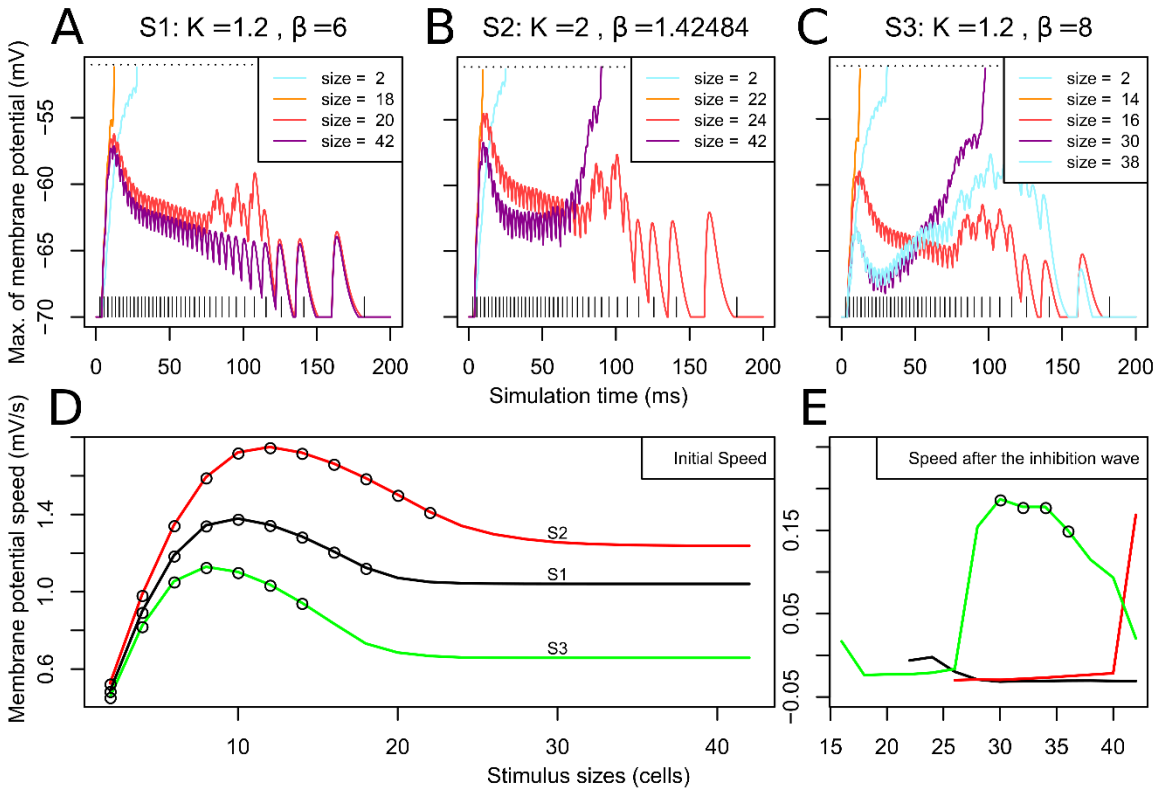

Figure 2-4: Overview of the membrane potential dynamics during SA1, SA2 and SA3. Subplot A-C: *Effect of the stimulation on the neighbourhood according to time. We report the membrane potential of the most excited neuron among the neurons situated along a line parallel to the stimuli and at 2 cells from it (x = 52). When a neuron on this line reaches its threshold (at -50 mV, see the dashed horizontal line), it means that a spiking cluster is created.* ***A, B and C*** *correspond to the 3 different MHs introduced in* ***Figure 2-2****; their parameters K and β (from equation 2) are indicated. For each MH, we plot the maximum of the membrane potential for the same sizes as shown in* ***Figure 2-3****.The vertical lines at the bottom represent the input spike train.* ***Subplot D:*** *Initial speed (averaged between 0 and 6 ms) of the membrane potential (in mV/s) according to stimulus size for SA1, SA2 and SA3. The circles plotted on the curves denote that, for these stimulus sizes, the membrane potential reached the threshold before 30 ms and led to one spiking cluster on the neural field.* ***Subplot E:*** *Speed of the membrane potential (in mV/s) between 30 and 90 ms when auto-inhibition prevented threshold being reached in the first rise, plotted according to stimulus size. The circles plotted on the curves denote that, for these sizes, the membrane potential reached the threshold sometime after 30 ms and there are two spiking clusters on the map.*

We can observe in all the simulations (**Figure 2-4**A, B, C, all curves) an early rise of membrane potential. This early rise is at the origin of all single spiking clusters observed in **Figure 2-3**. Moreover, **Figure 2-4**D shows the speed of this early rise (for the interval between 0 and 6 ms) for all stimulus sizes. This speed increases until an optimal size (10, 12 and 8 cells for S1, S2 and S3 respectively) and then decreases to a plateau. The obtained curve is analogue to what is found with the firing rate of neurons in surround suppression literature (Sceniak, Ringach, Hawken, & Shapley, 1999; Schwabe et al., 2006). Empty circles on the curves indicate that the

threshold is reached before 30 ms (i.e. a single spiking cluster is observed). Hence we can see that close to the stimulus size corresponding to the beginning of the plateau, the initial wave of excitation starts to fail to reach spiking threshold. Interestingly, in those conditions (size 20 and 42 of **Figure 2-4**A for instance), we can observe that the early rise is transient. This transient nature is explained further through the dynamics of excitatory and inhibitory influences in Appendix C. Interestingly, this transient rise in the membrane potential echoes the transience observed by Phongphanphanee et al. (2014) in the SCs as previously mentioned (see their figure 7A, left).

The two spiking clusters for larger stimuli occurred through a late second rise in membrane potential after 50ms (e.g. size 42 and 30 for S2 and S3). By observing the curve for size 20 in S1 **Figure 2-4**A, we can see that a late rise in the membrane potential occurs also for intermediate sizes, but insufficiently to produce late spiking clusters (see also size 24 for S2 and sizes 16 and 38 for SA3), this corresponds to the complete activity suppression shown on **Figure 2-3**. To examine this further, **Figure 2-4**E plots the mean speed of the membrane potential averaged between 30ms and 90ms to illustrate how the second rise varies over stimulus size. The time window used catches the variation for S3 especially well showing that the second rise of the membrane potential, like the first, also has an optimal stimulus size after which the rise speed decreases again and it fails to reach threshold (note that the pattern may be compared to **Figure 2-3**D).

3.3 Simulation Set 2: Spatial Interactions

Figure 2-5C shows a summary of the results for these simulations. The spiking clusters produced by the model indicate which locus has been selected as a target. Its deviation from stimulation B is shown as a function of distance between the two loci of stimulation. Negative values correspond to a deviation toward the locus of A. The three curves correspond to the three different intensity of stimulation tested for the point A (1333, 2000, 4000mV; B is always stimulated with 4000mV). Filled symbols indicate that only one spiking cluster was present on the network and open symbols that two clusters survived.

In the case of equal strength for both stimulations (green curve), for the first distances up to 14 cells, we observed one single resulting cluster (fusion phenomenon) that was in between

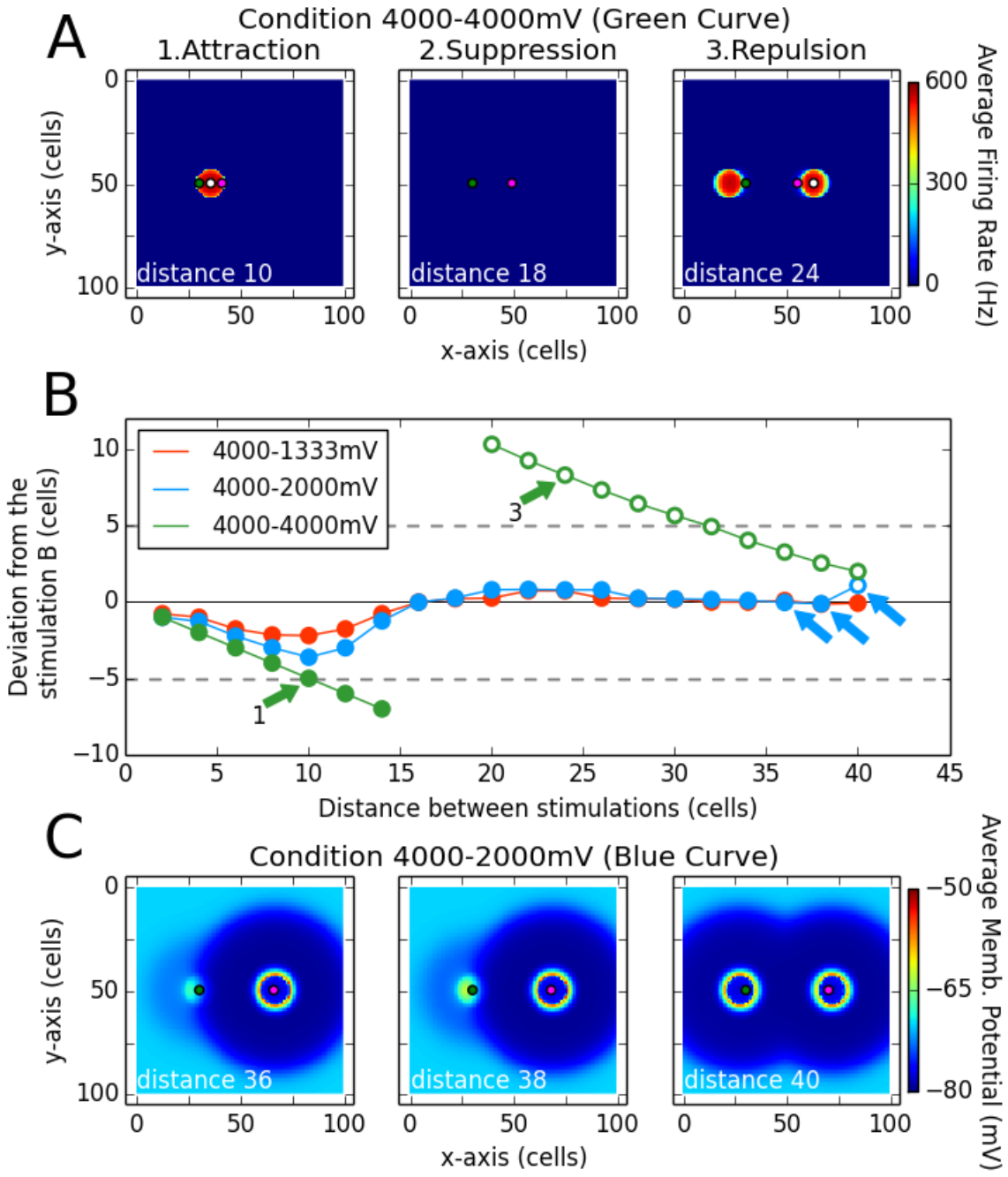

Figure 2-5: Interaction between two stimulation induced bumps according to their distances. *The magenta dot in subplot A and C represent the position of stimulation B, while the green dot represents the stimulation A. The white dot in subplot A is the centre of gravity of the spiking cluster the nearest from stimulation B. The plot B describes the deviation of that centre of gravity (white dot) from the stimulation B (magenta dot) on the x-axis. Filled dots denote there is only one spiking cluster on the map, while the unfilled dots denote there are two spiking clusters on the map. The simulation was run for different distance between the stimulation A and B (x-axis), and for different strength of the stimulation A (curves red, blue and green).Note that the subplot A shows an average of the firing rate over the simulation while the subplot B show an average of the membrane potential over the simulation.*

the two stimulation loci (see **Figure 2-5**A1 Attraction). That observation can be related to the activation merging found by Vokoun et al. (2014) in the SCs (see their Figure 3). Then for two following distances (16 and 18 cells), a complete suppression of activity on the map was observed (see **Figure 2-5**A2 Suppression). Finally, from a distance of 20 cells up to the largest tested distance (40 cells), two clusters are produced and the closer to the site of B is repulsed in the opposite direction with respect to A (positive values on y axis of the panel B). The panel A3 allows us to see that the same repulsion was observed for the cluster close to the A site. This repulsion phenomenon decreased as the distance between the two stimulating sites increased.

When stimulation B was stronger than stimulation A (blue and red curves), in almost every case only one cluster was produced: a winner-take-all mechanism occurred and selected a locus near stimulation B. Nevertheless, a deviation toward stimulation A is still observed up to the distance 16 cells: the spiking cluster appears in between the two stimulations. Note here that the selected locus is closer to the strongest stimulation and that it gets closer when the latter gets stronger. That bias toward the strongest stimulus is also observed in Vokoun et al. (2014). For larger separation distances, the winning cluster remained localized near site B. This result goes in line with the results of Phongphanphanee et al. (2014): when the stimulations are close enough, an activation is present at A and B sites while when the stimulations are more distant, no activity is recorded close to the stimulation A (the weakest) and a normal cluster is observed close to the stimulation B (the strongest). Nevertheless, the winner-take-all mechanism is not perfect: the selected locus is near to B but not aligned with it. Indeed a deviation away from stimulation A occurred, similar to what we observed with equal strength simulations.

Figure 2-5C shows the abrupt end of the winner-take-all phenomenon with stimulus distance[9] for the condition with A=2000mV (the panels correspond to the three blue arrows of **Figure 2-5B**). In panels C1 and C2, stimulation A is on the edge of influence of stimulation B. In panel C3 (distance = 40 cells), the activity at A escaped from the small inhibition influence of stimulation B and two clusters emerged – the system fails to select only one stimulus. That does not happen for the condition 4000mV-1333mV at distance 40: the stimulation A is then too weak to overcome the small inhibition influence of B.

[9] Note that, in the frame of this thesis and except if stated otherwise, "stimulus distance" will always refer to the distance between two stimuli, i.e., the inter-stimulus distance.

3.4 Simulation Set 2: Tight competition and addition of noise.

Our previous results for two stimulation inputs of exactly same strength show that for a given range of distances a complete suppression of activity is observed. This corresponds to a failure for the DNF-MH model to select only one target. One can suggest that this failure of the winner-take-all is due to 1) the absence of noise in our model or 2) the unnatural exact equality of the two stimulations in competition.

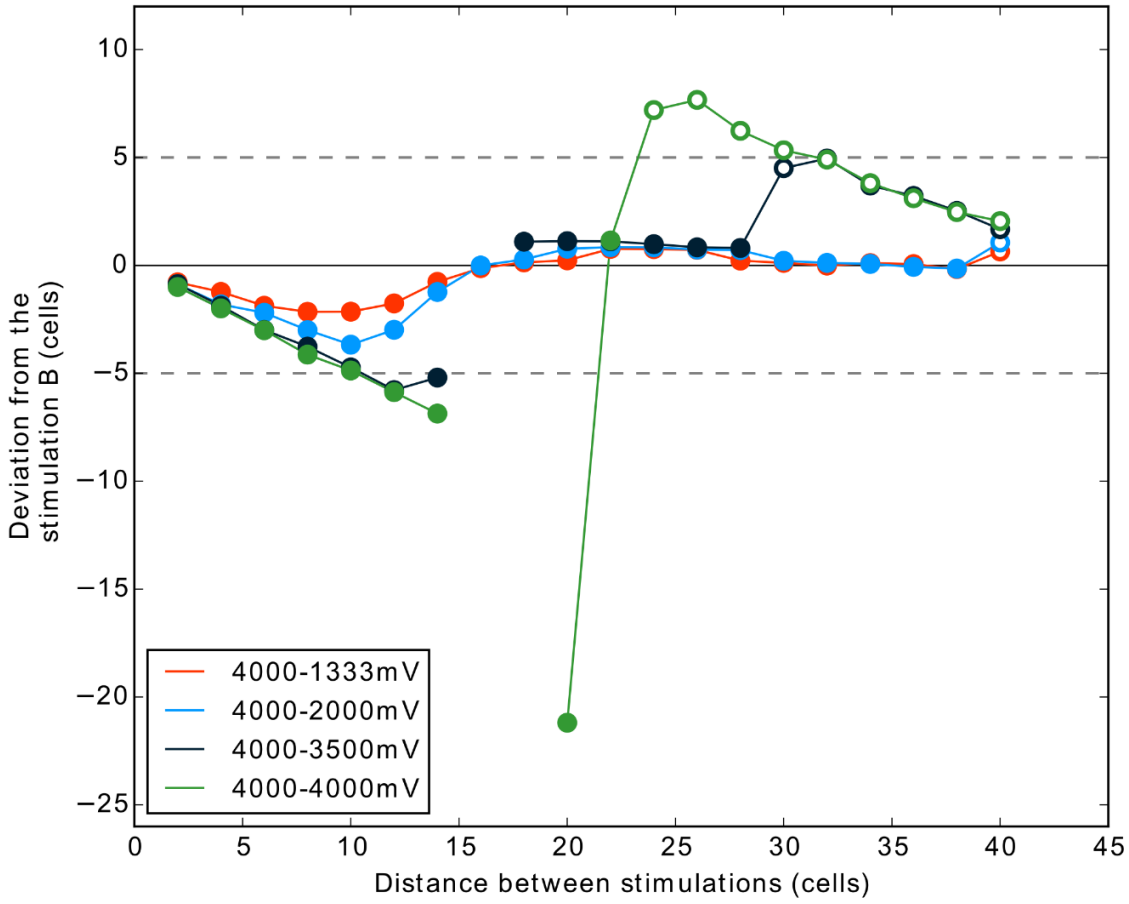

Figure 2-6: Interaction between two stimulations according to their distances, with noise and tight competition *(4000-3500mV). Same description as for* ***Figure 2-5****B.*

We tested here if the previous results, notably the suppression, can be obtained with the addition of noise and for close competition (3500mV vs 4000mV).

Figure 2-6 shows the results of one simulation with these conditions. The results are strongly similar to those obtained in the simulation without noise. The addition of noise, even if it helps to get only one winner (compare distance 20 and 22 in **Figure 2-6** and **Figure 2-5**B), does not

prevent the case of two-winner and no-winners in the 4000mV-4000mV condition. Interestingly, the condition 4000-3500mV (dark blue curve, **Figure 2-6**) shows that we can also obtain activity suppression when the two stimulations are not exactly of the same strength. This occurs for distance 16 and 18 cells, similarly to the equal strengths condition. However, in this case, the two-winner situation is not observed directly after the suppression phase. For some distances, the curve is similar to the one obtained in the condition 4000-2000mV. Nevertheless, finally stimulation A succeeds to give rise to a spiking cluster because the inhibition from stimulation B gets smaller after a certain distance (see **Figure 2-2** for the shape of a MH curve). Here, stimulation A being stronger than in the 4000-2000mV condition, it overcomes the inhibition of B (i.e. it results in two clusters) at a smaller distance.

4 Discussion

The aim of the present study was to get further insight into the properties -- and their consequences for saliency or target selection -- of Dynamic Neural Fields based on a Mexican hat kernel (DNH-MHs) in the specific case of short inhibitory influence. Indeed, this type of lateral connection has been recently demonstrated for a classical biological example of DNF-MHs, the superior colliculus (SC; see Introduction). We designed a simple one layer model implementing the most recent data concerning lateral interaction in this neural structure (Phongphanphanee et al., 2014) and we tested its properties. We observed that certain stimulus sizes could lead through centre-surround interactions to a complete suppression of the network activity, while larger sizes led to multi loci selection. This complete suppression, which led to no target selection, also occurred when two stimulations were presented simultaneously within a certain range of distances. For smaller distances, the model selected a position in-between, closer to the strongest stimulus (attraction/fusion), while for larger distances the model selected two loci that were deviated away from the stimuli positions (repulsion). We discuss these results of suppression and spatial deviation (i.e., attraction/fusion and repulsion) obtained here in view of neurophysiological, modelling and previous behavioural findings.

4.1 Suppression phenomena: Neurophysiology results

It may seem counterintuitive to observe complete suppression on a saliency map for large stimuli of interest. This result can nevertheless be related to previous neurophysiological, modelling and behavioural findings in the visuo-oculomotor system and may help to disentangle unanswered questions.

Suppression phenomena in which larger stimuli produce lower activity than smaller ones are well described in sensory systems and especially in the visual system (Allman, Miezin, & McGuinness, 1985; Series, Lorenceau, & Frégnac, 2003). Most of the time a decrease in the response is observed (either a decrease in the frequency of the response or/and in the number of spike emitted; see Hubel and Wiesel 1968), rather than a complete suppression as observed here. Nevertheless, phenomena of total suppression have also already been reported in physiological recordings. Goldberg and Wurtz (1972) showed a complete suppression of SCs response when increasing the size of a visual stimulus (see their Figure 4). Additionally, more recently, in a study on SCs receptive field, Wang et al. (2010) reported that the activity of SCs neurons was completely suppressed for large stimuli centred on the tested neurons (see their figure 5). Our study brings some clues concerning mechanisms underlying these suppressive phenomena. Indeed, their neural substrates remain debated (Sachdev, Krause, & Mazer, 2012). The origin of the suppression is proposed to be due to 1) a decrease of feedforward activation 2) interactions involving local lateral connections or, finally, 3) feedback connections from higher areas. The present study confirms, on a theoretical ground, that centre surround interactions in a single layer based on the most up to date physiological evidence from SC is sufficient to provide total suppression of the response for a certain range of stimulus sizes.

For any given surround suppression phenomenon, the present work provides predictions to test the hypothesis that it might be driven by short inhibitory lateral connections. First, increasing the size of a line stimulus should lead, after the suppression phase; to the reappearance of activation clusters on sites corresponding to extremities (see **Figure 2-3**). Second, this reappearance should be observed with a significant latency increase if a delayed wave of inhibition is present (see Appendix B, section 3.2). Third, when two stimulations are tested, maximal activity suppression should also be observed for a specific distance (see **Figure 2-5**).

4.2 Suppression phenomena: Modelling results

Similar models with MH connections have already been suggested to reproduce surround suppression (Sceniak et al., 1999; Schwabe et al., 2006; Spratling, 2010). Only Sceniak et al. (1999) also showed total suppression (see *their* figure 2F). Nevertheless none of them were constructed with spiking neurons. The patterns of activity at subthreshold level and before the first spike (section 3.2) gives an insight into how the *dynamic* of the inhibition and excitation can shape the suppression. In the present model, it is a delayed wave of inhibition – i.e. after an initial rise of membrane potential-- which drives the surround suppression. Note also that the model highlights that there is an optimal size of visual stimuli for which the latency to trigger a spiking cluster is minimized (**Figure 2-4**D). That aspect of the model is in line with the work of Marino et al. (2012) –see *their* figure 6F. Those authors were running a population rate base DNF-MH of the SCi (Trappenberg et al., 2001) and they used an arbitrary threshold to trigger saccades. They observed a U-shape relationship between the estimated reaction time and saccadic target sizes, but did not observe a total suppression as we did.

The total suppression (absence of spike) that we observed as a result of auto-inhibition might be due to the properties of our model. First, leaky integrate-and-fire spiking neurons implement *de facto* a gating mechanism: neurons keeps silent if the input in too low. Second, the strong coupling of our network allows strong self-sustained spiking clusters. The combination of both creates a switch-like responses of our model: either a region is ON (forming a spiking cluster), or it is OFF. That could explain the total suppression. However, it is reasonable to question whether such a switch-like winner-take-all is biologically possible. In fact, such switch-like responses are reported for neurons coding for competing stimuli in the optic tectum of the barn owl (Mysore, Asadollahi, & Knudsen, 2011) and in the SCs of the mouse (Phongphanphanee et al., 2014). Mysore et al. estimate that 48% of the neural population they tested was exhibiting switch-like responses while the remaining 52% was exhibiting gradual responses. From that, our model is predicting that total suppression due to a too large stimulus are likely to happen in the switch-like population of the SCs/Optic Tectum.

4.3 Suppression phenomena: Behavioural results

If the suppression phenomenon observed in our model exists in the oculomotor system, this predicts that large stimuli will lead to fewer saccades with short latency than would small stimuli. Ploner et al. (2004) observed this type of effect in a behavioural study: saccades with

short latency were less numerous for large targets (10°), whereas saccades with short latency were more frequent for small target sizes (1°). More precisely concerning this latency question, the U-shape curve for the relationship between the membrane potential evolution speed and the size of the stimulus (**Figure 2-4**D, see also figure 6F of Marino et al. 2012) is in line with the relationship shown by Boch et al. (1984) between express saccades latency and the size of the target (see *their* figure 5).

The observed suppression would similarly predict that larger distracting stimuli could paradoxically interfere less with saccades to a nearby target than might smaller distractors. Such a pattern was observed by Tandonnet et al. (2012) – and to which we will return in detail in Appendix A. Their work focused on the Global Effect, which is the tendency for saccades to land in between to nearby visual stimuli (Findlay, 1982). Using a target-distractor couple, they found a U-shaped curve for such deviation while increasing the distractor size: first the distractor is too small to have a strong influence, then its increase in size makes its influence grows, but from a given size its influence begin to decrease. This loss of weight for larger stimuli could be explained by a decreased response in a saliency map such as the SCs or the LIP. Finally, the results of Stigchel et al. (2012) consisting in a smaller extent of the global effect for large stimuli may also be explainable by a suppression of large stimuli. Note that while Tandonnet et al. (2012) observed the average shift of the landing positions, Stigchel et al. (2012) observed the split from unimodal to bimodal distribution. All these results suggest that different degrees of suppression are observable at the behavioural level. It remains to be investigated whether total suppression phenomena can also be detected – for single stimulus, and for two stimuli.

4.4 Spatial Deviation: the Fusion effect

Our DNF-MH demonstrates deviation of the spiking clusters from the initial input locations. Such deviation can be detrimental, for instance, when the DNF-MH is used as a target selection map which has to select among different points of interest sent by satellite structures. Indeed, with such deviation, the selected target would not correspond to any prior points of interest. We discuss here whether these deviations have already been observed at the neurophysiological, modelling or behavioural level.

When the model is stimulated at two nearby locations a single spiking cluster emerges in-between them. The cluster is closer to the stronger stimulation location – in proportion to its relative strength – and it is of the same width as spiking clusters induced by a single

stimulation. This phenomenon of *attraction (and fusion)* was described for the first time by Amari (1977) in a DNF-MH based on a firing rate neuron model. The findings of the present study extend these previous observations to a 2D spiking neuron networks.

On the behavioural side, the tendency for saccades to land in between two simultaneous and nearby visual stimuli is known as the Global Effect or saccade averaging (Findlay, 1982). Concerning the neurophysiological approach, Glimcher and Sparks (1993) showed that this fusion phenomenon could occur in the SCi when an intermediate saccade is made between two visual stimuli presented simultaneously. Edelman and Keller (1998) added that this could be the case for saccades of latency in the average range while two distinct bumps of activity would stand on the SCi for shortest latency saccades. However, whether a fusion of activity in the SCs or the SCi can explain the Global Effect is still matter of debate. Arai et al. (1994) implemented a saccadic system model using a DNF-MH to simulate the SC layers. Their model took into account the SC spatial compression and, in their test using fusion to explain the Global Effect, one can notice hypermetria (overshoot) of the output saccade (see *their* figure 10). Katnani and Gandhi (2011) brought further insight for that result: when the DNF-MH phenomenon of fusion is applied in SC space (Note that the SCs and SCi are assumed to have to an equivalent mapping; cf. Schiller and Stryker 1972), this would lead systematically to overshooting averaging saccades in external or retinotopic space. On the other hand, they demonstrated that a vector averaging of two steady bumps of the SC space would lead neither to a hypo- nor a hypermetria. They, however, note that if the phenomenon of attraction could lead to a wider bump of activity (wider on the axis formed by the two input stimulations, leading to an elliptic shape), the hypermetria would be corrected.

Recently, Vokoun et al. (2014) have reported in their work applying photodiode stimulations that on a coronal slice of the *superficial layers* of the rat SC- “simultaneous stimulation of two nearby sites resulted in a single, merged peak centred between the two sites”. They suggest that such a phenomenon could explain the Global Effect. Importantly, they observed that an activity bump induced by the simultaneous stimulation of two loci is wider than an activity bump induced by a single stimulation. That results interestingly echoes to a previous behavioural study observing that larger visual stimuli can lead to a wider distribution of saccade landing positions (Tandonnet & Vitu, 2013). Under the considerations of Katnani and Gandhi (2011) this spread of activation could correct the hypermetria issue discussed above, but it is important to note that a single layer bistable DNF-MH model such as ours could not

replicate such a spread of activity - the fused activity has the same width as that for a single stimulus because the stable cluster size is set by the width of the MH.

4.5 Spatial Deviation: the Repulsion effect

When two clusters of activity were induced by two stimuli, they tended to deviate away from each other (see **Figure 2-5**). Here also both the early work of Amari (1977) and the recent study of Almeida et al. (2015) already observed this phenomenon in 1D models. Again our results allow to extend these findings to a 2D situations (see also the Appendix B). To evoke this repulsion phenomenon, Amari (1977) explains that bumps of activity tend to climb up inhibition slopes. Then, the repulsion is reserved to MHs which have a range short enough to allow a stimulation to "climb" the outer inhibition slope of another.

Concerning the behavioural level, Wang et al. (2012) as well as Wang and Theeuwes (2014) suggest that if this phenomenon is present in the SC, it could explain the trends of saccade trajectories to deviate away from a distractor. Wang and Theeuwes (2014) also report a shift of the landing positions away from the previous fixation stimulus when varying its timing which might be explain by repulsion. However, to the best of our knowledge, repulsion in the bimodal distribution of landing positions to two simultaneously presented stimuli or in the internal representation of stimuli position has never been observed. This may be due to the difficulty to track back a phenomenon occurring in the SCs from behavioural data. For instance, the strongest repulsion effect we observed occurred when there are two spiking clusters emerging on the map. Nevertheless, if there is vector averaging downstream, at the behavioural level only a Global effect might be observed.

Finally, at the neurophysiological level, Vokoun et al. (2014) studied activations in coronal slices of the superficial layers of the rat SC after concomitant stimulation of 2 two sites. They did not observe any repulsion (nor any suppression) effect despite the exploration of numerous distances between the two stimulated sites. Hence, even though evidences have been found recently for a local Mexican hat kernel in the SCs (Phongphanphanee et al., 2014), the lack of concordance between the present study results and Vokoun et al. (2014)'s results question if the SCs can be modelled with a simple DNF-MH (see also the end of the previous section, 4.4). However, a possible alternative to explain this lack of concordance is that the coronal slicing used by Vokoun et al. (2014) may have damaged part of the lateral inhibition system altering the MH kernel, its size and its properties. Hence, further neurophysiological

works are required to shed more lights on 1) the link between fusion of activity in the SC layers and Global Effect, and 2) on what extent those natural phenomena can be modelled with a simple DNF-MH.

Interestingly, attraction and repulsion phenomena have recently been reported when using DNF-MHs to model spatial working memory tasks, and they have been successfully related to actual behavioural imprecisions (Almeida et al. 2015).

5 Conclusion

We constructed a DNF-MH integrating short range MH connections based on recent results obtained in the superficial layers of the SC, and we tested how it performs in very simple target selection tasks: 1) the localization of a single stimulus of different sizes; 2) the selection and localization of the strongest of a pair of stimulations.

Our work demonstrates that even a short range inhibition (i.e. only slightly larger than the excitation; ratio of 1.2) can enable a selection dynamic. However, it also highlights noticeable phenomena emerging from the model during those tasks: suppression, multi-spot selection, attraction/fusion and repulsion. If the DNF-MH is used as a target selection map as it is thought to be the case for the SCs, such attraction and repulsion would impair the spatial precision of the selection while the suppression would delay or hinder selection. In short, those properties suggest that the SCs is an imperfect winner-take-all selection system. At the same time, those properties constitute a collection of testable predictions to verify this point and the pertinence of using a DNF with short range MH to model the SCs. In parallel, future modelling work may investigate whether the phenomena we observed survive more advanced implementations of the SC dynamics. Notably, 1) when one implements the transient visual burst dynamics in SCs; 2) when one implements the SCi layer and the motor executions. This is partly what will motivate the modelling effort of Chapter 5.

Ultimately, this Chapter has introduced the basics of DNFs spatial interactions, the notions of merging/attraction/merging effect and of repulsion effect will be re-used in Chapter 3 and Chapter 4. We would also recommend the reading of Appendix A that explores the interaction of the merging effect with the auto-inhibition effect inside a single DNF. We particularly question whether such a configuration is sufficient to explain the result of Tandonnet et al. (2012) – mentioned in Section 4.3.

1

6 APPENDIX A: Global Effect and Auto-inhibition in the Superficial Layers of the SC?

6.1 Introduction

The Global Effect (GE, or averaging effect) is probably the simplest sensory-motor spatial interaction observable in the monkey and human. It refers to the tendency for the first landing position of saccades to be in between two nearby visual stimuli instead of there being an accurate saccade to one of the stimuli (Coren & Hoenig, 1972; Findlay, 1982).

Recently, the superficial layers of the SC have been suggested as the biological substrate of the GE (Vokoun et al., 2014) – notably because the authors observed in vitro a merging effect happening in the SCs while stimulating two regions of the SCi. In addition to this, early neurophysiological exploration of the SC showed that large stimuli can induce less activity than smaller ones in SCs neurons (Goldberg & Wurtz, 1972). Therefore, Vokoun et al. (2014)'s and Golberg and Wurtz (1972)'s results are suggesting that both auto-inhibition and GE are occurring in the SCs. Next to that we showed in this chapter that a single layer DNF model of the SCs can replicate both merging effect and auto-inhibition effect. In fact, the merging effect of DNF have already been suggested to explain the GE elsewhere (Arai et al., 1994). Thus, everything seems to fall into place: a single DNF model can generate the GE and the auto-inhibition effects; and all that in the SCs. However, it should be recalled that a more standard view of the GE localize it in the SCi or downstream (Edelman & Keller, 1998; Glimcher & Sparks, 1993). From that, there are two main hypotheses: 1) auto-inhibition and the GE happens at the same functional level; 2) the auto-inhibition and the GE does not happen at the same functional level. One way to address those hypotheses is to collect behavioural data of the interactions between auto-inhibition and GE and then explore the space of lateral connections that would allow those interactions to happen on the same single layer DNF. Our work shows that to consider that both effects happen at the same level would lead to elliptical lateral connections in the SCs; we then discuss why such an atypical solution favours the second hypothesis.

In the framework of Global Effect paradigms, the metaphor of the "centre of gravity" was introduced as the eyes often move closer to the largest or the brightest stimulus of the configuration (Deubel, Wolf, & Hauske, 1984; Findlay, 1982). However, based on the result of Goldberg and Wurtz (1972) and on the predictions that can be made for large stimuli in neural fields with lateral interactions (see above), Tandonnet et al. (2012) reasoned that the global

effect might be counter-intuitively less powerful for a large stimulus if it loses influence due to auto-inhibition. Consistent with this, their results showed that for small distractors, their apparent weight increases with size

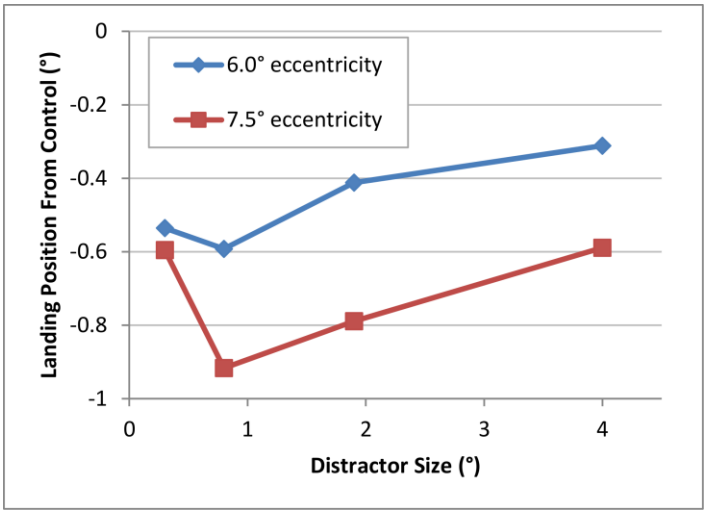

Figure 2-7: *Reversal pattern in global effect while the distractor's length increases observed by Tandonnet et al. (2012). Mean saccade landing positions in distractor trials relative to no distractor trials as a function of distractor length and target eccentricity for all participants. Asterisks indicate the statistically significant differences between neighbouring points ($p < 0.05$). In the behavioural study of Tandonnet et al. (2102), the target was a circle of 0.2° of visual angle. The distractor was a vertical line between the fixation cross and the target; its size could be 0.3°, 0.8°, 1.9° or 4° of visual angle. The target-distractor distance was kept at 3° of eccentricity throughout the conditions while they tested two eccentricity of the target -- 6° and 7.5°.*

(from 0.3° to 0.8°), but for further size increases (from 0.8° to 4°) the weight of the distractor seems to decrease, i.e. the eyes land closer to the target than for the 0.8° distractor size (more details in **Figure 2-7**). This result could be described as a reversal pattern (or U-shape) in the Global Effect. Because the reversal pattern was present at short reaction times, their results are likely to reflect an low-level interaction between Global Effect and auto-inhibition effect.

What is interesting with this experimental set up is that the distractor is a vertical line so that its size varies on the vertical axis while the fixation, distractor and target are aligned on the horizontal axis. Thus, the auto-inhibition effect is happening on the vertical axis while the Global Effect between target and distractor happens on the horizontal axis. If we find that our single DNF model needs an *elliptical* pattern of lateral connections to explain the results of Tandonnet et al. (2012), that would mean that two different radius of circular connections are needed to explain the interaction between GE and auto-inhibition. Assuming circular patterns to be more realistic, it would mean that GE and auto-inhibition occurs in two different DNFs.

6.2 Method

6.2.1 Mapping with the SC space and eyes landing position:

We used the same 100x100 neural network used in the present Chapter. Nevertheless, here we required a mapping between the network and collicular space to compute landing positions relative to the target and to account for the deformation of visual stimuli on the SC (see Figure 8 in General Introduction, Appendix, for an example). The area simulated with the modelled map is inscribed in a square of 3.67 mm of the spatial representation of the SC proposed by Ottes et al. (1986). Its upper corner position was at 0.15 mm on the rostro-caudal axis and at 1.83 mm on the medio-ventral axis – respectively the U and V axis in the Ottes et al. (1986) equations. Each neuron of the model represented a square of 1340 μm^2 (36.7 x 36.7 µm) of the SCs' tissue.

When the SCs model provides a single activation cluster, it was assumed that the SCi would trigger a saccade for that locus. The amplitude and the direction of this saccade are defined by mapping the centre of gravity of the activation cluster back from collicular space to retinal space. It is assumed that the model had reached a stable state after 150 ms, thus, the centre of gravity was computed during the last 50 ms of the 200 ms simulation. If the model gave rise to none or more than one activation cluster, no saccade was estimated.

6.2.2 Visual stimuli presented to the model:

In order to get a better understanding of the spatial configurations tested in Tandonnet et al. (2012), we projected that configuration from retinal space into collicular space with the equations of Ottes et al. (1986; see also **Figure 1-8** for an illustration). The transformation from retinal space to collicular space brings several insights. Firstly, in the collicular space, the target-distractor distance is larger for the conditions at 6° of eccentricity (14 cells, i.e. around 513 µm) than for the 7.5° of eccentricity one (12 cells, i.e. around 440 µm). Hence, the Global Effect occurring between the two conditions may not have the same strength: that is consistent with what has been observed by Tandonnet et al. (2012) (see **Figure 2-7**). Secondly, the collicular size of the distractor is globally larger in the conditions at 6° of eccentricity than it is in the 7.5° of eccentricity ones. Thirdly, the collicular image of the distractors were curved. Nevertheless, the curvature was small in these conditions, thus, it is assumed that it could be ignored and we used straight distractors.

Ultimately, we did not simulate an exact replication of Tandonnet et al. (2012). To increase the resolution of our analysis, we used a denser range of distractor sizes: from 2 to 40 cells in

increments of 2. Furthermore, we tested only for a distance of 12 cells between the target and the distractor -- corresponding to the 7.5° of eccentricity condition. The patterns of the stimulation used to simulate the inputs are the same as those used for in main Chapter, except that the maximum frequency of the distractor is at 400 Hz against 500 Hz for the target. The weight of the distractor is fixed at 2000mV whereas the target weight was fixed at 6000mV. That difference in weight was chosen to simulate a discrimination of the target/distractor in favour of the target – that is constant across the distractor sizes.

6.2.3 Parameters of the model:

The model parameters were the same as in the main Chapter (with K=1.2 and β=6.0) with few changes for the purpose of the study. The standard deviation σx of the MH was selected so that it replicated qualitatively the change in GE observed in Tandonnet et al. (2012) between the two conditions varying target eccentricity (6.0° and 7.5°). In particular, the deviation from the target was smaller for the condition with the largest target-distractor distance. Such a relation allows for constraining the size of the MH. Preliminary tests on the global effect between a distractor and a target (square of 2x2 cells, differing only by their intensity) showed that the absolute deviation from the target increases with the target-distractor distance until a *critical distance*, and then it decreases with the distance (see main Chapter). Therefore, it can be deduced that target-distractor distances used by Tandonnet et al. (2012) were larger than this *critical distance*. Importantly, that *critical distance* depends on the MH standard deviation. In order to replicate qualitatively the change in GE observed by Tandonnet et al. (2012), we fixed σx = 7.5 cells. With that, the GE disappears approximately at a stimulus distance of 550µm on the SC. That extend of the GE is in line with the results of Walker et al. (1997) when they are interpreted with the Ottes et al. (1986) equation.

The parameter σy (the standard deviation σy of the Mexican hat on the Y-axis) is our only free parameter so that to cover circular to elliptic pattern of lateral connections. We varied σy from a value of 3.5 – very elliptic -- to 7.5 – perfectly circular – in increments of 0.5 cells.

6.3 Results

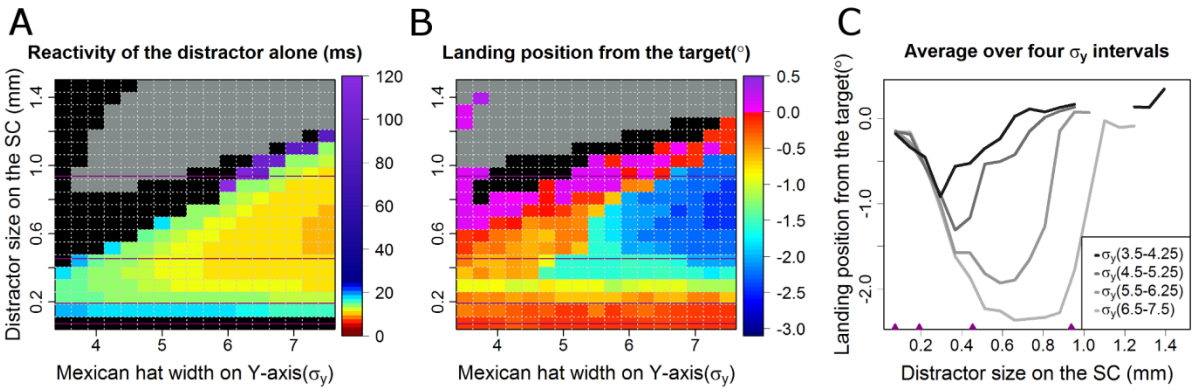

Figure 2-8: *Overview of our simulations of the global effect.* ***Subplot A:*** *Reactivity of the distractor alone: here, the time (in ms, see colour scale) for the distractor to reach threshold is measured without the target. The measure is done for the distractor sizes and the Mexican hat width (σy) tested in the main simulation (subplot B and C for the results).The black region denotes that complete auto-inhibition occurred, while grey denotes the occurrence of two late spiking clusters.* ***Subplot B:*** *Landing position from the target: estimation of eye landing positions (in °, see colour scale) for different distractor sizes and Mexican hat's width (σy). The estimation is done based on the centre of gravity of the spiking cluster during the last 50 milliseconds of simulation. A deviation of -3.0° (deep blue) means the eyes land on the distractor, while a deviation of 0° means the eyes land on the target (red). Positive values (magenta) indicate that eyes go beyond the target (hypermetria or repulsion). This overshoot was not observed in Tandonnet et al. (2012). As in subplot A, grey represents areas where more than one cluster of activation appeared on the map, while black represents areas where there is no spiking cluster.* ***Subplot C:*** *Average of landing positions curves over four Mexican hat width (σy), for comparison with* ***Figure 2-7****. Three columns of the subplot B are used to make one curve of the subplot C; except for the last interval σy (6.5-7.5) which uses 4 columns. Here the landing positions are plotted on the y-axis instead of using a colour range as in subplot B.* ***For all subplot:*** *The magenta triangle on the bottom (in C), or the magenta lines (in A and B) mark the distractor lengths used in Tandonnet et al.'s paradigm (2012).*

Figure 2-8A provides an overview of the latency of the distractor to lead to a spiking cluster (i.e., stable bump of activity) when it is presented without the target. The coloured cells show that the distractor is most reactive for some optimal size that changes according to the Mexican Hat Y-width. In particular, too large or too small distractors are less reactive; large stimuli become auto-inhibited. The black cells represents simulations where the auto-inhibition was so strong that no spiking cluster was created. Finally, grey cells indicate the simulations where the distractor led two or more spiking clusters – it was larger than the MH functional limits.

Figure 2-8B provides an overview of the GE – particularly the eye endpoint relative to the target – when both the target and distractor are presented. It can be observed that there is an obvious correlation between the GE and the distractor reactivity described in **Figure 2-8**A.

Importantly we obtained a qualitative replication of the GE reversal effect observed by Tandonnet et al. (2012) for all the values of σy that were tested (see the red to blue to red progression of the colour on each column). **Figure 2-8**C plots the results in a way that is easier to compare to the results of Tandonnet et al. (2012) – to keep that figure readable we selected only 4 representative values of σy. It appears that increases of σy (X-axis) are accompanied by an increase in the maximal deviation from the target (bluer colours) and also by an increase of the size of the distractor at which the reversal happens. Because of that it appears that the smallest values of σy lead to a better replication of the reversal observed by Tandonnet et al. (2012). Thus, when using a single layer DNF model, elliptical pattern of connections appears to be needed to describe the interactions between auto-inhibition and GE.

6.4 Conclusion

The models with the most elliptical MHs best match the behavioural data of Tandonnet et al. in the sense that their reversal phase is gradual – i.e. not abrupt. This appears to contrast with the usual assumption that lateral connections are approximately circular in collicular space.

Assuming that lateral connections are approximately circular in collicular space, this result suggests that the merging mechanism and the auto-inhibition mechanism observed in the SCs (Goldberg & Wurtz, 1972; Vokoun et al., 2014) could not explain alone the interaction between GE and auto-inhibition observed by Tandonnet et al. (2012). Instead, the GE and auto-inhibition observed by Tandonnet et al. (2012) would take place at two different functional levels. Particularly, using the DNF framework, one DNF would have a small MH to explain the auto-inhibition while the second DNF would have a larger MH to explain the GE through merging effect. One possibility is that the merging effect and the auto-inhibition happen in two different subpopulations of the SCs that have their own lateral connections. Another possibility is that the merging effect driving the GE happens on the SCi while the auto-inhibition occurs in the SCs. A last possibility is that the GE happens through a saccadic vector averaging downstream the SCi (i.e., the dynamic minivector summation, see in General Introduction) while the auto-inhibition happens in the SCs. In any case, the extent of the GE and the critical size for enabling auto-inhibition would be defined by two different mechanisms/populations.

A second provocative possibility is that both humans and monkeys actually have elliptical connection patterns in the SC. Since this has not been the focus of systematic investigation it could have escaped notice. Bozis and Moschovakis (1998) showed an elliptic shape of synapse

distribution from a single cell in the deeper layer of the squirrel monkey's SC (see *their* figure 2). The construction of such bidimensional map of SC connections is highly useful for modellers, and it would be interesting to reproduce their results in different layers and species.

7 APPENDIX B: Simulation Set 1, Generalization to 2D stimulus shapes

Our DNF-MH model of target selection map shows a phenomenon of total activity suppression related to stimulus size for 1D stimulus. Here, we generalize our observations to 2D stimuli by testing the behaviour of the model when stimulated with a circle and a rectangle of varying size. We used the reference MH (S1, K = 1.2 and β = 6.0).

Figure 2-9 shows results obtained for these tests conducted with 2D shapes. Columns 1 and 3 show average firing rate over the simulation period and columns 2 and 4 contain the spikes train of neurons on the diagonal of the map. Similar phenomena of activity suppression to those for the 1D stimulus are observed: spiking clusters did not emerge for size 18 for the square and for sizes 20-26 for the circle. Additionally for further increases of size, several clusters appear: from sizes 20 (square) and 28 (circle) four spiking clusters emerged (Note that activity for the circle segregates into 4 regions because the pixellation of our map, theoretically no point on a disk would be advantaged on a continuous competition field). Especially in the case of the circle, these clusters tend to move as if they are repulsed from the centre (lower panel of the column 4). This repulsion becomes weaker with size until a new spiking cluster emerges at the centre in addition of the four on its corners (not shown).

The spike trains (columns 2 and 4) also allow us to observe a latency increase for the appearance of clusters when increasing the size. For smaller sizes, below 18 (square) and 20 (circle), the unique cluster appears with almost no delay with respect to the onset of the stimulation. Conversely, when spikes appear for larger sizes, whether they finally disappear (size of 18 for the square or of 20-26 for the circle) or are part of stable spiking clusters (larger sizes), there is a short latency period of approximately 10 ms before their appearance. This latency increase is similar to the one observed when a 1D stimulus resulted in two clusters (see above) but of lower value: the latency increase for the 1D stimulus was around 70 ms. Finally, the first burst of spikes and the following gap (just at the beginning of the stimulation; middle and lower panels in the columns 2 and 4) can be respectively related to the initial rise of

membrane potential and to the wave of inhibition seen with 1D stimuli. These differences can be explained by the greater number of neurons interacting, which speeds and strengthens excitatory and inhibitory influence. Hence, apart from this difference in the latency, results for 2D shapes are similar to those obtained for the 1D stimulus (line).

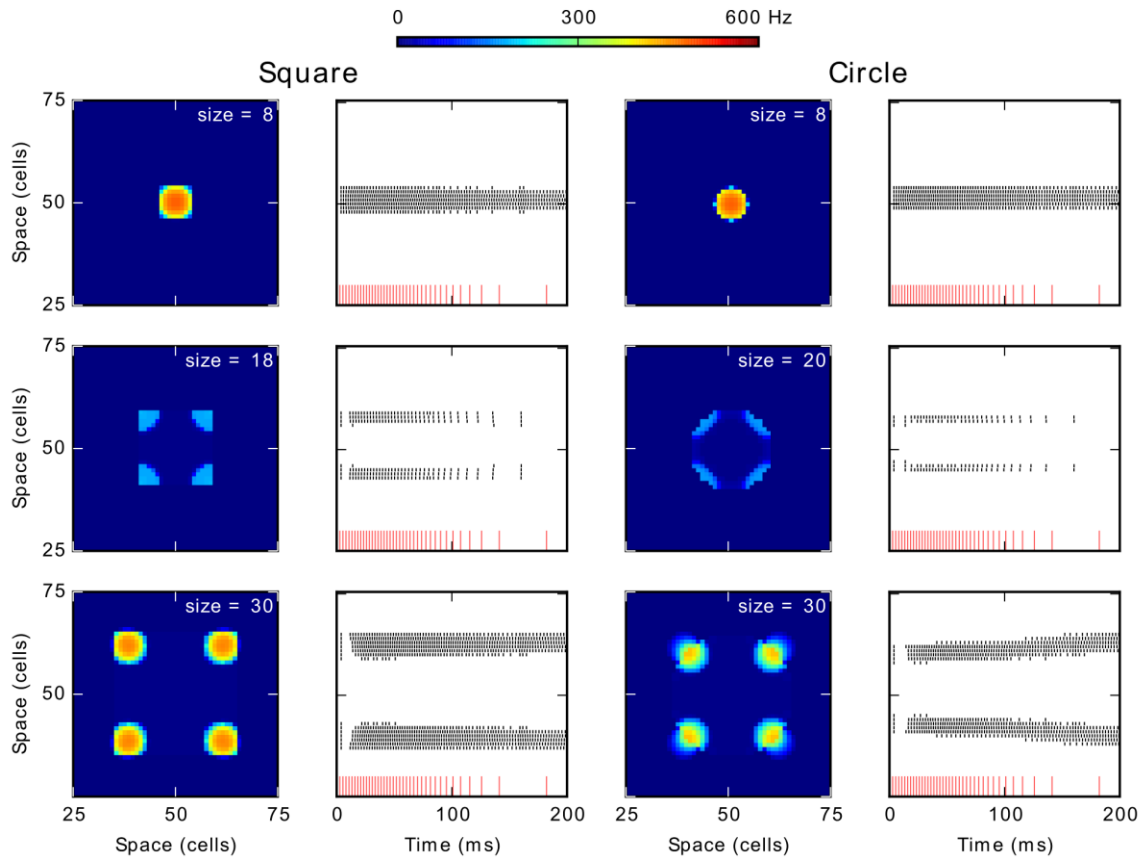

Figure 2-9: Suppression effect with a square and a circular shaped stimuli. Column 1 and 3 *show the average spike frequency (firing rate) in the neural map in hertz.* ***Column 2 and 4*** *show the spikes train of neurons according to time. The red vertical lines at the bottom represent the input spike train. The recorded neurons are those forming the diagonal of the neural field from the position (25, 25) to the position (75, 75).*

8 APPENDIX C: Simulation Set 1, Effect of Input Dynamic

To get a better view of the dynamics of inhibition and excitation, we compared these dynamics for a sustained input at 400Hz to those for the transient input with a Gaussian profile as previously used. **Figure 2-10** shows the strongest subthreshold activity near the stimulus in

these two conditions (panels A,B,C for transient input and panels D,E,F for sustained input) obtained with parameters of S3 (K = 1.2, β = 8.0). It highlights that the dynamic of the initial transient rise in membrane potential comes from a delayed wave of inhibition (Panels B, C, E and F). Indeed, the weight of excitation is twice that of inhibition, giving an initial advantage to the excitation, which the inhibition later catches up due to its larger decay time constant. Note that this wave of inhibition comes from remote units (see the MH in **Figure 2-2**) and, so, does not appear for small size (Panels A and D).

With the sustained input, we still observe a second rise in the membrane potential; the inhibition curve still decreases after having overtaken the excitation. As our recording takes place toward the extremities of the stimulus -- near the potential winner loci -- this decrease of inhibition thus comes from the decrease of activity of the middle of the stimulus (see **Figure 2-3**B size 42, and **Figure 2-3**C size 30, 38) silently losing the competition at sub-threshold level.

For a stimulus size of 36, no spike cluster is observed in this sustained input condition as opposed to the transient stimulus condition (**Figure 2-10**C, F). As mentioned above, the second membrane potential rise is weaker when using the sustained stimulation. Counter-intuitively, this suggests that to decrease or to stop the stimulation input --with the transient stimulation-- helped the membrane potential to reach the threshold. Two possible explanations are that 1) as the neurons are excitatory coupled, the most excited regions of the stimuli self-sustain their firing longer than the others when our input stops, and 2) the most inhibited regions lose their only source of excitation when our input stops. To then stop or decrease the input signal can accentuate disequilibrium in the competition and facilitate a target selection outcome.

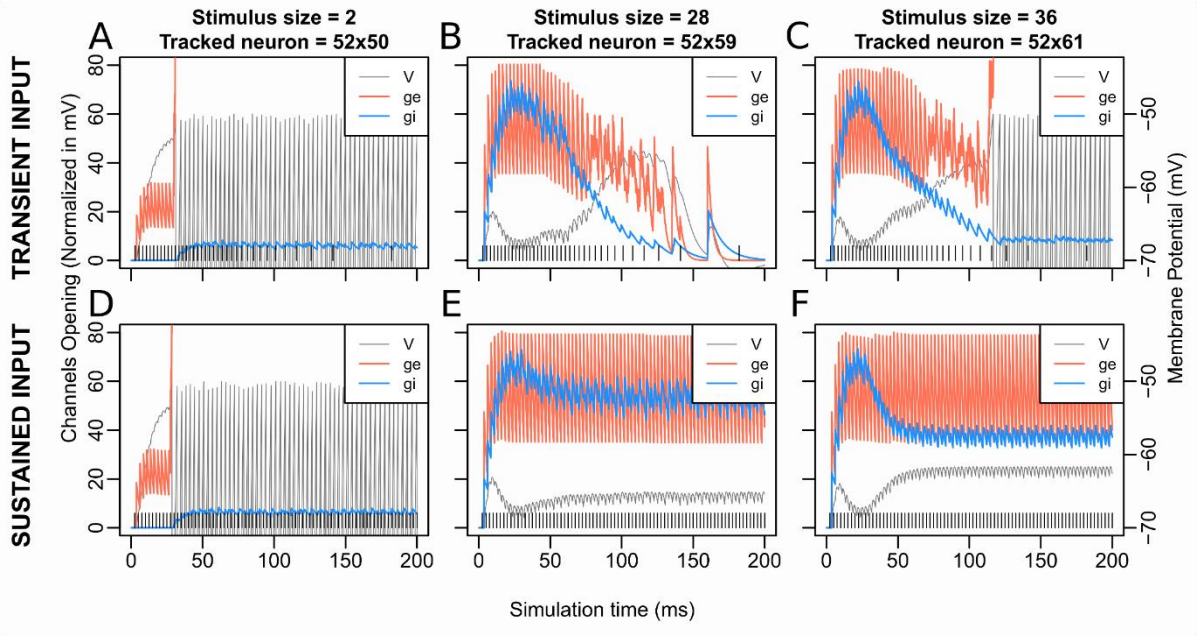

Figure 2-10: Excitatory and inhibitory channels opening and membrane potential according to time for transient stimulation (upper graphs) and sustained stimulation (lower graphs). *Data from SA3 (K=1.2, β=8.0) are shown here; similar curves can be obtained from the other conditions. The transient input (A,B,C) is the one used in the previous simulations and corresponds to a Gaussian (see F_s in Inputs and Methodology). The sustained input (D,E,F) set F_s = 400 Hz, e.g. the firing rate of the input stimulation is at 400 Hz and constant over the time. The vertical lines at the bottom represent the input spike train. The tracked neurons all come from the row at 2 cells from the stimulated neurons (x=52). At each time point, the following measures are extracted from the neuron that has the maximum membrane potential among the tracked neurons. The curve "V" is the evolution of the membrane potential over the time. "ge" or "gi" describe the evolution of, respectively, the number of excitatory or inhibitory opened channels on the neuron's membrane. However, for the sake of comparison, the number of opened channels ge and gi are multiplied by a scaling factor. Indeed, for any value of V: |Ee-V| > |Ei-V| where Ei and Ee are, respectively, the inhibition and the excitation equilibrium. Thus, an excitatory gate that opens always has more effect on V than an inhibitory gate. The scaling factors represent this difference by being* $\left|E_e - \acute{V}\right|$ *for ge and* $\left|E_i - \acute{V}\right|$ *for gi, with* $\acute{V} = (V_t - V_0)/2$.

Chapter Three: Deviation away from a previously fixated location

Evidence for a spatiotopic excitatory top-down signal?

Abstract:

When a decision is driving a saccadic eye movement, traces of the decision process can be inferred from the movement trajectory. This opens a small window on the interactions of endogenous and exogenous signals, which have been at play. For eye movement, the primary site for those interactions is normally assumed to be the superior colliculus (SC). For example, saccade curvature away from distractor stimuli was assumed to originate from a cortical distractor inhibition biasing activity on the SC. Recent neurophysiological work does not support this theory, and modellers have sought alternative explanations at a lower level: SC lateral inhibition or even brainstem execution machinery. The SC and brainstem are using a retinotopic representation of visual stimuli, thus these low level models could not explain saccadic deviation from a spatiotopic signal. We suggested that double-saccade paradigms can be used to distinguish whether a signal is retinotopic or spatiotopic, and help elucidating its origin. Here, we tested whether an initial fixation stimulus for one saccade creates deviation away in a second saccade in a spatiotopic manner. Our results favour such a spatiotopic effect and thus suggest that models considering only the SC and brainstem are not sufficient to explain saccadic deviation. We discuss the updates that each model would need to explain our results. In particular, we propose that they receive an excitatory and spatiotopic update, which, through a review of the previous literature, we identified as coming from the Lateral Intraparietal region (LIP).

1 Introduction

1.1 Using Saccade Curvatures to understand Decision Making mechanisms

In Chapter 2 we studied the interaction of retinotopic signals in the visuo-oculomotor pathway by means of a model of the SCs. Adopting a complete change of perspective, in the present Chapter we will detect the presence of retinotopic and spatiotopic signals in the visuo-oculomotor pathway by measuring the motor responses of human participants.

The selection of where-to-look-next embodies a complex decision-making process. As seen in the General Introduction, this process is based on the modulation and competition between exogenous stimuli (i.e. external events or processes relayed by sensory structures) and endogenous stimuli (i.e. internal events or processes relayed by cognitive structures). The study of saccade trajectories has suggested that the execution of the saccade can start before the selection of a single goal – from multiple endogenous and exogenous inputs - is completed (McPeek et al., 2003). Therefore, a trace of interaction between endogenous and exogenous stimuli can be deduced from saccade trajectories, making these valuable tools for understanding the decision-making dynamics in biological systems and for addressing how individuals and special populations differ in terms of modulating exogenous and endogenous stimuli.

However, it may be sometimes difficult to infer whether a signal has endogenous or exogenous origins from observing only the curvature it generated on a saccade. We propose in our study that a two-saccade paradigm can be used as an additional tool to distinguish if a signal is coded in a spatiotopic frame or a retinotopic frame. From this distinction, we can then identify the origin of the signal. We will particularly focus on the origin of the signal coding fixated stimulus.

1.2 Origin of Saccade Curvatures

The decision-making involved in where-to-look-next takes place on bi-dimensional neural maps that spatially code the position of the loci of interest. A good example is the Superior Colliculus (SC, see intro). Its intermediate layer represents the last action selection map before saccade execution. Importantly, it receives exogenous inputs – from the retina and V1 -- and endogenous inputs – from the Frontal and Parietal cortex. These inputs compete and are

selected by means of an accumulation-to-threshold system (Jantz et al., 2013) and an inhibitory system (Munoz & Istvan, 1998).

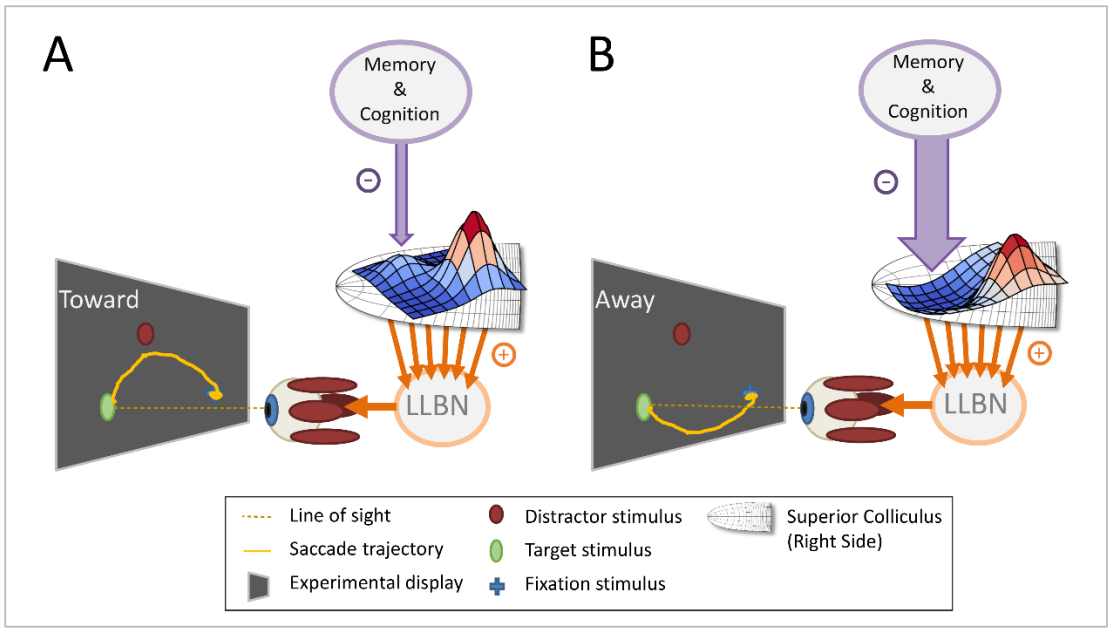

Figure 3-1: Diagrams displaying the classical model of saccade trajectory curvatures toward or away from a distractor *(see also McSorley, Haggard, & Walker, 2004, Figure 7.a). At saccade initiation, all the activity on the colliculus is taken into account by the Long-Lead-Burst Neurons (LLBN) to define the saccade direction: if there is a bump of activity on the distractor side, the saccade will deviate towards it; if there is an inhibition of activity on the distractor side, the saccade will deviate away from it. Target and Distractors indistinguishably ignite an exogenous and excitatory signal in the SC, which is believed to be a top down inhibition from memory and cognition structures that make deviation away possible (this in the frame of the classic theory – see the discussion for other models). Finally, note that whilst the correction of the trajectory is not addressed in this chapter, it is thought to be conducted by external structures such as the cerebellum (Quaia et al., 1999).*

When performing a saccade to a visual target, you may need to ignore one or multiple other goal-irrelevant stimuli -- i.e. distractors. Note that the target and the distractors represent excitatory exogenous signals for the SC. Furthermore, when a saccade to the target is triggered, the brainstem burst generator takes into account the activity of all the SC in order to create a velocity signal relevant for each of the extra-ocular muscles (see General Introduction). Thus, the trajectory of a saccade going to the target could either curve or deviate towards a distractor if its excitatory signal is still present in the SC during the saccade execution (see **Figure 3-1**A). And indeed, saccades deviating toward a distractor are accompanied by an activity corresponding to the distractor locus on the Superior Colliculus (SC) or on the Frontal Eye Field

(FEF) maps within an interval of -30 to 0 ms before the saccade (see McPeek, 2006 and McPeek et al., 2003).

When the saccade trajectory deviates – or curves – away from a distractor, a top-down inhibition process is considered (see **Figure 3-1**B): an endogenous and inhibitory signal would be acting on the SC from higher cognitive structures (McSorley et al., 2004). In support of this theory, neurophysiological studies have reported saccade curvature away from a deactivated SC locus (Aizawa & Wurtz, 1998; Quaia & Optican, 1998). Furthermore, Van der Stigchel (2010), in his literature review, reports 3 arguments in favour of a top-down action on the SC from behavioural studies: 1) prior knowledge of the target location can cause deviations away from a distractor (R. Walker, McSorley, & Haggard, 2006), 2) the difficulty in target/distractor discrimination can modulate the deviation away (Ludwig & Gilchrist, 2003), and 3) when using random dot kinematograms to cue the next target location, the difficulty of the perceptual decision (are dots moving left or right?) can modulate the deviation, that is, when the discrimination is easy the deviation away is stronger (McSorley & McCloy, 2009). Although 3) may be equivalent to 2), a fourth argument can be added: 4) the occurrences and the strength of deviations away from a distractor increase with saccade latency (Hermens, Sumner, & Walker, 2010, fig. 5; McSorley, 2006). This could be due to a slow and delayed top-down influence: it is often assumed that top-down pathways are slower than bottom-up pathways because they provide more refined information. Note that the spatial configuration of the distractor, target, and fixation stimuli also affects the deviation (McSorley, Haggard, & Walker, 2009; Van der Stigchel, Meeter, & Theeuwes, 2007), but this cannot be attributed specifically to a top-down inhibition mechanism.

1.3 Recent Debates Have Given Rise to New Retinotopic Models of Curvature Away

Although behavioural studies appear to support the top-down inhibition hypothesis, a recent neurophysiological result obtained by White, Theeuwes, and Munoz (2012) has challenged this account. In this experiment, monkeys were required to perform a simple saccadic task. In particular, for each trial, the monkey had to stare at a fixation cross, whereupon a paired target and distractor appeared (with or without an onset asynchrony). The monkey was trained to make a saccade to the target as soon as it appeared whilst ignoring any distractor. In trials with onset asynchrony, they expected to observe – during the interval where the distractor was

displayed alone – the trace of top-down inhibition at the distractor loci. Contrary to these expectations, no trace of inhibition was observed in the SC.

Since this study, models have been published to explain some or all the 4 behavioural points listed above with an alternative mechanism to top-down inhibition. These could be at the level of the SC, based on its local lateral interactions (Z. Wang et al., 2012; Z. Wang & Theeuwes, 2014) or below the SC, based on neural short term depression in the brainstem burst generator driving the eye muscles (Kruijne, Van der Stigchel, & Meeter, 2014). The latter authors present the top-down inhibition as "*more or less as a deus ex machina, called upon to explain deviation away when it occurs, yet remaining unexplained itself"* (Kruijne et al., 2014, p. 260). Note that those two models are based on structures that work with retinotopic coding (relative to the retina centre or current eye position).

1.4 Using Previous Fixation Spatiotopy to Test the Recent Models

The model of Wang and Theeuwes (2014), based on the assumed lateral connections in the SC, predicts an effect of the fixation point (the stimulus on which the participant has to fixate before the target and distractor appear) on the strength of the deviation away from the distractor. In particular, they expected the deviation to increase when the duration of the fixation stimulus was increased. They demonstrated the predicted effect and conclude that it is supportive of a SC origin of the deviation away phenomena.

However, their conclusion linking the fixation effect they observed to the SC may be somewhat premature. The SC is a retinotopic structure, and their experiment did not address the issue of whether the fixation effect is coded in a spatiotopic frame or a retinotopic frame. Unlike the latter, the former frame is unaffected by eye movements, and single saccade paradigms cannot distinguish these two frames[10]. Note that a spatiotopic frame would *also* be in contradiction with the model developed by Kruijne et al. (2014), as the brainstem burst generator is coding eye movements in retinotopic coordinates. Thus, our study proposes to test both models by

[10] The centre of the coordinate system of a retinotopic frame is anchored to the retina. Thus, the position of an object in that frame is affected by eye movements. On the other hand, spatiotopic frames have a centre of coordinate system which is anchored to something else than the eyes (head, navel, ground for instance), and thus they are unaffected by eye movements. In order to distinguish in which frame a stimulus is coded, two saccades are needed. A first saccade is made after the stimulus presentation so that the memory trace of that stimulus will either move with the visual field shift (retinopic frame) or not (spatiotopic frame). Here it is important to note that the trace will be at a *different* position in the visual field depending on the frame in which it is coded. Then, when a second saccade is made, its curvature is measured in order to deduce the location of the trace of the stimulus and reveal its frame.

introducing a two-saccade paradigm that addresses the question of spatial frames. Jonikaitis and Belopolsky (2014) have recently used a two-saccade paradigm to find evidence for deviation away from the spatiotopic representation of a *distractor*. However, as we will see in the discussion (Section 5.2), their results may be due to the interaction of two retinotopic mechanisms. Furthermore, our work extends that of Jonikaitis and Belopolsky (2014) by assessing deviations away from the spatiotopic representation of a *previously fixated stimulus* – as opposed to a distractor. Finally, we open up an in-depth discussion on the modifications needed for the models of both Kruijne et al. (2014) and Wang et al. (2012; 2014) to explain our results and spatiotopic deviations.

Previous studies concerned with free viewing or visual search (Bays & Husain, 2012; Klein & MacInnes, 1999; Smith & Henderson, 2011, 2011; Sogo & Takeda, 2006) have shown that previous fixation zones may be memorized and affect future saccade plans – the most famous effect being the inhibition of return (Posner & Cohen, 1984; Sumner, 2006). Specifically, the work of Sogo and Takeda (2006) demonstrates that saccades tend to deviate away from previous fixation zones and suggest an effect of the 3 last fixation zones. This would support a spatiotopic effect of previous fixation on the current saccade. However, in this free viewing experiment, it is unclear whether the deviation is caused by the fixation representation or simply by the residual activation of previous saccades. Indeed, it has been shown that previous saccades can allow for residual activity in the motor map, which is *retinotopic*, and affect future saccade plans (A. J. Anderson, Yadav, & Carpenter, 2008; Z. Wang, Satel, Trappenberg, & Klein, 2011). This residual activity is also related to the well-known companion of inhibition of return: the saccadic momentum (Klein & MacInnes, 1999; Smith & Henderson, 2009, 2011). The effect of a residual activity of the previous saccade on the current saccade would be simple: it would curve the current saccade away from the previous fixation because the vector of the previous saccade was logically pointing away from that previous fixation.

Our present work proposes to demonstrate the presence of a deviation away from the spatiotopic representation of a previously fixated stimulus, while controlling for residual activity. Because we are using an original two-saccade paradigm, our demonstration is composed of the following two steps: Experiment 1 shows that deviation away from the previous fixation location can be obtained on the second saccade, whilst Experiment 2 answers the afore-mentioned question. In particular, it yields evidence for the notion that the second saccade's deviation is caused partly by the spatiotopic representation of the previous fixation stimulus, and partly by residual activity of previous saccades. This evidence then joins the

recent findings of Jonikaitis and Belopolsky (2014) on target-distractor competition (see discussion for more details) to support a spatiotopic frame for deviation away phenomena. We finally discuss how the models of Wang et al. (2012; 2014) and Kruijne et al. (2014) could be updated. We suggest primarily that an excitatory spatiotopic influence from the Lateral Intraparietal region could serve as a satisfactory addition to both models.

2 General Method

As mentioned at the end of the introduction, our work consists of two experiments (Experiments 1 and 2). We will describe here the method, which was employed in all of them, though more specific details will be given in separate sections dedicated to each experiment (sections 3.1, 4.1).

2.1 Nomenclature

In the following text, the coordinates on the screen are given in polar coordinates as (eccentricity; direction) degrees. When not specified, the origin of the coordinate system is the centre of the screen, although some coordinates may be given relative to another stimulus (eccentricity; direction; stimulus name). The X-axis is always pointing right and the Y-axis pointing down, such that the points with a null direction angle are on the right side and points with a positive direction angle are on the bottom side (see **Figure 3-2**A).

The expressions F, S_1 and S_2 refer to the Fixation Cross, Stimulus 1 and Stimulus 2, respectively. Saccade 1 and Saccade 2 will refer to the first saccade of the participant that aims toward S_1 – and S_2 – respectively. Finally, G_1 refers to the optional temporal gap between F and S_1.

Note that in the present study, onset/offset are synonyms of start/end or appearance/disappearance. In our analysis, five different time durations will be frequently used: ΔGap, the gap between Fixation offset and S1 onset; ΔS1, the duration of S1 presentation; ΔFromFix.1, the time passed since Fixation offset when Saccade 1 ends; ΔFromFix.2, the time passed since Fixation offset when Saccade 2 starts; ΔInterSacc., the duration between Saccade 1 offset and Saccade 2 onset (see **Figure 3-2**B, C).

Note the following relationship:

$$\Delta FromFix.2 = \Delta FromFix.1 + \Delta InterSacc.$$

Figure 3-2 gives a visual summary of the protocol events, along with the five durations mentioned previously. Details of the protocol are described below.

2.2 Procedure

The procedural set-up of the next three experiments will follow the same pattern of events as that described in **Figure 3-2**B. In all the experiments, there are three types of trials: control trials, single stimulus trials, and double stimuli trials, which will be described below. The control trials were present in case we needed a reference to compute the curvature of saccades. The single stimulus trials where used to prevent the participant anticipating a second saccade. For each experiment (unless otherwise specified) a participant would complete two experimental sessions of approximately 1 hour, separated by at least one night. Each session consisted of setting the chair and chin-rest for the participant to sit comfortably; a 13-point calibration of the Eyelink 2000 Eye tracker; 160 control trials; 640 trials mixing randomly single-stimulus and double-stimuli trials. A break was suggested to the participant at every 200 trials, and a re-calibration was conducted every 400 trials.

For single and double stimuli trials, the participant was required to fixate a "+" fixation cross F of size 0.2° on the screen. The fixation cross F could appear at the position (r_F; 0°) or (r_F; 180°); respectively, which we refer to as F_R and F_L. Note that r_F is a placeholder. The participant was asked to look at F and press the space bar of the keyboard placed in front of him to confirm that he is fixating and ready to start the trial. The space bar press triggers a timer and F disappears at a random time picked up from a uniform distribution $U(500\ ms, 1100\ ms)$. According to the experimental details listed below, a gap G_1 where no stimuli are drawn on the screen can occur. In both single stimulus and double stimuli trials, this optional gap G_1 was followed by the presentation of a circular stimulus S_1, of size 0.4° , at position (r_S; 90°) or (r_S; -90°) (i.e. S_1 was on the vertical central axis of the screen, either on the top or bottom part of the screen). In the double stimuli trials, the presentation of S_1 was followed directly with the presentation of S_2 which will be the vertical mirror image of S_1 -- i.e., if S_1 is at (r_s; -90°), S_2 will be at (r_s; 90°); S_2 shape is identical to S_1. The participant was instructed to move his/her eyes onto the stimuli which appear on the screen in order of appearance. Once the sequence of stimuli is completed, a new trial began.

With respect to the control trials, these were similar to the single stimulus trials, except that F and S_1 were shifted to the vertical line at the centre of the screen while F was specifically placed at the mirror position of S_1. This condition collects a set of vertical saccades, the amplitude of which is similar to those made from S_1 to S_2 in the double stimuli trials.

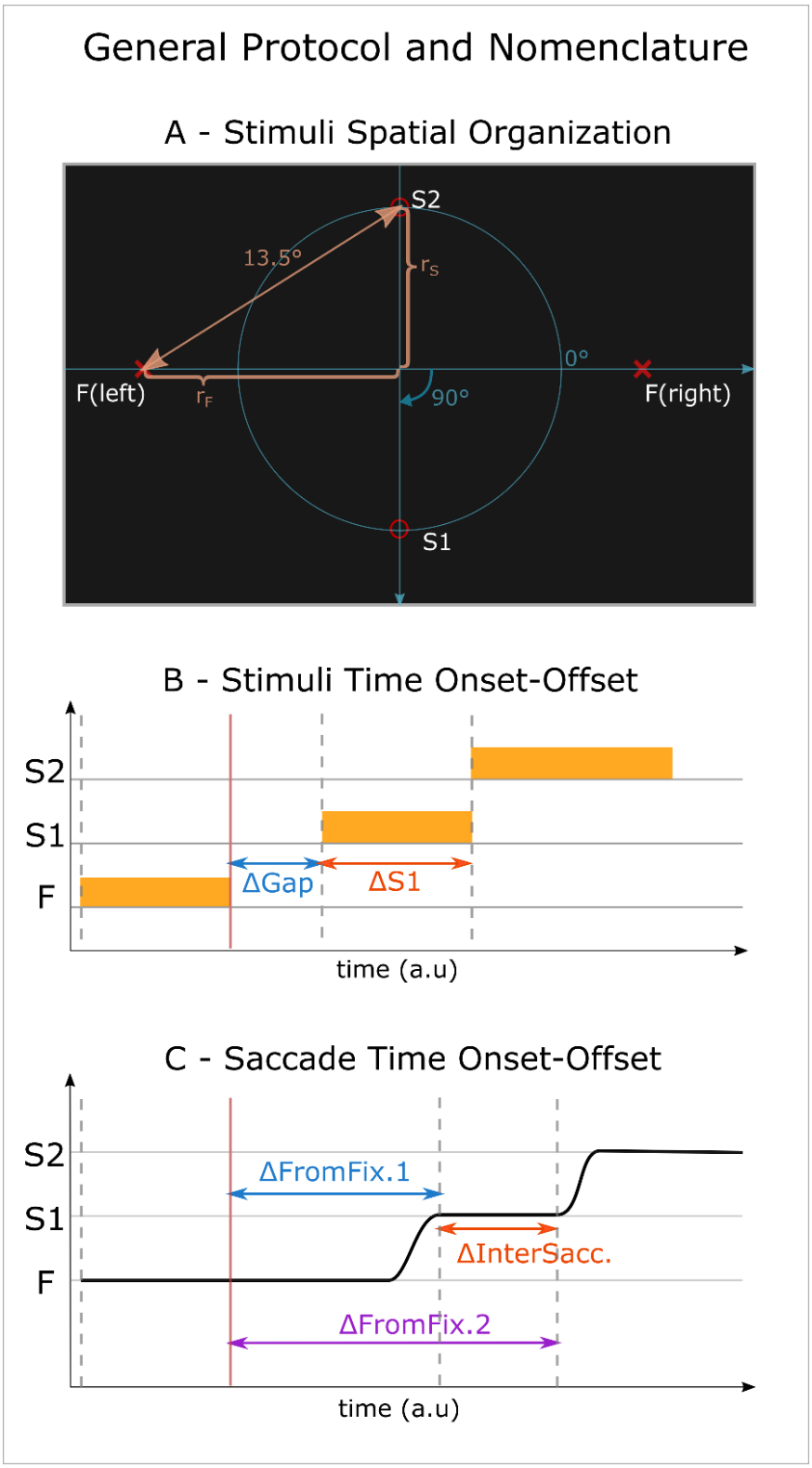

Figure 3-2: Description and Nomination of the Different Critical Time Spans Present in the Experiment *(see details in the main text). Note that in subplot A, only the red lines are visible to the participants.*

A final thing to consider for the further sections is that S_1 and S_2 are always at 13.5° from fixation F. From now on, we will report S_1 and S_2 positions relative to F_L as (13.5°; D_S; F_L) instead of reporting r_S and r_F. **Figure 3-2**.A helps to quickly understand the configuration of the stimuli. The experiments were programmed using python with the library *pygame* (more information at http://www.pygame.org/wiki/about) and the library *pylink* provided by SR research. The code source of Experiment 2 can be found at:

https://github.com/Nodragem/SuppData-EyeTrackingExp-Sources.

2.3 Data Cleaning and Extraction

The EDF files obtained from one experimental session with the Eyelink eye tracker were translated into tables and gathered in a HDF5 file for rapid and easy access with python. Reading and plotting of the data were primarily carried out by using 3 python libraries: *matplotlib, pandas*, *numpy* (respectively, refer to: Hunter, 2007; McKinney, 2010; Walt et al., 2011).

A home-made program opened the tables for each session and detected the saccades for each trial. A saccade is detected and marked if:

- the acceleration is greater than 6,000 °.s^{-2},
- the absolute velocity of the eye is superior to 10°.s^{-1},
- the amplitude of the detected saccade is superior to 5.4°.

A trial is suspected for rejection by the program if it complies with at least one of the following points:

1. no saccade or fixation marks have been found,
2. the number of detected saccades does not match with the expected number of saccades on that type of trial,
3. the reaction time or one (or more) of the intersaccadic times is too short or negative (inferior to 80 ms),
4. at least one of the saccade durations is longer than 150 ms,
5. at least one of the saccades contains positions outside the screen or missing data,
6. the last detected saccade has no end.

Following this, the trajectories of all trials were plotted (x and y against time). In this procedure, the experimenter checks all trials, one by one, to confirm the selection made by the

program. Most of the trials suspected by the program were then rejected. The reason for not rejecting some of them could be because points 4 and 5 were too strict. With respect to point 4, an oscillation artefact at the end of a saccade could lengthen its duration without affecting its initial trajectory, where we measure the deviation. Further discussion of this type of artefact can be found in Nyström, Hooge, and Holmqvist (2013). In relation to point 5, a saccade could be usable even with a small missing data gap. Finally, some trials have been rejected in addition to those suspected by the program. One reason is that a saccade inferior to 5.4° of amplitude could be made inappropriately by the participant and would not be detected by the program.

The percentage of rejected *trials* will be reported for each experiment separately.

All sources are available at: https://github.com/Nodragem/Eyetracking-Analysis-tools.

2.4 General Deviation measure

To measure the deviation, we extracted the saccade of interest from each of the analysed trials. We computed the distance of the trajectory points from a straight line drawn between the start and the end point of the saccade. A negative deviation corresponds to a deviation on the left of the straight line. This deviation from the straight line is given as a function of time in visual degrees (see **Figure 3-3**): the time course is aligned on the start of the saccade and we take the deviation at 20 milliseconds to be the initial deviation.

Note that usual measures of saccadic deviation/curvature do not consider the deviation over time, but over space. Given the fact that we are searching for an effect that is assumed to be a function of time and which may only affect the start of the saccade, we considered it judicious to 1) consider the deviation over time, 2) align our data on the saccade onset and 3) measure the deviation at a fixed and early time from that saccade onset (at 20 ms).

Finally, in Experiment 2, we used the distance in deviation between F_L and F_R conditions respectively when the Fixation is on the left or on the right. For instance, if the deviation in F_L is -3° in average and it is 4.5° in F_R , the distance is 7.5°. We call this measure the Distance in Initial Deviation (IDD_{LR}, see **Figure 3-4** for an example) and we used it to examine whether the amplitude of deviations decreased in both Fixation conditions.

It is important to note that, as we always compared the conditions F_L and F_R with each other, it was not necessary to use the vertical saccade controls.

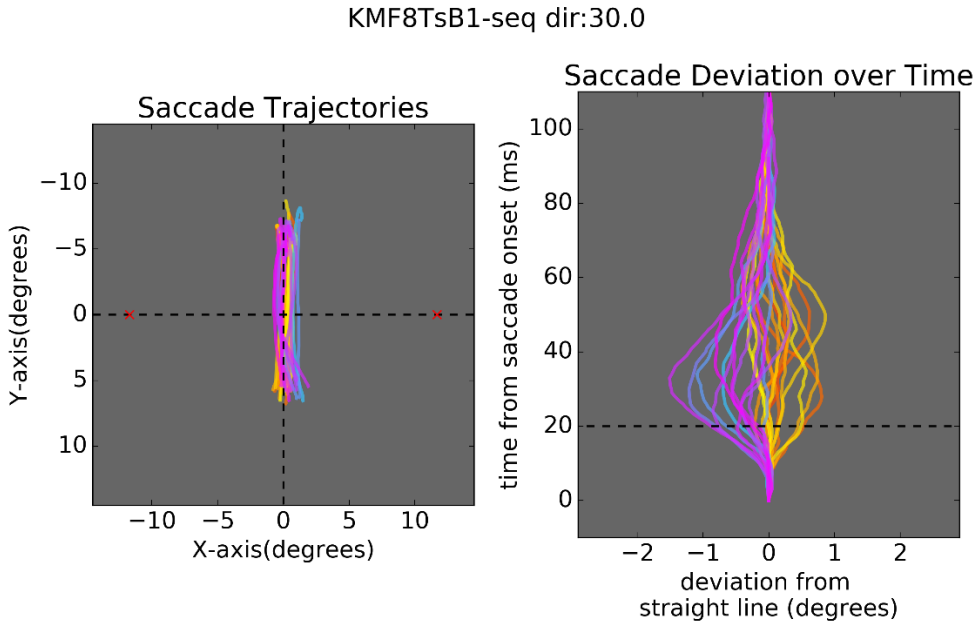

Figure 3-3: Deviation measure. *The plots are based on a saccade sample from participant KM in Experiment 1.* ***Left Subplot,*** *the second saccade of the double-stimuli condition has been extracted and plotted over space.* ***Right Subplot,*** *the distance from the straight line - was computed for each of the saccades. Negative values are on the left of the straight line while positive values correspond to the right. The initial deviation to be reported in the following sections corresponds to the intersection with the vertical dash line drawn at 20 ms.*

2.5 Statistical Methods

We chose mainly to employ the Bayes Factor framework for analysis of our data. One reason is that classical tests cannot test for an *absence* of an effect. In the pilot experiment (Experiment 1), we were *a priori* interested in quantifying the evidence for an *absence* of an effect on the initial deviation, since results of this sort would lead us to discontinue the study. Similarly in Experiment 2, the selection of one hypothesis (more details in section 4.1) over another may be based on the *absence* of an effect. Another reason of using Bayes analysis is that all the data points of the participants (80 measures per conditions per participants) can have a weight on the analysis. This allows us to quantify effects at the intra-subject level. This is particularly relevant for a pilot experiment such as Experiment 1, which included few participants. In Experiment 2, we collapsed the data to their mean (1 mean per condition per participant) in order to have a straight comparison with a Classical Method, but also because the independent variable is the difference of curvature between two conditions (see IDD_{LR} in the previous section).

We employed the R package *BayesFactor* (see Rouder & Morey, 2012 for more details on Bayes Factors for regression model selection; Rouder, Morey, Speckman, & Province, 2012 for more details on Bayes Factors for ANOVA designs). Our interpretation of the Bayes Factor (BF) testing a model 0 against a model 1 (BF_{01}) was in accord with the scale proposed by Raftery (1995, Table 6). This table is displayed below (**Table 1**).

Table 1: *Interpretation of the Bayes Factor in Terms of Evidence.*

Bayes Factor BF_{01}	Pr(H_0|Data)	Evidence
1-3	.50-.75	Weak
3-20	.75-.95	Positive
20-150	.95-.99	Strong
>150	>.99	Very Strong

We will nevertheless present a classical two-way analysis of variance (ANOVA) for the main results of our work in Experiment 2, in order to confirm that the outcome of both analyses corroborate our conclusions. We used the statistical software R, specifically the function ezANOVA() from the *ez* package, which is specialized in within-subject design (http://cran.r-project.org/web/packages/ez/index.html).

3 Experiment 1

3.1 Aims and Procedural Details

In this pilot experiment, we were testing whether (and to what extent) we can detect a deviation away from the fixation on the second saccade (Saccade 2) in double-stimuli trials. We anticipated that the effect would be observable at the single subject level due to both the relatively simple mechanisms thought to be at play and the simplicity of the paradigm. We ran only 4 participants for one session of 800 trials each – i.e. 320 double-stimuli trials per participant. The Dependent Variable was the initial deviation measured, as described in Figure 2. Our Independent Variables were merely 1) the side of the fixation stimulus (Left or Right) at the beginning of the trial in order to assess our main point; and 2) the distance between S1 and S2 (30 and 60 directional degrees) in order to guide our choice of distance for the next experiment. The gap duration between F and S1 (ΔGap) was equal to zero. The duration of S_1

(ΔS_1) was equal to 500 ms in single-stimulus trials and distributed between 250 ms and 450 ms during double-stimuli trials (see Figure 1.B).

3.2 Results

The mean rate of rejected trials across participants was approximately 2.7 %. A graphical summary of the data can be found in **Figure 3-4**; it also illustrates the Distance in Initial Deviation (IDD) between the conditions F_L and F_R.

Inspection of **Figure 3-4** reveals that the second saccade features a clear deviation away from the initial fixation position. For instance, the 95% confidence intervals for the saccade deviation at 20ms from saccade onset (see insets of **Figure 3-4**) shows that the deviations are significantly more rightward when the fixation is on the left (see red bars in both insets). Reciprocally, the deviations are significantly more leftward when the fixation is on the right (see blue bars in both insets). Note also that the deviations are greater for the distance of 60 degrees between S1 and S2. These impressions of the data are confirmed by the Bayes Factor analysis -- the model that considers an interaction between S1-S2 Distance and Fixation side is classed as the best model. The pre-eminence of the interaction model is unambiguous as it has a BF of $612.16 \pm 3.74\%$ when tested against the second best model which considers a main effect of Fixation side (BF > 150 corresponds to *very strong evidence*, see **Table 1**).

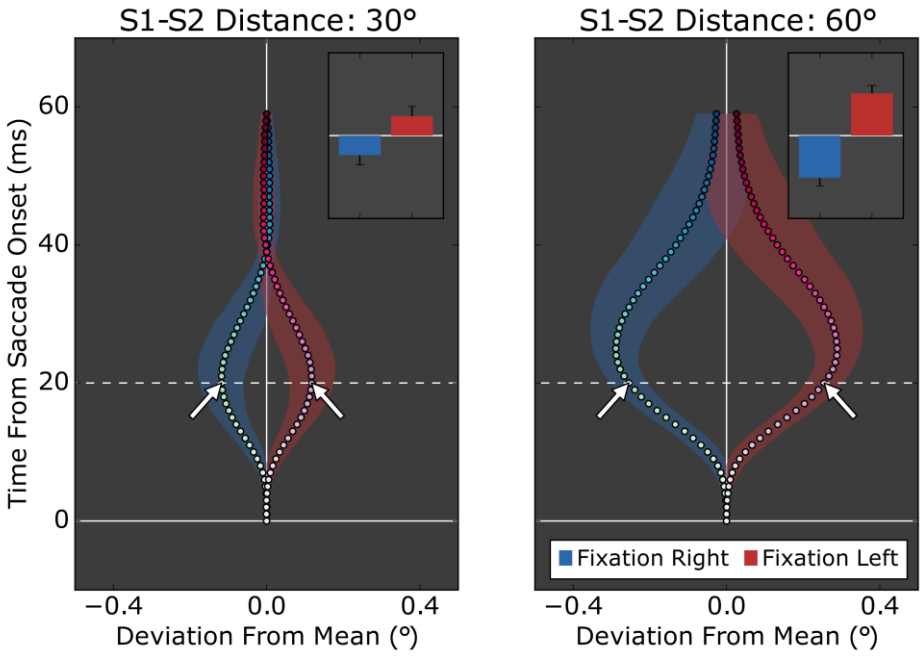

Figure 3-4: Average Saccade Curvatures due to Fixation Side across all participants according to Fixation side (Left or Right) and Stimulus Distances (30° and 60°). *The dotted curves represent the average saccade curvatures. The saccade curvature of each participant has been centred on the average trajectory of the participants for each stimulus distance in order to highlight only the effect of the Fixation Side – and so its clear interaction with Stimulus Distance.* ***Insets:*** *The initial deviations at 20 ms, indicated with white arrows in the main plots, are represented as a bar plot. The error bars and error contours denote the confidence interval at 95% with a within-subject correction (Cousineau, 2005) based on 80 data points per participant in each condition.*

4 Experiment 2

4.1 Aims and Procedural Details

The aim of this experiment was to finally specify the mechanism underlying the curvature of the second saccade -- deviating away from the previous fixation. As a reminder, two mechanisms have been suggested: **Hypothesis 1**, it is a memorized and spatiotopic image of F which causes the deviation; **Hypothesis 2**, it is residual activity from Saccade 1 which deviates Saccade 2 away from F.

Hypothesis 1 can be tested by varying the time from Fixation offset when Saccade 2 starts (ΔFromFix.2), whilst **Hypothesis 2** can be tested by varying the intersaccadic duration (ΔInterSacc.). On one hand, varying the duration of S1 (i.e. *ΔS1)* could be used as a proxy to vary *ΔInterSacc.* but it would also vary *ΔFromFix.2* (*ΔFromFix.2 = ΔFromFix.1 + ΔInterSacc.*, see

Figure 2C). Thus, varying the duration of S1 alone is not sufficient to differentiate **Hypothesis 1** from **Hypothesis 2**. On the other hand, the creation of a gap between F and S_1 (named Gap, see Figure 2C) can be used as a proxy to vary ΔFromFix.2 without varying ΔInterSacc. In particular, the duration of this gap (i.e. ΔGap) would be a proxy to vary ΔFromFix.1. Consequently, varying ΔGap is a good way to specifically address **Hypothesis 1**, but it would not address **Hypothesis 2**.

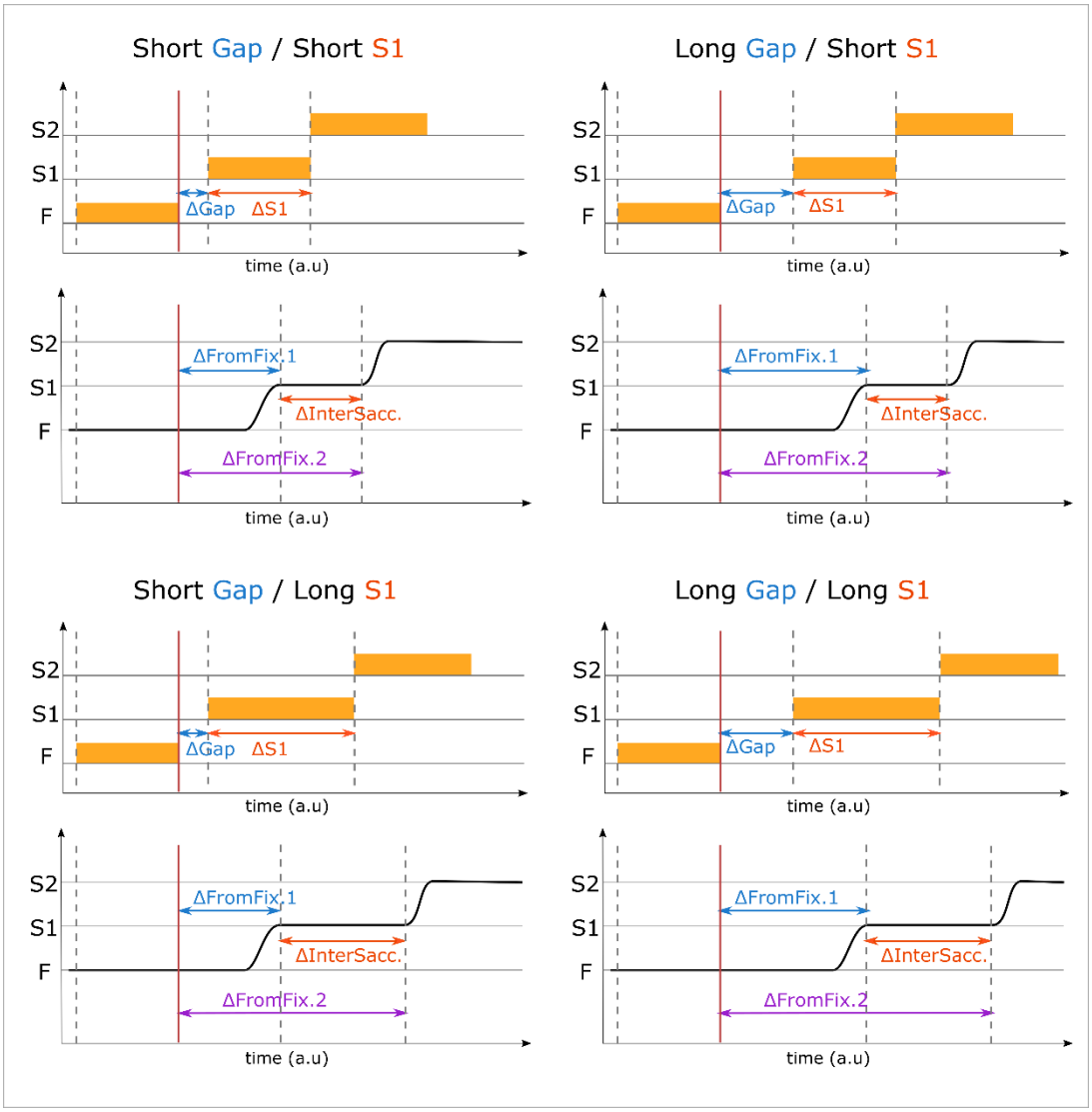

Figure 3-5: Summary of the Various Conditions of the Paradigm. *Note that for the sake of simplicity we represent the average timing: the randomness in timing is detailed below. The distance S_1S_2 was of 60 directional degrees. For* short S1 *trials, ΔS1 is randomly taken from a uniform distribution between 250 ms and 450 ms, while for* long S1 *trials it was taken between 550 ms and 750 ms. For* short Gap *trials, ΔGap is randomly selected from a uniform distribution between 0 ms to 200 ms while for* long Gap *trials, ΔGap is picked between 300 ms to 500 ms. Note the equality of variation used for ΔGap and ΔS1. We mixed all the conditions in a random and balanced way. Each participant was tested in two experimental sessions.*

In order to concurrently address both hypotheses, we propose the following. First, we assume that *Saccade 1* and *Saccade 2* durations and the reaction time of the participants to S1 and S2 presentations will be sufficiently constant over the conditions (i.e. same distribution). Second, we assume that both the Fixation representation and the residual activity are transient and so their effects on *Saccade 2* decrease over time. On the basis of these assumptions, a change of 200 ms – for instance – in ΔGap would create a change of 200 ms in ΔFromFix.1; a relationship which would also be held between changes in ΔS1 and *ΔInterSacc*. We then created two levels for ΔGap: *short Gap* and *long Gap*; and two levels for ΔS1: *short S1* and *long S1*. We chose the duration of ΔS1 and ΔGap levels so that 1) the combination *short Gap / short S1* gives a short *ΔFromFix.2*, 2) the combinations *short Gap / long S1* and *long Gap / short S1* give a similar, medium *ΔFromFix.2*, and 3) the combination *long Gap / long S1* gives a long ΔFromFix.2 (see paradigm details in **Figure 3-5**).

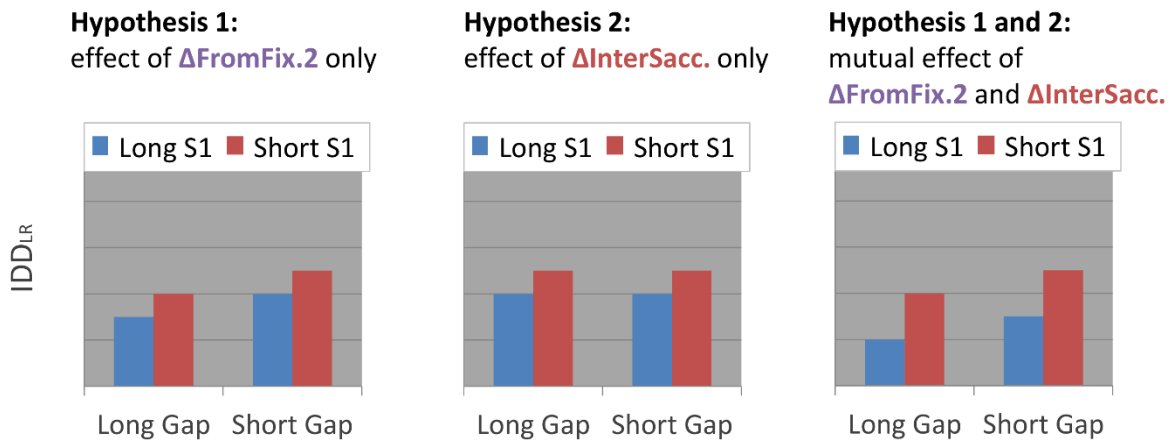

Figure 3-6: Summary of Expected Results for the two-way ANOVA according to the hypotheses. *Note that in **Hypothesis 1** (left plot), the two middle bars - red and blue - are of equal height, Furthermore, the effect of S1 duration is larger than the effect of Gap duration. In **Hypothesis 2** (middle plot), the bars sharing the same colour are of the same height. In **Hypothesis 1 and 2** (right plot), the two middle bars - red and blue - are not of equal height. Furthermore the effect of S1 duration is larger than the effect of Gap duration.*

If **Hypothesis 1** (inhibition from previous fixation) is exclusively correct, the deviation of *Saccade 2* depends only on ΔFromFix.2. We should observe a main effect of ΔGap and ΔS1 while the deviation should be equal for *short Gap / long S1* and *long Gap / short S1* conditions. In other words, the effect size of ΔS1 and ΔGap are equal. If **Hypothesis 2** (residual saccade activity) is exclusively correct, the deviation depends only on ΔInterSacc, and we should obtain a main effect of ΔS1 but not from ΔGap. If **Hypothesis 1 and 2** are mutually correct, the deviation will

depend on ΔInterSacc. and ΔFromFix.2, and we should obtain a main effect of ΔGap and ΔS1 while the deviation should be smaller for the *short Gap / long S1* condition than for the *long Gap / short S1* condition (the ΔFromFix.2 is equal but ΔInterSacc. differs). In other words, the effect size of ΔS_1 is larger than the effect size of ΔGap (see **Figure 3-6** for a graphical representation).

To reduce the number of statistical models tested by the Bayes Analysis, the Independent Variable we chose to work with is the Distance in Initial Deviation for Saccade 2 between F_L and F_R conditions (we will refer to it as $IDD_{LR,}$ as in Experiment 1). This change in independent variable also allowed us to assess the effect of ΔS1 (*short S1* and *long S1*) and of ΔGap (*short Gap* and *long Gap*) on the IDD_{LR} with a two-way Analysis of Variance (ANOVA). However, this also means that we work with one IDD_{LR} per participant per condition (instead of one measure per trial as in Experiment 1). Because of this, and also because we have now mixed conditions with different stimulus timings, we chose to increase the number of participants to 14 (9 males).

4.2 Results

We rejected, in total, 3 participants based on their proportion of rejected trials (proportion greater than 40% - see Appendix 6 for details on trial rejections and a sample of ill-distributions for ΔInterSacc and ΔFromFix.2).

A classic two-way ANOVA detected a significant effect of ΔS1 and ΔGap on IDD_{LR} and no interaction between them (for further details - **Figure 3-7**). In addition, we ran a paired t-test comparing the changes in IDD_{LR} observed when varying ΔGap and when varying ΔS1: the change caused by ΔS1 is significantly greater, $t(21) = 2.14$, $p=.044$. The fact that both main effects are significant and that ΔS1 has a larger effect supports the idea that **hypotheses 1 and 2** are coexisting (see section 4.1 and **Figure 3-6**).

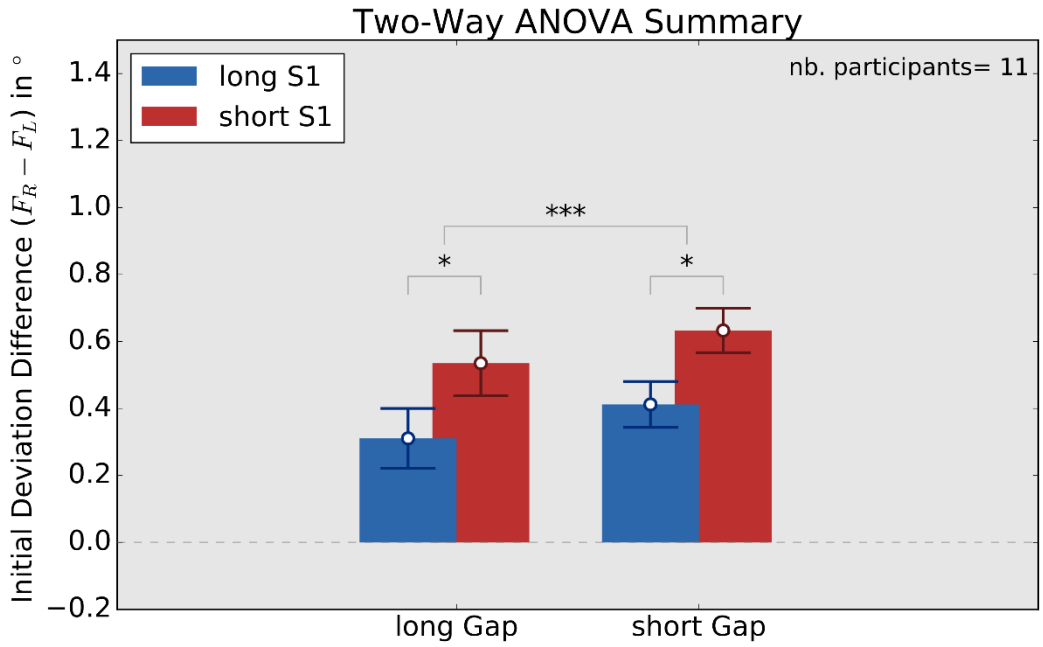

Figure 3-7: Summary of the two-way ANOVA conducted in Experiment 2. *Error bars display the within-subject standard error of the mean for a 95% confidence interval. The two-way ANOVA within participants yielded a main effect of* ΔS_1, $F(1,10) = 8.869, p = .0139, \eta_G^2 = 0.154$, *such that the average* IDD_{LR} *was significantly higher for* short S1 *(M = 0.584 , SD = 0.314) than for* long S1 *(M = 0.361, SD = 0.201). The main effect of ΔGap was also significant,* $F(1,10) = 12.166, p = .00584, \eta_G^2 = .0351$, *such that the average* IDD_{LR} *was significantly higher for* short Gap *(M = 0.523 , SD = 0.236) than for* long Gap *(M = 0.423 , SD = 0.238). The interaction was not significant,* $F(1,10) = .00301, p = .957, \eta_G^2 = .00001$

To further confirm our finding, we ran a Bayesian analysis with the same data set. We tested all possible models combining *Participant*, ΔGap and ΔS1 and their interactions (i.e. interactions between Participant and Dependent Variables are now tested).

Table 2: *Bayes factor top-down analysis on Initial Difference in Deviation (Left-Right).*

	Effect of Omission	BF		Interpretation Tag	Polarity
[1]	ΔGap:ΔS1:Participant	1.02	±5.26%	weak	none
[2]	ΔGap:Participant	3.88	±4.26%	positive	against
[3]	ΔS1:Participant	5.29E-04	±4.65%	very strong	in favour
[4]	ΔGap:ΔS1	2.37	±5.96%	weak	against
[5]	Participant	3.53E-09	±5.19%	very strong	in favour
[6]	ΔGap	0.196	±6.07%	positive	in favour
[7]	ΔS1	0.248	±4.46%	positive	in favour

Note. The symbol ":" indicates interactions. Bayes Factor against the full model: $IDD_{LR} \sim \Delta S1 + \Delta Gap + Participant + \Delta S1{:}\Delta Gap + \Delta S1{:}Participant + \Delta Gap{:}Participant + \Delta S1{:}\Delta Gap{:}Participant$.

Table 2 reports the effect of omitting each Dependent Variable and interaction from the full model (i.e. the model with all the variables). A BF inferior to one means that to omit the variable is detrimental to the full model – i.e. the evidence is *in favour* of an effect of the variable. Matching the BFs with the interpretation tags of **Table 1** (in italics), we can see that there is *positive* evidence in favour of an effect of both ΔGap and ΔS1, consistent with the results of the above ANOVA. There is also *very strong* evidence in favour of an interaction between Participants and ΔS1 and *positive* evidence against an interaction between Participants and ΔGap. Furthermore, the best model reported by the analysis is the following:

$$IDD_{LR} \sim \Delta S_1 + \Delta G_1 + Participant + Participant{:}\,\Delta S_1$$

Its BF against the next best and simpler model – which simply *ignores ΔGap* – is approximately 7.23 ($\pm$4.27%). This constitutes *positive* evidence for a clear pre-eminence of the best model over the other models.

Finally, considering the best model, we tested if $E(\Delta S_1) > E(\Delta G_1)$ --where $E()$ stands for the effect size-- from its *posterior distribution*. We extracted 10,000 points from the *posterior distribution* of ΔS1 and of ΔGap in order to estimate the probability of $E(\Delta S_1) > E(\Delta G_1)$ and of $E(\Delta S_1) < E(\Delta G_1)$identifying the best model. To obtain the BF of each hypothesis against the best model, we multiply each of them by their prior probability, which is 0.5 (we assumed that both are equally possible). We get $BF_{\Delta S_1 sup}$ and $BF_{\Delta G_1 sup}$ against the best model. From this:

$$BF_{(\Delta S_1 sup\ vs.\ \Delta G_1 sup)} = \frac{BF_{\Delta S_1 sup}}{BF_{\Delta G_1 sup}} = \frac{1.603}{0.397} = 4.037$$

This BF is greater than 3 and so suggests that our data constitute *positive* evidence for E(ΔS1) > E(ΔGap) – the effect size of S1 duration is greater than the effect size of Gap duration. To conclude, the results of the Bayesian Analysis are compatible with those of with the ANOVA and support the idea that **hypotheses 1 and 2** are mutually correct: the deviation away that we observed is caused by both a spatiotopic influence and a retinotopic residual activity.

5 Discussion

Revealing the spatial frame of saccades is a way to put to the test recent models of saccade curvatures (Kruijne et al., 2014; Z. Wang & Theeuwes, 2014) that are based on retinotopic brain regions. Our work set out to demonstrate an influence of the fixation stimulus on subsequent saccade trajectories as suggested in previous studies (Sogo & Takeda, 2006; Z. Wang & Theeuwes, 2014). The originality of our work is that, contrary to Wang and Theeuwes (2014), we looked specifically for an influence of the *spatiotopic* representation of the previous fixation by using a double saccade paradigm. Furthermore, in contrast with Sogo and Takeda (2006), we controlled for the aftereffect of previous saccades which could have the same consequences as the influence of the fixation stimulus on the ongoing saccade trajectory.

Our double saccade paradigm consisted of trials on which the participant first had to stare at a fixation stimulus F. When F disappeared, the participant performed two saccades (Saccade 1 and Saccade 2) to two different locations indicated sequentially on the screen with stimuli S_1 and S_2. Our first experiment shows that the trajectory of the second saccade deviates away from the previous fixation F. The second experiment demonstrates that both the time elapsed from Fixation offset to Saccade 2 onset, and the inter-saccadic time from Saccade 1 offset to Saccade 2 onset are both influencing the deviation. This demonstrates that one part of the deviation is caused by the spatiotopic representation of F and one other part is caused by the aftereffect of the first saccade (residual activity).

5.1 Link with Jonikaitis and Belopolsky (2014) and with Inhibition of Return

Interestingly, our evidence for spatiotopic influences on saccade trajectories is supported by the recent behavioural work of Jonikaitis and Belopolsky (2014). In an experimental set-up where participants have to achieve two saccades – as in ours - they demonstrated that the second saccade trajectory deviates away from the spatiotopic representation of a distractor and not from its retinotopic representation. To the best of our knowledge, only our work and their study have yielded evidence for a spatiotopic frame of deviation phenomena. Such spatiotopic deviations could not be explained by the low-level mechanisms proposed by Kruijne et al.(2014) and Wang et al.(2012; 2014). However, Jonikaitis and Belopolsky (2014) did not control for saccade residual activity; we will discuss in the next session (5.2) the

possibility that the model of Kruijne et al.(2014), combined with saccade residual activity, could explain their results.

It is also worth noting that there are encouraging links between our work and the literature on inhibition of return during visual search (overt attention IoR). Indeed, the deviation away from a previously fixated stimulus could be linked to overt attention IoR – i.e. saccades to a previously fixated position take longer to trigger (Klein & MacInnes, 1999). Further, the deviation caused by the residual activity from a previous saccade could be linked to the saccadic momentum – i.e. saccades with a similar vector as the previous one are more probable (A. J. Anderson et al., 2008; Smith & Henderson, 2009). Both effects are usually reported together, and our paradigm may be a solution to study them separately. However, it is important to be cautious: work has shown that deviation away phenomena and *covert* attention IoR can be based on different mechanisms (Godijn & Theeuwes, 2004). The same conclusion has been reached for the priming compatibility effect – an analogue of IoR -- and deviation away (Hermens et al., 2010; Sumner, 2007 for a review on the compatibility effect). Furthermore, *similar* mechanisms can be *separate* mechanisms. For instance, the priming compatibility effect has been shown to be implemented separately for manual and eye movement (Sumner et al., 2007). In parallel with this, it has been demonstrated that there is a distinct cortical and collicular IoR for covert attention (Sumner, Nachev, Vora, Husain, & Kennard, 2004). Thus, we believe that to link *overt* attention IoR to our results is not trivial. At the very least, the time course of our deviation away effect will need to be explored. At most, different mechanisms of overt IoR may need to be distinguished and localized before being compared with our results.

Note that a quantitative measure of the residual effect over time would require an increase in the precision with which deviation is measured. In this case, human participants may need training sessions before collecting the data in order to minimize superfluous and missing saccades, as well as any disruption induced by the introduction of a gap.

5.2 Discussion in the light of Kruijne et al. model: fatigue in the brainstem burst generator

The model of Kruijne et al. (2014) is based on fatigue (resembling Short Term Depression, STD)[11] occurring in the saccade burst generator in the brainstem. They assume one stem per

[11] STD refers to a decrease on the neuronal sensitivity to its input when this one is sustained

saccadic direction (left, right, up, down) and a fatigue mechanism in the Long-Lead-Burst neurons (LLBNs). The LLBNs are known not to be inhibited by the omnipause neurons between saccades (Scudder, Kaneko, & Fuchs, 2002, see also General Introduction). In addition a visually evoked signal on the SC can activate the LLBNs (Rodgers, Munoz, Scott, & Paré, 2006). Subsequently, a distractor could activate the LLBNs and cause a sort of fatigue of those neurons, which will modify the trajectory of the next saccade. A distractor placed to the right of the target would fatigue the right LLBNs stem: this imbalance would then cause a saccade deviation to the left. As the SC connections to LLBNs are heavier for eccentric positions, the fatigue caused to the LLBNs would increase with distractor eccentricity, resulting in a stronger deviation (in line with Van der Stigchel et al., 2007). Along the same line of reasoning, a long presentation of the distractor would also increase the fatigue of the LLBNs. Their theory is rather appealing in the way in which it explains the major phenomena that top-down inhibition control was given credit for (see the four points mentioned in the Introduction, Section 1.2).

In our experiment, however, their theory predicts a deviation toward the previous fixation point, which is not what we observed. For instance, if the first saccade is toward the right, their model suggests that the right LLBNs are fatigued for the second saccade: the second saccade would deviate toward the left, towards the previous fixation. Furthermore, our work shows that the saccadic curvatures can be partially explained by the time from previous elicited saccades (the intersaccadic interval ΔInterSacc.). This is likely to originate from a saccadic residual activity in the SC, as assumed by the work of other authors (A. J. Anderson et al., 2008; Hooge & Frens, 2000; Klein & MacInnes, 1999; Smith & Henderson, 2009; Z. Wang et al., 2011). Note that this saccadic residual activity has an opposite effect to the fatigue mechanism proposed by Kruijne et al. (2014). They failed to consider this residual activity because they developed their model to explain a single-saccade paradigm. Their model might be revised to treat saccade-evoked activation of LLBNs differently from stimuli-evoked activation of the LLBNs. The former would produce residual activity in the SC or LLBNs, whilst the latter would produce fatigue in the LLBNs.

With such a revision of the model, results such as those of Jonikaitis and Belopolsky (2014), which suggest deviation away from the spatiotopic representation of a distractor -- might be reduced to an explanation in terms of a simple interaction between both SC's residual activity and brainstem fatigue. Indeed, it should be noted that the retinotopic representation is less eccentric in their *green* condition (see their figure 1.E) than in their *purple* condition. Hence, in their *green* condition, the fatigue caused by the distractor is smaller than the fatigue caused in

the purple condition. The residual activity caused by the first saccade could be such that it would overcome the *green* condition's fatigue but not the *purple* condition's fatigue.

Our experiment, on the contrary, does control for residual activity from previous saccades, and still finds evidence for a deviation away from the spatiotopic representation of a previous fixation stimulus. Such a deviation away in a spatiotopic frame cannot be explained by Kruijne et al.'s model. A second revision of the model could then add either a satellite structure, which would send spatiotopic signals to the SC/LLBN – or a feedback mechanism that would automatically shift the SC's signal when a saccade occurred.

5.3 Discussion in the light of Wang et al. model: lateral interactions in the SCi

The model of Wang et al. (2012; 2014) is based on spatial interactions occurring between stimuli on the Superior Colliculus (SC) map. These spatial interactions assumed that the SC is reducible to a Dynamic Neural Field with a Mexican hat kernel. The Mexican hat kernel defines the way that all neurons in the field connect with neighbouring neurons. In particular, it excites its close neighbours, inhibits its remote neighbours, and does not connect at all with distant neighbours. The kernel resembles a Mexican hat (MH) as shown in **Figure 3-8** and it defines three interaction zones centred around the stimulus locus: a circular attraction zone, a ring repelling zone and a no-interaction zone beyond that ring (Amari, 1977) [note that **Figure 3-8** is a one-dimensional cut of the MH - thus the circle and the ring are reduced to segments]. Similar to what was observed in Chapter 2, when two stimuli of the same strength are presented to the neural field:

- If they are in the attraction zone of the other, they give rise to a bump of activity in between their two loci;
- If they are in the repelling zone, the activations evoked by each stimulus repel each other, each of them giving rise to an eccentric bump of activity;
- If they are in the no-interaction zone, each stimulus gives rise to a bump of activity centred on its locus.

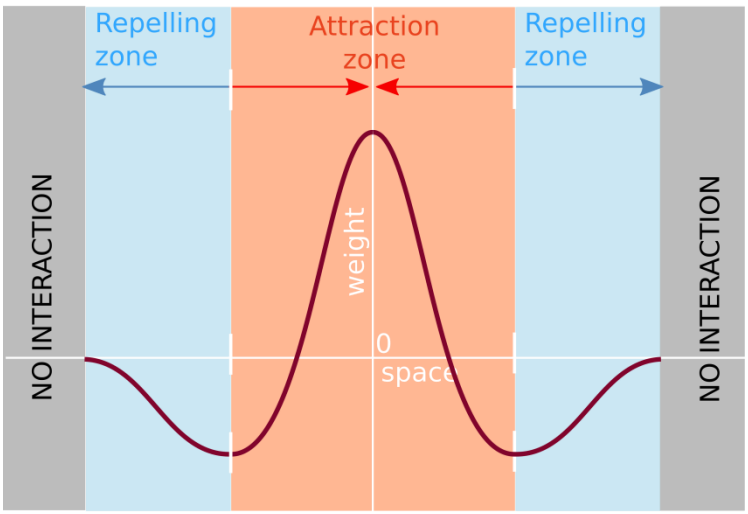

Figure 3-8: Mexican Hat Connection Kernel and the interaction regions assumed by Wang et al. (2012; 2014)'s model.

With this simple attraction/repulsion model, Wang et al. (2012; 2014) successfully explained the relationship between deviation and distractor-target separation observed in the previous literature, notably based on McSorley et al. (2009)'s data and on a meta-analysis across 12 data sets.

Furthermore, as a fixated stimulus also evoked a MH activation of the SC, they considered that the timing of the fixation stimulus could affect the trajectory of the next saccade. In their experiments (Z. Wang & Theeuwes, 2014) where they generated curvatures away from a distractor, they report that, indeed, the fixation timing (overlap vs. gap) influences the deviation *and* the amplitude of the saccades. This influence is in line with a Fixation-Target repelling effect cumulating with a Target-Distractor repelling effect. This demonstration of their theory is elegant and Kruijne et al.(2014)'s model could not account for such a fixation stimulus effect on saccade trajectory. Indeed, the fixation zone of the SC presumably does not activate the LLBNs and/or at least, would not activate a specific direction in the LLBNs.

However, to place the Mexican hat kernel (which drives the attraction/repulsion) and the fixation representation specifically in the SC without considering any external updates prevents their model from explaining our results. Indeed, in that case, no spatiotopic representation of the fixation is reaching the deviation mechanism (i.e., the Mexican Hat kernel). In fact, it has already been suggested that there are several fixation inhibitory influences coming from more than one pathway (Sumner, Nachev, Castor-Perry, Isenman, & Kennard, 2006). Hence, as for the model of Kruijne et al. (2014) a revision of their model could

add either a satellite structure which would send spatiotopic signals to the SC – or a satellite structure which would shift the SC's signal when a saccade occurred. Alternatively, the Mexican Hat kernel could be operating directly from a spatiotopic structure.

5.4 An Excitatory Spatiotopic Signal from the Lateral Intraparietal Area

Our suggested revisions for the two aforementioned models have in common the proposal of a spatiotopic excitatory signal in the SC -- as both models need an excitation of the SC to create deviation phenomena. It is important to mention that the traditional explanation of deviation away phenomena – as opposed to the aforementioned proposition-- is a top-down inhibition influence on the SC (McSorley et al., 2004). This top-down inhibition could be spatiotopic. We discuss next what may be inferred from the previous literature.

It should be noted that structures downstream (or parallel to) the SC have been suggested for driving spatiotopic updating (Bozis & Moschovakis, 1998). Bozis and Moschovakis's work demonstrates that a simple feedback of the brainstem burst generator to the SC (known from Moschovakis, Karabelas, & Highstein, 1988), makes spatiotopic updating possible. Note that the brainstem burst is correlated with the velocity of the saccade. Their idea was to feedback this velocity related burst to the SC with asymmetric connections so that the activity on the SC moves as the eyes move. This is important, since they successfully implemented a simple neural mechanism to update retinotopic representations to spatiotopic representations.

However, several pieces of evidence appear to favour a top-down origin of the spatiotopic representations. First, it has been shown that spatiotopic representations often happen late and gradually compared with those of the retinotopic system (Golomb, Chun, & Mazer, 2008; Hilchey, Klein, Satel, & Wang, 2012; Mathôt & Theeuwes, 2010; Pertzov, Zohary, & Avidan, 2010). Second, human participants can voluntarily block the build-up of a spatiotopic representation when the task requires them to maintain only a retinotopic representation (Golomb, Chun, & Mazer, 2008, experiment 3). Third, it is known that cortical lesions can hinder the completion of saccadic tasks requiring spatiotopic update (Duhamel, Goldberg, Fitzgibbon, Sirigu, & Grafman, 1992; Heide, Blankenburg, Zimmermann, & Kömpf, 1995). The work of Heide et al. (1995) is of particular interest. In a double-step task, two target stimuli were presented one after the other, and the participant had to make a saccade to each of them in order. The presentation of the second target stopped before the initiation of the first saccade. The second target then had to be memorized and its representation needed to be

spatiotopically updated on the SC to trigger the relevant saccade. Note that if the second target has been still displayed after the end of the first saccade, the spatiotopic update would have not been needed. Heide et al. (1995) showed that a lesion in the Posterior Parietal Cortex causes an increase in errors for the second saccade – suggesting that it is involved in the spatiotopic update that the second saccade requires. Interestingly, the dorsolateral prefrontal cortex, which has been suggested to implement a top-down inhibition influence on the SC (Meeter et al., 2010) does not appear to be involved in the spatiotopic coding of the second saccade, and neither is the Frontal Eye Field (FEF, replicated in other studies such as Rivaud, Müri, Gaymard, Vermersch, & Pierrot-Deseilligny, 1994; Schiller & Chou, 1998). Finally, the main area projecting to the SC from the Posterior Parietal Cortex is the lateral intraparietal area (LIP, Paré & Wurtz, 1997). Note that both LIP and FEF are also strongly interconnected (Andersen et al., 1990).

In addition, in both LIP and FEF –which are both top-down structures projecting to the SC – the neural population coding for the postsaccadic location of the visual stimuli seems to be activated before the saccade (Goldberg & Bruce, 1990; Goldberg, Colby, & Duhamel, 1990; Kusunoki & Goldberg, 2003; Umeno & Goldberg, 1997): this could correspond to an anticipated spatiotopic update. Furthermore, neurophysiological work have demonstrated that such predictive activations also occur in specific cells of the SCi, i.e., the quasivisual cells (Mays & Sparks, 1980; M. F. Walker, Fitzgibbon, & Goldberg, 1995). These findings support the possibility of a spatiotopic excitatory update of the SCi: notably its quasivisual neurons would reflect an anticipated spatiotopic update sent and generated by the LIP.

5.5 Conclusion

We have demonstrated that both residual activity from previous saccades and the spatiotopic representation of previously fixated stimuli can influence the trajectory of the current saccade. This influence is translated into a trajectory deviation away from the previously fixated stimulus. These findings call for current retinotopic models on deviation to update and take into account spatiotopic representations. In particular, we suggest that the Lateral Intraparietal area would be a good candidate to provide excitatory spatiotopic signal to the SC.

6 APPENDIX A: Rejection of Trials in Experiment 2

The average rejection rate of trials was very high compared to the pilot experiments (27 %) and it justifies *a posteriori* our choice of increasing our sample size. This high rejection rate could be due to the introduction of a gap or the fact that we mixed the conditions. Indeed, participants have reported finding it difficult to not move their eyes during the long gap (ΔGap) and they found themselves making predictive saccades. The uncertainty of a long or short gap may also prevent them from adopting a strategy to stabilize their eyes. It is also important to recall from Section 2.2 that the trial rejection algorithm is sensitive to early and/or superfluous saccade.

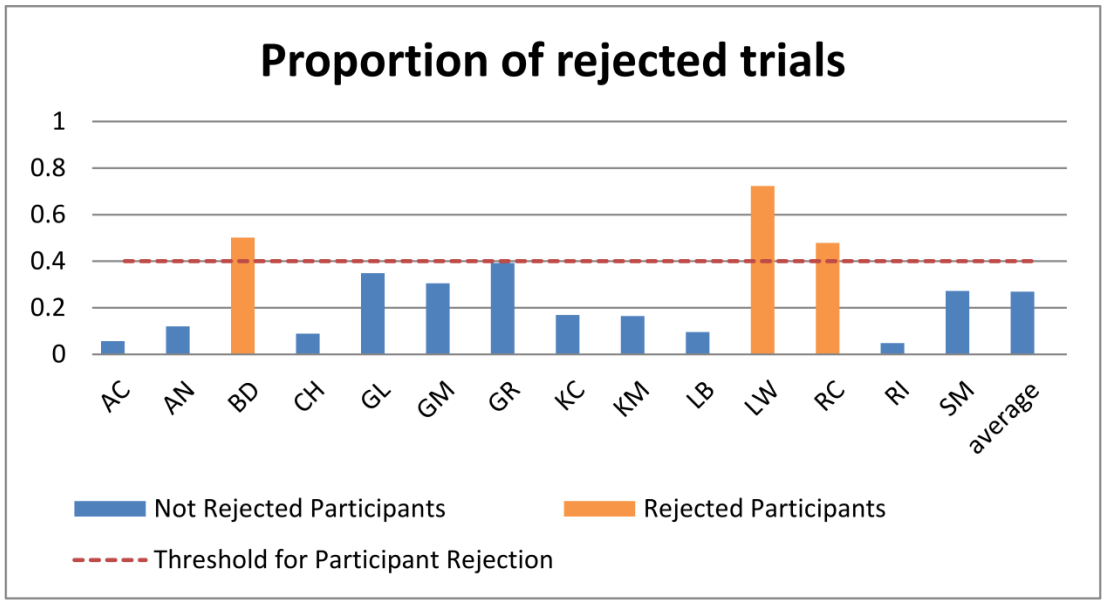

Figure 3-9: Rejection of Participants based on the proportion of rejected trials for Experiment 2.

We rejected in total 3 participants based on their proportion of rejected trials (greater than 40% - see **Figure 3-9** for a summary of trial rejection), concluding that the gap had been too disruptive on their performance. It is worth mentioning that a good data set for testing our hypotheses should show:

1. A similar distribution of ΔInterSacc - when comparing the condition$[S1_{short}|G1_{short}]$ with $[S1_{short}|G1_{long}]$ or when comparing $[S1_{long}|G1_{short}]$ with $[S1_{long}|G1_{short}]$,

2. A similar distribution of ΔFromFix.2 when comparing $[S1_{long}|G1_{short}]$ with $[S1_{short}|G1_{long}]$.

These are the necessary requirements for ΔS1 and ΔGap being good proxies for ΔInterSacc and ΔFromFix.1 respectively and for our ANOVA being interpreted as in Section 4.1. Interestingly, the 3 rejected participants suffered from an ill-shaped distribution of ΔFromFix.2 and ΔInterSacc. Figure 11 and Figure 12 show an example of, respectively, well and ill-distributed ΔFromFix.2 and ΔInterSacc. (from the analysed and rejected data respectively).

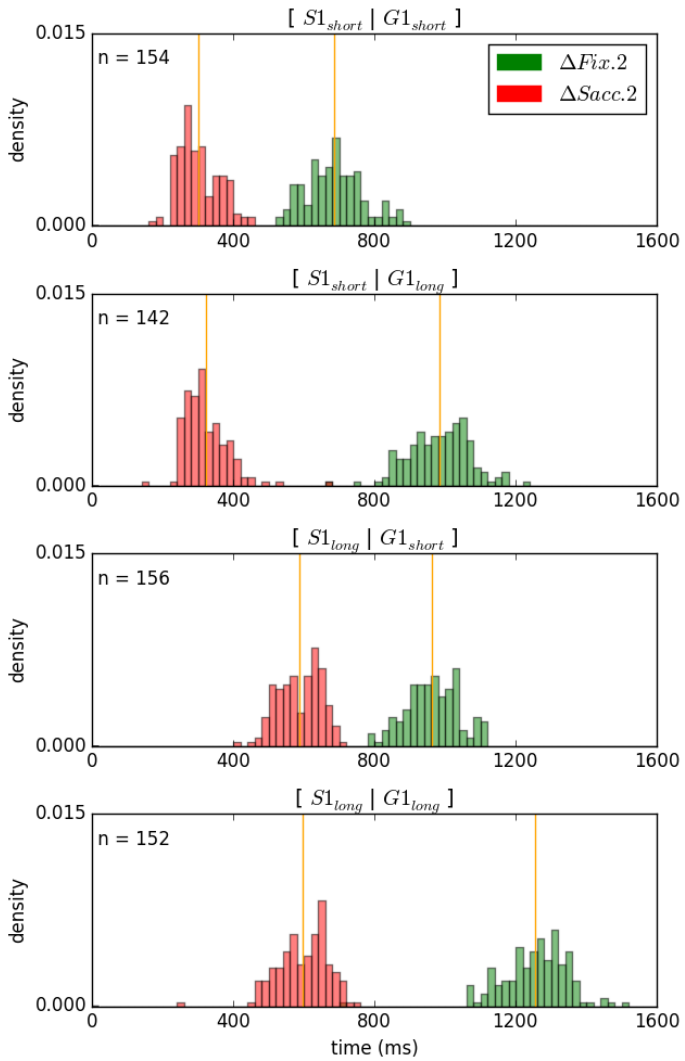

Figure 3-10: Example of a Good distribution of ΔFix.2 and ΔSacc.2 from Participant AC. *These distributions are in agreement with the assumption made for using, respectively, ΔS1 and ΔG1 as proxy for varying ΔSacc.2 and ΔFix.1..*

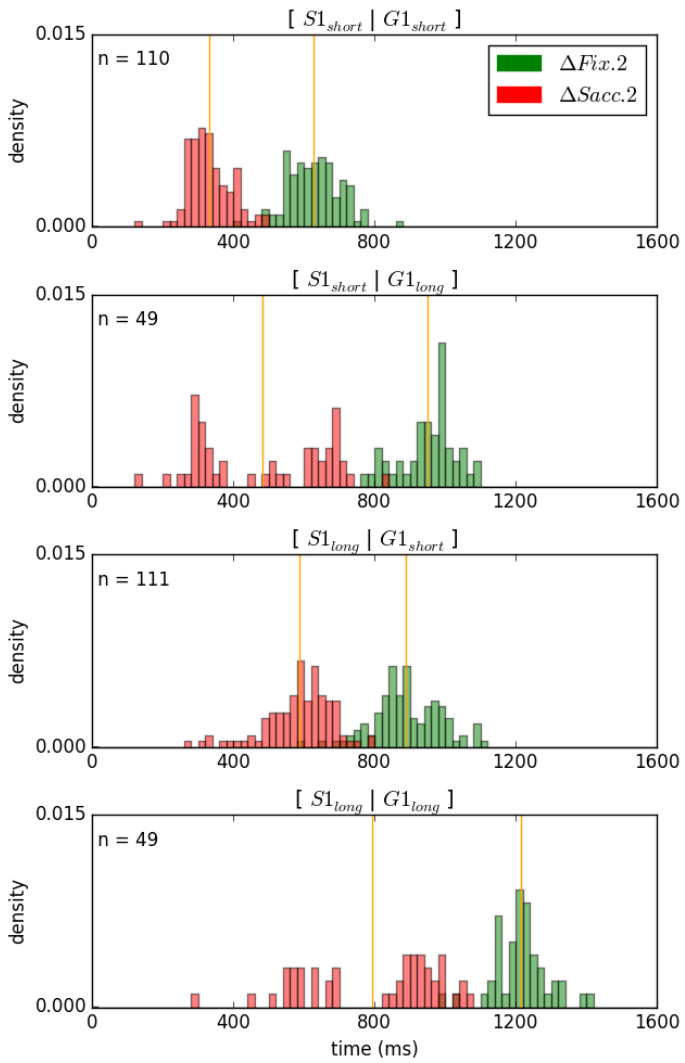

Figure 3-11: Example of an ill-shaped distribution of $\Delta Fix.2$ and $\Delta Sacc.2$ from Participant BD.

1

Chapter Four: The Bimodal Global Effect as a new Window on Decision Making Processes

Determining the Spatial Profile of the Effect of Probability of Occurrence and Top-down Discrimination.

Abstract

The Global Effect (GE) refers to the tendency for saccades to first land in between two nearby visual stimuli – forming a unimodal distribution -- instead of being an accurate saccade to one of the stimuli – forming a bimodal distribution. Considering the motor map of the Superior Colliculus, several mechanisms were suggested: either there are two visually related bumps of activity that merge into one bump through lateral interactions, or there are two bumps that do not merge and the structures downstream somehow compute a spatial average. Based on the latter hypothesis, we explored whether a GE is still detectable for bimodal distribution of saccades. By proposing a simple mechanism underlying the Bimodal GE, we introduce this measure as a new window on Decision Making processes -- as compared to saccade trajectories.

As a showcase of our measure, we chose to use it to examine the two major kinds of endogenous signals at play during decision-making –selection history signals and goal-related signals, respectively. In particular, we selected the following two factors: 1) the probability of the occurrence of two stimuli on a trial, and 2) whether the participant is required to discriminate and aim for a target on two stimuli trials. We measured the Bimodal GE for several inter-stimulus distances to obtain a spatial profile of the signals.

Our work reports that Bimodal GE can be successfully used to probe both types of signals. Interestingly, their spatial profiles differ -- the effect of the probability of occurrence is symmetric and decreases with stimulus separation, while the effect of discriminating a target is maintained across separations and is asymmetric, occurring only on the side of the distractor. This suggests that the former effect changes the response property of the motor map, while the latter specifically gives a boost to the target location.

1 Introduction

1.1 Main question

Most decision-making processes depends on the execution of an action expressing the decision. In this situation, no matter how efficient a decision-making system, its expression will ultimately be limited by the mechanisms used to translate decisions into action. We saw in the General Introduction that the SC serves as a sensori-motor interface for eye movement to which several decision processes can converge. Interestingly, the SC appears to trigger a saccade based on a simple threshold mechanism rather than on the *completion* of the inputting decision processes. Thus, a saccade can serve as a window opened on the SC, and/or on a specific decision process. For instance, in the previous chapter, we analysed the curvature of saccade trajectories to address the origin of a specific signal in the SC. Saccade curvature is a well-established tool to probe the mechanism of action selection, but it suffers from some limitations. First, the underlying mechanisms are debated or not fully understood – particularly with respect to curvatures away from a distractor (as seen in the previous Chapter) and the correcting part of curvatures (Quaia et al., 1999; Walton, Sparks, & Gandhi, 2005). Second, they are computationally heavy to extract, store, and handle. Third, they are ambiguous to measure (see Ludwig & Gilchrist, 2002 for a review of different methods to quantify saccade curvatures). In this chapter, we will introduce a new, lightweight, and simple measure – the Bimodal Global Effect -- to use as an alternative window on decision processes.

1.2 Origin and mechanisms of the Global Effect

Decisions are often translated into ocular and/or hand movements landing on or pointing to a visual item in the environment. In such a decision-making situation, each available decision option is attached to a visual item and a motor response. It has been shown that visual stimuli not relevant to the current task – i.e., a distractor -- can interact with the relevant visual item, leading to inaccurate or altered expression of the decision. One famous example is that when two close visual stimuli are presented simultaneously, eye and/or hand movements directed to one of them tend to land in between the two stimuli (saccade averaging: (Findlay, 1982); see (Sailer, Eggert, Ditterich, & Straube, 2002). This phenomenon, termed the Global Effect (GE) or saccade averaging, could represent a fundamental limitation in rapid action selection: although the decision of where-to-go may be made with precision at some higher level, the spatial

proximity between items on the motor map can make the decision ineffective (for more studies on the Global Effect, see: Findlay, 1982; Heeman, Theeuwes, & Van der Stigchel, 2014; Tandonnet, Massendari, & Vitu, 2012; S. Van der Stigchel & Nijboer, 2013; Walker, Deubel, Schneider, & Findlay, 1997). Alternatively, for the experimenter, the GE can provide a tool with which to examine decision making processes. It is therefore important to understand the mechanism underlying the GE.

It is important to note that the space of the decision-making depends on the space of motor responses. In the case of eye movement, a two-choice decision would be projected onto the two dimensions of SC; each option being a bump of activity (R. W. Anderson et al., 1998). It is thought for a long time that the SC is involved in the GE, as saccade averaging occurs when stimulating two coordinates in the SC (D. A. Robinson, 1972). However, the actual mechanism underlying the GE is not clear. Because the SC has local lateral connections (Isa & Hall, 2009 for a review on lateral connections in the SC), it is often assumed that the bumps can interact. In Dynamic Neural Field models of the saccadic system, two proximal bumps would merge into a single bump, which would explain the GE (see Chapter 2 and Arai, Keller, & Edelman, 1994; Kopecz & Schöner, 1995; Wilimzig, Schneider, & Schöner, 2006). This merging of the two bumps of activity has been reported to occur in both the superficial layers (Vokoun et al., 2014) and the intermediate/deep layers (Edelman & Keller, 1998; Glimcher & Sparks, 1993). However, the work of Edelman and Keller (1998) also reports two bumps of activity during averaging express-saccade, which means that the mechanism thought to underlie the Global Effect still remains a matter of debate (Gandhi & Katnani, 2011). Interestingly, the GE has been successfully modelled without any merging mechanism – i.e., conserving two bumps of activity in the SC -- by using the vector summation theory or quaternion coding (see General Introduction and Arai & Keller, 2005; Tweed & Vilis, 1990; Van Opstal & Van Gisbergen, 1989).

In a conservative definition of the GE, the effect is considered to be present when we observe a unimodal distribution of the landing positions in between two simultaneously presented stimuli -- a *genuine global effect*, (Van der Stigchel, Vries, Bethlehem, & Theeuwes, 2011). It is considered absent, however, when a bimodal distribution is observed. The GE disappears with stimulus separation, and theoretically there is a bifurcation of unimodal to bimodal at a certain distance— considered to be around 20-35° in visual space (Ottes, Van Gisbergen, & Eggermont, 1984; Van der Stigchel & Nijboer, 2013; R. Walker et al., 1997). However, it appears that the presence of GE is not as simple as a clear demarcation from a unimodal to bimodal distribution. Indeed, it has been reported that saccade endpoint still deviates toward the centre when the

distributions are bimodal (Arai, McPeek, & Keller, 2004; Van der Stigchel et al., 2011). We have chosen to call this phenomenon *Bimodal GE*.

Thus, the definition of GE we use here extends to any spatial deviation of the saccade endpoints toward a non-target stimulus. We then distinguish unimodal GE, corresponding to the genuine global effect, from bimodal GE. We will see in the discussion that the bimodal GE framed in the vector summation theory readily allows for inferences to be made on the decision processes or signals that a paradigm would isolate.

1.3 Aims and Hypotheses

Decision-making involves both exogenous signals – e.g., from stimulus properties -- and endogenous signals –e.g., from internal processes. It is known that properties of the stimuli can influence the Global Effect; endpoints of saccades tend to go closer to the larger (Findlay, 1982), or more salient stimuli (Deubel et al., 1984). Yet, little is known regarding which of the *endogenous* signals can modulate the GE, and the properties of such modulations. Endogenous signals can be divided into two types - goal-related and history-related - as suggested recently by Awh, Belopolsky and Theeuwes (2012). We decided to explore the effects of both kinds of signals with the Bimodal GE. This also permits the possibility of demonstrating that the Global Effect can be influenced by both kinds of endogenous signals.

The results of Ottes et al. (1984) and Walker et al. (1997) are classical references on the Global Effect and yet, a possible discrepancy can be found when comparing them. In the former study (*their* figure 6D), it appears that a bimodal Global Effect is still present for a stimulus distance[12] of 90° (directional angle) while in the latter study (*their* figure 6B and 7B), the measured Global Effect is very small at distance 45° and absent at distance 90°. As the measures reported by both research groups are different, it is difficult to quantitatively judge this possible discrepancy without replicating their experiments. Interestingly, there are two main differences between their methods. Before describing these differences, it is important to note that both studies intermixed trials with two stimuli with trials with one stimulus. The first difference is the *type of stimulus pair:* Ottes et al.'s study used two identical stimuli without specific instructions while Walker et al.'s used a target/distractor pair instructing the participant to ignore the distractor and aim for the target. The second difference concerns *the*

[12] It should be recalled that "stimulus distance" refers to the inter-stimulus distance, as it was noted in Chapter 2

frequency of occurrence of the stimulus pair: Ottes et al.'s study used a low frequency (10%), whilst Walker et al.'s employed a high frequency (on most of the trials). We chose to take these two factors as starting points to explore which endogenous signal could modulate the GE as 1) they are respectively linked to goal-related and history-related signals, 2) they are keys factors in designing GE experiments, and 3) they give us scope for assessing the possible discrepancy between the two afore-mentioned studies.

The important difference when using a target/distractor pair compared to using two identical stimuli is that, in the former case, a discrimination has to be intentionally made to select the instructed target, and thus involves a top-down process. A second experiment by Ottes, Van Gisbergen, & Eggermont, (1985) reported no difference from their initial results when using a target-distractor couple. Although their conclusion is not based on any strong statistical method, it has been acknowledged for a long time that GE is immune to top-down influences. Nevertheless, recent results have demonstrated that this is not the case (Aitsebaomo & Bedell, 2000; Heeman et al., 2014; Hermens, Ghose, & Wagemans, 2013). The work of Heeman et al. (2014), in particular, shows that to give the mere instruction to aim for one of the stimuli of a discriminable pair modifies the GE; to be more specific - the unimodal distribution of landing positions is shifted toward the targeted stimulus. Given that this study was carried out with only one stimulus distance, we thought it necessary to extend their work in order to examine the spatial profile of this top down influence that modulates the strength of the GE. As we will see in the discussion, the spatial pattern of GE modulation will also help us to distinguish between different sorts of mechanisms.

The other key factor we tested is the probability of stimulus occurrence. It is important to distinguish the probability of occurrence from spatial probability. The latter gives an advantage to frequently aimed positions and biases the GE toward that position (He & Kowler, 1989). The spatial probability of targets has been shown to be coded in SC (Basso & Wurtz, 1998) and may originate from FEF (C.-L. Liu et al., 2011). With regard to the mere probability of stimulus *occurrence*, there is, to our knowledge, no behavioural work addressing its effect on GE. Interestingly, it has been shown that the probability of both target occurrence (Jüttner & Wolf, 1992) and distractor occurrence (Goldstein & Beck, 2013) has an effect on saccade reaction times. Furthermore, some studies have suggested that the Locus Coeruleus – i.e. the norepinephrine system – responds to the relevance, novelty, and infrequency of stimuli (Alexinsky, Aston-Jones, Rajkowski, & Revay, 1990; Preuschoff, 't Hart, & Einhauser, 2011; Privitera, Renninger, Carney, Klein, & Aguilar, 2010) with more or less habituation (Aston-

Jones et al., 1994; Vankov, Hervé-Minvielle, & Sara, 1995). Interestingly, the norepinephrine system is thought to modify the responsiveness of neurons in diffuse parts of the brain involved in decision making or in perception through coarse projections (Aston-Jones & Cohen, 2005; Hurley, Devilbiss, & Waterhouse, 2004). Such an effect of norepinephrine has been observed in SC neurons (Mooney, Bennett-Clarke, Chiaia, Sahibzada, & Rhoades, 1990; Tan, Mooney, & Rhoades, 1999; Y. Zhang, Mooney, & Rhoades, 1999) and some studies have demonstrated direct projections of the Locus Coeruleus to the SC (Arce, Bennett-Clarke, & Rhoades, 1994; S. B. Edwards et al., 1979; Mooney et al., 1990). Taken together, these findings encourage testing of the hypothesis that the frequency of occurrence of the stimulus pair can modulate the strength of the GE. If this is indeed the case, it would support the notion that this signal is sent to the SC.

To summarize, we hypothesized that the type and the frequency of occurrence of the stimulus pair can modify the strength of the GE, and we assumed that they respectively control a goal-related and a history related signal. Our paradigm consisted of four conditions: two factors (*Pair-Type; Pair-Frequency*) of two levels (respectively *T-Same/T-Different; F-20/F-80*). These conditions were arranged across 8 stimulus directional distances in a classical Global Effect paradigm. We will show that *Pair-Frequency* and *Pair-Type* are both able to exert an effect on GE. Interestingly, our measurement highlights a distinct spatial pattern of the GE modulation across stimulus distances for each effect. Based on the vector summation theory, we will argue that an easy correspondence can be made between the pattern of GE modulation and the shape of the goal-related or history-related signal sent to the SC. Thus, we conclude that the bimodal GE represents an interesting tool for exploring decision-making processes.

2 Methodology

2.1 Participants

Four naive individuals and the author (25-27 years old; 3 male [BD, GM, RI] and 2 female [KM, AN]) participated in the experiment. All had normal visual acuity. BD and GM are occasional smokers. No participants reported drug or alcohol dependencies or sleeping disorders. Ethical approval was obtained through the local ethics committee.

2.2 Apparatus

Participants performed the experiment in a quiet dark room. They sat at a distance of 72 cm from a display monitor with a 100 Hz refreshing rate. Its dimensions were 36.60 cm in width and 29.30 cm in height for a density of pixels approximately 35 pixels per centimetre. The monitor was covered with a red filter. A measure of luminance homogeneity was made to check if any unusual behaviour might be expected (see **Figure 4-1**). For instance, note the drop of luminance on the bottom left. This might have led to lower reaction times of the participant when stimuli were displayed in this part of the screen, which could also have had the effect of biasing decisions if one of the options was located in that corner.

Eye movements were recorded with an Eyelink 2000 system (Tower mount system; SR Research Ltd., Canada), an infrared video-based eye tracker that has a spatial resolution of 0.01° (average accuracy measured by constructor: typically between 0.25° and 0.5°). It was used at a time resolution of 1000 Hz while the participant's chin was resting on the headset pad. Only the left eye was recorded.

The experiment was programmed with *pygame*, a python library that provides graphic and input management, and *pylink*, the official Eyelink library for python. The code can be found at: https://github.com/Nodragem/Chapter-GlobalEffect-Experiment1

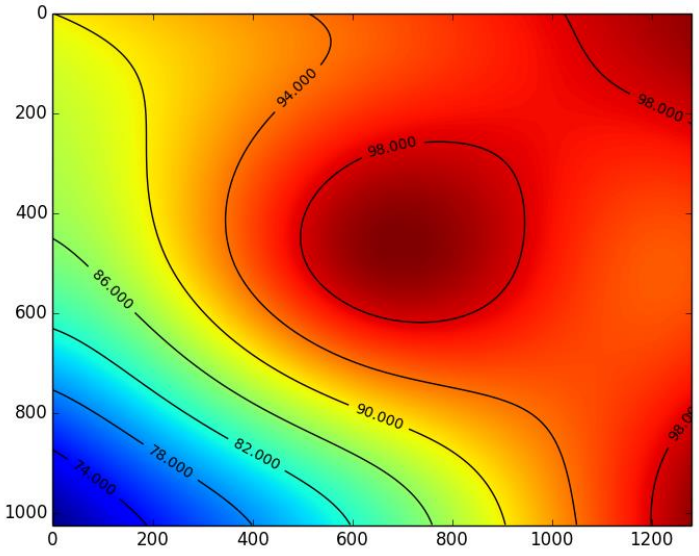

Figure 4-1: Luminance homogeneity of the monitor display. *The luminance is expressed as a percentage and is relative to the central luminance of* 4.5 $cd.m^2$*. The graph interpolates measures taken at 9 positions.*

2.3 Stimuli and Procedure

The participants were required to undertake 8 sessions of 1600 trials each (8x60min); each session being separated at least by one night. A break was offered every 200 trials while a break and a calibration on 13 points were imposed at every 400 trials. Each session tested only one of the 4 following conditions: *F-20/T-Same*, *F-20/T-Different*, *F-80/T-Same*, *F-80/T-Different*.

Trials in any of these conditions followed the same template: the participant started by staring at a white fixation cross of 0.4° on a black background at the centre of the screen. After a random interval of 500-1000ms, the fixation cross disappeared and a target element S1 (luminance: 4.5 $cd.m^2$) was presented at an eccentricity of 13.5° of visual angles (see **Figure 4-2**A and B) while its direction could have been any one of the 32 directions tested. We tested 8 directions per quadrant (given in directional angles, see **Figure 4-2**A): from +5.625° to +45° by step of 5.625° for the top right quadrant; the vertical mirror images of these directions are tested in the top left quadrant; and the horizontal mirror images of the top quadrant directions are tested in the bottom quadrants (see Figure 4-2A). For a certain percentage of the trials, an additional stimulus S2 is simultaneously displayed at the horizontal mirror image of the target. For instance, if S1 is presented at -45°, the additional stimuli S2 will be displayed at 45° of angular direction (and 13.5 of eccentricity). We refer to those trials as double-stimulus trials. The stimulus S1 was displayed for 800ms while the S2 was displayed for 700ms. Following this, the screen was cleared and a new trial began.

We tested 4 conditions. In *F-20/T-Same*, and *F-80/T-Same*, the additional stimulus S2 was identical to the stimulus S1 but 12.5% brighter. All the participants reported not having noticed this difference in luminance. For these conditions, the participants were simply asked to move their eye to any presented stimulus as quickly and precisely as possible. They did not receive further instructions for the case of double-stimulus trials, as in the study by Ottes et al. (1984). In *F-20/T-Different* and *F-80/T-Different* conditions, the additional stimulus S2 was of a different shape to S1 and was also 12.5% brighter. For these conditions, we defined S2 as a distractor and S1 as the target. The participants were instructed to ignore the distractor and to move their eyes to the target as quickly and precisely as possible. Finally, in *F-80/T-Different* and *F-80/T-Same* conditions, the additional stimulus was presented 80% of the time, while its frequency was set up at 20% for *F-20/T-Different* and *F-20/T-Same* conditions.

For all the participants, the distractor and the target of *T-Different* conditions could either be a circle or a diagonal-cross of 0.8°. The circle stimulus was defined as the target for BD and AN,

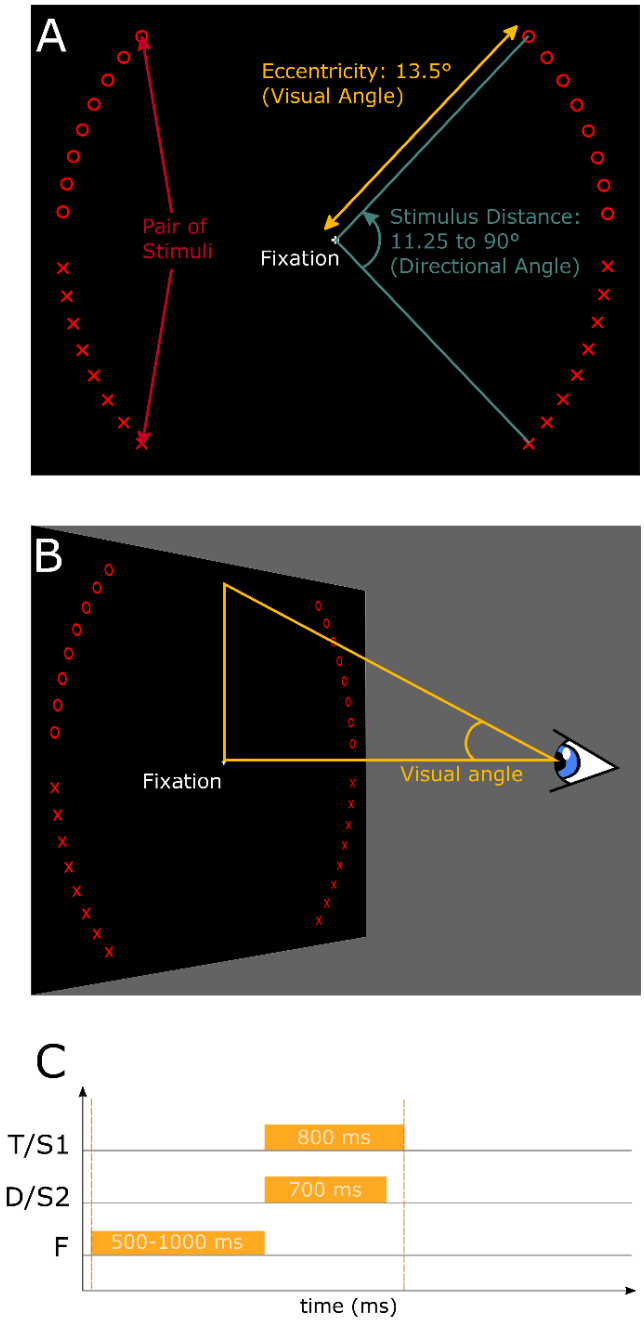

Figure 4-2: Summary of the Paradigm. A: *This graph locates the possible position of the stimulus on the monitor's display during a trial. For the sake of readability, we only show the case where the target is a circle and the additional stimulus is a diagonal-cross (Condition T-Different). Further, the target is only on the top part of the screen in this example: a reflection on the x-axis of this figure would show the possible remaining stimulus configurations.* ***B:*** *This plot displays what we refer to as visual angle; i.e. the angle formed between two positions on the screen and the recorded participant's eye. Note that eccentricities and landing positions are given in visual angle; only stimulus distances are given in directional angle.* ***C:*** *A pair of stimuli –S1 and S2, or T and D -- appear on the screen simultaneously after the offset of the fixation cross F. The duration of F is randomly distributed between 500 and 1000 ms.*

while the diagonal-cross was the target for GM, KM, and RI. The distractor logically inherited the remaining shape: it was a circle if the target was a diagonal-cross and vice versa. Hence, the *F-20/T-Same* condition is similar to that employed in the paradigm of Ottes et al. (1984) while the *F-80/T-Different* condition is close to that used in the work of Walker et al. (1997). For all the participants, the sessions were ordered as follows: *F-20/T-Same*, *F-20/T-Different*, *F-80/T-Same*, *F-80/T-Different*, *F-80/T-Different*, *F-80/T-Same*, *F-20/T- Different, F-20/T-Same*. While we would usually counterbalance the order across participants, here we thought it was useful to keep this order. First, the two F-20 blocks were separated by four F-80 blocks in order to diminish any habituation to the low frequency condition. This choice was prompted by our hypothesis concerning the role of the Locus Coeruleus, which is subject to habituation (see Introduction). Second, this arrangement enables a fairer comparison with the procedure used by Ottes et al., (1984). Indeed, the *F-20/T-Same* condition needs to appear first in order to maintain the effect of surprise that is likely to have occurred in the work of Ottes et al. (1984): the participants were not told that there would be trials with two stimuli. The palindrome order within participant was used to minimize any linear training effects. We also checked that our results hold when order effects are taken into account.

3 Data Analysis

All the analyses were conducted with *scipy* (McKinney, 2010), the scientific package for python (e.g. www.python.org), and with *ipython 2.0* (Perez & Granger, 2007).

3.1 Saccade Detection and Cleaning

A custom algorithm detected saccade end points for each trial as being the first data point at which the eyes had a velocity below 10°.s^{-1}, an acceleration below 6.000°.s^{-2}, and a shift from the fixation above 1.0°. The algorithm found potential saccade initiation by looking for the last data points at which the eyes had a velocity below 30°.s^{-1}, an acceleration below 6000°.s^{-2}, and a shift from fixation below 0.3°. The difference in criteria for saccade end and start points were implemented to deal with an artefact that can occur at the end of saccades (see Nyström et al., 2013, for more information of this post-saccadic oscillation artefact). Our algorithm tends to catch the landing position of the saccade after this artefact, which is exactly what we require. The algorithm also detected trials containing more than one saccade, and these were deleted from the analysis here.

A second algorithm was run across the results of the first algorithm and highlighted suspect trials according to the following rules: 1) there were missing values or gaze positions outside the monitor (40 pixels of tolerance) during the saccade, 2) either no start or no end of the saccade was detected, 3) the time between the target onset and the detected start of the saccade –i.e. the reaction time-- was less than 80ms, 4) the saccade duration was longer than the reaction time, and 5) the position shift from the fixation was less than 7.5°. After the list of suspects had been created, the experimenter undertook a visual check of all the trials for approval of this list. Most of the amendments to the list either involved excusing a suspect trial that presented a position outside the monitor display, or rejecting a trial that presented a blink. The trials with gaze positions outside the monitor display were kept if explicable in terms of an obvious drift of the fixation point in the recording system.

After cleaning, the loss rates were 1.7%, 4.5%, 1.5%, 3.4% and 2.2% for AN, BD, KM, GM and RI, respectively.

3.2 Landing Positions

We assumed that, for all the trials that passed the cleaning step, the participants were properly fixating on the initial cross. Hence, our coordinate system is centred on the gaze position at the start of the saccade. The landing positions correspond to the endpoint positions of the first saccade produced after the onset of the stimuli.

For each of the 8 stimulus distances that we tested, there were 4 possible target positions (one per quadrant); for the analysis, the data were mirrored and combined so that we considered only one target position per stimulus distance.

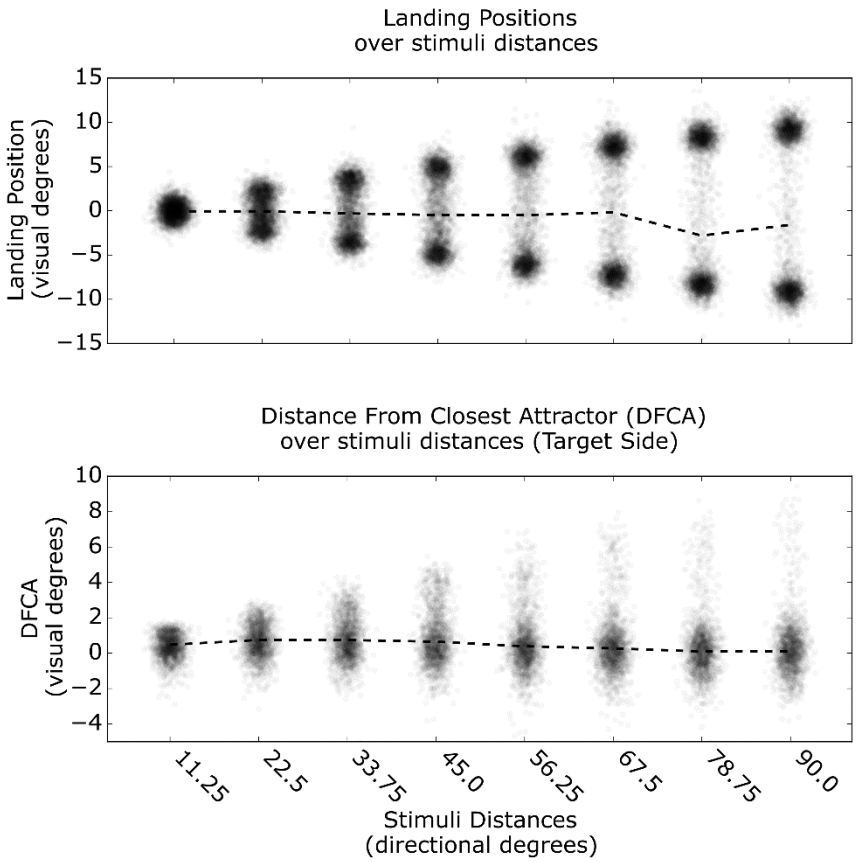

Figure 4-3: Presentation of the Distance from the Closest Distractor on Target Side. *The transformation that the DFCA makes on the landing positions can be observed by comparing the top plot and the bottom plot (see section 3.3 for further details). The DFCA on target side is no more than the landing positions on target side in double-stimulus trials centred on the mean of the landing positions in single-stimulus trials. The dashed lines represent the medians of the distributions. The data are from all the participants.*

3.3 Measure of the Global Effect: the Distance from the Closest Attractor

We are interested in testing the effect of *Pair-Frequency* (i.e., F-20 / F-80) and *Pair-Type* (i.e., T-same / T-Different) on the Global Effect (GE). Here, we use a general definition of the GE rather than the restricted definition requiring a unimodal distribution (see Introduction).

Previous measures in the literature often assume a unimodal distribution of the landing positions and measure the GE from the mean landing position of saccades (Casteau & Vitu, 2012; Heeman et al., 2014; R. Walker et al., 1997). Here, however, we want to quantify GE in bimodal distributions. Moreover, we would like to address the possible asymmetry in GE

between the two modes. Indeed, in our different conditions, the levels T-Different and T-Same manipulate the symmetry of the stimulus pair, and this could affect the symmetry of the GE. For these reasons, our new GE measure divides the landing positions into two groups: those directed towards the target, and those directed towards the distractor. We also computed a control position for each group from the single-stimulus trials – this estimates the mean of the landing positions in the case where the target or the distractor is presented alone. We then examined the deviation of each group from their control. The controls were computed across the four screen quadrants (we mirrored the data and collapsed them to one quadrant), and are distance specific (i.e. one control per distance), participant specific, and block specific (to correct for calibration discrepancies). As we collapsed the four quadrants into one, we had the same control for the target side and distractor side: we only changed its sign. We named the measure the Distance From the Closest Attractor (DFCA) – the attractors being the control positions. For the landing position *i* and on the y-axis, this is defined mathematically, by:

$$DFCA_i = \min(|C_1 - y_i|, |C_2 - y_i|)$$

Where C1 and C2 are the control position.

Figure 4-3 shows the DFCA for saccades directed toward the target. Note that another major difference with the usual measure of the GE is that we get one measure per trial, which allowed us to use more powerful statistic tools (thus increasing the statistical power).

3.4 Statistical analysis

The statistical analysis of this data set was challenging for the following reasons: 1) we wanted to use all the data points in the statistical analysis in order to detect small effects, 2) the DFCA violates the assumptions of normality, and 3) Participants need to be treated as a random effect. A standard ANOVA would collapse the participant's data points to their mean and this is not appropriate considering the fact that we ran only 5 participants. Furthermore, it would not make use of the statistical power permitted by a *per trial* measure of the GE. Concerning the violation of normality, it appears to be a false problem in our case: it is not the distribution of the participant means which is not normal but the DFCA distribution within a participant. Furthermore, we are, in fact, interested in how much the outliers (the centric saccades) shift the mean of the DFCA distribution – because these saccades are the most representative of the GE. Consequently, using a statistical model that assumes a normal distribution is not a problem as long as *it is sensitive* to outliers. Finally, we choose to report two statistical tests: 1) a multiple

comparison approach using a non-parametric Mann-Whitney U-tests along with a within-participant correction; and 2) a parametric Bayesian top-down test of the possible mixed linear models considering the participant as a random effect.

3.4.1 Running Mann-Whitney U-tests:

To test statistically the difference in DFCA across conditions and distances, the saccades of all the participants were gathered (as in Van der Stigchel & Nijboer, 2013). **Figure 4-3** shows an example of the resulting DFCA distributions. This led to an average of 389 trials for each distance in each condition for the conditions *(T-Same | F-20)* and *(T-Different | F-20)* and an average of 1,543 trials for the conditions *(T-Same | F-80)* and *(T-Different | F-80)*. Given that the distributions of DFCA were suspected to be non-normal we decided to use the non-parametric independent 2-group Mann-Whitney U-test to test for mean differences (the `wilcox.test(x, y, paired=FALSE)` in R). The R code sources and data are available at: https://github.com/Nodragem/Chapter-GlobalEffect-Statistic. In order to focus on differences within participants, and because the U-test does not apply this by itself, we applied a within-subject correction (Cousineau, 2005) to our data set. This means that we centred the data of each participant on the same mean. The condition effects (difference between conditions) are reported with the Hodges–Lehmann estimator (HLΔ). It is the median of all possible differences between the N measures in one condition and the M measures in another condition (N x M combinations). A non-parametric 0.95 confidence interval for HLΔ accompanies these estimates. Finally, the Common Language Effect Size (CLES) (McGraw & Wong, 1992; Vargha & Delaney, 2000) from the R package `orddom` is reported. Indeed, the CLES simply estimates the probability that a DFCA randomly picked from one distribution is higher than a DFCA randomly picked from another distribution -- also known as the Probability of Superiority. Generally speaking, a CLES of 0% (or 100%) would mean that the first distribution is lower (or higher) and does not overlap with the second distribution. When the CLES is at 50% the medians of both distributions are aligned.

Using the DFCA, we first addressed the effect of *Pair-Type.* We ran one U-test for each of the eight stimulus distances testing for an effect of *Pair-Type* (level *T-Different* against level *T-Same*). Thereafter, the same procedure was repeated to test the effect of *Pair-Frequency* across stimulus distances (level *F-20* against level *F-80*). It should be noted that the p-values for a set of tests were corrected according to Bonferroni's correction.

3.4.2 Bayesian Mixed Models: Top-Down analysis.

Although the U-test procedure tried to correct for within-participant variance, the fact that we gathered the data of all the participants into one distribution could be considered as problematic. In order to address this concern and to double-check our results using an alternative method, we conducted a Bayesian Mixed Models top-down analysis with participants as a random factor (Rouder & Morey, 2012), using the Bayes Factor package in R, available at: http://bayesfactorpcl.r-forge.r-project.org/).

Top-down analyses are based on a reference model, often referred to as the full model. In a preliminary step, the test estimates how good the full model is in explaining the data. In a second step, it estimates how good each model that omits one - and only one - variable of the full model is in explaining the data. In the Bayes Factor framework, we are given the weight of evidence for each omitting model against the full model. This tells us how much each variable plays a role in explaining the data. The weight of evidence provided is the Bayes Factor (BF). Bayes Factors are odds which tell us if the data that we observed are more likely to happen either when the omitting model is assumed to be true or when the full model is assumed to be true. When the BF is smaller than 1 it favours the full model – and so supports a role of the omitted variable - when it is higher than 1 it favours the omitting model – and so gives support for the claim that the omitted variable has no role.

Our interpretation of the BF, in the case where it tests a model 0 against a model 1 (BF_{01}), will follow the scale proposed by (Raftery, 1995). A reproduction of this table can be found below.

Table 3: Interpretation of the Bayes Factor in Terms of Evidence.

Bayes Factor BF_{01}	Pr($model_0$|Data)	Evidence
1-3	.50-.75	Weak
3-20	.75-.95	Positive
20-150	.95-.99	Strong
>150	>.99	Very strong

4 Results: Distance From Closest Attractor

Observation of **Figure 4-4** reveals that the DFCA initially increases and then decreases with the stimulus distances, which is how the GE is expected to fluctuate when the landing position is not normed by the stimulus distance. It is important to recall that the DFCA divides the landing positions into two groups: 1) the points closer to the target/S1 and 2) the points closer to the distractor/S2. From this, we computed their distance from the corresponding control. It is important to note that the proportion of landing positions between the two aforementioned groups was reasonably balanced in all conditions and participants; see Appendix B, **Figure 4-15**. We propose an overview of the data at participant level in Appendix B.

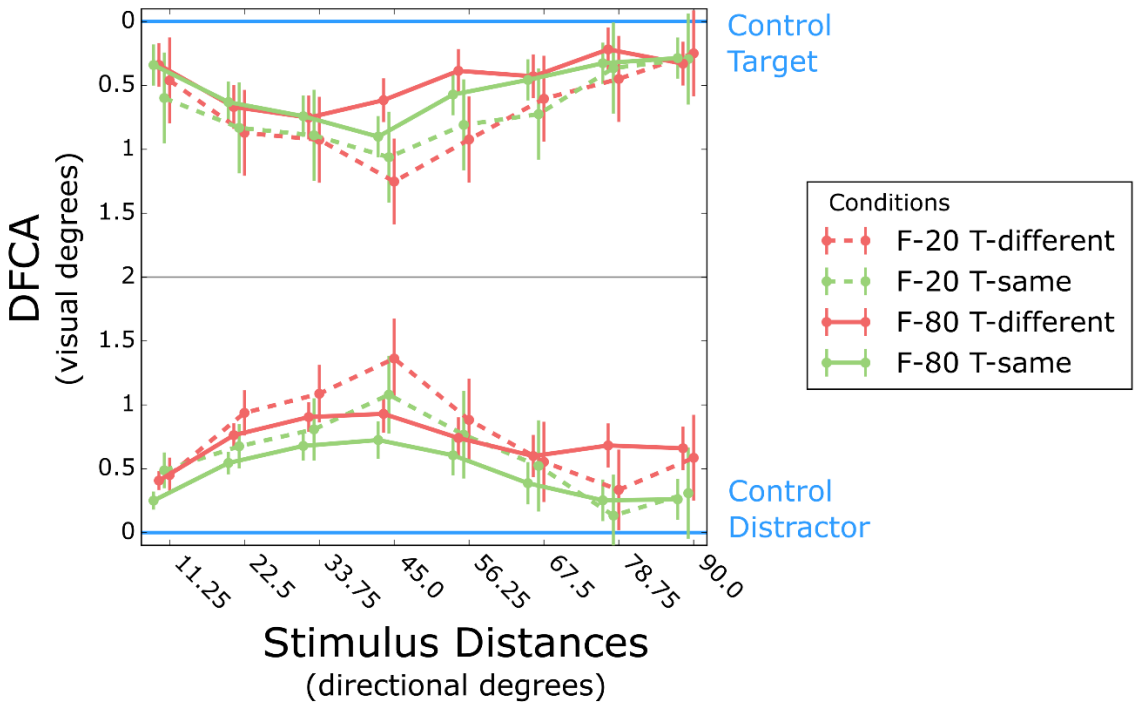

Figure 4-4: Overview of the Distance From the Closest Attractor (DFCA) over stimulus distances and between conditions. *The figure shows the mean of the distributions with the parametric 95% confidence intervals; the upper part displays the curves for the DFCA on the target side, and the lower part displays the curves for the DFCA on the distractor side.*

4.1 Mann-Whitney U-tests: Asymmetric Effect of Pair-Type and Symmetric Effect of Pair-Frequency

Table 4 and Table 5 report the results of the U-tests for *Pair-Type* on the target and distractor sides, respectively. Table 6 and Table 7 report the results of the U-tests for *Pair-Frequency*, again on the target side and distractor side. Finally, **Figure 4-4** provides a summary of all the tables.

Figure 4-5A shows that the U-tests yielded significant effects of *Pair-Frequency* both on the S1 side and the S2 side. In particular, **Figure 4-5**A suggests a symmetric increase of the GE when double-stimulus trials are rare (F-20). For both the S1 and S2 side, the increase in GE observed in F-20 tends to increase progressively with the stimulus distance, up to distance 45°, upon which it decreases. Finally, the effect of F-20 on the S2 side tends to decrease more rapidly with the stimulus distance in comparison with the S1 side. This small asymmetry could be attributed to the slight difference in luminance between stimulus S1 and S2 (We shall recall that in the Condition *T-Same*, S2 is similar to S1, but slightly brighter so that it matches the distractor luminance that is used in the *T-Different* conditions).

Interestingly, for the factor *Pair-Type* described in **Figure 4-5**B, the U-tests revealed 1) a significant effect for all distances but one (56.25°) on the distractor side and 2) a significant effect on the DFCA only at one distance (45°) on the target side. Furthermore, the effect on the distractor side is an increase in GE as opposed to the effect on the target side, which is a decrease in GE (**Figure 4-5**B, or Tables 7, 8). Specifically, our results suggest that the distribution of DFCA on the distractor side shifts toward the centre in *T-Different* conditions and that the effect size is rather regular over stimulus distances with a decrease around distance 56.25°. On its side the significant effect at distance 45° on the target side shifts the distribution toward the target. However, **Figure 4-4** suggests that the specific effect at distance 45° has opposite directions in F-80 conditions and F-20 conditions. This discrepancy makes this effect difficult to interpret and suggests an interaction between Frequency and Type. In summary, we observe an asymmetric increase in the GE when the participant is asked to aim towards a target and avoid a distractor (T-Different), whilst saccades directed to the distractor tend to be shifted toward the centre.

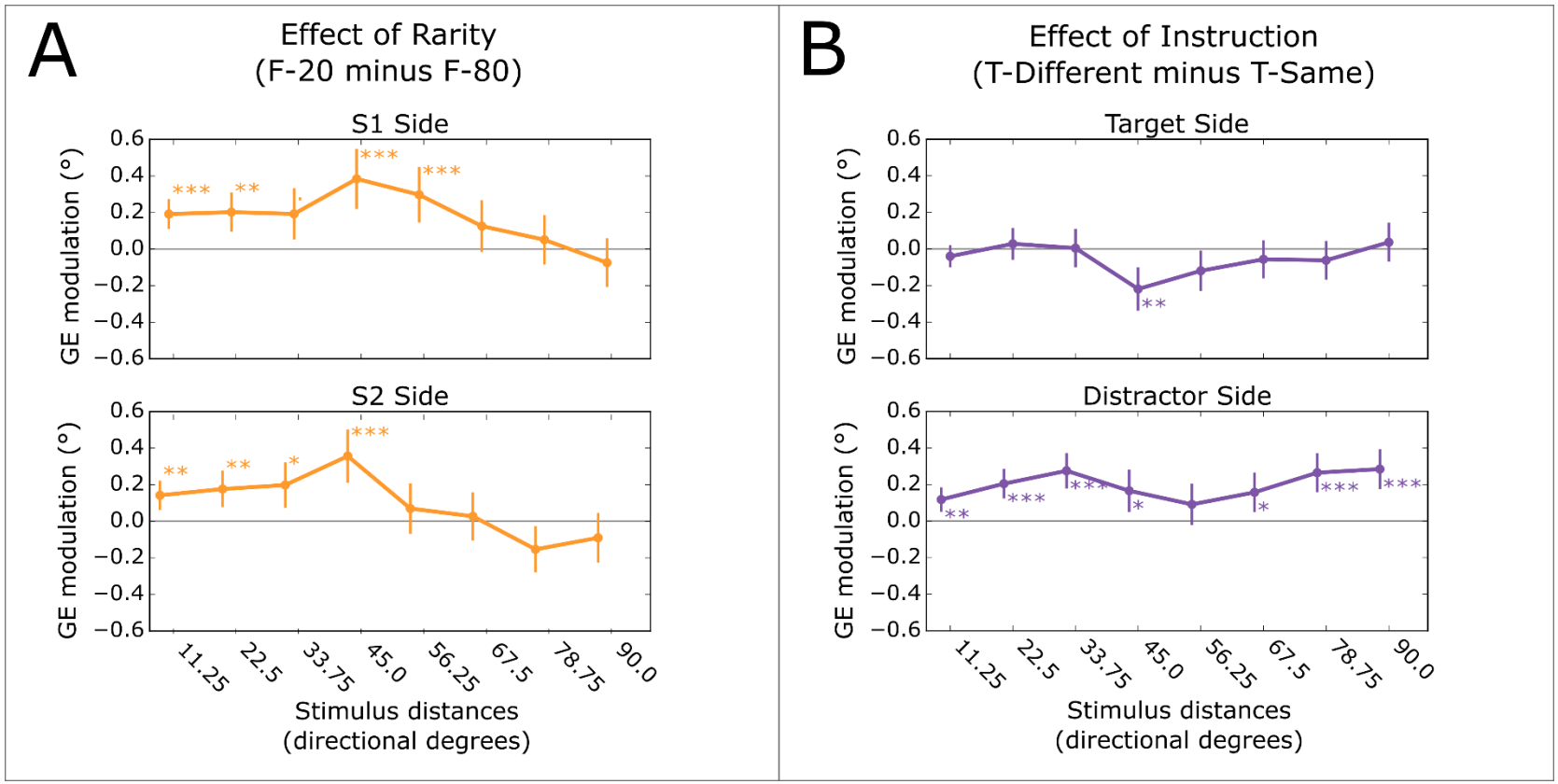

Figure 4-5: Summary of the Mann-Whitney U-tests. *Each plot shows the difference in DFCA between the two conditions, which we name the GE modulation: a positive number means that there is a larger GE in F-20 than in F-80 conditions (in* ***subplot A****) or a larger GE in T-Different than in T-Same conditions (in* ***subplot B****). Note that a larger GE means a deviation of landing position towards the centre. Each plots shows the Hodges–Lehmann estimators (HLΔ) of the GE modulation – i.e. the median of the DFCA differences (see section 3.4.1) - with 95% confidence intervals. The stars represent the level of significance as in Table 5 and Table 6.* ***A:*** *We ignored the factor Pair-Type, mixing the conditions T-Same and T-Different. Note that we refer to S1 and S2 as the two stimuli presented simultaneously; S2 corresponds to the slightly brighter one in T-Same conditions and to the distractor in T-Different conditions.* ***B:*** *We ignored the factor Pair-Frequency, mixing the conditions F-20 and F-80. Note that the stars displayed in the graphs represent the degree of statistical significance for the HLΔ being different from zero.*

Table 4: Target Side U-tests over distances for a distractor type effect (T-Same against T-Different):

Distance	U-stat		p-value	n.Td	n.Ts	CLES	HLΔ	95% CI	
11.25	433851		1.00E+00	981	915	51.67%	-0.040	-0.102	0.022
22.5	460714		1.00E+00	997	909	49.16%	0.028	-0.059	0.115
33.75	458158		1.00E+00	983	930	49.88%	0.005	-0.101	0.110
45	412946	**	2.78E-03	998	914	54.73%	-0.219	-0.338	-0.099
56.25	432647		2.55E-01	1063	863	52.84%	-0.119	-0.230	-0.011
67.5	479230		1.00E+00	1065	925	51.35%	-0.056	-0.161	0.049
78.75	430544		1.00E+00	1035	858	51.52%	-0.062	-0.168	0.045
90	451448		1.00E+00	1007	881	49.11%	0.037	-0.070	0.143

Note. Refer to Table 2 note.

Table 5: Distractor Side, U-tests over distances for a distractor type effect (T-Same against T-Different):

Distance	U-stat		p-value	n.F8	n.F2	CLES	HLΔ	95% CI	
11.25	452304	**	5.10E-03	970	1023	54.42%	-0.118	-0.185	-0.050
22.5	423556	***	5.45E-06	950	1024	56.46%	-0.205	-0.285	-0.125
33.75	413434	***	3.81E-07	948	1017	57.12%	-0.275	-0.373	-0.177
45	451307	*	3.88E-02	953	1022	53.66%	-0.166	-0.282	-0.051
56.25	442758		8.91E-01	877	1054	52.10%	-0.091	-0.204	0.021
67.5	397084	*	3.35E-02	869	990	53.84%	-0.157	-0.266	-0.050
78.75	415780	***	7.91E-06	904	1055	56.40%	-0.265	-0.372	-0.159
90	406350	***	2.51E-06	915	1026	56.72%	-0.284	-0.394	-0.176

Note. Refer to Table 2 note.

Table 6: Target Side, U-tests over distances for a distractor frequency effect (F-20 against F-80):

Distance	U-stat		p-value	n.F8	n.F2	CLES	HLΔ	95% CI	
11.25	225235	***	2.52E-05	1550	346	58.00%	-0.192	-0.273	-0.111
22.5	259148	**	1.35E-03	1516	390	56.17%	-0.202	-0.309	-0.097
33.75	252640	.	5.10E-02	1555	358	54.62%	-0.193	-0.332	-0.055
45	228095	***	3.26E-05	1566	346	57.90%	-0.384	-0.549	-0.219
56.25	245242	***	7.39E-04	1565	361	56.59%	-0.297	-0.449	-0.148
67.5	279013		6.15E-01	1625	365	52.96%	-0.126	-0.268	0.014
78.75	267306		1.00E+00	1536	357	51.25%	-0.051	-0.186	0.085
90	287083		1.00E+00	1525	363	48.14%	0.074	-0.059	0.207

Note. Refer to Table 2 note.

Table 7: Distractor Side, U-tests over distances for a distractor frequency effect (F-20 against F-80):

Distance	U-stat		p-value	n.F8	n.F2	CLES	HLΔ	95% CI	
11.25	376754	**	4.34E-03	1556	437	44.59%	0.142	0.062	0.222
22.5	344744	**	4.80E-03	1582	392	44.41%	0.176	0.076	0.275
33.75	360737	*	1.44E-02	1538	427	45.07%	0.198	0.074	0.320
45	387352	***	1.15E-05	1537	438	42.46%	0.356	0.210	0.503

56.25	323915	1.00E+00	1517	414	48.42%	0.069	-0.069	0.208
67.5	299833	1.00E+00	1451	408	49.35%	0.027	-0.105	0.158
78.75	302211	1.29E-01	1532	427	53.80%	-0.154	-0.281	-0.028
90	295816	1.00E+00	1540	401	52.10%	-0.090	-0.226	0.047

Note. Refer to Table 2 note.

4.2 Top down Bayesian Analysis: Evidence against Interaction between Pair-Type and Pair-Frequency

The result of the comparisons between omitting the model against the full model can be seen in Table 8. In addition to the main effects, the top-down analysis tested for an interaction of *Pair-Frequency* and *Pair-Type* with the DFCA *Side* (i.e., S1/S2 or Target/Distractor sides). Furthermore, we chose to test for an interaction effect between *Pair-Frequency* and *Pair-Type*, and between *Pair-Frequency* and *Distance* as the possibility of such interactions was raised in the previous sections.

This analysis (see Table 8) suggested a main effect of *Distance*, *Pair-Type* and *Pair-Frequency*. It also supports an interaction of *Pair-Frequency* with *Distance* and no interaction between *Pair-Type* and *Distance*. Moreover, very strong evidence was found for an interaction of *Pair-Type* with DFCA *Side*. This corroborates that the GE increases only on the distractor side when the distractor has to be discriminated and avoided – i.e., the effect of *Pair-Type* on GE is asymmetric. Interestingly, the evidence for an interaction between DFCA *Side* and *Pair-Frequency* is weak; there is not enough evidence to conclude either against or in favour of the interaction (i.e., whether the effect is symmetric or not).

We thought that this uncertainty could be caused by an interaction with *Distance*. In the previous section, the effect of *Pair-Frequency* appeared to decrease more rapidly over distances on the distractor side (**Figure 4-4**C). We therefore ran an alternative full model taking into account the interaction *Distance:PairFrequency:Side*. The top-down analysis yielded strong evidence (BF=24.1± 27.0%) against such an interaction. Considering that the analysis was still in favour of an interaction *Distance:PairFrequency* (BF= 0.058±7.6%), this result suggests that the effect of *Pair-Frequency* is symmetric (i.e., no effect of *Side*).

Finally, returning to the main analysis (Table 8), there is strong evidence against an interaction between *Pair-Frequency* and *Pair-Type*. It can also be noted that there is strong evidence against a participant effect, due to the within-participant correction applied previously.

Table 8: Bayes factor top-down analysis on DFCA.

	Omitted Effect	BF		Interpretation Tag	Polarity
[1]	PairFrequency:PairType	72.1	±35.79%	strong	against
[2]	Distance:PairType	15.2	±25.57%	positive	against
[3]	PairFrequency:Side	1.29	±7.76%	weak	against
[4]	Distance:PairFrequency	0.0799	±7.57%	positive	in favour
[5]	Side:PairType	1.00E-15	±6.67%	very strong	in favour
[6]	Participant	9.25E+6	±7.22%	very strong	against
[7]	Distance	1.0E-18	±9.92%	very strong	in favour
[8]	PairFrequency	8.21E-12	±6.95%	very strong	in favour
[9]	Side	15.9	±8.05%	positive	against
[10]	PairType	0.00220	±13.03%	very strong	in favour

Note. The symbol ":" indicates interaction. Against denominator: DFCA ~ PairType + Side + PairFrequency + Distance + Participant + PairType:Side + PairFrequency:Distance + Side:PairFrequency + PairType:PairFrequency

We shall recall that we used a particular ordering of our condition blocks. We thought there was perhaps a surprise effect in the paradigm employed by Ottes et al. (1984) as the participants were not told that there would be double-stimulus trials. A Wilcoxon rank-sum test conducted on the DFCA between the first block and the second block of *F-20/T-same* yielded a significant difference (W= 12E+7, p=0.002) with a small effect size (-0.04°) compared to the effects observed in **Figure 4-5** (from 0.2° to 0.4°). Thus, it appears that any surprise effect across participants was small or did not last long enough within the first block to produce a large overall effect. Finally, it is important to test whether the effects that we reported in the results section can be explained by an ordering effect. We ran a Top-down Bayesian Analysis with a full model taking in account the effect of blocks in addition to the effects found earlier (labelled *in favour* in Table 8). Even though there is strong evidence for an effect of block, the effects previously reported are maintained (see Table 9).

Table 9: Bayes factor top-down analysis on DFCA, Ordering Effect (i.e., effect of Block).

	Omitted Effect	BF		Interpretation Tag	Polarity
[1]	Distance:PairFrequency	0.00281	±4.74%	very strong	in favour
[2]	Side:PairType	9.23E-16	±14.2%	very strong	in favour
[3]	Block	0.0276	±3.96%	strong	in favour
[4]	Distance	3.58E-100	±4.41%	very strong	in favour
[5]	PairFrequency	9.62E-13	±3.99%	very strong	in favour
[6]	PairType	0.00139	±27.26%	very strong	in favour

Note. The symbol ":" indicates interaction. Against denominator: DFCA ~ PairType + PairFrequence + Distance + Block + Participant + PairType:Side + PairFrequence:Distance

5 Discussion

In the present study, we examined whether the strength of the Global Effect (GE) and spatial profile can be modulated and controlled by endogenous signals that are supposedly external to the SC. Confirmation of this possibility would then promote the GE to the rank of a tool that permits the assessment of signals involved in decision-making processes. In particular, we tested for the two main categories of endogenous signals – goal-related and history-related – by means of the following two factors in our paradigm: 1) the requirement *or not* to discriminate and aim for a target during the two-stimulus trials (*Pair-Type*: T-Different | T-Same); and 2) the frequency of occurrence of the two-stimulus trials (*Pair-Frequency*: F-20 | F-80). Our paradigm was based on a simple saccade-to-target task in which trials could involve the presentation of either a single stimulus or a pair of stimuli, with eight possible stimulus distances. We first introduced a new measure – the Distance From the Closest Attractor, which quantifies the GE for bimodal distributions of landing positions for each stimulus side. Next, using a non-parametric test, we highlighted an effect of the aforementioned factors on the GE. The GE increased on both stimulus sides –i.e. symmetry - when the double-stimulus situations were rare (F-20) compared to when they were frequent (F-80). This effect of *Pair-Frequency* decreased with stimulus distances. On the other hand, only the GE on the distractor side increased – i.e. asymmetry - when the participant had to discriminate and aim for a target among two dissimilar stimuli (T-Different) compared to when the participant was making a free choice toward one of two similar stimuli (T-Same). This effect of *Pair-Type* was stable for almost all of the tested stimulus distances. Thus, *Pair-Frequency* and *Pair-Type* draw two clearly distinguishable patterns in terms of modulating the GE. We will next discuss the possible mechanisms that could be responsible for such a difference.

5.1 The Global effect: more than one mechanism?

The Global Effect (GE) has been defined on many occasions over the years. It has been proposed that the *genuine GE* involves the observation of a unimodal distribution instead of a bimodal distribution when comparing with single target controls (Van der Stigchel & Nijboer, 2013). A more general definition is that the GE is an increase of centripetal saccade endpoints compared to a single target control condition. In the latter definition, one can still observe GE in bimodal distributions, and instances of this version of the GE have been observed in the past (Arai et al., 2004; Van der Stigchel et al., 2011). The purpose of the work presented here was to

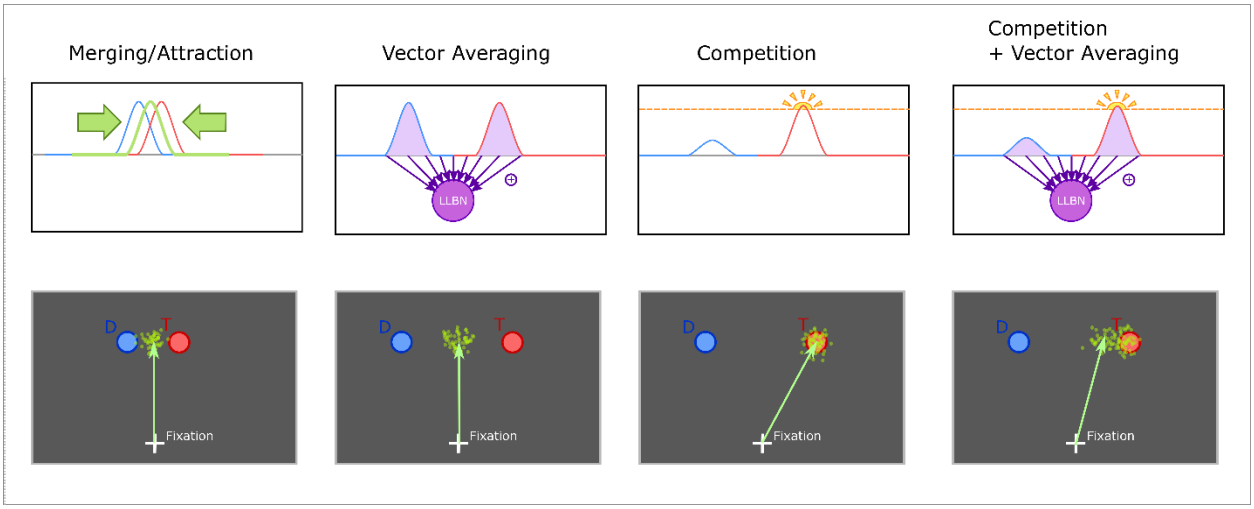

Figure 4-6: Summary of Different Mechanisms at Play during Saccadic Action Selection. *We suggested that the combination of competition and vector averaging (or vector summation) leads to what we call the bimodal Global Effect (schema on the right), see text for details. In the figures of the bottom row, we represent the spatial configuration of different stimuli (D: distractor; T: target) on the monitor screen; the green arrow represented the average saccadic vector while the green dots draw the distribution of the saccade endpoints.*

quantitatively report this effect. However, such a GE raises some issues when it comes to determining its underlying mechanism. There are two common accounts that have been proposed to explain the GE (see next page).

The first common account of the GE (see **Figure 4-6**, first column) is based on the hypothesis that the Superior Colliculus (SC) behaves as a dynamic neural field with short-range excitation and long- range inhibition. A strict and hard bifurcation from unimodal to bimodal distribution is easily reproducible even with a simple noise-free dynamic neural field model (see Chapter 2). A merging mechanism allows the bumps of activity induced by two close stimulations to merge into a single bump of activity (Amari, 1977). However, such a merging mechanism cannot explain the observation that saccade endpoints deviate toward the centre for bimodal distributions. In other words, it cannot explain the bimodal GE.

A second common account of the GE (see **Figure 4-6**, second column) is based on the vector averaging (which we argued to be explainable with the vector summation theory in General Introduction) that occurs downstream the SC. This population-coding mechanism does not merge close activity; it simply triggers the saccade that corresponds to the centre of gravity of the SC activation. When the GE occurs for express saccades, we can observe two bumps of activity in the SC (Edelman & Keller, 1998), a situation whereby only a population-coding

mechanism could explain the GE. However, this mechanism fails to explain the transition from unimodal to bimodal distributions of landing positions; on its own, for a specific pair of stimuli, it would always produce centred unimodal distributions. In other words, it would be unable to explain a bimodal GE.

Thus both common accounts of the GE failed to explain the bimodal GE. Before suggesting a solution, we need to highlight another important mechanism (see **Figure 4-6**, third column) at play in neural field models of the SC, which is not directly linked to GE, that is, the race/competition mechanism. When two remote stimuli are presented to the neural field, each induces a bump of activity. This is the first bump, which reaches an arbitrary threshold that wins and triggers an eye movement to the corresponding stimulus. Additionally, long-range inhibition (if present) can prematurely bias the race to threshold: if one of the racers gains enough of an advantage over the other, this other will begin to decrease – and may be doomed to lose. This competition is noisy, and can be lost by even the strongest stimulus. These occasions would occur at a rate inversely proportional to its contrast with the weaker stimulus.

The solution we suggest to explain the bimodal GE is a combination of the race/competition mechanism and of the vector averaging (see **Figure 4-6**, last column). When the winning stimulus reaches the threshold to trigger a saccade, the losing stimulus has raised a certain amount of activity in the SC. As seen in Chapter 3, which concerned saccade curvatures, the execution of the saccade can start before the selection of a single goal has been completed (McPeek et al., 2003). The bumps of activity induced by both the winning and losing stimuli is unselectively taken into account by the downstream vector averaging mechanism. As a result, there can be a centripetal deviation from the winning stimulus that is proportional to the performance of the losing stimulus on that trial.

It should be noted that the genuine GE is expected to decrease with stimulus distances, a relationship that we have also found when measuring the bimodal GE (see **Figure 4-4**A). In our frame of explanation, this decrease in GE with stimulus distance may be caused either by: 1) a stronger mutual inhibition between the two stimuli whilst their distance increases – decreasing the activity of the loser -- or 2) a spatial release of the inhibition that the substantia nigra pars reticulata (SNr) applies in the SC. This disinhibition zone would be centred on the race-winner so that the activity of the loser decreases as it moves further away from the winner. Indeed, the SNr is known to release its otherwise tonic inhibition of the SC during saccade execution. Furthermore, it is known to project topographically to the SC (Hikosaka &

Wurtz, 1983) and to have large receptive fields – i.e., low spatial resolution (Basso & Wurtz, 2002; Handel & Glimcher, 1999).

Finally, if an external structure/top-down process were to modulate the proposed GE mechanisms, it could do so by either 1) selectively helping or penalizing competitors or 2) modifying the race/competition mechanisms such as the threshold or the weight of lateral inhibition. Note that a third way would be to hinder the downstream averaging mechanism but we did not need to turn to this possibility to interpret our results.

5.2 Modulation of the Global Effect by Target Aiming Instruction

5.2.1 Link to previous literature

While recording saccade endpoints, Heeman et al. (2014) measured a shift in the mean of their distribution toward the target when the participants were instructed to aim for a specific stimulus from the presented pair. Their observation was made in a genuine Global Effect - i.e. unimodal distribution. They showed that this shift is observed for fast reaction time saccades. This suggests that the process of target discrimination has an early influence on the decision-making processes. The authors concluded that GE is not immune to top-down processes – indeed, target discrimination is considered to happen in cortical structures which project onto the SC (see Introduction). Note that a close replication of their analysis, method, and results can be found in Appendix A, section 6.2. Our work brings to light a new piece of information for understanding the top-down modulation observed by Heeman et al. (2014). Using a measure of GE on bimodal distributions, we succeeded in highlighting that it is primarily the endpoints of the saccade directed toward the distractor that are subject to a deviation. Moreover, this deviation is centripetal – i.e. toward the centre - (when comparing T-Different with T-Same) and is stable across stimulus distances. Note here that this centripetal deviation away from the distractor is consistent with the deviation toward the target that was observed by Heeman et al. (2014).

In addition, it should be noted that a very similar experiment to the one reported here has been conducted using monkeys. In particular, the results of a study by Chou, Sommer, and Schiller (1999), appear to run counter to those reported here: they found that there is a weaker GE when the monkey is instructed to aim for a specific target compared to when he is not (T-Different against T-Same, in our experiment). A starting point for explaining this discrepancy could be that they worked with stimuli differing in colour, while we worked with stimuli that

differed in terms of shape. Such a difference in the modality of the discrimination can influence the GE: it has been reported that distractor/target pairs defined by colour generate a weaker GE (Findlay & Gilchrist, 1997). Thus, the possibility of an interaction between the instruction conditions and the modality of the discrimination should not be ignored. A further explanation comes from the fact that Chou et al. were qualitatively judging whether the landing position distributions were unimodal to infer the presence of the GE. It is possible that our DFCA measure – which is quantitative - would detect a deviation on the distractor side. Although the authors do not specify this notion, their figure 12, bottom right, points toward this possibility if the top right stimulus is the target.

5.2.2 Revealed Mechanisms: Facilitation of the Target stimulus

We can readily explain our results with the bimodal GE mechanism presented above (Section 5.1). **Figure 4-7** summarizes the activity pattern that we assumed to be present in the neural field during the conditions T-Different and T-Same, when the distractor wins and when the target wins. In order to have a good understanding of **Figure 4-7**, it is important to note that: 1) the GE measured on the target side comes exclusively from situations where the target wins and so 2) the GE measured on the target side gives us an idea of the sub-threshold activity in the distractor side – and vice-versa.

For now, let us consider the purple curve in **Figure 4-4**B on the target side, which shows the difference in GE between the condition T-Different and the condition T-Same. For the sake of simplicity, let us momentarily assume that this purple curve is straight and at zero. This means there is no change in GE observed on the target side: the activity of the loser – i.e., the distractor - was the same in conditions T-Different and T-Same. This is represented with our model in **Figure 4-7** (On the 'Target wins' row, the blue bumps are the same). This suggests that there is no additional external signal penalizing or helping the distractor in T-Different when compared with T-Same. Having established the general pattern, it should be noted that the purple curve in **Figure 4-4**B is not perfectly flat, and is significantly below zero at Distance 45. This means there is an inhibition at the distractor location, which decreases the GE on the target side. The fact that this occurs only for a specific range of target-distractor distances suggests that there is a ring of inhibition around the target. This could possibly be related to Mexican hat shaped lateral connections, or it could be an artefact from inter-individual differences (we return to this issue in Appendix B, section 7.2).

On the other hand - using the same reasoning - let us consider the purple curve on the distractor side in **Figure 4-4**B. This curve indicates that there is globally a positive change in the GE for all distances when comparing T-Different with T-Same. The fact that there is a positive change in the GE on the distractor side means that the activity of the loser – i.e., the target - was stronger in T-Different than T-Same (this is represented in **Figure 4-7**, on the 'Distractor wins' row, the red curves are different). In particular, the target was aided by an external signal in condition T-Different. Again, it should be noted that the purple curve in **Figure 4-4**B is not entirely straight on the distractor side; there is a noticeable decrease at Distance 56.125, which could be taken to indicate a ring of inhibition around the distractor. This, again, could possibly be related to Mexican hat shaped lateral connections or it could be an artefact of inter-individual differences (further details in Appendix B, section 7.2).

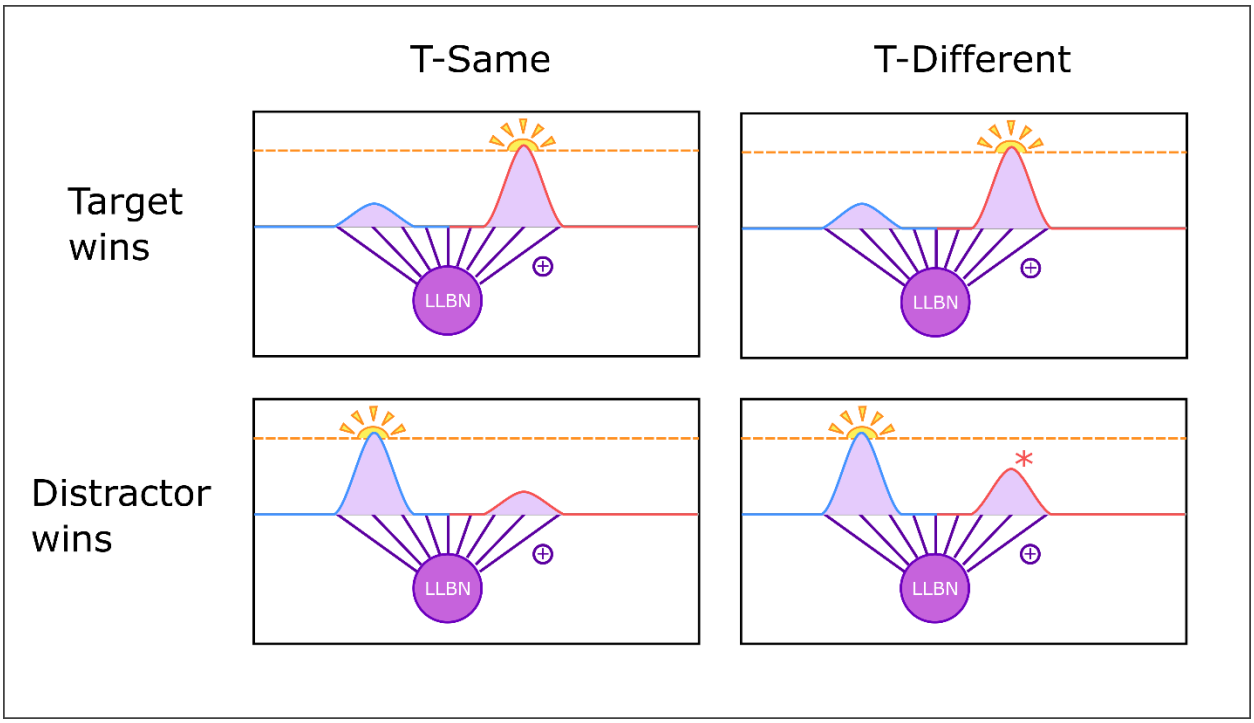

Figure 4-7: Effect of Instructions (i.e. PairType: T-Same or T-Different) on the Bimodal Global Effect. *Target is in red and distractor is in blue. Our results (see* ***Figure 4-4****B purple curves) reported an increase in the bimodal Global Effect only on the distractor side when using a couple target/distractor instead of two undistinguishable stimuli. When the distractor was selected to trigger a saccade (bottom row), there was still some activity on the target side (red curve) creating a centripetal deviation of the landing positions – i.e. the Global Effect. The increase in the Global Effect on the distractor side means that the activity on the target side was larger in the T-Different than in the T-Same condition. This suggests that the target location is receiving help in the T-Different condition.*

In the T-Different condition, instructions were given to the participants to aim for a target stimulus and ignore the distractor. It is assumed that in this situation, top-down mechanisms are attempting to discriminate the target (Ipata, Gee, Goldberg, & Bisley, 2006; Schall & Hanes, 1993; Schall, Hanes, Thompson, & King, 1995; N. W. D. Thomas & Paré, 2007; Wardak, Olivier, & Duhamel, 2002) while the visual bottom-up signals of the stimuli compete on the SC. It has been a matter of debate as to whether the discrimination system inhibits the distractor location or helps the target location in the SC (McSorley et al., 2004). Here, our work yields evidence supporting the presence of an excitatory signal sent on the location of the target stimulus, with no evidence supporting the possibility of inhibition of the distractor. It is important to note that the excitatory boost given to the target could not be inferred from analysing the difference in saccadic reaction times between T-Different and T-Same when the target wins. Indeed, the task of discriminating between a target and a distractor makes the reaction time slower for most participants (see **Figure 4-8**) so that it hides any excitatory effects.

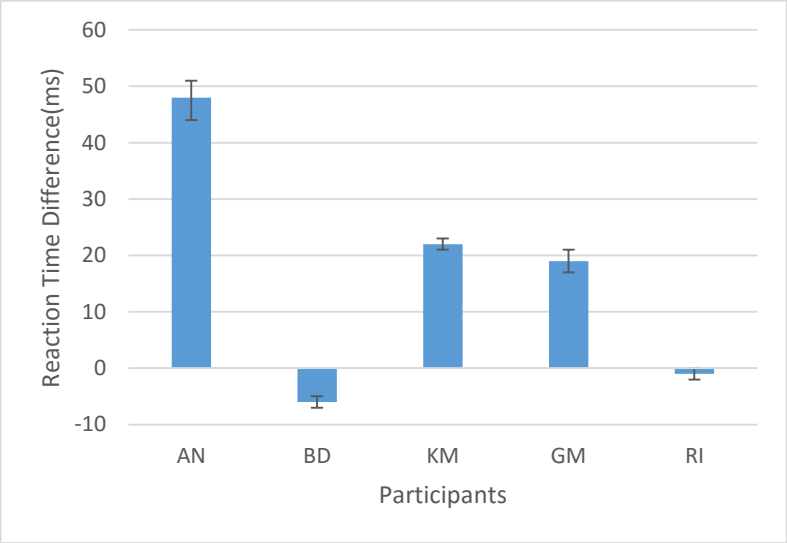

Figure 4-8: Differences in Reaction Times between conditions (T-Different – T-Same). *We plot the median estimate of the difference and its 95% of confidence intervals from a Wilcoxon rank sum test with continuity correction.*

Finally, as mentioned earlier, the bimodal GE decreases with stimulus distance (see **Figure 4-4**A, any curves), an effect that could be caused either by mutual inhibition or spatial disinhibition of the SNr (see section 5.1). The fact that the effect of T-Different does not decrease with stimulus distances suggests that its mechanism is not interacting with the mutual inhibition or with the SNr's signal. For instance, it is known that the FEF is involved in

target discrimination (Schall & Hanes, 1993) and has direct projections to the brainstem saccade burst generator, bypassing the SC to control saccades (Schiller & Chou, 1998; Schiller & Sandell, 1983; Schiller, True, & Conway, 1980). In the eventuality that there is mutual inhibition occurring in the SC, and that a boost to the target is provided by the FEF, it follows that at least part of this enhancing effect is not altered by mutual inhibition. With regard to spatial disinhibition from the SNr, it is possible that both its inhibitory signal and the excitatory signal of the FEF are linearly summed in the SCi, leading to no interaction. Indeed, such linear summation of signals in the SCi have already been reported (Phongphanphanee et al., 2014).

5.3 Modulation of the Global Effect by Frequency of Choice Occurrence

5.3.1 Link to previous literature

Previous studies have shown that the probability of a stimulus appearing at a specific location can influence the GE (He & Kowler, 1989). This stimulus location probability has been shown to influence the preparatory signal in the SC. It increases the preparation signal at the most probable locations (Dorris & Munoz, 1998) which is in line with the work of He and Kowler (1989). Our work goes further and suggests that a probability of occurrence, which, unlike location probabilities, has no spatial dimension, can influence the GE. To the best of our knowledge, the effect of the frequency of occurrence of double-stimulus trials had never been addressed prior to the present study.

5.3.2 Revealed Mechanism: a Global Modulation of the Competition

As there is no spatial dimension attached to a frequency of occurrence, our hypothesis is that the factor *Pair-Frequency (F-20 / F-80)*, which controls the frequency of double-stimulus trials, will have an unselective effect on the entire selection map (i.e. the SC). This would be consistent with there being a global projection of the Locus Coeruleus to the SC (Arce et al., 1994; S. B. Edwards et al., 1979; Mooney et al., 1990), which is known to respond to frequency of occurrence and uncertainty (Duzel & Guitart-Masip, 2013).

Let us consider the orange curves of **Figure 4-5**B. These curves show the difference in the GE in condition F-20 (low frequency of two-stimulus trials) and condition F-80 (high frequency of two-stimulus trials). We can readily observe an increase in the GE in the F-20 conditions, for the shortest stimulus distance, on both stimulus sides (target and distractor, top and bottom plot). Within the framework of the GE mechanism introduced earlier, the fact that the GE

increases on both sides means that whichever wins the competition, the loser was more active in F-20 than in F-80 conditions (this is represented in **Figure 4-9**). This *unselective effect* (occurring regardless of the winner) is in line with our afore-mentioned hypothesis.

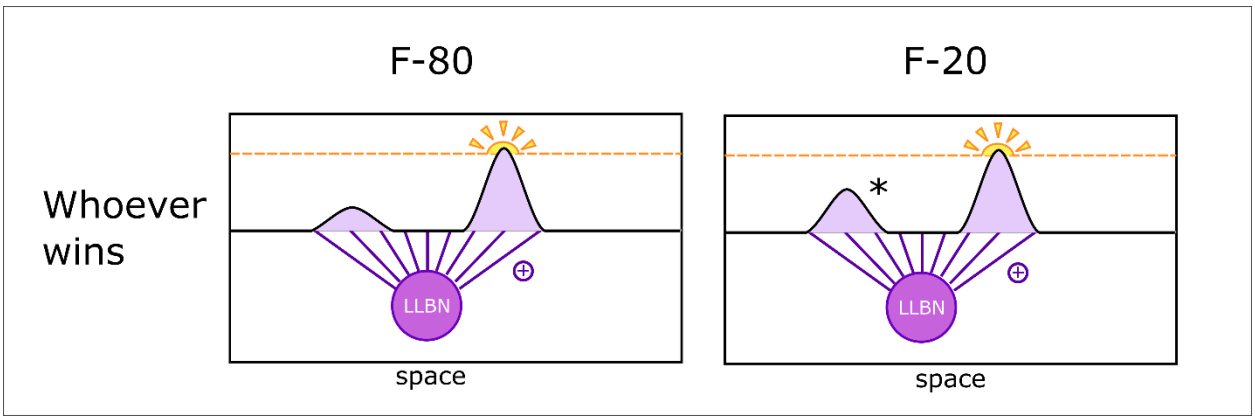

Figure 4-9: Whichever wins the competition, the loser receives more activation in condition F-20. *This increases the bimodal GE on both stimulus sides (see the orange curves, target and distractor side in* ***Figure 4-4****B).*

In addition, it can be observed that the effect of F-20 decreases with the stimulus distance. As mentioned earlier, the bimodal GE also decreases with stimulus distance (see **Figure 4-5**A, any curves). This was explained by means of either an increasing mutual inhibition with stimulus distance or spatial disinhibition from the SNr. The fact that the effect of F-20 decreases with stimulus distance suggests that its mechanism is interacting positively with mutual inhibition and/or spatial disinhibition. This means that the effect of F-20 is directly affecting the property of the neurons that are involved in mutual inhibition and/or spatial disinhibition. This would be consistent with the idea that an external structure, e.g., the Locus Coeruleus, is affecting the responsiveness of SC neurons (see the adaptive gain theory, Aston-Jones & Cohen, 2005).

Finally, note that the effects on reaction time distributions were not consistent across all the participants. However, a pattern that we observed for three of the five participants is discussed further in Appendix 7.1.

5.4 On Ottes et al. (1984), Walker et al. (1997), and Ordering Effect

It appears that our experiment has yielded a number of interesting findings, along with the tools for understanding and interpreting these results. However, we conclude with one of our initial aims which was to test if there is an actual difference in the GE when comparing the

results of Ottes et al. (1984), which encouraged our use of condition F-20 / T-Same, and the results of Walker et al. (1997), which prompted us to use condition F-80 / T-Different. Importantly, their results can be compared only for a stimulus distance of 90°. The hypothesis was that rarity and/or lack of instructions would increase the GE. First, we found that rarity can increase the Global Effect on both target and distractor sides. However, given that rarity had no significant effect at the distance of 90°, this does not support a difference between the results of Ottes et al. (1984) and Walker et al. (1997). Second, we detected that the presence of instructions (T-Different) increased the GE, but only on the distractor side. Unfortunately, Walker et al. (1997) could not detect this asymmetric effect in their study because this was not possible with their measures. To conclude, the measure of GE and general paradigms used by both Ottes et al. (1984) and Walker et al. (1997) were quite different, making it difficult to assess an effect of frequency (Pair-Frequency) and instructions (Pair-Type). Based on a novel definition of GE, our work has yielded evidence and details of these effects, whilst suggesting a possible mechanism to interpret them.

5.5 Conclusion:

The present work has generated a novel way to assess decision processes and signals occurring in an action selection map such as the SC. In particular, we have examined a different aspect of the Global Effect, which we have termed the bimodal Global Effect (GE). Unlike the traditionally defined Global Effect (R. Walker et al., 1997), the bimodal GE can be observed for distant stimuli and for bimodal distributions. We provide a measure to quantify the bimodal GE and we also suggest a biologically coherent mechanism to account for the phenomenon. We suggest that the mechanism underlying the bimodal GE differs from the merging mechanism that has sometimes been proposed to explain the traditional Global Effect (see Section 5.1). Furthermore, using this novel aspect of the GE, our work provides a deeper understanding of how frequency of choice and active discrimination modulate decision-making. Indeed, the specified mechanism of the bimodal GE is shown to be of great use in interpreting the modulations that occur on the side of the stimulus that loses the race to trigger a saccade. In combination with the reaction time distributions, which allow us to interpret what happened on the race winner side, the bimodal GE may become a powerful tool for specifying the precise spatio-temporal patterns of endogenous/exogenous signals on an action selection map. It can be noted that additional future directions and guidelines concerning inter-individual differences can be found in the concluding remarks of Appendix B.

6 APPENDIX A: Replication of Previous Studies

6.1 A Replication of Goldstein and Beck (2013): Reaction Time and Distractor Presentation Frequency

One of the expected effects of manipulating the frequency of distractor presentation (two stimuli trials) is to affect the saccade reaction times (RT) as observed by Goldstein and Beck (2013). The **Figure 4-10** shows the distribution of RT observed for each participant and conditions. The effect observed by Goldstein and Beck (2013) was an increase of 60ms of the RT mean in the low frequency condition while they used a couple target/distractor – i.e. this should correspond to our F-20 / Different condition. In our data, the RT of BD and RI seems to not have been affected by the conditions, whereas AN, KM, and GM show a clear effect of Frequency which interacts with the type of double-stimulus (T-Same or T-Different). F-20 makes the responses faster in T-Different whereas it makes them slower in T-Same. Thus, the effect of F-20 we found in T-Different is totally opposite to the effect found by Goldstein and Beck (2013). Nevertheless, this can be explained by the fact that in their paradigm the target position was quite predictable which reduced the need for discrimination. From this, their task may be closer to our T-Same condition -- the results of which are in the same direction as theirs.

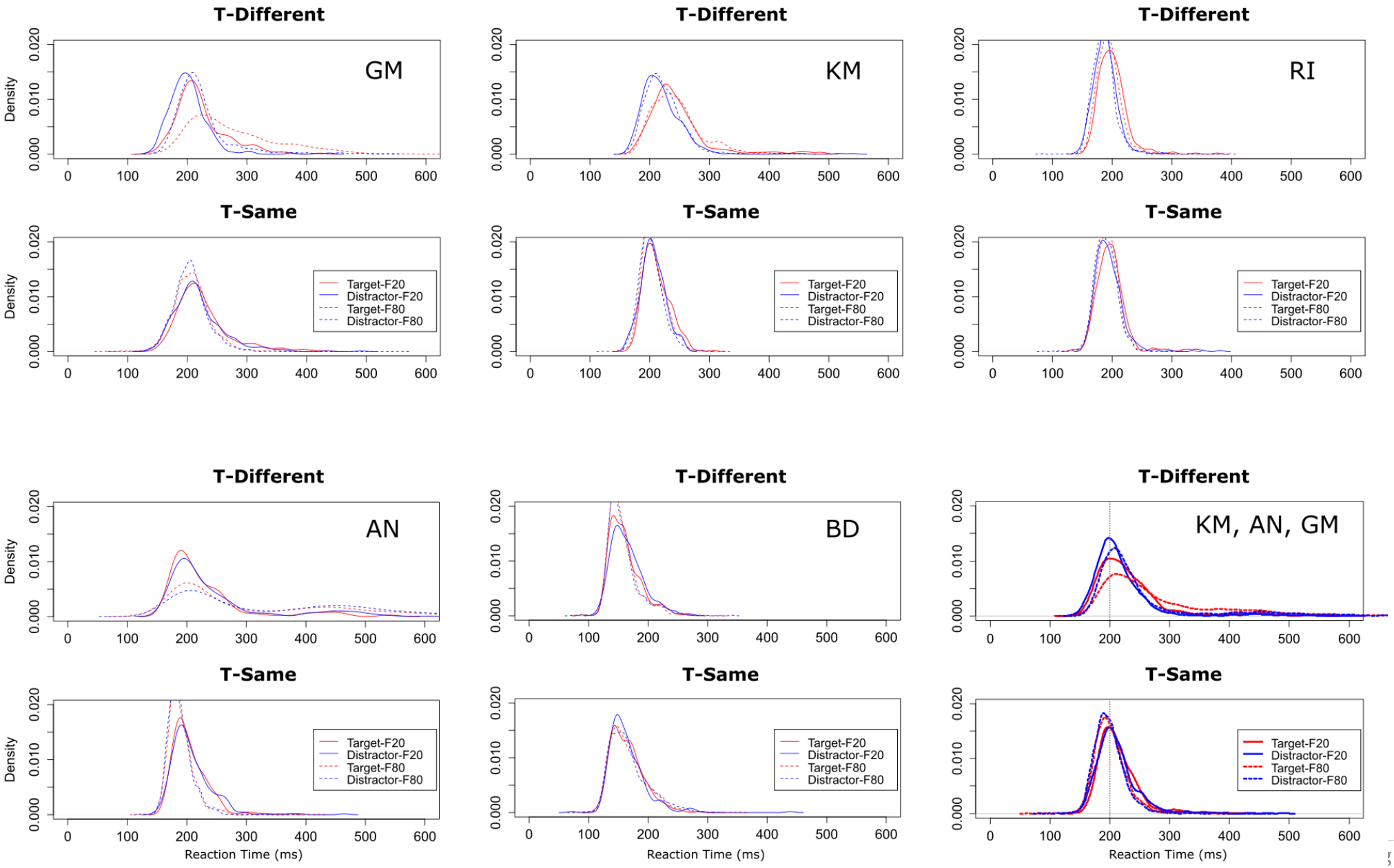
T-Different
GM
KM
RI
T-Same
AN
BD
KM, AN, GM
Density
Reaction Time (ms)
Target-F20
Distractor-F20
Target-F80
Distractor-F80

Figure 4-10: Distribution of Reaction Time per condition and per participant. *We show the kernel density estimation curves of reaction time distributions. Note that what we are concerned about here is the relative position of the solid lines (condition F-20) compared to the position of the dashed lines (condition F-80). For KM, AN, and GM, the condition F-20 give rise to quicker reaction times than condition F-80 (the positive slope of solid lines are on the left on the dashed lines) in the condition T-Different, while we observed the exact opposite in the condition T-Same. For RI, the pattern in T-Different is the same as in T-Same and they correspond to the pattern of KM, AN, GM in T-Same. This suggests that RI was not able to do the discrimination task in T-Different, and answer as if he was in T-Same condition (see also Figure I). Finally, BD shows no obvious pattern, or maybe a pattern opposed to KM, AN, GM in T-Different. Note also that BD has very impressively short reaction times. One may think he has issues in discriminating the target as RI but Figure I tells us that he was actually successful in discriminating the target and avoiding the distractor.*

6.2 Replicating Heeman et al. (2014): Effect of the Additional Stimulus Type on the Global effect.

Here we will focus on the effect of the *Pair-Type* on the Global Effect as in the work of (Heeman et al., 2014). In their work, they proposed to test the effect of the instructions on the Global Effect. Their paradigm was split into three blocked conditions, which is echoed in our paradigm:

- **Double No instruction:** the participants are presented with a pair of stimuli (green and red) and are told to make saccades to the presented stimuli; no target was specified. *This is similar to our T-Same level* of the factor *Pair-Type.*
- **Double Instruction:** the participants are presented with a pair of stimuli and are told to make their saccades to the red target and ignore the green distractor. *This is similar to our T-Different level* of the factor *Pair-Type.*
- **Single:** the participants are presented with a single stimulus, and are told to make their saccade to that stimulus. *This is similar to our trials with one stimulus.* Note that our paradigm differs from theirs by mixing single stimulus trials with double-stimulus trials.

They tested on only one stimuli distance at which the Global Effect is strong. Specifically, their tests have been done for a stimuli distance where the landing positions are shaping a centred unimodal distribution. They find a deviation of the distribution toward the target when for the condition “instruction” compared to the condition “no instruction”; and that even at short saccade latencies. This means the global effect, which is thought to be a low-level phenomenon, can be affected by top-down structures at an early stage.

To fit with the experiment of Heeman et al. (2014), we take into account only our data for the two smallest tested distances (11.25 ° and 22.5°). We proceed to a similar transformation of our landing positions data as Heeman et al. (2014). Namely, we normed our data with the absolute mean of landing positions in the single stimulus trials -- note that Heeman et al. (2014) instead normed their data according to the stimulus position. Then, if the index is equal to 1 or -1, the eyes have landed where they would have for a single stimulus. In the level *T-Different*, the index -1 correspond to the distractor stimulus while the index 1 correspond to the target stimulus.

While Heeman et al. (2014) have chosen to test if the mean of their distributions are different from zero (the perfect averaging); we have chosen to test for an effect of the factor *Pair-Type* with non-paired t-tests between *T-Same* and *T-Different* trials within participants. Our method has the following advantages: 1) it addresses more directly the effect of *Pair-Type*, 2) it gives more power by using all the landing positions recorded for each participants, 3) it addresses inter-individual differences. Furthermore, testing *T-Same* against *T-Different* controls for the bias in brightness we have between the stimuli in our paradigm (the brightness bias may deviate distributions toward -1 as for KM, see Figure 4-11; for details on the paradigm see Section 2.3).

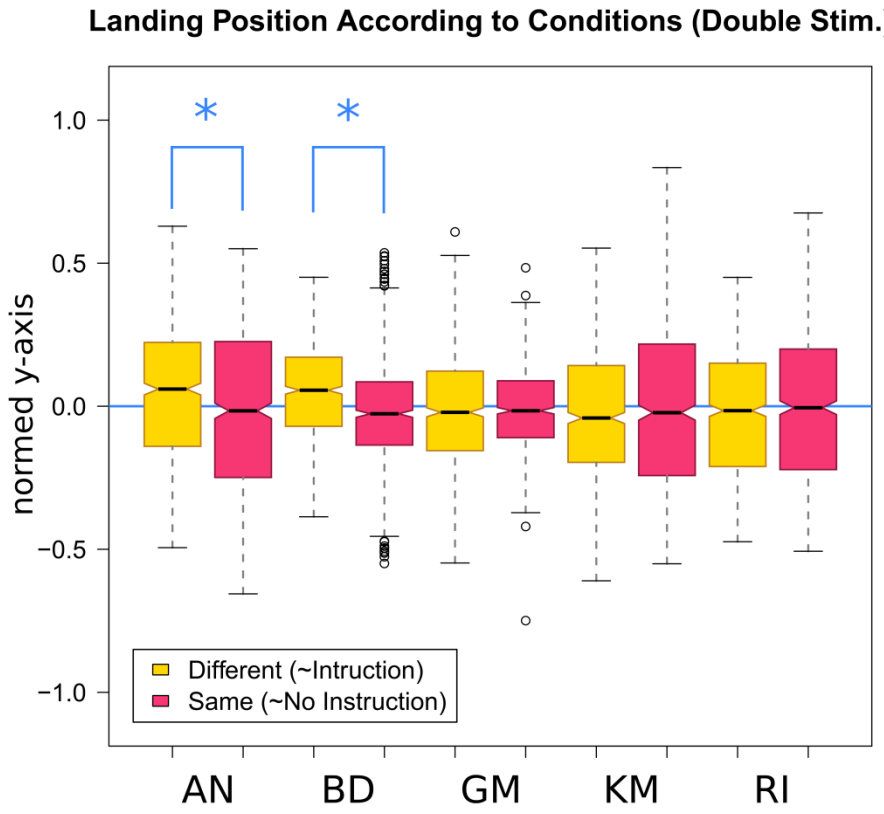

Figure 4-11 : Summary of the non-paired t-test within participants.

The results of the t-tests are reported graphically in **Figure 4-11** and the statistics are gathered in Table 10. After Bonferroni correction, only AN and BD show a significant effect of *Pair-Type*. In line with Heeman et al. (2014), those two participants show a deviation of their landing positions toward the distractor when we used a couple target-distractor compared to when we used a couple of undistinguishable stimuli. The deviation from zero observed in Heeman et al. (2014) is reported to be around 0.3 -- i.e. 15% of the target-distractor distance. The deviation we observed, however, is around 0.061 -- i.e. 3% of the target-distractor distance. Note that, although our normalization methods are slightly different – see above - this difference could not explain such a difference in effect size. For instance, the Cohen's d in the experiment 1 of Heeman et al. (2014, p.32) is 0.306/0.21 = 1.457; while for BD, it would be 0.0708/0.1765 = 0.4011.

Table 10: Summary of the non-paired t-test for each of the participants. The p-values are corrected with the Bonferroni method.

Name	p-value	t-value	FD	M(T-Diff.)	M(T-Same)	SD(T-Same)	SD(T-Diff.)
AN ***	1.17E-04	4.243	1518.585	0.0412	-0.0100	0.218	0.257
BD ***	3.63E-14	7.860	1512.353	0.0464	-0.0244	0.164	0.189
GM	1.000	-0.504	1440.515	-0.0152	-0.0108	0.196	0.144
KM	1.000	-0.862	1502.761	-0.0244	-0.0139	0.221	0.253
RI	0.904	-1.339	1539.935	-0.0206	-0.0053	0.214	0.237

****: p < .001, M: Mean, SD: standard deviation, FD: Freedom Degrees, T-Diff.: T-Different.*

Finally, we also tested if *Pair-Frequency* has an effect on the Global Effect. Using the same method as above, only GM appeared to show a significant effect of Frequency (p = 0.00821, t=3.166, FD=495.202).

To double-check our results, we used the Bayes Factor package (see Rouder, Morey, Speckman, & Province, 2012), which is based on multilevel models allowing to use all the trials of the participants to increase power. We tested all possible interactions between *Participant*, *Pair-Frequency, and Pair-Type*. The favoured model was considering an effect of:

Participant + Stimulus-Type + Participant:PairType.

This model was preferred with a BF of 12.978 ±4.54% against the best model considering *PairFrequency* (in addition) and preferred with a BF of 46,256.68 ±2.82% against the best model ignoring *Participant:PairType* interaction. In short, the Bayes Factor model ranking reflects exactly the previous result: there is no effect of Pair-Frequency, and there is an effect of Pair-Type depending on the participants.

7 APPENDIX B: Within Participant Analysis

7.1 Reaction Time Analysis

To get a better understanding of the mechanisms underlying the effect of condition F-20, we examined the reaction times (RT) in more detail. We decided to particularly focus on a very clear pattern shown by three participants. The reader needs to keep in mind that, as there are only 3/5 participants who display this pattern, it may not be a typical case. Nevertheless, we thought it was an interesting and clear enough pattern to be worthy of the reader's attention. **Figure 4-12** shows the three participants overall RT while plots for all the participants are

available in Appendix 7.3.3. In short, for those three participants, there is a different effect of F-20, according to whether the participant is in T-Different or T-Same conditions. When the participant is in T-Different, reaction times are faster in F-20 condition (compared to F-80) for both stimulus sides. When the participant is in T-Same condition, reaction times are slower in F-20 condition for both stimulus sides. We want to remind the reader that such an interaction effect of

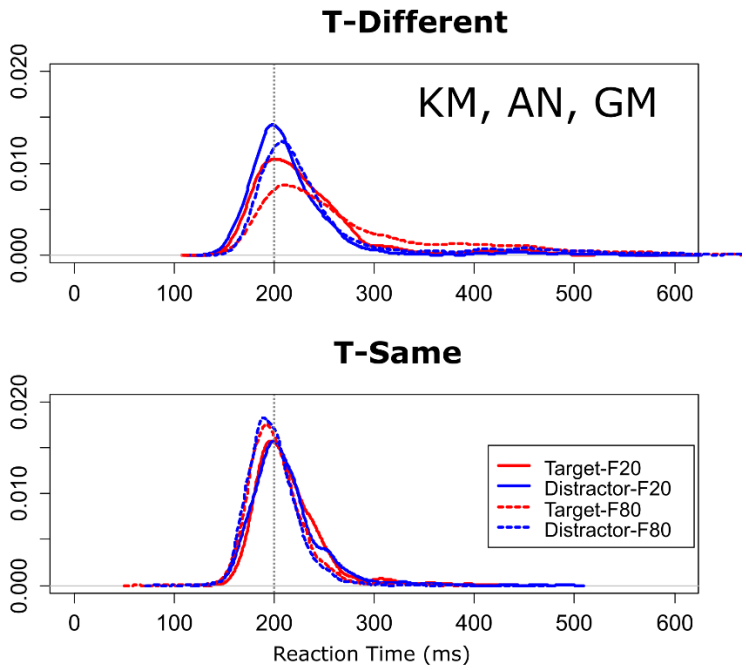

Figure 4-12: A Clear Pattern of Inversion of the Frequency Effect on Reaction Times between the condition T-Different and T-Same. *We mixed the reaction time distributions of KM, AN and GM and we show the resulting density curves. RI and BD was ignored for the illustration as they do not show the pattern we want to comment on. Their distributions and those of all participants are available in appendix. Please note that what we are concerned about here is the relative position of the solid lines (condition F-20) compared to the position of the dashed lines (condition F-80). The condition F-20 give rise to quicker reaction times than condition F-80 (the positive slope of solid lines are on the left on the dashed lines) in the condition T-Different, while we observed the exact opposite in the condition T-Same.*

Pair-Frequency (F-20, F-80) and *Pair-Type* (T-Same, T-Different) *on the bimodal GE* was discarded with strong evidence from our Bayesian Analysis (see Table 8). The reaction times essentially tell us about the speed of the winner while the bimodal GE tells us about the strength of the loser at saccade time. Thus, in T-Same, F-20 makes the loser greater and the winner slower (compared to F-80). Inversely, in T-Different, F-20 makes the loser greater and the winner faster (compared to F-80). Then, in T-Same, a low frequency of double-stimulus

trials (F-20) makes the competition tighter, while in T-Different, a low frequency of double-stimulus trials (F-20) gives a boost to both the winner and the loser.

The unselective boost happening during the T-Different condition could be linked to the Locus Coeruleus keeping a *tonic activation* during frequent events (see Aston-Jones & Cohen, 2005) and thus tonically *suppressing* the visual response (Y. Zhang et al., 1999) during double-stimulus trials in F-80. Furthermore, it has been shown that the Locus Coeruleus is more likely to make phasic responses to novel stimuli, to stimuli evoking goal-directed processes (Bouret & Richmond, 2009) and to rare events (Aston-Jones & Cohen, 2005). In the condition F-20 / T-Different, the double-stimulus trials are rare and the shape of the distractor is novel. Thus it is the optimal combination of factors for inducing a phasic response of the Locus Coeruleus – and thus a relaxation of inhibition of visual stimuli – thereby giving a boost to the winner and the loser.

However, such an explanation does not account for what happens to T-Same condition. We need more neurophysiological study on the effects of Frequency of Occurrence on the SC to progress in our understanding – and to possibly succeed in linking these phenomena to the Locus Coeruleus.

7.2 Bimodal Global Effect

In the main text, **Figure 4-4** described the average effect of the Rarity of the pair of stimuli (F-20 minus F-80 conditions) and the Discrimination Task (T-Different minus T-Same) across participants. Such an average allows for easier readability of the effects but it can be ambiguous. For instance, when one effect is positively significant at the average level, there are several possibilities at the participant level: 1) the effect is positive and consistent across all the participants, 2) a majority of participant shows no effect or a slightly negative effect and a minority show a strong positive effect, 3) a majority of the participants show a positive effect and a minority show no effect or a slightly negative effect. On the other hand, when one effect is not significant at the average level, there are also several possibilities at the participant level: 1) there is consistently no effect across all the participants, and 2) there are strong inconsistent effects that compensate for each other.

Figure 4-13 shows that the effect of Rarity (which was presented in **Figure 4-4**A, orange curves) appears to be consistent for all the participants on both stimulus sides. There is, however, a participant that appears to present an extremely large effect on S1 Side. **Figure**

4-14 shows that the effect of the Discrimination Task (which was presented in **Figure 4-4**B, purple curve) appears to be consistent for all the participants on the side of the distractor. Interestingly, some participants show positive slopes across stimulus distances (GM, BD) whilst some other participants show negative slopes across stimulus distances (RI, KM). Thus the effect that we thought to be stable across distances (**Figure 4-4**B, Distractor Side) is, in fact, an average of curves with positive slope and curves with negative slope. This could also explain the indentation of the purple curve in **Figure 4-4**B at distance 56.25. On the target side, the effect of the Discrimination Task is *inconsistent* between participants – some participants have a negative effect, and some others have a positive effect. That suggests that the absence of a significant effect on the target side that we observed at the average level (in **Figure 4-4**B) is caused by inconsistent effects between participants, rather than no effect. Here, it should be recalled that, in the main discussion (section 5.2), we concluded that we did not detect any Top-down inhibition of the Distractor signal. In fact, it appears that there is possibly strong modulation of the distractor signal at the participant level. The negative GE modulation found for BD and GM could betray a Top-down inhibition of the distractor signal for those participants. It could also explain the indentation of the purple curve that we observed at distance 45 in **Figure 4-4**B.

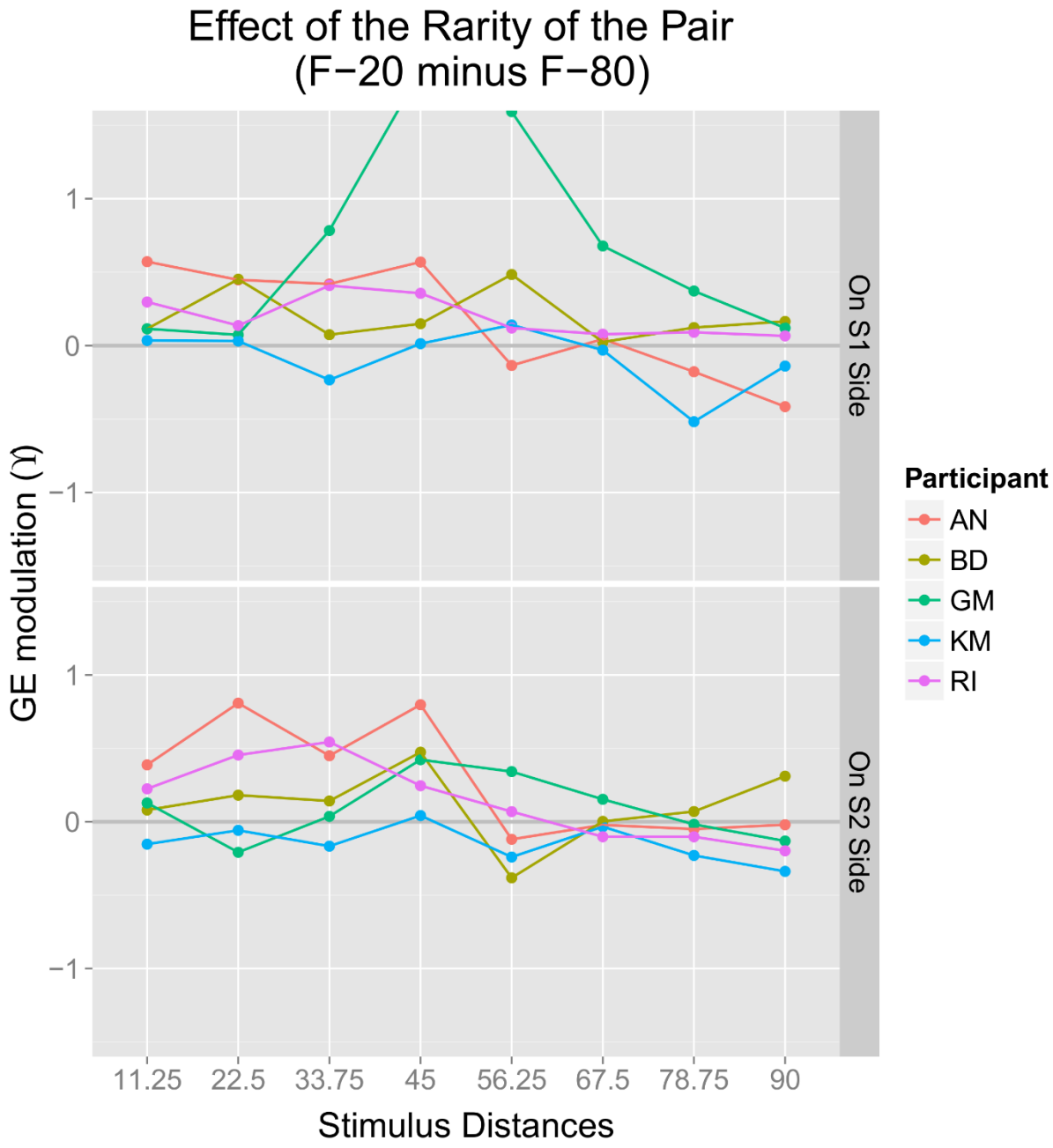

Figure 4-13: Effect of the rarity of the stimulus pair on the bimodal Global Effect (GE), for each participant, and across the tested distances.

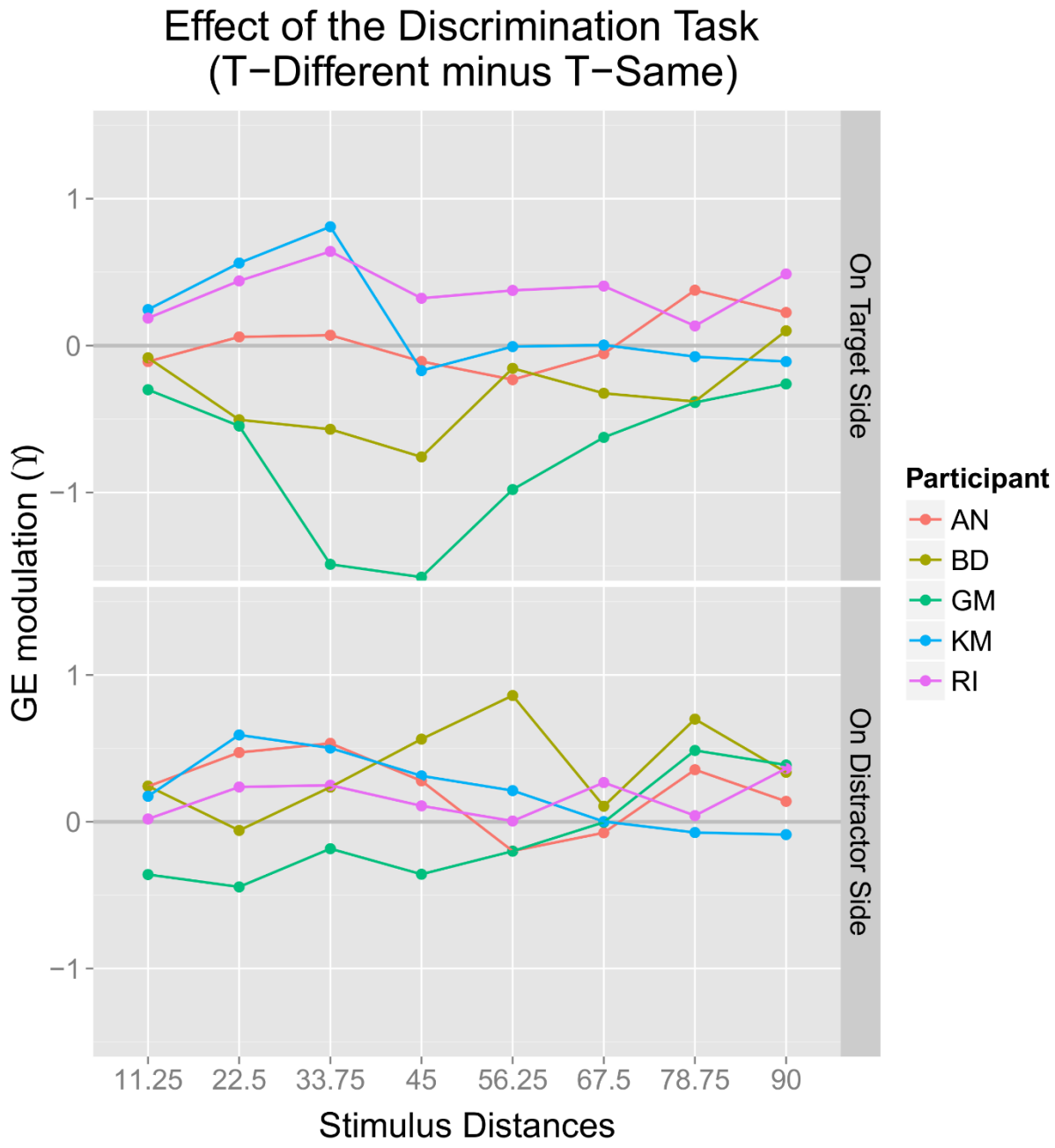

Figure 4-14: Effect of the Discrimination Task on the bimodal Global Effect (GE), for each participant, and across the tested distances.

7.3 Inter-individual heterogeneity

7.3.1 From mid-line distribution

The percentage of landing positions on the target side and on the additional stimulus side are plotted in **Figure 4-15**, for each condition, and on average over the target-distractor distances. A similar distribution for the *T-Same* (double target) conditions is found over participants. All of them showed a slight unbalance toward the additional stimuli, which were brighter. GM appears to be slightly more affected by this unbalance than the others, while RI seems less affected in *F-80/T-Same* with a distribution very close to 50-50.

In the *T-Different* (target-distractor) conditions, two groups stand out: the participants who succeed to inhibit the additional (and brighter) stimulus — AN and BD — and the participants who do not succeed in inhibiting the additional stimulus — GM and KM. The last group is, indeed, more attracted by the additional stimuli when they are told it is a distractor: compare T-Same with T-Different. Note that GM is considerably better at avoiding the distractor in the *F-80* condition (high frequency of two-stimulus trials), and KM shows also a slight improvement. Outside of these two groups, there is RI who gets a similar distribution whenever he was required to ignore a distractor or to cope with two targets. This consistency in his behaviour may come from a difficulty to do the task properly, or a lack of involvement from the participant.

Overall, it appears that we succeeded in making the discrimination task in T-Different – i.e. to discriminate which stimulus is the target -- difficult enough to keep a good number of saccades toward the distractor and to allow their analysis. However the difficulty may have been too high for RI.

7.3.2 Deviation from the Closest Attractor

Figure 4-16 shows the DFCA for each participant averaged over all the conditions. These measures of the Global Effect (how far away are the landing positions from the closest stimulus) allow us to appreciate the heterogeneity of the results. It seems that GM and BD present a strong Global Effect: there is large centripetal deviation of landing positions, and it stays for large stimulus distances. On the other side, RI, AN and KM seem all to be rather less sensitive to Global Effect. Hence, a new clustering has emerged, compared with the previous section.

7.3.3 Reaction times

Figure 4-10 suggests to us that AN may have waited until the last moment before moving her eyes in T-Different conditions, a possibility that was confirmed verbally by the participant after interview. This difference of AN compared to the other participants can be corrected by giving clearer instructions. The participant BD also stands out from the others with very fast reaction times. He also shows no difference in reaction times between the different conditions (see **Figure 4-10**) as RI. However, the mid-line distribution (previous section 7.3.1) shows that RI was not properly performing the discrimination task in T-Different, while BD had no problem. Thus, BD seems to form a special case.

7.3.4 Symmetry of responses

As described in the method and analysis section, the data analysis is made by mirroring the landing positions: 4 position settings (of the stimuli) are used to address one distance ($8\ distances \times 4\ settings = 32\ target´s\ positions$). Our mirroring assumes that a symmetry of stimuli give a symmetry of responses. However, we found out by accident that our assumption is not as systematic as we would have expected.

Indeed, on **Figure 4-17**, it seems that some participants strongly favour upward saccades whatever the position of the stimuli on the screen. With the graphs shown in **Figure 4-17**, we understand the participant RI's results in **Figure 4-15** (response accuracy): most of the time, he goes first to the bottom stimulus, whatever the distractor or the target. As the target appears 50% of the time on the bottom part of the screen, RI gets 50% of landing positions toward the target and 50% toward the distractor. Though RI is an extreme case, this attraction for the bottom stimulus is also observable for KM for all the conditions and for AN in the conditions *C-same* where, obviously, the choice top/bottom was free.

7.3.5 Summary

Our group of 5 participants is heterogeneous:

On the side of response accuracy, KM and GM are strongly attracted by the distractor while BD and AN successfully avoid the distractor; RI does not discriminate between target and distractor;

On the side of the Global Effect, BD and GM show a strong GE over large stimulus distances, while AN, RI, KM show a small GE;

On the side of reaction time, BD stands out from the others with a very short reaction time; But AN, KM and GM stand out by showing a very clear and interpretable pattern of RT between conditions.

On the side of the absolute direction of saccades, KM and RI present a strong attraction to the top stimuli (upward saccades). AN shows this attraction only in free-choice (T-Same).

The heterogeneity of the group is summed up in Table I. These groups are not based on statistical clustering and we did not test their statistical significance.

Table I: Summary of Inter-Individual Heterogeneities.

Participants	RA	DFCA	RT Speed	RT Pattern	ADS
AN	++	--	--	++	+/-
BD	++	++	++	--	++
GM	--	++	+/-	++	++
KM	--	--	+/-	++	--
RI	+/-	--	+/-	--	--

Note. RA for from Response Accuracy, DFCA for Distance from the closest attractor, RT Speed for Reaction Time Speed, RT Pattern for Reaction Time Pattern, ADS for Absolute Direction of Saccades. We classed the performance of the participants on the different measures, with ++ denoting a good performance, +/- denoting an average or neutral performance and –- denoting a poor performance.

7.4 Concluding Remarks

The point that follows from the previous sections is that it may be worthy to analyse and understand data at the participant level. In fact, the Global Effect/Reaction Time model that we are working with is a participant level model: it models one individual. Thus, it makes perfect sense to interpret the data – i.e., create an instance of the model -- for each individual separately.

We believe that there are two possibilities for coping with heterogeneity. The first possibility is that the experimenter succeeds in finding an experimental paradigm that adapts to any kind of participants so that he/she collects homogeneous data with consistent effects between participants. In that case, the experimenter can create a single instance of his model to interpret the data at the level of the population (average level). The second possibility is that the experimenter cannot find an experimental design that gums out or controls for the heterogeneity between participants. In that case, the experimenter can create one instance of his model for each participant so that it might reveal a category of participants in the population.

In practice, the experimenter who uses a single instance of a model to explain the behaviour of the participant population while that population is heterogeneous is creating a Chimera model. A Chimera model, by trying to fit a heterogeneous population made of lions, snakes and goats, leads to an imaginary monster that is useless to understand how the actual lions, snakes and goats operate in the population.

Thus, a logical future direction for our bimodal GE measure – and its use in the assessment of decision making processes -- is to improve the paradigm in order to reduce heterogeneity that we can control, and also to create tools for 1) fitting an implemented version of our model at an individual level, and 2) assessing the presence of clusters of participants in the parameter space. This enterprise may require a larger set of participants.

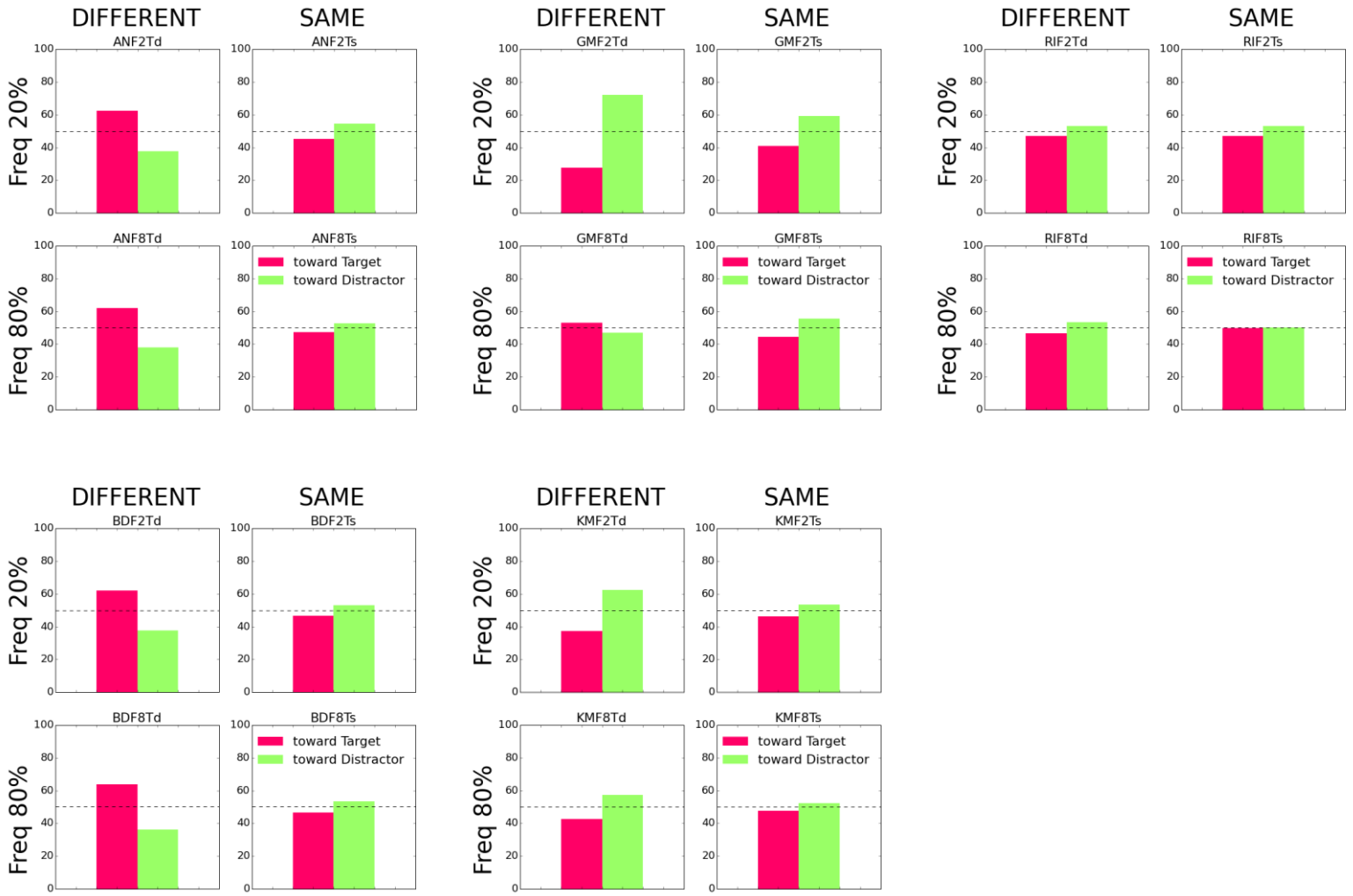

Figure 4-15: From mid-line distribution or Response accuracy or Proportion of saccade made toward the target and toward the distractor. *Note that in T-Same (SAME on the graph), the "distractor" was identical to the target: that was just a pair of identical stimulus, the distractor side being slightly brighter (of 12.5%).*

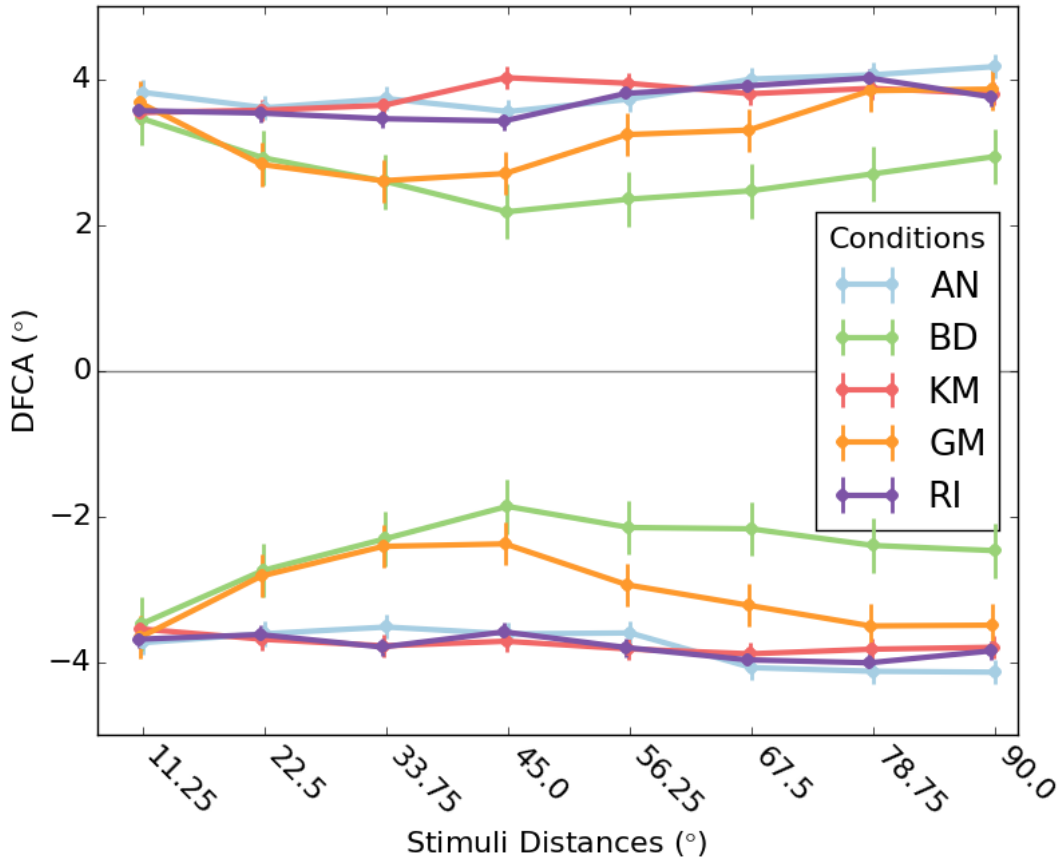

Figure 4-16: Average over all condition of the DFCA on target and distractor side for each participant. *Note that in T-Same condition, the pair of stimuli are similar but one is slightly brighter than the other; the distractor side refers to this slightly brighter stimulus.*

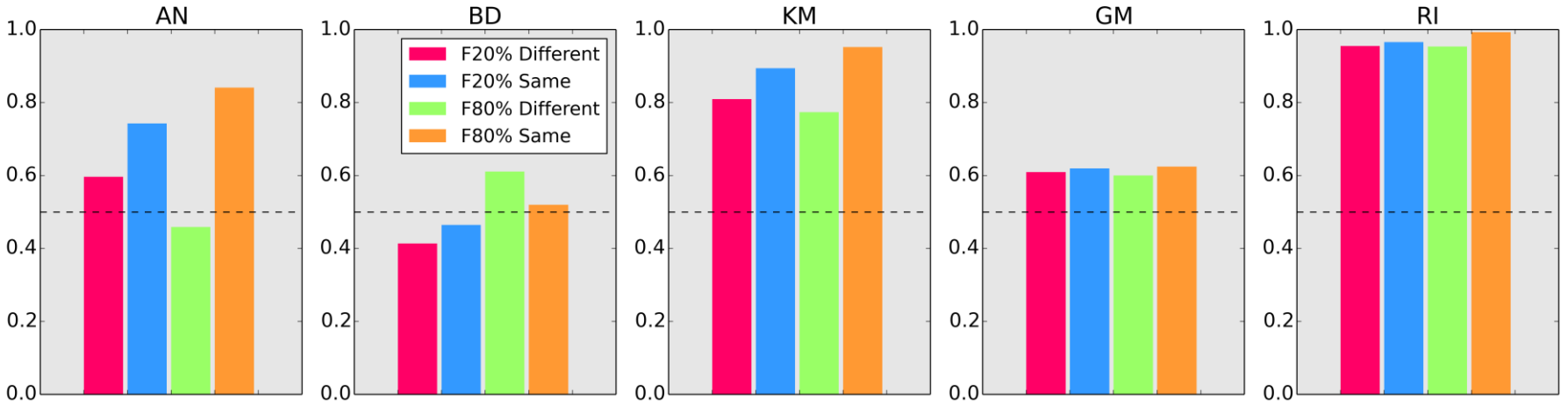

Figure 4-17: Proportion of Upward saccades for each participant in each condition. *As the stimuli presentation was balanced, the proportion of upward saccade is expected to be 0.5 (50% of the time the participants go upward, 50% of the time, the participants go downward). It is here obvious that some participants had a strong bias to making upward saccades. Interestingly, for AN who succeeded to discriminate the target and to avoid the distractor, the bias appears only during free choice (T-Same condition). Such a facilitation of upward saccade is in line with the work of (Bell, Everling, & Munoz, 2000, fig. 3, pro-saccade curves).*

Chapter Five: From neurons to behaviour

An attempt to replicate the superficial and intermediate layers of the Superior Colliculus from neurophysiological data.

Abstract:

Can we climb up the chain of events from neurons to macroscopic behaviour? Recent progress in recording technology allows neurophysiologists to assess more easily the dynamic of neural ensembles while recent hardware and software allows modellers to easily build complex neural ensembles of spiking neurons. Finally, abstract models of neural ensembles have been successfully used to explain macroscopic behaviours. Thus, Psychology, by way of the new avenue opened on neural ensembles, has the tools to resolve the chain of events from single neurons to macroscopic behaviours.

Recently Phongphanphanee et al. (2014) applied neural ensemble recording technology to the Superior Colliculus. The authors suggested that the connection patterns that they observed in the superficial layers (SCs) and the intermediate layers (SCi) can explain the dynamic that they recorded in those layers – respectively a winner-take-all dynamic and an accumulator dynamic. Our work aims to test the link that they made between the connection patterns and the dynamic of each layer.

Using a homogeneous spiking neuron network, we found that the connection patterns and single neuron models that we interpreted from their data does not lead to the dynamic that they reported. On the side of the SCs model, the winner-take-all dynamic could be obtained if we added a stronger inhibition and removed the delay between excitation and inhibition. Our work also highlights that there were possibly two different types of neurons in the population recorded by Phongphanphanee et al. (2014). On the side of the SCi model, no solution was found to replicate the accumulator dynamic. It is the single neuron model of SCi neurons that appears to be at fault. We finally discuss what data are needed to improve our model and the fitting of its parameters.

1 Introduction

Can we climb up the chain from neurons to behaviour? When the behaviourists laid the foundations for what is now known as modern psychology, they stated that the smallest explanatory units of Psychology are stimuli and responses – at macro-level. This was done for the sake of limiting the scope of conjecture to what we could measure at the time. And, even if this level of study is still one of the most interesting, technology and scientific progress now allow scientists 1) to *study* and 2) to *model* single neurons *and* neural ensembles. Furthermore, the behaviour of some neural ensembles can be successfully linked to the behaviour of the organism under scrutiny. Then, a logical progression of Psychology would be to work on scaling its smallest explanatory units down to neurons; i.e. to work on linking neurons to behaviour in a systematic way. Our work represents a modest contribution towards achieving that aim. While in Chapter 2, we shaped a network model for it to behave in the same way as the Superior Colliculus, in the present chapter, we shape a network model to resemble as closely as possible the neurophysiology of the Superior Colliculus. In other words, in Chapter 2, we aimed to replicate a function and we deduce the structures that are necessary to achieve this function; in the present chapter, we aim to replicate a structure and hence we observe if its emergent functions replicates the expected functions of a given brain structure. Note that the two approaches – let us call them functional and structural -- are totally opposite, and complementary. To draw an analogy with building a house, in the functional approach, we would lay bricks with hypotheses regarding what a house should provide to be comfortable; in the structural approach, we would lay the bricks as we see them from the neighbour's house and then we would test if it is comfortable. Note that the structural approach is limited by what is observable, and hence, by technology. The brain structure that we model, the Superior Colliculus, is involved in the action selection for orienting movements, and we hope our work could provide a basis for future development in our understanding of the spatio-temporal interactions between stimuli during decision making, addressed in Chapters 3 and 4.

1.1 From single neuron recording to behaviour

Progress in technology such as intra-cellular recording (Cole & Curtis, 1939; Young, 1936), the voltage clamp (Hodgkin & Huxley, 1952; Marmont, 1949; please note the implication of Cole), and the whole cell patch clamp (Neher & Sakmann, 1976) have revolutionized the way that we can assess neurons. These technologies have made it possible to model very precisely the behaviour of a single neuron (Hodgkin & Huxley, 1952), a single membrane channel (for instance Shouval, Bear, & Cooper, 2002) or a single synapse mechanism

(Stevens & Wang, 1995; Tsodyks, Pawelzik, & Markram, 1998). The Hodgkin & Huxley model has given rise to a number of simplified or derivative versions named "spiking neuron models". These are all based on a dynamic description of the membrane potential and are able to initiate spikes, i.e. action potentials. Importantly, their parameters can be estimated from single neuron recording – as the original model was constructed around that method. Note finally that, synaptic, channel or other kinds of mechanisms can be easily added to these single neuron models.

Despite huge progress in understanding single neuron mechanisms, our understanding of neural ensembles has lagged far behind. However, since then, some recent technological progress has opened up some possibilities for moving forward: the recording of neural ensembles now represents a promising direction in modern neurophysiology (Nicolelis, 2007; Taketani & Baudry, 2006) that has attracted a lot of interest. In fact, multi-electrode arrays were invented in the 70s (Gross, 1979; C. A. Thomas, Springer, Loeb, Berwald-Netter, & Okun, 1972; Wise & Angell, 1975), but it is only recently that they have begun to be used intensively due to the development of computers, which can now manage large streams of data (Fejtl, Stett, Nisch, Boven, & Möller, 2006). This recent revival of multi-electrode array technology has brought with it a renewed interest in its development that, in turn, is promising to benefit from the advances in nanotechnology (Spira & Hai, 2013). For now, this technology allows scientists to make extra-cellular recordings or stimulation at more than one locus - in *in vitro* slices (Gross, 1979) or *in vivo* brain structures (D. Paré & Collins, 2000; Rousche & Normann, 1998). For instance, a 16x16 array can probe 256 loci / cells. Despite the advantages of multi-electrodes, extra-cellular recording is not as precise and informative as intra-cellular recording. Thus, a powerful combination is to use whole-cell recording at the same time as multi-electrode array stimulation. This combination allows scientists to readily stimulate neurons at different positions in a neural structure while making an intra-cellular recording at another (fixed) position. If the intracellular recording is made in *voltage clamp* mode, the experimenter can observe the postsynaptic currents induced by the stimulated neurons on the recorded neuron. From these recordings, neural mechanisms, synaptic mechanisms and the spatial patterns of the connections in the neural ensemble can be inferred. Finally, other promising recording systems of neural ensembles have been developed in parallel such as the two-photons voltage imaging (Peterka, Takahashi, & Yuste, 2011) or multi-electrode arrays allowing intracellular-like recordings (Hai, Shappir, & Spira, 2010a, 2010b; J. T. Robinson et al., 2012).

To our knowledge, the application of neural ensemble recording technology to the study of the SC is relatively recent, and includes voltage imaging (Vokoun et al., 2014), multi-

electrode extracellular field potential (Phongphanphanee, Kaneda, & Isa, 2008), and a combination of multi-electrode arrays and whole-cell patch clamp (Phongphanphanee et al., 2014).

In the meantime, tools to simulate spiking neuron networks have been developed in abundance (e.g. MOOSE, NEURON, GENESIS, NEST, CSIM, Nengo, PCSIM, ANNarchy, Brian Simulator). They have become easier to use, with most of them proposing a python script interface or a graphical interface. Most of them facilitate the use of parallel threads on a single PC -- optimised for multicore processors and graphic cards – or the use of supercomputer (i.e. cluster) in order to optimize their computational power. Finally, progress has been made to facilitate neuron model fitting (Rossant et al., 2011; Rossant, Goodman, Platkiewicz, & Brette, 2010). In short, spiking neuron network simulators have been made to work easier and faster. And some laboratories have started to use them for modelling the SC (Morén et al., 2010, 2013) and decision making systems (Lo & Wang, 2006; X.-J. Wang, 2002).

Until now, most of the recent models of action selection for eye movement have been based on the high level of abstraction of dynamic field (these include, among others, Bompas & Sumner, 2011; Marino, Trappenberg, Dorris, & Munoz, 2012; Meeter, Stigchel, & Theeuwes, 2010; Schneegans, Spencer, Schöner, Hwang, & Hollingworth, 2014; Trappenberg, Dorris, Munoz, & Klein, 2001). These authors demonstrate successfully that macro-level behaviour can be explained with idealistic and simplified dynamic neural ensembles – the approach being functional – i.e., to find how to lay bricks together so that they explain a specific set of behaviours. The novel neurophysiological approach offered by neural ensemble recording along with the optimization of spiking neuron simulators invites us to push models further toward neurophysiology. In particular, in the light of both the successes and shortcomings of simplified dynamic neural ensembles to explain behavioural data, we could build neurophysiology-based models that connect neurons to behaviour. Ultimately, those models could replace debatable and limited arbitrary/default choices – such as the saccadic threshold (Jantz et al., 2013) - with an actual mechanism that can be studied and tested.

In the present work, we will investigate if it is possible to replicate the behaviour of the two main layers of the SC from the recent work of Phongphanphanee et al. (2014). In this study, they used whole-cell patch clamp recording in combination with multi-electrode array stimulation. Whilst it would be ideal to obtain a working model from the first iteration, our objective is admittedly more modest: it is to open a dialogue with neurophysiologists on what is needed to achieve a realistic model.

1.2 Phongphanphanee et al. (2014): a neurophysiological review of the SC.

We based most of our work on only one neurophysiological study (Phongphanphanee et al., 2014) conducted on rodents. The recent work of Phongphanphanee stands out from other neurophysiological studies in three ways. First, it reports results for both the SCi and the SCs. Second, by using whole-cell recording in combination with micro-array electrodes, their results cover a large range of mechanisms and parameters such as the cell membrane and synaptic dynamics, the connection patterns in the network, and the behaviour of the network when presented with one or two simultaneous stimulations. Third, despite this large amount of data, they propose a simple and clear view of the SC: two layers, one stereotype of neurons per layers, one connection pattern per layer and importantly, one network behaviour per layer. Thus their work, by virtue of covering a wide range of parameters, and by the attractive simplification of the SC that it assumes, is very suitable for being modelled and tested.

Phongphanphanee et al. (2014) assumed that there is only one type of neuron (i.e., a stereotype) per SC layer, only one connection pattern per layer, and only one function per layer. With regard to the SCi, they suggested that it is a temporal and spatial accumulator. They observed 1) an accumulation of the delivered input pulses over time; 2) an equality in the extent of the lateral connections for excitation and inhibition; 3) an equality of the strength of excitatory and inhibitory synaptic currents (see Appendix A, section 6.3.3, p. 5-52, for further details); 4) the linear summation of the bumps of activity induced by two close stimulations; and 5) the absence of an interaction between the bumps of activity induced by two remote stimulations. They conclude that the SCi is shaped to achieve decision making in the sense that it behaves similarly to a race model system. In terms of the SCs, they observed: 1) transient responses to input pulses; 2) an extent of inhibitory lateral connections that is larger than that of the excitatory connections; 3) a strength of excitation synaptic currents that is twice that of the inhibition synaptic currents; 4) the non-linear interaction of the bumps of activity induced by two close stimulations (i.e. the resulting activity is greater than the linear sum); and 5) a winner-take-all interaction between remote stimulated regions (i.e. the strongest induces a bump whilst the weakest does not). They conclude that the SCs is shaped to select the highest saliency from a saliency map through a winner-take-all system.

In a preliminary study, we used the procedure described by Phongphanphanee et al. (2014) using the whole-cell patch clamp method in order to fit a neuron model for the SCs and SCi. This section, which can be found in Appendix A (section 6), covers the replication of the

observation 1) for both SCs and SCi. In the present chapter, we will focus on testing whether the connectivity bricks 2) and 3) lead to the network behaviour 4) and 5). This would then corroborate the respective conclusions that Phongphanphanee et al. (2014) reached with respect to the functions of the SCs and SCi.

2 Method

2.1 Summary of Method

In a preliminary study (see Appendix A, Section 6), we built two neuron models that estimate the behaviour of single neurons found in the SC of the rodent. Each model represents a hypothetical *stereotype* neuron: one stereotype for the SCs and one for the SCi. Here, using these models, our aim will be to test if an homogenous dynamic neural field (DNF) is sufficient to account for the *in vitro* behaviour of, respectively, the SCs and SCi observed in Phongphanphanee et al. (2014). More specifically, our aim will be to address the suggested link between the pattern of lateral connections and the behaviour of the SCs and SCi. Indeed, the authors, in their conclusion, suggested very precise parameters for the lateral connection settings in the SCs and in the SCi, which they assumed to drive the behaviour of the DNF. Specifically, the authors reported a *winner-take-all behaviour* in the SCs and a *non-competitive accumulator behaviour* in the SCi (see **Figure 5-1**, in the next section, for a schematic of those behaviours with a one dimensional DNF).

However, we consider that, when framed into a model, the parameters for the lateral connection settings suggested by Phongphanphanee et al. (2014) are subject to unknown rescaling and to interpretation (we will return to some ambiguities in their paradigm in the Discussion, Section 4.3). The unknown rescaling effects could be due to, for instance: 1) the fact that they are working on mice while DNF models have been primarily used to model human/monkey data, 2) the fact that they are working with an actual SC, while we are working with a simplification of this structure (we will return to this issue in the Discussion). Furthermore, testing only whether Phongphanphanee et al.'s specific sets of parameters lead to the behaviours that they observed (i.e, winner-take-all and non-competitive accumulator) is not sufficient to determine which of those parameters are necessary for one of those behaviours to occur. Hence, for those reasons, we decided to explore a space of parameters that comprises and extends the region corresponding to their results. However, the experimental paradigm of Phongphanphanee et al. is complex and for the sake of computation, data visualisation and manageability, we could not explore the space of parameters using a simulation paradigm with more than one condition (as we will

see, simple paradigms allow us to construct a grid of exploration). Therefore, we decided to divide our work into two phases: an exploration phase and a testing phase. In Phase 1, we explored a space of parameters using a single condition paradigm. This condition allowed us to detect whether a set of parameters leads to a winner-take-all or a non-competitive accumulator behaviour.. In fact, the model was presented with two stimulations for a fixed strength and for a fixed distance. In Phase 2, we selected the most promising connection settings from Phase 1 and tested them further with a precise replication of the procedure used by Phongphanphanee et al. (2014). In particular, Phase 2 tested the effect of inter-stimulation distance and stimulation strength. It should be noted here, that regardless of the results of Phase 1, the set of parameters suggested by Phongphanphanee et al. (2014) was, by default, always part of the sets tested in Phase 2. We apply this process first for the SCs model and then for the SCi model.

2.2 Equation and Parameters of the lateral connections

The general equation of the neural field model is described in Appendix A (section 6.2.2). It is similar to the one described in Chapter 2 except that we used the neuron models that we built in Appendix A (section 6) so that they fit the single neuron data in Phongphanphanee et al. (2014)'s work. Note that the neural field is spatially unidimensional. Another difference from Chapter 2 is how we simulated the lateral connections. Here, the excitatory and inhibitory connections are separated and overlapping: there is one Gaussian kernel for the excitatory connections and one Gaussian kernel for the inhibitory connections (instead of using a Mexican hat). This method used more memory of the hosting computer but it maps more closely onto actual neurophysiological connections. If we consider a pair of neurons, one at position *k* and the other at position *j*, the connection kernel can be written as (in relation to equation 1, appendix 6.2.2):

$$W_e(j,k) = A_e \exp\left(\frac{-(j-k)^2}{2\sigma_e}\right) \ and \ W_i(j,k) = A_i \exp\left(\frac{-(j-k)^2}{2\sigma_i}\right)$$

To this, we add the possibility of synaptic delays D_e and D_i; these are the delays between a pre-synaptic spike and its effect on the post-synaptic neurons. The subscripts *e* and *i* denote *excitation* and *inhibition* respectively.

Finally, we scaled our neural field to a size of 200 neurons; we decided that a distance of 1 cell would correspond to a distance of 10µm in the SC.

2.3 Phase 1: Exploration of Several Lateral Connection Settings

During the exploration phase, we used the same paradigm using different connection settings of the model. The paradigm replicated one of the double stimulation conditions used by Phongphanphanee et al. (2014): it consisted of delivering 11 pulses at 200Hz at two positions on the map simultaneously, with a distance of 48 cells (corresponding to 480 µm). The input consisted of two mock neurons controlled by the experimenter. One of the input pairs was half the strength of the other. The strongest one was connected to the neural field with a strength of 0.6nS for the SCi model and of 5.0 nS for the SCs model. We selected these strengths so as to ensure that even the weakest input would initiate one spike when tested on the single neuron model (see the details of the single neuron model in Appendix, Section 6). The aim of the exploration will be to detect whether there are sets of parameters that lead to a winner-take-all (for the SCs model) or a non-competitive accumulator behaviour (for the SCi model). **Figure 5-1** summarizes into a schematic the patterns of activity to be expected in a one dimensional DNF if a set of parameters leads to one of those desired behaviours. It can be noted that the schematics are represented in the same format as the results of the exploration in sections 3.2 and 3.3 in order to ease the comparison.

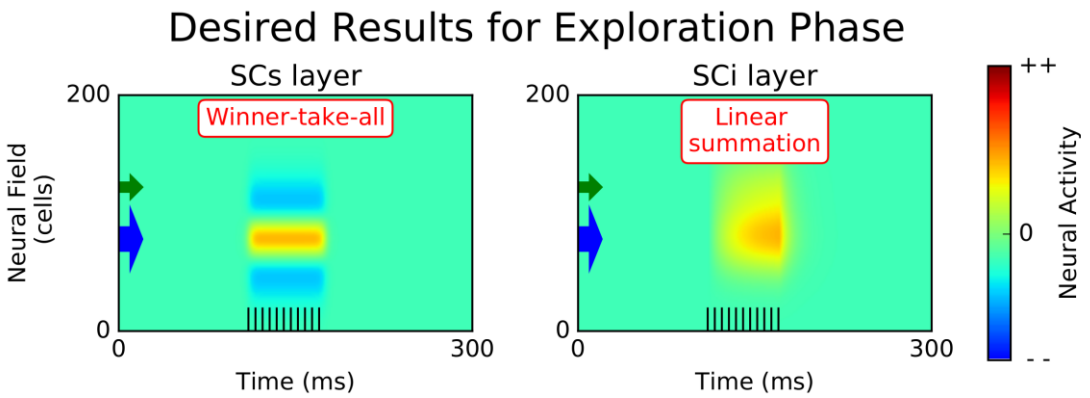

Figure 5-1: Desired Results of the Models for the Exploration Phase. *Both subplots represent respectively a schematic of the behaviour of the SCs and the SCi reported by Phongphanphanee et al. (2014) when stimulated unevenly at two locations. Note that the SC map is reduced to a one dimensional DNF. The blue arrow represents the position of the strongest stimulation electrode on the DNF, while the green arrow represents the position of the weakest one (half of the strength of the other). The train of black vertical lines at the bottom of each plot represents the 11 input pulses delivered by each stimulation electrode.* ***In the SCs:*** *a winner-take-all behaviour is reported: only the location receiving the strongest stimulation activates.* ***In the SCi:*** *a non-competitive accumulator behaviour is reported: both stimulated locations get activated and their activity sums up (linear summation). The exploration across different parameters of lateral connections in section 3.2 (for the SCs model) and 3.3 (for the SCi model) aims to find which set of parameters lead to those patterns.*

We explored four components of the lateral connections: 1) the *inhibition extent ratio,* which is the ratio of the standard deviation of the inhibitory and excitatory Gaussian ($\sigma e/\sigma i$), 2) the *inhibition strength ratio* which is the ratio *Ae/Ai*, 3) the *connection coupling* which is the overall strength of the lateral connection $\frac{(A_e+A_i)}{2}$ and 4) the *synaptic delay ratio* which is the ratio *De/Di*. We proceeded in the following way:

Inhibition Extent Ratio:

The spatial extent of the inhibition and excitation was tested across 3 levels:

- $\sigma_e > \sigma_i$: where the extent of inhibition is 1.5 times smaller than that of excitation ,
- $\sigma_e = \sigma_i$: where the extent of inhibition is equal to that of excitation,
- $\sigma_e < \sigma_i$: where the extent of inhibition is 1.5 times larger than that of excitation.

Note that $\sigma_e < \sigma_i$ corresponds to what is observed in the SCs while $\sigma_e = \sigma_i$ corresponds to the SCi according to the observations of Phongphanphanee et al. (2014).

For the SCs, the smallest connection extent (e.g., the value of σ_i in $\sigma_e > \sigma_i$ condition) was fixed at 13 cells (130 μm) in order to match what is observed in Figure 4D (electrical stimulation) of Phongphanphanee et al. (2014). For the SCi, the smallest connection extent was fixed at 19 cells (190 μm) based on Figure 6D (electrical stimulation) of Phongphanphanee et al. (2014). The aforementioned values (i.e., 13 and 19 cells) were used by default in $\sigma_e = \sigma_i$ conditions. Note that these estimations would be substantially different if we were using the photo-uncaging stimulation data of Phongphanphanee et al. (2014); this last kind of stimulation excites a smaller area of neural tissue.

Inhibition Strength Ratio:

The weight of the excitation to the inhibition is tested under 3 levels:

- $A_e > A_i$: where the strength of inhibition is 2.0 times weaker than that of excitation,
- $A_e = A_i$: where the strength of inhibition is equal to that of excitation,
- $A_e < A_i$: where the strength inhibition is 2.0 times that of excitation.

Note that the first setting corresponds to the observations of Phongphanphanee et al. (2014) in both the SCs and SCi (see appendix 6.2.6 and 6.3.3 for more details).

See the following factor for the absolute strength values.

Connection Coupling:

The coupling defines the absolute strength of the lateral connections at 3 levels:

- *Low Coupling:* where A_e, the excitatory strength is fixed at 0.2 nanoSiemens for the SCs model and at 0.1 nanoSiemens for the SCi model,
- *Medium Coupling:* where A_e, the excitatory strength, is fixed at 0.4 nanoSiemens for SCs model and at 0.2 nanoSiemens for the SCi model,
- *High Coupling:* where A_e, the excitatory strength, is fixed at 0.8 nanoSiemens for SCs model and at 0.4 nanoSiemens for the SCi model.

Note that the data of Phongphanphanee et al. (2014) does not provide an estimation of the coupling. Theoretically, if the coupling is low, the neurons are not very sensitive to the activity of their neighbours and are mostly driven by the input stimulation. If the coupling is high, the neurons are more sensitive to the activity of their neighbours: they will be less influenced by the input stimulation if a neighbour is spiking. High coupling plays a role in generating both self-sustained activity (after input removal) and winner-take-all dynamics.

Synaptic Delay:

We tested the model with two synaptic delay levels:

- *Same Delay ($D_e = D_i$):* where all delays are randomly selected between 2.0-2.8 ms,
- *Different Delay ($D_e < D_i$):* where D_e is between 2.0 and 2.8 ms and D_i is between 6.9 and 7.8 ms.

Note that *Different Delay* corresponds to what was reported by Phongphanphanee et al.(2014) in the superficial layer of the SC. Since no information was given for the SCi, we assumed *Same Delay* by default.

2.4 Phase 2: A Replication of Phongphanphanee et al.'s Double Stimulation paradigm

On the basis of the results of the exploration phase, we selected the connection settings that produced behaviour similar to that observed by Phongphanphanee et al. (2014), and we tested them further. Notably, for this testing phase, we replicated the paradigm that corresponds to Figures 9 and 10 of Phongphanphanee et al.(2014), which test different inter-stimulation distances and stimulation strengths. As in the exploration section, we connected two input neurons to the neural field to simulate the two stimulation electrodes. One stimulation is half the strength of the other – note that the input connection strengths were the same as those described in Section 2.3. We tested 4 distances: 15, 30, 45, 60 cells corresponding respectively to 150, 300, 450, 600 µm, as in the original paradigm. Referring to S1 as the strongest stimulation and S2 as the weakest, we had 4 stimulation conditions: *Condition S1* and *Condition S2*, where we applied a single stimulation corresponding either

to S1 only or to S2 only; *Condition S1 + S2*, where we applied the stimulation S1 and S2 simultaneously for a given distance (uneven double-stimulation); and *Condition S1 + S1'*, where we applied the stimulation S1 at two locations simultaneously for a given distance (even double-stimulation). *Condition S1 + S2* replicates the condition used in *their* Figure 9E, F, G while *Condition S1 + S1'* corresponds to the condition used in *their* Figure 9B, C and 10B, C. In fact, our paradigm is slightly more complex than that employed by Phongphanphanee et al. (2014) since, unlike in the current study, they did not test several distances for *Condition S1 + S2*.

Finally, Phongphanphanee et al. (2014) made their intra-cellular recording for neurons near to one of the stimulation loci, but these supposedly did not receive direct input from the stimulating electrode. Furthermore, they applied an intra-cellular solution that prevented the recorded neurons from spiking. To match those conditions, we attached to our network a pair of special neurons – one for each stimulation locus. These special neurons were connected to the network with the same lateral connections as the neurons localised at the stimulation loci. Thus, these special neurons responded as if they were part of the network and as if they were located at the stimulated locations. These special neurons had no direct connection from the stimulation input and they had no spiking threshold, preventing them from spiking – so that they replicate the experimental conditions.

Figure 5-2 and **Figure 5-3** present schematics that summarize the expected results according to Phongphanphanee et al. (2014)'s observations – note, however, that some of the schematics (in red background) are reasonable extrapolations of their results for the conditions they did not test directly. Thus, those schematics represent the desired results for the SCs and SCi models. Moreover, the schematics have a similar format to that of Figure 9.E in Phongphanphanee et al. (2014) and, importantly, they share the format of the results in sections 3.2 and 3.3 for ease of comparison. In these sections, the crucial point of comparison for the SCs models (**Figure 5-6**, **Figure 5-7**) will be the replication of a non-linear interaction / auto-catalyst for short inter-stimulation distances (the winner-take-all for long distances should be validated in the Exploration phase). For the SCi models (**Figure 5-9**), the crucial point will be to obtain linear summation of activity for any inter-stimulation distances.

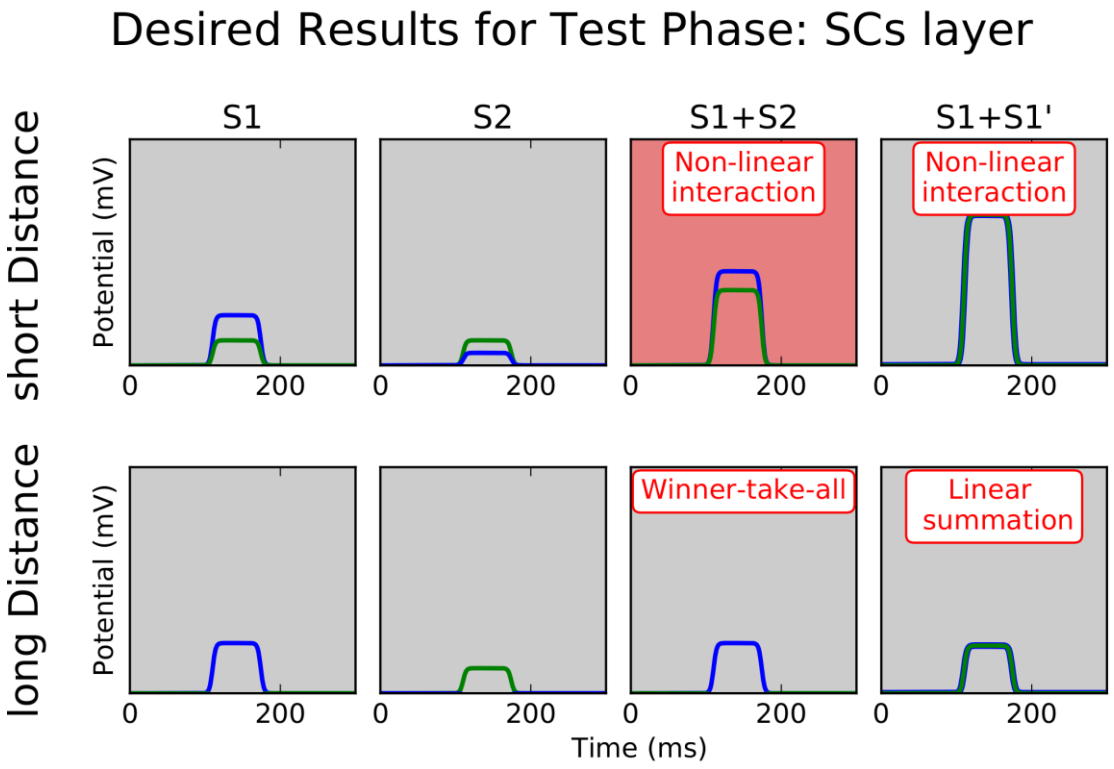

Figure 5-2: Desired Results for the Test Phase: Model of the Superficial Layer of the Superior Colliculus. *The subplots represent schematics of the expected behaviour of the SCs for the different conditions (S1 only, S2 only, S1 + S2, S1 + S1') of the Test phase according to the results of Phongphanphanee et al. (2014). As opposed to the Exploration phase, the Test phase tests several distances between the two stimulation locations. The activity of the DNF at these locations is reported by the blue and green curves (corresponding respectively to the arrows of* ***Figure 5-1****).* ***Short Distance****: for Condition S1 + S2, the resulting activity at a location near the stimulation (for example, the blue curve) is expected to be higher than the linear sum of the activity at that location (in our example, the sum of the blue curves) observed in both S1 only and S2 only. This phenomenon is referred to as positive non-linear interaction, or auto-catalyst, and it is also expected in Condition S1 + S1'.* ***Long Distance:*** *for uneven double-stimulation (S1 + S2), a winner-take-all is expected: only the activity induced by S1 (the strongest stimulation) survives, while the activity induced by S2 is completely inhibited. For even double-stimulation (S1 + S1'), a linear summation of the activity induced by the stimulations (S1 only and S1' only) is expected. The grey schematics are based directly on the observations of Phongphanphanee et al. (2014, Figure 9), while the schematics in red are extrapolations.*

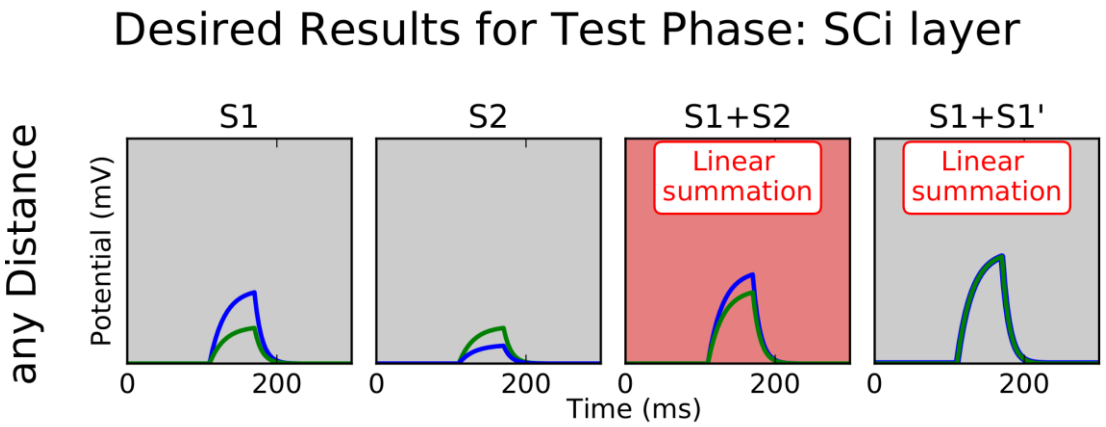

Figure 5-3: Desired Results for the Test Phase: Model of the Intermediate Layer of the Superior Colliculus. *Same description as in* ***Figure 5-2****.* ***Any Distance:*** *although different distances between the stimulation electrodes are tested, a similar pattern is expected for all of them. Based on Figure 10 in Phongphanphanee et al. (2014), for even (S1 + S1') and uneven (S1 + S2) double stimulation, a linear summation of the activity induced by each stimulation is expected. In other words, the green (or blue) curve in Condition S1 + S2 is simply the sum of the green (or blue) curves in S1 only and S2 only conditions. The grey schematics are based directly on the observations of Phongphanphanee et al. (2014, Figure 10) while the schematics in red are extrapolations.*

3 Results

We recommend downloading the PDF version of the figures as they offer the best quality and readability. In particular, they allow the reader to zoom in on each simulation and to distinguish the individual neurons.

The PDFs are accessible at:

https://drive.google.com/folderview?id=0B_xgBelrpzdta2ZVTWR4UUFxLWM&usp=sharing.

Note that we still provide a printed version for each figure in the present document.

3.1 A General Word on How to Read the Exploration Results

Figure 5-5 and **Figure 5-8** will present the main results of the exploration phase undertaken for, respectively, the SCs model and SCi model. However, before addressing them further in sections 3.2 and 3.3, we will take some time to explain how to read the subplots that they consist of and how those subplots have been organised into a grid layout.

Figure 5-4 corresponds to a single subplot from **Figure 5-5**. As with each subplot in **Figure 5-5**, **Figure 5-4** describes the behaviour of the neural field when using a specific set of

parameters for the model (see figure legend for further details). The behaviour described is in response to the double-stimulation paradigm presented in Section 2.3. The plot shows how the membrane potential (colour-axis from blue to red) of the neural field's cells (on the y-axis) evolves over time (the x-axis). As expected, the double-stimulation results in increasing the membrane potential at two locations on the neural field after time t=110 ms (the input initiation); this can be observed with the colour going from green to red. When a high membrane potential (red) is immediately followed by a small membrane potential (blue/green), this means that the considered neuron has spiked: the sharp passage from red to blue/green corresponds to a reset of the membrane potential. It can be noted that our model of the SCs, by means of the short term depression mechanism we implemented, replicates the transient responses to a step current that was observed by Phongphanphanee et al.(2014). In most of the configuration, it can also be said that the location of the strongest input is the bottom one (position 78), since it emits spikes first and most frequently. Finally, note that a red boomerang shape as in **Figure 5-5** C, E and F means that the spiking activity has spread over space and finally died: the connection setting led to an instable behaviour of the network.

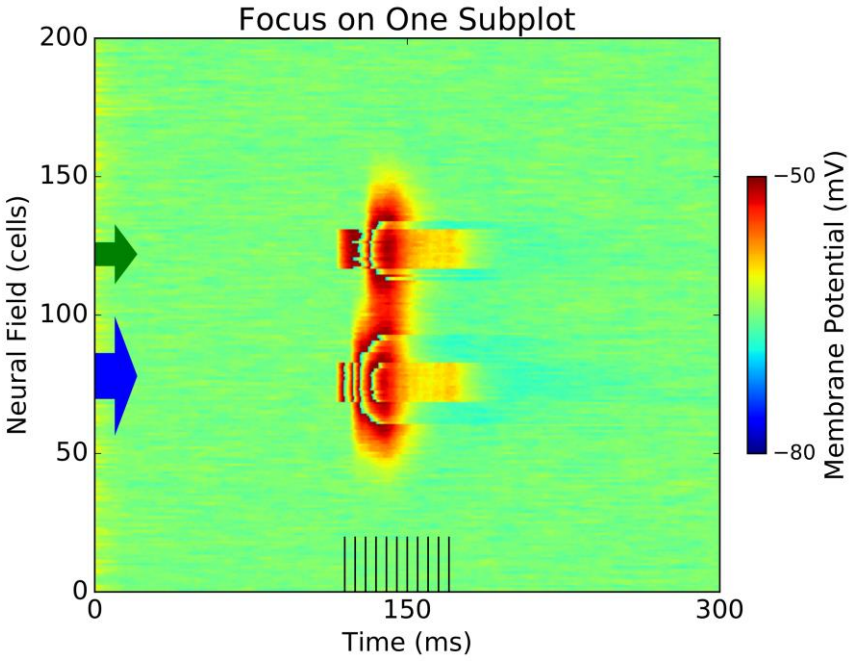

Figure 5-4: *Focus on One Subplot of* ***Figure 5-5****. This subplot corresponds to the central red-framed subplot of* ***Figure 5-5****, which corresponds to one of the parameter sets deduced from Phongphanphanee et al.'s observations. Specifically, the parameter set is:* Inhibition Extent Ratio: *σe < σi;* Inhibition Strength Ratio: *Ae > Ai;* coupling: *Medium;* delay: *Different (2.0-2.8ms for excitation, 6.9-7.8ms for inhibition, more details in method, section 2.3). The spiking neural field, prepared with this parameter set, is fed with two temporary and simultaneous inputs as described in 2.3. The y-axis represents the spatial position of the cells in the neural field; the x-axis represents the time of the simulation; the coloured-axis represents the membrane potential of each cell through the simulation.*

The grid layout of **Figure 5-5** provides an overview of the effect of the different factors under scrutiny (see Section 2.3). The figure consists of 6 grids distributed across 2 rows and 3 columns; each grid is a 3 by 3 grid of subplots (for a total of 54 simulations). The 2 rows of grids correspond to the Delay parameter (Same, Different), and the 3 columns of grids correspond to the Coupling parameter (Low, Medium, High). For each grid, the 3 rows of cells/subplots correspond to the Inhibition Extent Ratio parameter ($\sigma e < \sigma i$, $\sigma e = \sigma i$, $\sigma e > \sigma i$) and the 3 columns of subplots correspond to the Inhibition Strength Ratio parameter ($Ae < Ai$, $Ae = Ai$, $Ae > Ai$). On a general note, a brief overview of the different effects of these parameters can be given (see **Figure 5-5)**. With respect to the Delay parameter, the condition *Different* strengthens the transient response of the SCs while adding a subsequent wave of inhibition. This effect can be observed, for instance, when comparing the top left subplot of **Figure 5-5**B and **Figure 5-5**E (Medium Coupling). An increase in the Coupling parameter leads to a greater contrast in activity and can cause instability in the model – though surprisingly it did not help to achieve self-sustained activity. For example, this effect can be observed with a comparison among the red-framed subplots shown in **Figure 5-5**D, E, F. Finally, increasing the Inhibition Extent Ratio or increasing the Inhibition Strength Ratio both participate in making the model stable. In **Figure 5-5**C (High Coupling, Same Delay), for instance, the middle row of subplots shows the effect of the Inhibition Strength Ratio (note that the inhibition decreases rightward) whilst the middle column of subplots shows the effect of the Inhibition Extent Ratio (note that the inhibition decrease downward). It can be noted that ratios in favour of excitation are not necessarily leading to an unstable model (see bottom right subplots of **Figure 5-5**D, E).

3.2 SCs model: Exploration and Double-Stimulation Results

Phongphanphanee et al. (2014) reported that the SCs map behaves as a winner-take-all field. In particular, if two remote regions are stimulated, the strongest stimulated region will be the only one to show activity. However, when the two stimulations are of the same strength, Phongphanphanee et al. (2014) reported no winner-take-all. Importantly, when two stimulated regions overlap, they observed a level of activity that is more than the sum of the levels of activity that the two stimulations would generate separately (positive non-linear interaction).

Figure 5-5 reports the results of the exploration phase for the SCs model. The interesting outcome of this exploration is that none of the connection settings led to a clear winner-take-all as reported by Phongphanphanee et al. (2014) and described in **Figure 5-1** (left panel). In addition, none of the connection settings created self-sustained spiking clusters

after the offset of stimulation; rather they produced a transient spiking response. Even more interestingly, the red-framed connection settings (in **Figure 5-5**D, E, F) – which correspond to our interpretation of Phongphanphanee et al. (2014) -- do not lead to any visible inhibition between the two stimulations. Indeed, the delay of the inhibition allows a strong uninhibited initial burst at both stimulation loci. Without this delay in inhibition (see **Figure 5-5**B, top-right subplot), we can observe a disturbance in the spike train induced by the upper stimulation, but no winner-take-all. While the red framed subplots (in **Figure 5-5**D, E, F) correspond to our interpretation of Phongphanphanee et al. (2014)'s results, it appears that only the blue-framed settings (in **Figure 5-5** A, B, C) lead to no spike on the weaker side. From that, we selected the red-frame settings in addition to the blue-framed settings for further examination in the testing phase – i.e., our more complete replication of Phongphanphanee et al. (2014)'s paradigm.

Figure 5-6, A and B, present the results of the testing phase for the *red-framed setting* (see red frames in **Figure 5-5**). They allow us to check more precisely if there is competition between the two stimulations by 1) adding control conditions (S1 only, S2 only), 2) testing several distances, 3) representing the membrane potential with a curve – instead of colour gradients. Each cell of the grids of **Figure 5-6A** presents the results of one simulation, in a similar way to **Figure 5-4**. **Figure 5-6A** contextualizes what is presented in **Figure 5-6B**. We used blue and green arrows in **Figure 5-6A** to indicate the position of the neurons recorded for **Figure 5-6B** (blue and green curves respectively). Note that those neurons are the threshold-free neurons described in the method section. To summarize, it is clear from **Figure 5-6B** that there is no winner-take-all or competition observed between the two stimulated regions: in *Condition S1 + S2* (D45, D60), both the blue and green peaks have the same size as in the control conditions (unlike the desired behaviour in **Figure 5-2**, long distance). For small distances (D15, D30), we observed that there is summation of the peak of activity induced by the two stimulations. For instance, at low and medium coupling, the green peak of activity in *Condition S1 + S2* is higher than in *S1* or *S2* conditions. However, the resulting peak of activity in *Condition S1 + S2* is not greater than the linear sum of the peaks of *S1* and *S2* conditions (unlike the desired behaviour in **Figure 5-2**, short distance). This means that there is no positive non-linear interaction (i.e., auto-catalyst) as the one observed in Figure 9D of Phongphanphanee et al. (2014). In fact, in our case, the resulting peak in *Conditions S1 + S2* can be smaller than the linear sum of the peaks of both *S1* and *S2* conditions. This can be observed, for instance, with the green peaks in **Figure 5-6**B, at D15.

Figure 5-7 shows the results of the testing phase for the *blue-framed settings* (see blue frames in **Figure 5-5**). The representation of the data here is similar to that used in **Figure**

5-6. For these connection settings, we observed a winner-take-all similar to that observed by Phongphanphanee et al. (2014, see *their* Figure 9E, F, G) in *Condition S1 + S2*. This can be observed at distances D30 and D45 for all Coupling levels. Specifically, in **Figure 5-7**B, the green peak that is otherwise induced by the weaker stimulus (S2) is not present in *S1 + S2* conditions (similarly to the desired behaviour in **Figure 5-2**, long distance). For distances D15 and D60, the green peak is present: there is no winner-take-all. Also, when S1 is presented with an equal strength stimulation S1', no winner-take-all is observed at any distance (similarly to the desired behaviour in **Figure 5-2**, long distance). Indeed, in **Figure 5-7**B, the green and the blue peaks observed in *Condition S1 + S1'* are both similar to the blue peak in *S1* conditions – thus S1 and S1' appear to not disrupt each other. This result is in line with the absence of winner-take-all interaction between equal strength stimuli observed by Phongphanphanee et al. (2014, see *their* Figure 9B, C, D). Despite the absence of winner-take-all, there is notably still mutual inhibition between equal strength competitors: in *Condition S1+S1'*, S1 caused a smaller increase of membrane potential than in *Condition S1 + S2*. In terms of the excitatory interaction, in **Figure 5-7**B, we do not observe any positive non-linear interaction as compared with Phongphanphanee et al. (2014)'s Figure 9D and our **Figure 5-2** (the interpretation of the curves in **Figure 5-7** is therefore similar to those of **Figure 5-6** above).

Finally, one of the most striking differences between the simulated results and the desired results described in **Figure 5-2** (based on Phongphanphanee et al., 2014) is the pattern of the membrane potential response to the stimulations. Our membrane potential curves show a well-defined transient increase followed by a wave of inhibition, while the curves generated in the study by Phongphanphanee et al. (2014) show an accumulation to a stable value (see *their* Figure 9). Note that in *their* study, the curves displayed in (*their*) Figure 9 are quite different from those displayed in (*their*) Figure 1C. Our single neuron model of the SCs neurons was based on (*their*) Figure 1C. The curves of their Figure 1C - as opposed to their Figure 9 - presents a transient response (we will return to this issue in the Discussion, Section 4.1).

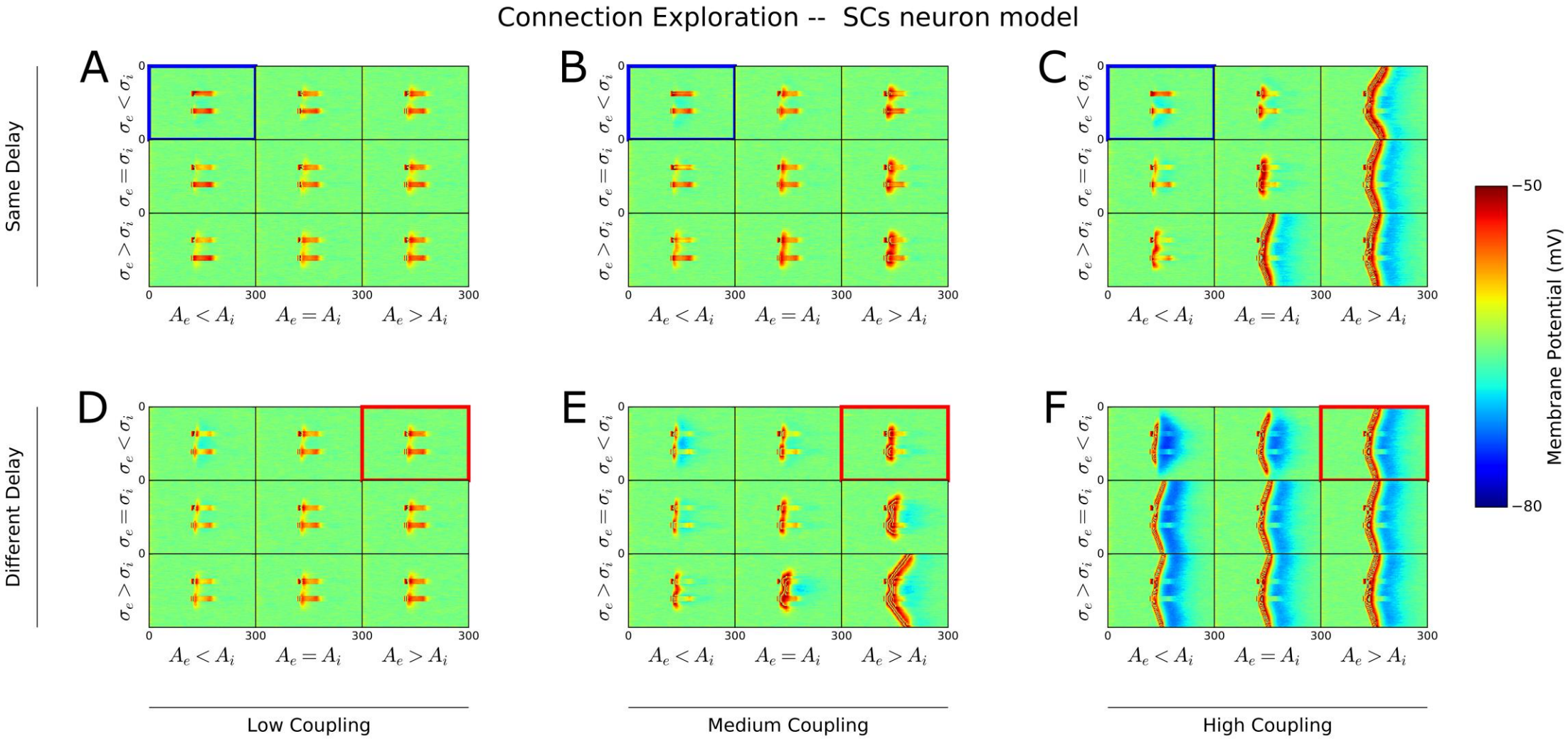

Figure 5-5: Exploration of lateral connection settings for SCs model. *Each plot cell represents time on the x-axis and the neural field space on the y-axis, so that each row represents the data of one neuron. The colour, running from deep blue to deep red, indicates the membrane potential of the neurons, red being the highest. The red frames indicate the connection settings corresponding to those of Phongphanphanee et al. (2014). Further tests of the red-framed and the blue-framed settings are displayed in, respectively,* ***Figure 5-6*** *and* ***Figure 5-7****.*

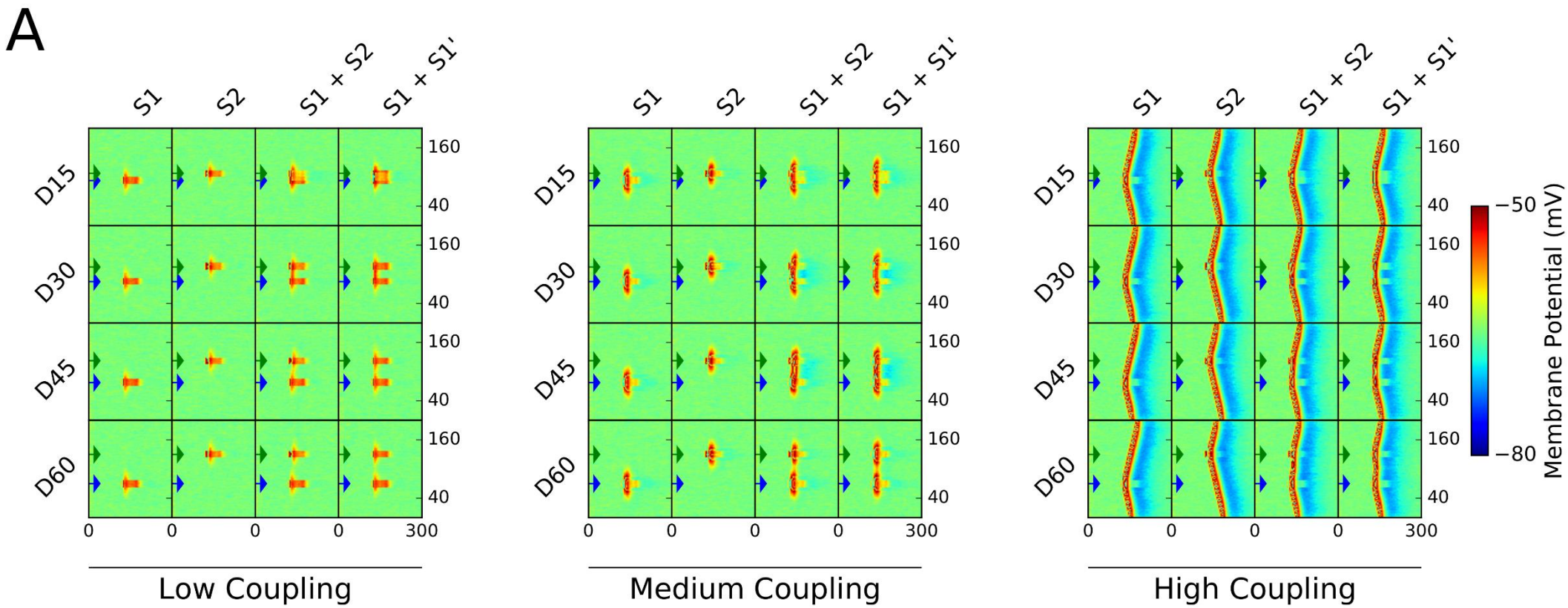
A
S1
S2
S1 + S2
S1 + S1'
D15
D30
D45
D60
160
40
0
300
Low Coupling
Medium Coupling
High Coupling
−50
−80
Membrane Potential (mV)

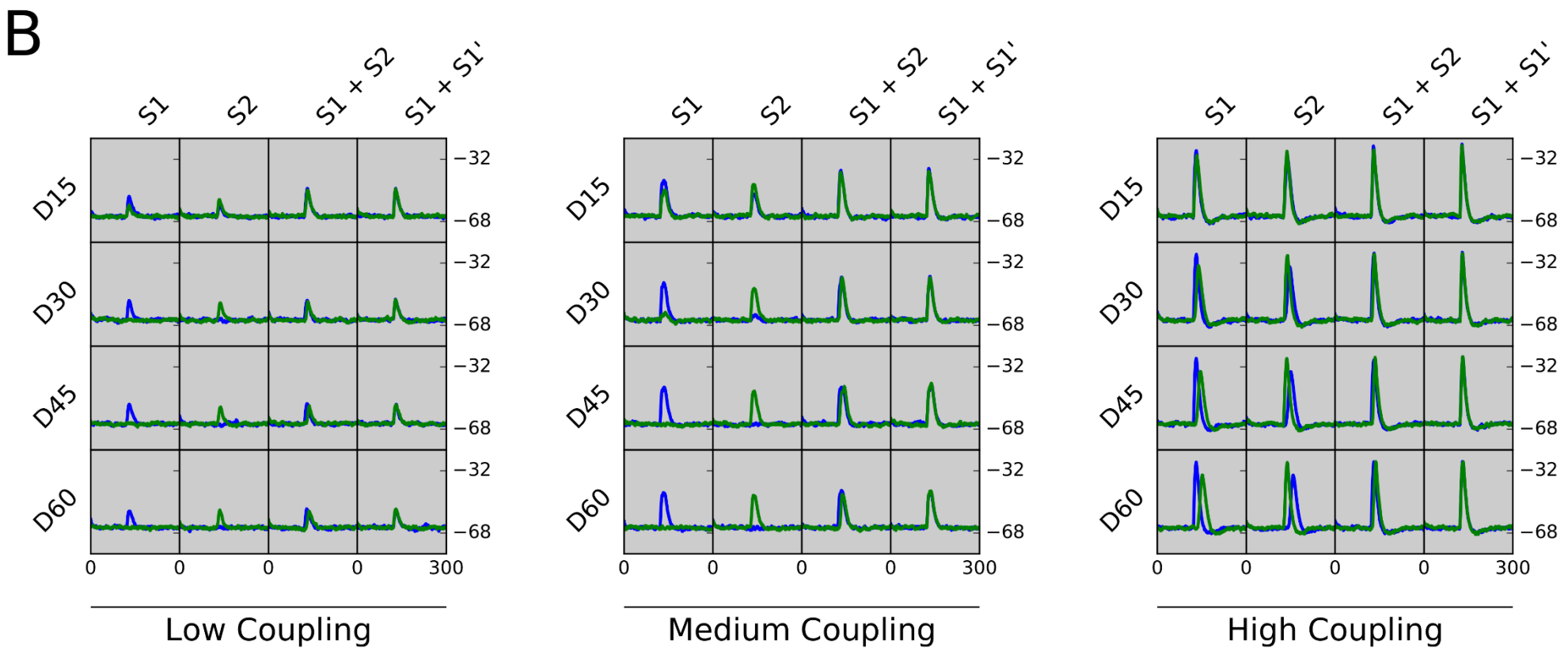

Figure 5-6: Double-stimulation paradigm with the red-framed connection setting *(see red frame in* ***Figure 5-5****).* ***A:*** *the plot shows the membrane potential of each neuron of the field evolving over time. Each grid of the plot represents one level of coupling. In each grid the different rows feature different distances between the two stimulations (D15 is 150µm for instance). The columns denote the different conditions described in the method (S1 only, S2 only, S1+S2, S1+S1'). **B:** we report the membrane potential curves for the neurons located at positions marked with the green and the blue arrows on the top figure. These neurons did not have a threshold and they were not directly connected to the input stimulation.*

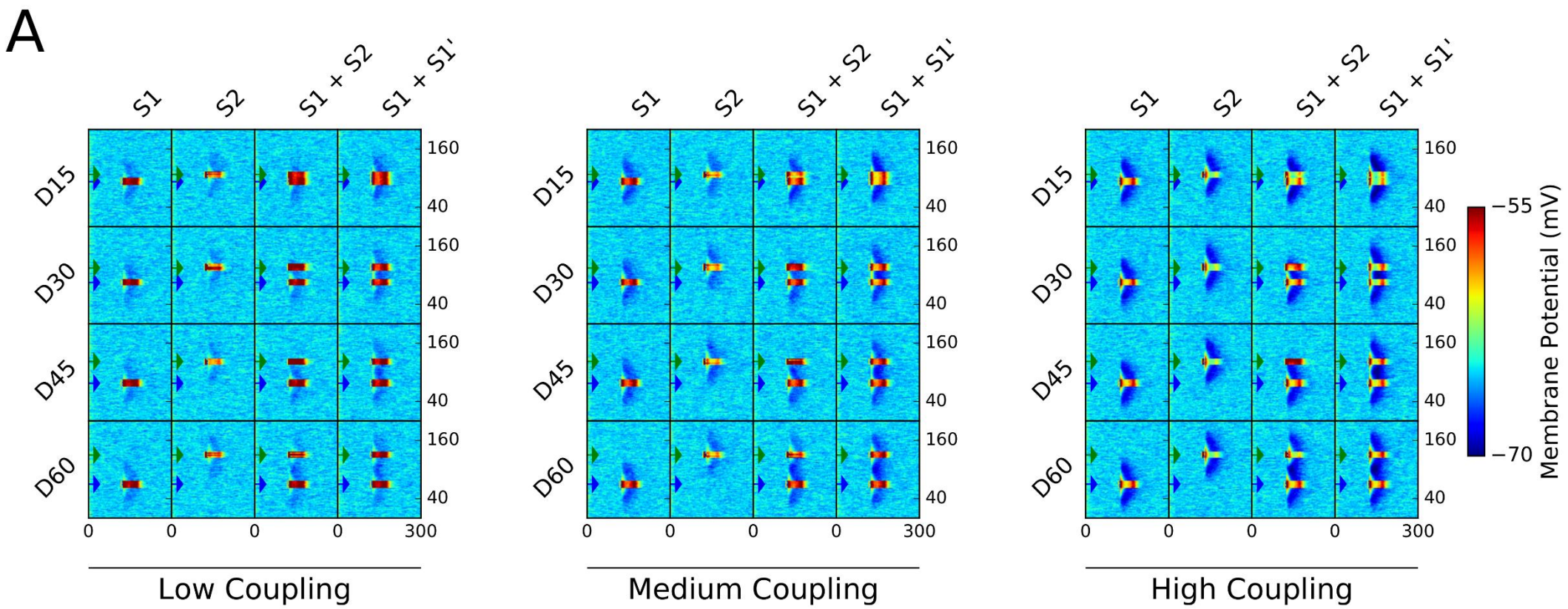
A
S1
S2
S1 + S2
S1 + S1'
D15
D30
D45
D60
160
40
0
300
Low Coupling
Medium Coupling
High Coupling
−55
−70
Membrane Potential (mV)

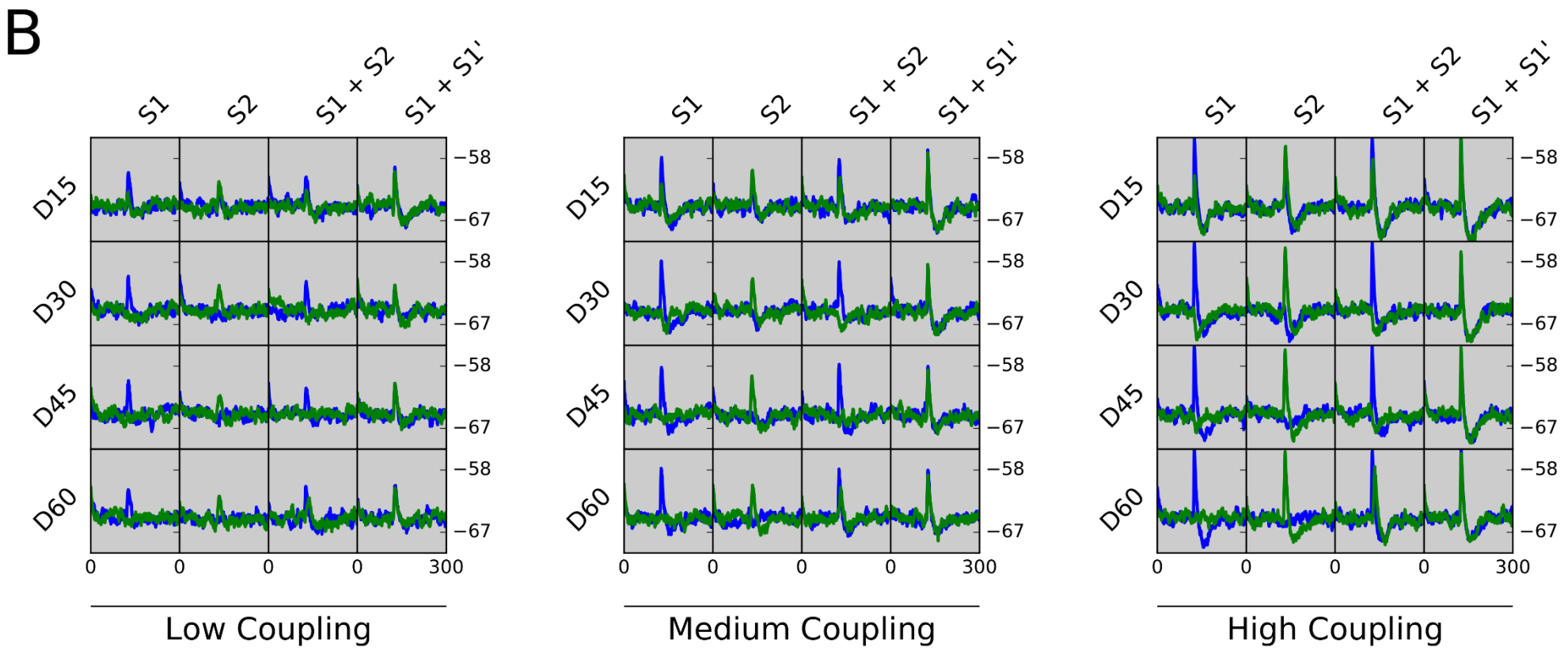

Figure 5-7: Double-stimulation paradigm with the blue framed connection setting *(see blue frame in Figure 2). The description is the same as that given for Figure 3.*

3.3 SCi model: Exploration and Double-Stimulation Results

Phongphanphanee et al. (2014) reported that the SCi map behaves as an accumulator, without competition between two stimulated regions. Importantly, when two stimulated regions overlap, they observed a linear summation of the activity of the two regions.

Figure 5-8 displays the results of the exploration phase for the SCi model (similar to **Figure 5-5** for the SCs model). The interesting outcome of that exploration is that most connection settings led to the same kind of behaviour (except when unstable) and they clearly failed to replicate the behaviour reported by Phongphanphanee et al. (2014). In other words, none of the tested sets of parameters led to a clear linear summation such as described in **Figure 5-1** (right panel). Note that the effects of the factors we tested are similar to the observations reported with the SCs model in Section 3.1. The connection settings corresponding to the suggestions of Phongphanphanee et al. (2014) are framed in red. As the results are quite similar for all the connection settings (except when unstable), we will use only the red-framed subplot at Medium Coupling as a reference in the following description.

In all connection settings the neurons that were stimulated spiked immediately after the first stimulation pulse was delivered (it is important to recall that the stimulations consisted of 11 pulses at 200Hz). It is only after this initial spike (and the reset) that the stimulated neurons began to work as accumulators. When in accumulator-mode, the neurons accumulated the input pulses up to the spiking threshold, whereupon they spiked and reset, and began again. It is important to note that the accumulation is taking place at the level of the membrane potential: as there is no spike, no interaction between the two stimulated locations is possible and extra-cellular recording would register no firing rate. Note that it is only when the stimulated neurons spike that they interact with their neighbours. Thus, as most of the connection settings lead to relatively *long* sub-threshold accumulation of the input, interactions are very limited. When there are spikes emitted in one of the stimulated regions, there are two things happening in parallel: 1) there is a decrease of membrane potential in the stimulated regions due to the reset mechanism, 2) there is an increase in the membrane potential in the immediate neighbourhood of the stimulated region -- that is, the postsynaptic potential. It appears that the postsynaptic potential caused by one stimulated region has too limited a spatial extent to affect the accumulation occurring in the other stimulated region. As a result, it can be observed that: 1) the level of activation in between the two stimulated regions appears to be a linear summation of the postsynaptic potentials of both stimulated regions; 2) the two stimulated

regions are accumulating their input in an independent manner. This is possibly because the two stimulated regions are too far apart.

In summary, it appears that, whatever the connection settings, our model of a single neuron of the SCi fails to generate a simple temporal accumulation – i.e., it always begins with an initial spike. Furthermore, no connection setting appears to generate a linear summation of activations observable in or near the stimulated regions. As no connection setting appears to be encouraging in terms of replicating the behaviour of the SCi reported by Phongphanphanee et al. (2014), we chose only the red-framed settings for further examination in the testing phase.

Figure 5-9 reports the results of the test phase for the red-framed connection settings. The representation of the data is similar to that displayed in **Figure 5-3** and **Figure 5-6**. It shows the membrane potential of threshold-free neurons at the location of the stimulation, for the connection setting framed in red in **Figure 5-8**. These special neurons received input only from the neighbouring area and not from the input stimulation. It is clear when comparing **Figure 5-9**B with **Figure 5-3** that we did not obtain the desired results for the SCi layer. Indeed, we did not observe any sum of activity for the tested inter-stimulation distances: 1) the curves of *Condition S1 + S2* cannot be explained by the addition of the curves of *S1 only* and *S2 only*; 2) the curves of *Condition S1 + S1'* cannot be explained by adding the curves of *S1 only* and *S1' only* (the *condition S1'* only is not shown: it would be similar to *S1 only*, switching the blue and green colour). In summary, the model fails to replicate the summation of activity reported by Phongphanphanee et al. (2014), even when the inter-stimulation distances are short.

Intentionally Blank Page

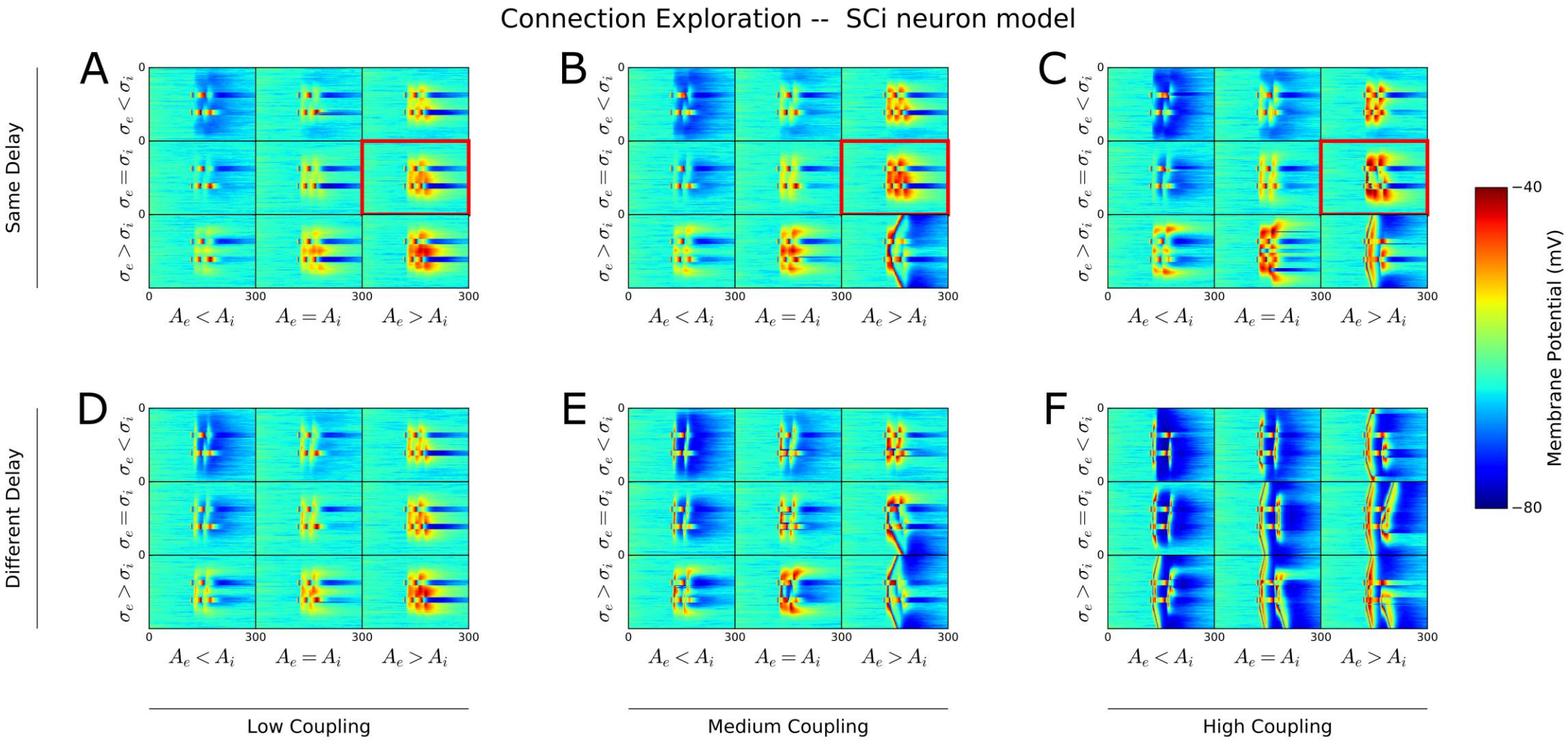

Figure 5-8: Exploration of lateral connection settings for the SCi model. *The description is the same as that given for* ***Figure 5-5****. The red-framed plots correspond to the connection settings we interpreted from Phongphanphanee et al. (2014).*

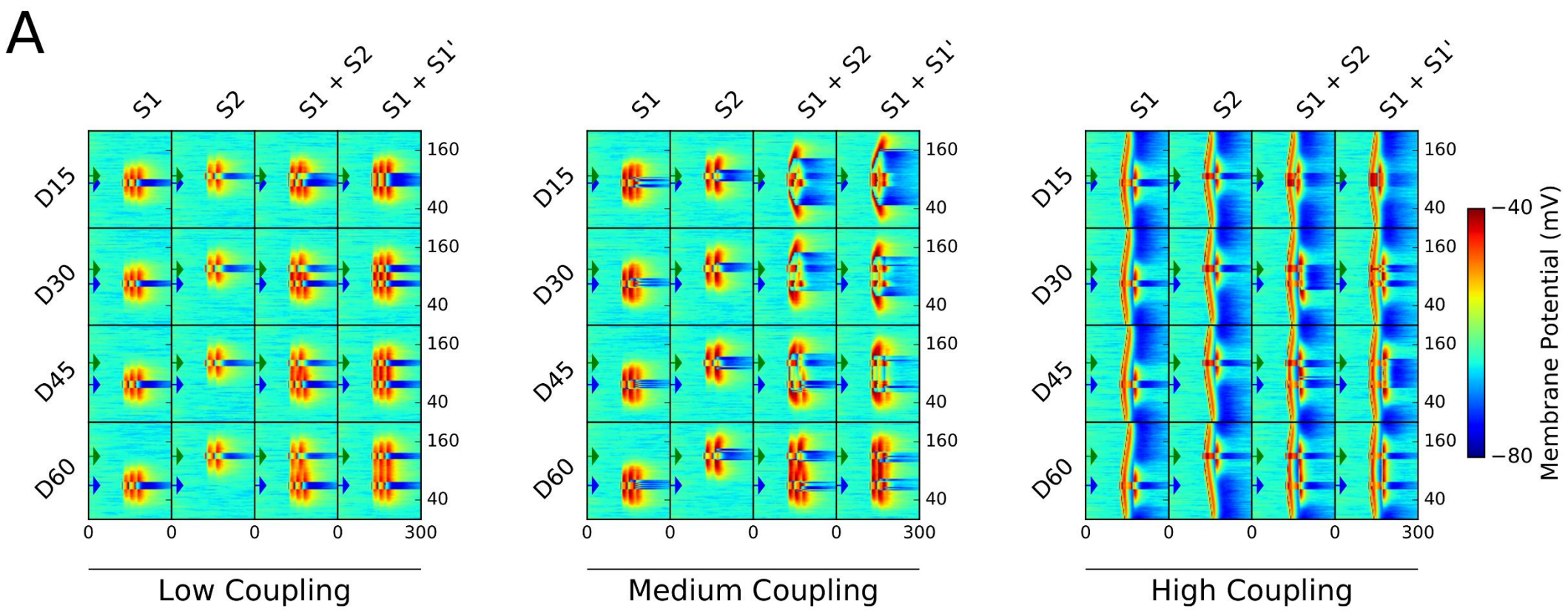
A
S1
S2
S1 + S2
S1 + S1'
D15
D30
D45
D60
160
40
0
300
Low Coupling
Medium Coupling
High Coupling
−40
−80
Membrane Potential (mV)

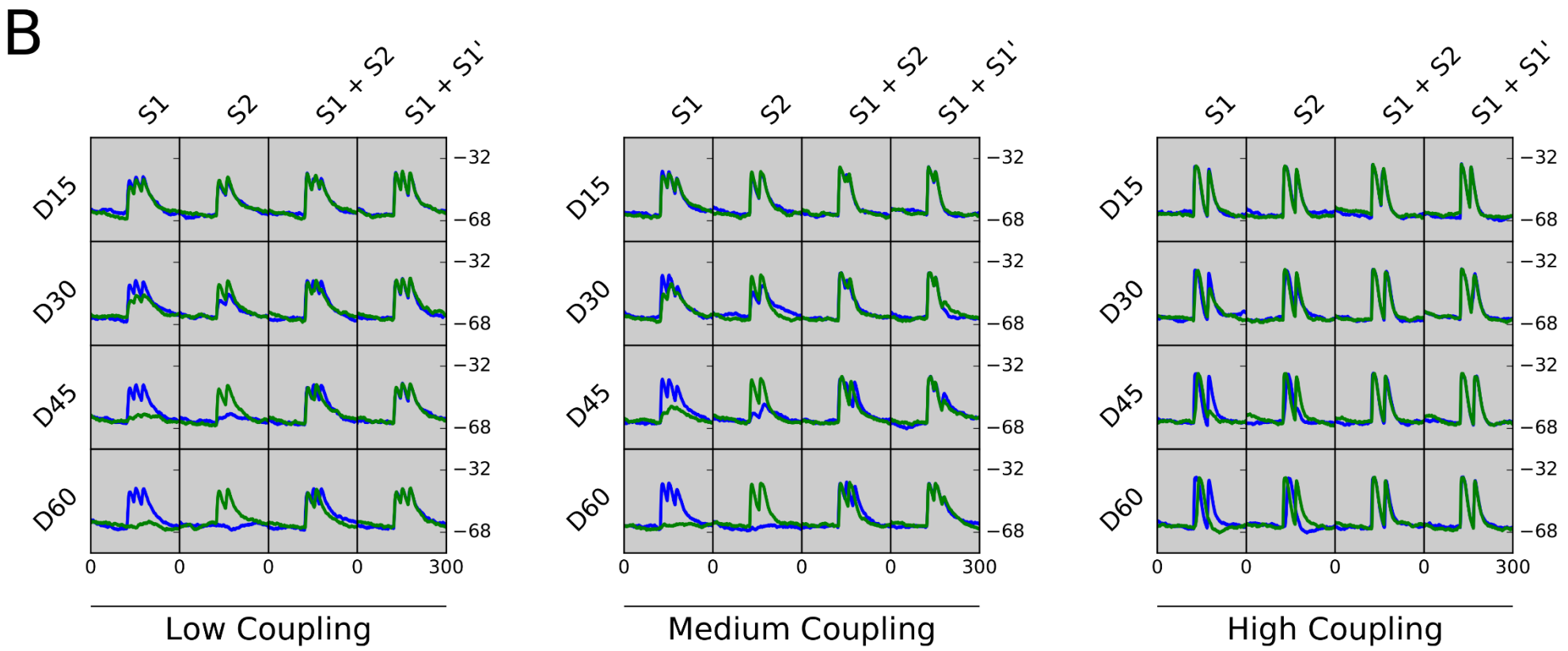

Figure 5-9: Double-stimulation paradigm with the red-framed connection setting *(see red frame in* ***Figure 5-8****). The description is the same as that given for* ***Figure 5-6****.*

4 Discussion

With the development of neural field models that are able to successfully explain behavioural data, the development of new techniques of neural ensemble recording and the development of spiking neuron network simulators, it appears that the neurosciences hold all the keys to connecting neurons with actual behaviour. It is from this perspective that our current work has developed. In particular, we aimed to follow up a recent study that made use of neural ensemble recording in the Superior Colliculus (Phongphanphanee et al., 2014). The work presented in this chapter is a preliminary attempt to use those first recordings to build a model of the Superior Colliculus from a basic neurophysiological perspective.

Our aim was to address the claims of Phongphanphanee et al. (2014): we tested whether the specific connection patterns that they reported to have found in the SCs and SCi could replicate the behaviour of the SCs and SCi that they observed when implemented in a homogenous DNF. Note that the single neuron model used to build our DNFs is described in Appendix A. As a precautionary measure, and to allow deduction of the parameter roles, we explored the parameter space that surrounds the reported pattern of connectivity. We found that the connection setting that we interpreted from Phongphanphanee et al. (2014) does not produce the neural behaviour they observed. In particular, we observed neither a winner-take-all dynamic for the SCs or a spatial or temporal accumulation for the SCi. Nevertheless, for the SCs model, our exploration revealed a connection setting that produces a winner-take-all dynamic. This connection setting is actually close to what the results of Phongphanphanee et al. (2014) suggest except that it uses 1) equal delay of excitation and inhibition, and 2) stronger inhibition. Interestingly, the SCs neuron model leads to transient responses that were not observed in the original data that we attempted to replicate. This phenomenon was observed in another part of the work of Phongphanphanee et al. (2014) that we used to configure the single neuron model (Appendix, Section 6.3.2.). Finally, no solution was found for the SCi model. The single neuron model that we constructed for the SCi is potentially unable to explain the SCi dynamics – and this may be particularly due to a premature spike at the onset of the input.

We will discuss here how the transient response can be linked to the literature. We will then consider what might be improved in the model, along with the sort of data that are required from neurophysiology in order to achieve these improvements.

4.1 Superficial layer of the SC: two neural populations to explain transient visual bursts and winner-take-all?

A considerable discrepancy can be noticed between the present results and those of Phongphanphanee et al. (2014). In particular, our attempt to replicate their double stimulation paradigms for the SCs network (see **Figure 5-6** and **Figure 5-7**, for comparison with *their* Figure 9E) yielded a very clear transient increase of the membrane potential for the recorded neurons, which is translated into a transient burst of spikes in the stimulated regions. In their study, Phongphanphanee et al.(2014) observed no transient increase while they reported a clear winner-take-all dynamic (see *their* Figure 9E). The clear transient response that we observed is in accordance with 1) the pulse-decay pattern of the synaptic current that they observed in *their* Figure 7, and 2) the pulse-step pattern of the membrane potential that they observed in *their* Figures 1C and 2B. In fact, our model of a single neuron of the SCs was designed with a synaptic short-term depression so that it replicates the pattern observed in *their* Figure 7, 1C and 2B (see Appendix A, Section 6.3.3 -**Figure 5-13**). Surprisingly, this aspect of the neural response disappears upon inspection of their Figure 9E. Thus, the discrepancy between our observation and theirs could be a result of the discrepancy between their Figure 1C, 2B -- which we used to build the single neuron model-- and their Figure 9 – which we used to test the neural field model. It is possible that their assumption of neural homogeneity is flawed, and that there are, in fact, different types of neurons in the SCs. If this is the case, one category of neurons could play a role in a winner-take-all mechanism whilst another category could be involved in transient responses.

Interestingly, it is worth noting that a localized transient visual burst (of firing rate) on the SC map in response to a visual stimulus is actually observed in SC studies on regular saccades (Dorris, Olivier, & Munoz, 2007; Dorris, Paré, & Munoz, 1997; Mays & Sparks, 1980; Munoz & Wurtz, 1995a). This transient visual related burst is thought to originate from the SCs and to play an important role in orienting responses in general (Boehnke & Munoz, 2008) and in the generation of express saccades (Isa, 2002; Marino, Levy, & Munoz, 2015). Importantly, it is the case that the transient visual burst is not subject to any strong competition or to any winner-take-all dynamic. Indeed, it has been shown that the transient visual burst occurs for any stimuli presented in the visual field irrespective of whether it is the target of a saccade (McPeek & Keller, 2002a). Furthermore, in models that have been successful in explaining reaction time distribution of saccadic eye movements, the presence of an early transient visual burst for both distractors and target represents an essential cogwheel (Bompas & Sumner, 2011; Trappenberg et al., 2001). Thus, it appears that from the perspective of this literature, our model fares rather well when implementing the red-

framed connection settings (in **Figure 5-6**), which do not produce a winner-take-all and correspond to the connection setting suggested by Phongphanphanee et al. (2014).

Nevertheless, Phongphanphanee et al. (2014) reported a winner-take-all dynamic that our model cannot explain with the connection setting that they suggested. Our blue-framed connection setting, which replicated the winner-take-all system, helps us to understand why the red-framed setting does not. The important difference between the red and blue-framed setting is that, in the former setting, the inhibition is delayed relative to the excitation. This delay of the inhibition increases the amplitude of the transient burst and makes simultaneous stimulations *immune* to competition – preventing any winner-take-all. Thus, because this mechanism is systematic, it is difficult to reconcile the delays of inhibition and excitation reported by Phongphanphanee et al. (2014) with the winner-take-all dynamic that they observed. Further investigations *in vitro* and further improvements of the model will be needed to understand the origin of these *a priori* puzzling discrepancies. For now, our hypothesis is that there are, at least, two categories of neurons in the SCs: one would drive winner-take-all sustained responses while the other would drive non-competitive transient responses. The idea that all the SCs neurons are not all following a winner-take-all dynamic is supported by results from the Optic Tectum of the barn owl, where some neurons display switch-like responses (that can be related to winner-take-all dynamic) while other neurons display gradual responses (Mysore et al., 2011). Therefore, an interesting direction would be to break the assumption of neural homogeneity in the SCs/SCi that was adopted by Phongphanphanee et al. (2014).

4.2 Intermediate Layer of the SC: Toward an improved model

Although we can argue that the results of our DNF model of the SCs network makes sense on the basis of the previous literature on transient visual burst, our DNF model fails to reproduce the observation of Phongphanphanee et al. (2014). It replicates neither the winner-take-all that they observed in the SCs or the spatial and temporal accumulation observed in the SCi. We will address the directions for future improvements of the model in this section.

At the level of the single neuron (a complete discussion is available in Appendix A, Section 6.4), we suggest that a more complete mechanism of spike-frequency adaptation is needed, possibly along with an escape noise (stochastic threshold) to increase the flexibility of our model. Indeed, it has been difficult to fit the SCs and particularly the SCi neuron models to the f-I curves of Saito and Isa (2003) – see Appendix A, **Figure 5-15** . This is because the f-I curves reported by those authors are very linear while common integrate-and-fire models

make non-linear f-I curves. To add an escape noise would help in obtaining spikes for very small currents without having to decrease the time constant of the membrane. This would make the f-I curves more linear and would prevent the premature spike that we observed at stimulation onset. A spike-frequency adaptation could also help in attaining a more linear increase of the f-I curves.

Importantly, such improvements should be accompanied by a better fitting method of the single neuron model. Here, we had to work with the recording that Phongphanphanee et al. (2014) and Saito & Isa (2003) published. The fitting of spiking neuron models to single neurons would be facilitated if the neurophysiologists knew specifically what kind of data to record in order to fit a model. For instance, when intra-cellular recording is available, well-defined procedures exist such as the dynamic I-V (current against voltage) curve estimation (Badel, Lefort, Berger, et al., 2008; Badel, Lefort, Brette, et al., 2008) where the neurophysiologist needs to record the single neuron response to fluctuating current only for a few seconds. From that, the modeller can attain a very precise model of the single neuron. Furthermore, the relatively short time of recording needed readily allows the recording of a large amount of neurons. We believe that by way of a cluster analysis across all the fitted neurons on the parameter space, this fitting method would allow us to assess quantitatively whether - and to what extent - there are different types of neurons in the SCs and SCi. It should be noted that extra-cellular recording can also be used to parameterize spiking neurons (Jolivet, Lewis, & Gerstner, 2004; Rossant et al., 2011). In fact, extra-cellular recordings have been used successfully to characterize a complete neuronal population of retinal ganglion cells and their functional connectivity (Pillow et al., 2008). Thus, an interesting direction would be to replicate that latter work for the different neural populations in the SCs and SCi.

One important direction for both modellers and neurophysiologists is to integrate the neural diversity of the SC, and most importantly, to unify the different perspectives of that diversity (morphology, firing pattern, location in the SC, receptor type, neurotransmitter type). We will return to that point in the General Discussion.

4.3 Feedback to Phongphanphanee et al. and to the neurophysiology community

Our attempt to translate the work of Phongphanphanee et al. (2014) into a model of the superficial and intermediate layers of the SC was a very insightful experience. From this work, the following three questions have emerged: 1) What could be improved in their paradigm in order to make it more relevant for a modeller? 2) What kind of information

was lacking, which would be needed for modelling? 3) What could be done next? Some possible answers to these questions are described next

1. The electrical stimulation used by Phongphanphanee et al. (2014) may be complicated to model and may not be the most relevant for the study of a network. For instance, it is unclear whether the electrical stimulation was exciting both local inhibition and local excitation neurons at the same time. It would be a welcome improvement to select exactly which types of neurons are stimulated. Indeed, under natural conditions, external excitation may synapse selectively with the local excitatory neurons, or with the local inhibitory neurons. Failure to control which neuron receives direct stimulation may change the general dynamics of activation. Alternatively, it may be interesting to stimulate axons reaching the SC instead of the SC itself. This was the approach adopted by Saito and Isa (2003), in order to get a better idea of the natural behaviour of the SC.

2. A helpful addition would be to use TTX (tetrodotoxin) to block spikes from presynaptic cells as a control for the results presented in their Figures 1.C, 5.C, and 7. Indeed, the electrical stimulation itself may affect the recorded neurons and there is no way of knowing to what extent their observations are the result of the electrical stimulation alone, or the effect of the presynaptic spiking neurons.

3. In relation to point 2, the size of the neural region that is stimulated – and hence the number of activated neurons - is unknown. For instance, it appears that the glutamate photo-uncaging method stimulates less neurons than the electrical stimulation method (this is detailed in the next point). Having an estimation of how many pre-synaptic neurons are spiking is essential, in order to make a good estimation of the synaptic current recorded in whole-cell patch clamp. It should be recalled that by default and for the sake of simplicity, we assumed there to be only one pre-synaptic neuron spiking (Appendix A). This problem is also related to defining the neural density in the SC.

4. In relation to point 3, the size of the neural region that is stimulated may be different from the size of the neural region that is indirectly activated. More precisely, there are, at least, two possible situations that might have occurred whilst Phongphanphanee et al. (2014) made their whole-cell patch clamp recording:

- First, there are no strong recurrent excitatory connections in the network (i.e., a low coupling). Here, the stimulated region and the activated region are equal. Importantly, the size of the activated region depends on the properties of the stimulation. In this

case, the experimenter observed mono-synaptic responses of the recorded neuron from few spikes coming from a relatively small region of stimulated neurons.

- Second, there are strong recurrent excitatory connections in the network (i.e., a strong coupling). The stimulation has triggered an auto-catalyst that led to a self-sustained activation of a region of the SC layer. This region is emitting many spikes and corresponds with what we referred to as spiking clusters in Chapter 2. Importantly, the size of this region only depends on the lateral connections. In this case, the experimenter observed mono and multi-synaptic responses of the recorded neuron from a cluster of spiking neurons initiated by the stimulation.

5. It is important to note here that these two cases represent the extreme end of a continuum. The fact that the network does not continue to spike after the removal of electrical stimulation in the study by Phongphanphanee et al. (2014) suggests that there is no self-sustained activity (spiking cluster). This could mean that both SCs and SCi do not have strong recurrent connections (i.e. they have a low coupling). Furthermore, in the SCi, there is a difference in results when using uncaging photo-stimulation and using electrical stimulation (see *their* Figure 6D and E): the regions of activation are larger when using the electrical stimulation (size ratio of 2; Full Width at Half Maximum: 450µm against 224 µm). This leads to the suggestion that the size of the activated region depends on the type of stimulation, which is typical of a low coupling network. With regard to the SCs, a coupling that is too low would prevent any winner-take-all dynamic (because of the absence of strong interactions between stimuli). Interestingly, Phongphanphanee et al (2014) reported winner-take-all in the SCs. In fact, in the SCs, the size ratio of activated surface between the electrical stimulation condition and the uncaging photo-stimulation condition is smaller than that observed in the SCi (see Figure 4D and E): the ratio is at 1.2 (Full Width at Half Maximum: 331µm against 272µm). This smaller effect of the input property suggests that the SCs has a higher coupling than the SCi, making its activation less sensitive to a change in the input. The SCs coupling would be high enough to enable competition, and low enough to prevent self-sustained activity. Note that the short term depression allowing the transient response of the SCs would also help preventing self-sustained activity.

6. Related to point 4, and assuming there is a category of neurons in the SC that behave as a DNF, we believe that a measure of their coupling is needed. Note that this measure would also be useful to parameterize DNF models of the SC that do not use spiking neurons. Indeed, the level of coupling is a fundamental question for understanding the capabilities of a network. If the coupling is low, the neurons are mostly driven by the

input stimulation. If the coupling is high, the neurons are less influenced by the input stimulation once they start spiking. The test that we suggest is to conduct a double-stimulation paradigm, where there is an onset asynchrony (OA) between two close stimulations. The experimenter would estimate the position of the resulting bump of activity just after he applied the second stimulation. In a low coupling network the final bump of activity will be closer to the loci of the second stimulation, while for the high coupling network the final bump of activity would be closer to the locus of the first stimulation. The way in which the centre progresses from the first to the second stimulation locations across the OAs would reveal the degree of coupling.

7. The paradigm would gain from a single pulse condition for the voltage clamp condition. The voltage-clamp condition allows us to achieve the current input, whilst a one-pulse condition would have directly given us the synaptic pulse function. The use of TTX would have confirmed the presynaptic nature of the pulse; while the uniqueness and the delay of the pulse would have confirmed its mono-synaptic nature.

8. To finish, Phongphanphanee et al. (2014) noticed an excitation delay of 2.38 ± 0.41 ms and an inhibition delay of 7.79 ± 0.90 ms in the SCs, but did not report any delay measurement for the SCi.

5 Conclusion

To connect neural behaviour to macroscopic behaviour is not a trivial enterprise and so we shall begin by looking at small, easily accessible, and old – i.e. basic -- brain regions. Indeed, it would be logical for a trainee architect to start replicating standard houses before beginning to replicate eccentric skyscrapers (to follow the analogy in the introduction). Most of the basic knowledge accumulated while building houses will be essential to the architect when building skyscrapers. A tiny brain structure such as the SC already presents an amazing level of complexity, and modellers need to work in close collaboration with psychophysicists and neurophysiologists in order to ascertain which complexity is functionally needed, and which complexity is superfluous. For instance, attempts such as that reported by Morén et al. (2010, 2013) were made to incorporate a high degree of complexity into a model of the SC, but only few functional benefits were extracted from it. To return to the house analogy, we could spend a long time developing a machine to observe very precisely the wallpapers for each wall of our neighbour's house. From that, we could spend even more time developing a machine able to replicate exactly those wallpapers. However, if we had in mind the function of the house, i.e., to be comfortable, we

would realise that we could choose any wallpaper that we wished. To understand what is wallpaper and what is functionally necessary in terms of the SC is essential, and it will help the modeller to avoid getting lost in superfluous complexity when confronted with more complex brain regions. Maintaining an appropriate balance between complexity and functionality needs to be at the core of any enterprise attempting to connect neurons to behaviour.

6 APPENDIX A: Estimation of the single neuron models

6.1 Introduction

In the present work we are attempting to extract the parameters of two neuron models: one model will try to fit a typical neuron of the SCs and another will try to fit a typical neuron of the SCi. Indeed, one of the assumptions made in the work of Phongphanphanee et al. (2014) is that there is only one type of neuron for each SC layer. As several electrophysiology methods will be referred to in this section, such as the current clamp, the voltage clamp, and whole-cell recording. A brief introduction to those methods is given next.

It is now more than 60 years since Kenneth Cole, Alan Hodgkin and Andrew Huxley made one of the most spectacular and formidable breakthroughs in Neurophysiology, Neurosciences, and Computational Neurosciences (Nobel Prize in Physiology or Medicine in 1963). Re-introducing the squid giant axon as a medium to study neurons (after Young, 1936), their work has led to 1) the first tools for intra-cellular recording of the membrane potential of neural cells (Cole & Curtis, 1939; Curtis & Cole, 1942); 2) the first tools for recording post-synaptic currents through voltage clamp (Hodgkin & Huxley, 1952; Marmont, 1949, with Cole), and 3) the first modular and long-lasting model of a biological neuron (Hodgkin & Huxley, 1952). The majority of current spiking neuron models (such as Brette & Gerstner, 2005; Izhikevich & others, 2003) are simplifications of Hodgkin and Huxley's model. Those pioneers introduced *the current clamp method* that allows for the injection of a current into a cell to observe its membrane potential (the difference in ionic charges between the inside and outside of the cell) and *the voltage clamp method* that maintains the membrane potential to a fixed value and makes explicit the currents passing through the cell's membrane.

The whole-cell patch-clamp has refined the use of these methods (Hamill, Marty, Neher, Sakmann, & Sigworth, 1981; Neher & Sakmann, 1976, Nobel Prize in Physiology or Medicine, 1991). The electrode consists of a microscopic glass pipette containing a thin metal. The electrode is filled with a solution mimicking the intra-cellular solution of neural cells, and is delicately attached to a neural cell by suction: hence, a membrane region is captured inside the electrode. Subsequently, a little more suction is applied so that the captured membrane region breaks, mixing the intra-cellular solution and the pipette solution. The metal wire is now recording the whole-cell potential. This method allows for high precision and can be used to access any types of neurons, of all sizes. Interestingly, while the technique was limited to *in vitro* study, it is now used *in vivo* with head-

immobilized anaesthetized animals (for instance, Ferster & Jagadeesh, 1992), awake animals (for instance, Margrie, Brecht, & Sakmann, 2002) along with freely moving animals (A. K. Lee, Manns, Sakmann, & Brecht, 2006).

Interestingly, paradigms can be organised in order to observe specifically the excitatory or inhibitory post-synaptic currents (E/IPSP) received by the recorded neuron. For instance, in order to filter the EPSPs and to reveal only the IPSPs, the experimenter will apply a *voltage clamp* to the recorded cell so that its membrane potential is kept at the Nernst Potential of the excitatory ions. This Nernst potential is the equilibrium of the excitatory ions: no excitatory ion is attracted outside or inside the neural cells. Thus, there is no ion passing through excitatory receptors when they get opened due to a pre-synaptic spike. In other words, the excitatory flux of the recorded neuron is frozen.

6.2 Method

6.2.1 Summary of Method:

Here, we overview the method that we developed to set up and parameterize a single neuron model from neurophysiological data. Two models will be constructed; one for SCs neurons and one for SCi neurons. Starting with a simple conductance based integrate-and-fire model as seen in Equation 1, we added new mechanisms on top of this when it was needed to reproduce or come closer to a data set. Note that our work mainly focuses on the rodent SC as it is the main source of intra-cellular data.

The recent work of Phongphanphanee et al. (2014) gathers data on both SCs and SCi. We will particularly use three of their experiments on a single cell here: 1) the one pulse stimulation in current clamp condition, 2) the eleven pulse stimulation in current clamp condition, and 3) the eleven pulse stimulation in voltage clamp condition (see details of these conditions in the sections below). Although, Equation 1 contains many parameters, most of them are fixed to default values that are coherent with previous neurophysiological work (seen in Chapter 2). This allows estimation of the following parameters: the excitatory post-synaptic current (EPSC) time constants τ_e^r and τ_e^d, the inhibitory post-synaptic current (IPSC) time constants τ_i^r and τ_i^d, the membrane capacitance Cm and the leak conductance gL. Note here that the membrane potential (MP) decay time τm is defined by Cm/gL. Note also the difference between excitatory post-synaptic current (EPSC) and excitatory post-synaptic potential (EPSP), the latter being the effect of the former on the membrane potential.

We first estimate τm and τ_e^d from the single pulse current clamp data. Second, we get a second estimation of τ_e^d, as well as an estimation of τ_e^r, τ_i^r and τ_i^d by fitting the eleven pulse voltage clamp data. Third, still using the eleven pulse voltage clamp data, we scaled our stimulation input to produce the same EPSC and IPSC amplitudes. With those scaled EPS**C**/IPS**C** amplitudes, we inferred the membrane potential constants *Cm* and gL from the resulting EPS**P**/IPS**P** amplitude reported in the eleven-pulse current clamp condition. Note that using the potential response to a known current is a common way to find *Cm* and gL (Brette & Gerstner, 2005).

In a last section, we set up wA and τA (the spike adaptation) for the neuron models parameterized with Phongphanphanee et al. (2014)'s data to reproduce the relation *input current* to *firing rate* (f-I curves) observed in Edwards, White, & Platt (2002) and in Saito & Isa (2003) on the SCs and SCi.

6.2.2 Equation of the General Neuron Model:

$$
\begin{cases}
C_m \dfrac{dV}{dt}(n,t) = \\
\quad -g_L(V-E_L) - g_e(V-E_e) - g_i(V-E_i) - g_A(V-E_A) + I_{Ext} + \xi(t)) \\
g_e(n,t) = \displaystyle\sum_{j\in N}\sum_{s\in S_j} W_{nj}^e\, \alpha_e(t-t_j^s) \\
g_i(n,t) = \displaystyle\sum_{j\in N}\sum_{s\in S_j} W_{nj}^i\; \alpha_{Inh}\left(t-t_j^s\right) \\
g_A(n,t) = \displaystyle\sum_{s\in Sn} w_A\, \alpha_A(t-t_n^s) \\
\alpha_e(t) = \dfrac{1}{1-(\tau_{\mathrm{e}}^{\mathrm{d}}/\tau_e^r)}\left[e^{-t/\tau_{\mathrm{e}}^{\mathrm{r}}} - e^{-t/\tau_{\mathrm{e}}^{\mathrm{d}}}\right] \\
\alpha_i(t) = \dfrac{1}{1-(\tau_{\mathrm{i}}^{\mathrm{d}}/\tau_i^r)}\left[e^{-t/\tau_{\mathrm{i}}^{\mathrm{r}}} - e^{-t/\tau_{\mathrm{i}}^{\mathrm{d}}}\right] \\
\alpha_A(t) = \frac{1}{\tau_A} e^{-\frac{t}{\tau_A}} \text{ if t > 0 and = 0 otherwise.} \\
\text{With } V(t) \text{ resetting to } V_{reset} \text{ if V(t)} > \mathrm{V_{threshold}}
\end{cases}
\qquad (1)
$$

The equation describes the dynamic of our neural field of spiking neurons with *V(n, t)* being the membrane potential of the neuron *n* at time *t*. The membrane potential *V(n,t)* has a tendency to return to its equilibrium E_L with a time constant of $\tau_m = C_m/g_L$. The way in

which g_e and g_i works is exactly that described in Chapter 2 (ge and gi). The only difference is the notation. We chose here to directly describe the function g_e and g_i rather than their differential equations. This notation has the advantage of explicitly presenting g_e and g_i as a sum of post-synaptic current pulses of shape $\alpha_{e/i}(t)$. These synaptic pulses are readily described with a known function that we can fit to a data set. As opposed to Chapter 2, we decided here that the synaptic pulses are a *double* exponential function with a rising and a decay time constant – in Chapter 2 the rising phase was instantaneous.

In addition to this, we have I_{Ext} which is used to input the current into the neuron for current step paradigms, and we have $\xi(t)$ which is a weak Gaussian white noise on the membrane potential (σ = 10.0 pA for SCs neurons and σ = 2.0 pA for SCi; in order to obtain a similar noise).

Finally, the main addition to the equations of Chapter 2 is the term $g_A(V - E_A)$ which allows for spike frequency adaptation – i.e. when stimulated with a step current, a neuron shows a reduction in the firing rate of its spike response following an initial increase (see Benda & Herz, 2003 for a complete overview). We followed the adaptation model suggested for the Adaptive Exponential Integrate-and-Fire Model (Brette & Gerstner, 2005). However, we made the decision to 1) ignore the membrane voltage adaptation for the sake of simplicity – we do not need sub-threshold resonance, and 2) add a Nernst potential E_A to the spike-adaption as in Treves (1993) so that *V(t, n)* cannot reach improbable values. With these changes, it becomes clear that the spike frequency adaptation mechanism is equivalent to recurrent inhibition (i.e. the neuron inhibits itself as if it was connected to itself). This mechanism will be helpful to explain the firing rate of neurons in Section 6.3.4.

6.2.3 Data extraction method

We contacted the laboratory that conducted the experiments reported in Phongphanphanee et al. (2014), but the principal investigator explained to us that he has a team working on a model based on this data set and so he preferred to restrict access to the relevant data.

To extract quantitative data from the various figures displayed in Phongphanphanee et al. (2014), we used the promising desktop version of WebPlotDigitizer (release 3.7, downloaded at http://arohatgi.info/WebPlotDigitizer/index.html). We also used the PDF measure tools of Abode Acrobat Reader DC when we simply wanted to extract the amplitude of a curve. For the single pulse current clamp condition, we extracted the curves 3, 4, 5 of *their* Figure 1C (for the SCs, blue curves) and of *their* Figure 5C (for the SCi, blue curves). For the eleven-pulse voltage clamp condition, we manually estimated an average

curve from each condition (EPSC/IPSC x SCi/SCs) of *their* Figure 7. For the IPSC curve of the SCs, it was ambiguous to extract an average trend, so we extracted two curves. Finally, with regard to the eleven-pulse current clamp condition, we only needed an estimation of the EPSP amplitude -- i.e. the difference from the peak to the baseline of the EPSP – in order to get a scale. However, this was needed for conditions similar to those represented in *their* Figure 7. Thus, we measured the EPSP amplitude of curves 4 and 5 in *their* Figure 1C – for the SCs – and 4 and 5 in *their* Figure 5C – for the SCi.

Finally, we used Acrobat Reader's measuring tools to extract the number of spikes according to the injected current from Figure 4C of Saito and Isa (2003).

6.2.4 Reproducing the Single Pulse Current Clamp data

Phongphanphanee et al. (2014) prepared *in-vitro* horizontal slices of the SCi and SCs that are comparable to a neural field map. During current clamp conditions, a single cell was selected for recording with a whole cell patch clamp technique. The current clamp means that the experimenter fixed the input current to a fixed value -- here zero -- and recorded the membrane potential of the cell. While this cell was recorded the experimenter applied electrical stimulation (extra-cellular current injection of 120-180μA) at different positions on the SCs or SCi slices (or maps).

For the sake of calculus, we based our estimation of τm and τe on the following neuron model that simplifies Equation 1 by ignoring the Nernst potentials:

$$\tau_m \frac{dV(t)}{dt} = -V(t) + \frac{1}{g_L} \sum_{j \in N} \sum_{s \in S_j} W_{ij}^e \, \alpha_e(t - t_j^s) \qquad (2)$$

Here, the variable V*(t)* represents the membrane potential of the recorded cell. The variable $\alpha_{Exc}(t - t_j^s)$ is the EPSC caused by a single pre-synaptic spike – i.e. the synaptic current pulse.

From the shape of the curves in their figure 1C/5C, we assumed that the electrical stimulation caused only one neuron to spike once and so it caused only one synaptic pulse in the recorded cell. By solving Equation 2, we can describe ϵ(t) the membrane potential response for one synaptic pulse (see Gerstner, 2001):

$$\epsilon(t) = \int_0^\infty e^{-s/\tau_m} \alpha(t - t_0^{(0)} - s) \; ds \qquad (3)$$

Where $t_0^{(0)}$ is the time of the spike of the pre-synaptic neuron and where $\int ds$ is an integral over time. We consider the excitatory current pulse $\alpha(t - t_j^{(f)})$ to be a simple exponential pulse of decay τe:

$$\alpha(t-s) = \frac{1}{\tau_e} e^{-\frac{t-s}{\tau_e}} \text{ where t > s and 0 otherwise,} \quad (4)$$

And thus we obtain (see Gerstner, 2001):

$$\epsilon(t) = \frac{1}{1-(\tau_e/\tau_m)}\left[e^{-t/\tau_m} - e^{-t/\tau_e}\right] \quad (5)$$

This double exponential curve starts with an increasing part that is followed by a decreasing part. The variable τ_e is the *rising time constant* while τ_m is the *decay time constant*. We used an optimization algorithm to fit ϵ(t) to the data extracted from Phongphanphanee et al. (2014). The algorithm minimized the integral of the squared errors between currents over time and returned an estimation of τm and τe. We used the optimisation function `minimize` (default method) of the python *scipy* package.

6.2.5 Reproducing the Eleven Pulse Voltage Clamp data

This step will allow us to estimate the time constant of the excitation and inhibition synaptic pulse $\alpha_e(t-s)$ and $\alpha_i(t-s)$. We will see in the result that we also need time rising constants but for now, we explain the meaning of a Voltage Clamp from the perspective of the model. Let us return to Equation 1 (ignoring the spike adaptation gA as it is not relevant here):

$$C_m \frac{\delta V}{\delta t} = -g_L(V - E_l) - g_e(V - E_e) - g_i(V - E_i) + I_{ext} \quad (1)$$

As Phongphanphanee et al. (2014), we want to clamp the voltage at E_e (which is 0mV, the reversal potential of glutamate receptor channels). This means that V is frozen:

$$C\frac{\delta V}{\delta t} = 0 \; ; \; V = E_e \quad (6)$$

Phongphanphanee et al. (2014) did this in order to neutralize the EPSC to study the IPSC. If the cell does not receive any synaptic input ($g_e = g_i = 0$), we obtain from (1) and (6):

$$\Rightarrow I_{clamp}^{Ee} = g_l(E_e - E_l) \tag{7}$$

Where I_{clamp}^{Ee} is the current that the experimenter needs to apply to the neurons to keep the voltage at E_e. Now, let us consider that the cell receives a synaptic input ($g_e \neq 0$; $g_i \neq 0$):

$$C\frac{\delta V}{\delta t} = 0 \; ; \; V = E_e \tag{8}$$

$$\Rightarrow I_{total} = g_l(E_e - E_l) + g_e(E_e - E_e) + g_i(E_e - E_i) \tag{9}$$

$$I_{total} = I_{clamp}^{Ee} + g_i(E_e - E_i) \tag{10}$$

In more detail:

$$I_{total} - I_{clamp}^{Ee} = (E_e - E_i)\sum_{n\in N}\sum_{s\in S_n} w_n\,\alpha_e(t - t_s^n) \tag{11}$$

Where N is the ensemble of neurons connected to the recorded neurons, S_n is the ensemble of spike times of a neuron *n*, and w_n is the connection of the *n*-th neuron with the recorded neuron.

Assuming that the remote electrical stimulation has made only one neuron spike once by a pulse in the ensemble N, we have the following simplification:

$$I_{total} - I_{clamp}^{Ee} = \; w_0(E_e - E_i)\sum_{s\in S_0}\alpha_e(t - t_s^0) \tag{11}$$

Where the S_0 are the times of stimulation pulse (which are known) and w_0 is the weight of the stimulated neuron to the recorded neuron. Similarly for a clamp to Ei, we get:

$$I_{total} - I_{clamp}^{Ei} = \; w_0(E_i - E_e)\sum_{s\in S_0}\alpha_i(t - t_s^0) \tag{12}$$

$I_{total} - I_{clamp}^{Ei}$ was reported by Phongphanpannee et al. (2014) in their Figure 4B, 6B and 7. We used the right part of Equations 11 and 12 to manually fit the extracted data from Figure 7. We ignore w_0 (Ei – Ee) for now by norming the data to 1. To improve our estimations compared with section 6.2.4 we assume that $\alpha_e(t - s)$ is a double exponential function – instead of a simple exponential -- of rising constant τ_e^r and decay constant τ_e^d. The same applies to $\alpha_i(t - s)$. Fitting the data will then bring us an estimation of τ_e^r , τ_e^d , τ_i^r and τ_i^d.

The reproduction of the SCs data required a little more effort than in the case of the SCi. Indeed, Phongphanphanee et al. (2014) observed that both EPSC and IPSC of the SCs are made of a lightning increase followed by a decreasing phase. Note that the decreasing phase was occurring *during* the electrical pulse stimulation. To make such a pattern possible, we gave a weight of 1 to the first synaptic pulse (W_{init}), and a weaker weight to all following synaptic pulses ($W_{follower}$). Extending the equation (12), we obtain:

$$I_{total} - I_{clamp}^{Ei} = W_{init}\alpha(t - t_0) + W_{follower}\sum_{s \in S_0} \alpha_i(t - t_s^0) \quad (13)$$

Where t_0 is the first spike of the pre-synaptic neuron (i.e. the hypothetical single stimulated neuron), and where S_0 includes all the spike times of that neuron except t_0. With this equation, one can find a value of $W_{follower}$ such that the follower pulses are weaker than the decay time $\tau_{e/i}^d$ of $\alpha(t - s)$ and so the PSC would decrease after the first stimulation pulse. This diminution of weight after a fist spike can biologically be explained with short-term synaptic plasticity, or more specifically a *short-term depression*. In fact, our simple approach can be easily replicated with the more complete model of Tsodyks, Pawelzik, & Markram (1998). A second biological possibility is that the weight diminution comes from a decrease in the excited population through delayed local inhibition feedback. But as we do not know the size of the stimulated population, we cannot test this possibility.

6.2.6 Reproducing the Input Scale

Now that we have obtained the shape of the synaptic current by estimating τ_e^r , τ_e^d , τ_i^r and τ_i^d , we manually fit w_0 to scale equation (11) and (12) to the synaptic current amplitude of *their* Figure 4B and 6B. Note here that *their* figure 7 is normed to 1 and so it cannot be used. One can notice that $w_0(E_i - E_e)$ is the amplitude A of one synaptic current pulse. We can then simply measure A in Phongphanphanee et al.(2014)'s figures and divide it by $(E_i - E_e)$ to obtain w_0.

Because an EPSP is a type of integral of the EPSC, a specific EPSC pattern produces in our model a specific EPSP amplitude. As we now have a scaled EPSC estimation, we can search which combinations of gL and Cm would produce an EPSP of the same amplitude as that observed in Phongphanphanee et al. (2014)'s Figure 1C and 5C. To optimize two variables with only one measure (the EPSP amplitude) would lead to a number of possible combinations (the optimisation is under constrained). Fortunately, from section 6.2.4, we have fixed τm, the membrane decay time and we know that Cm/gL = τm. We take arbitrary initial values of C_m^{init} and g_L^{init} verifying:

$$\frac{C_m^{init}}{g_L^{init}} = \tau_m \tag{13}$$

These arbitrary values are linked to the actual values by k:

$$\frac{C_m}{g_L} = \frac{k.C_m^{init}}{k.g_L^{init}} = \tau_m \tag{14}$$

Now, we are optimizing only one variable *k* to make Equation (1) fit the EPSP amplitude, and so only one solution is possible. The actual transformation of EPSC to EPSP is described by Equation (1). As it is difficult to integrate, we simulate a spiking neuron implementing Equation (1) in Brian Simulator. We use the parameters we estimated in the previous section. To reproduce the conditions of Phongphanphanee et al. (2014), the simulated neuron is fed with 11 pulses of weight w_0 separated by 5 ms and its spiking threshold is set at 100 mV to prevent any spike. We varied manually *k* until the membrane potential of the simulated neuron performs a bump (EPSP) similar in amplitude to that observed in the neurophysiological data.

6.2.7 Fitting the f-I Curves reported by Saito and Isa (2003)

At this point, we have all the neuron parameters we need to reproduce the E/IPSC and E/IPSP observed by Phongphanphanee et al. (2014). More precisely, we modelled 1) the E/IPSP shapes defined by the synaptic time constants and 2) the current to voltage relationship (PSC to PSP) defined by *Cm* and *gL*.

However, we have not yet replicated how the neurons spike when they are fed with a specific input current. For this we may need parameters w_A and τA (in Equation 1). To begin with, the relationship between input current and firing rate of the neuron is usually described as an f-I curve (f: firing, I: input). One important point is that the f-I curve is not systematically explained by the current to voltage relationship (I-V curve), due to a phenomenon called *spike frequency adaptation*. This spike adaptation works exactly as an automatic and immediate auto-inhibition of the neuron for each of its spikes. The spike adaptation is defined by variable *gA,* parameters w_A and τA in Equation 1. The parameter w_A can be seen as the weight of the auto-inhibition, and τA is its decay time. Note that to set the f-I curve close to the target biological range is important as the stability and the behaviour of the network depend on it.

An interesting part of this section, we believe, is that we will not be using the data of Phongphanphanee et al. (2014), but that of Saito and Isa (2003). The latter provides complete f-I curves for several neurons in the SCs and the SCi. Note that their results for the

SCs are in line with the work of Edwards et al. (2002), which we have also been considering throughout this work.

Using the SCi and SCs neuron models that we have built throughout the previous sections, we reproduced the paradigm of Saito and Isa (2003). We injected into the model cell a step current of 400ms in duration and amplitude of either 40, 120, or 200 pA. We then counted the number of spikes and inferred the firing rate. For both SCs and SCi we tried to match manually the firing rates to Saito and Isa (2003)'s results. Note that, as the f-I curves for the SCi and SCs were not qualitatively different (compare their figure 5C1 and 5A1), we used only one set of values to match the firing rates.

6.3 Results

6.3.1 Reproducing the Single Pulse Current Clamp data

The results here are relatively straightforward and are summarized in **Figure 5-10**. All the optimisations we ran converged easily to a solution. Across the three optimisations we made to fit the SCs data, the estimation average of τ_m – the membrane potential decay time – was 6.41 (±3.02 or ±47%) and the estimation average of τ_e^d – the excitatory post-synaptic decay time -- was 1.62 (±0.86 or ±53%). With regard to the SCi optimisation, the estimation average of τ_m was 57.70(±9.36 or ±16%) and the estimation average of τ_e^d was 5.63(±0.71 or ±13%). Note that the variance in the SCi estimations is smaller than in those of the SCs (in percentage of the mean).

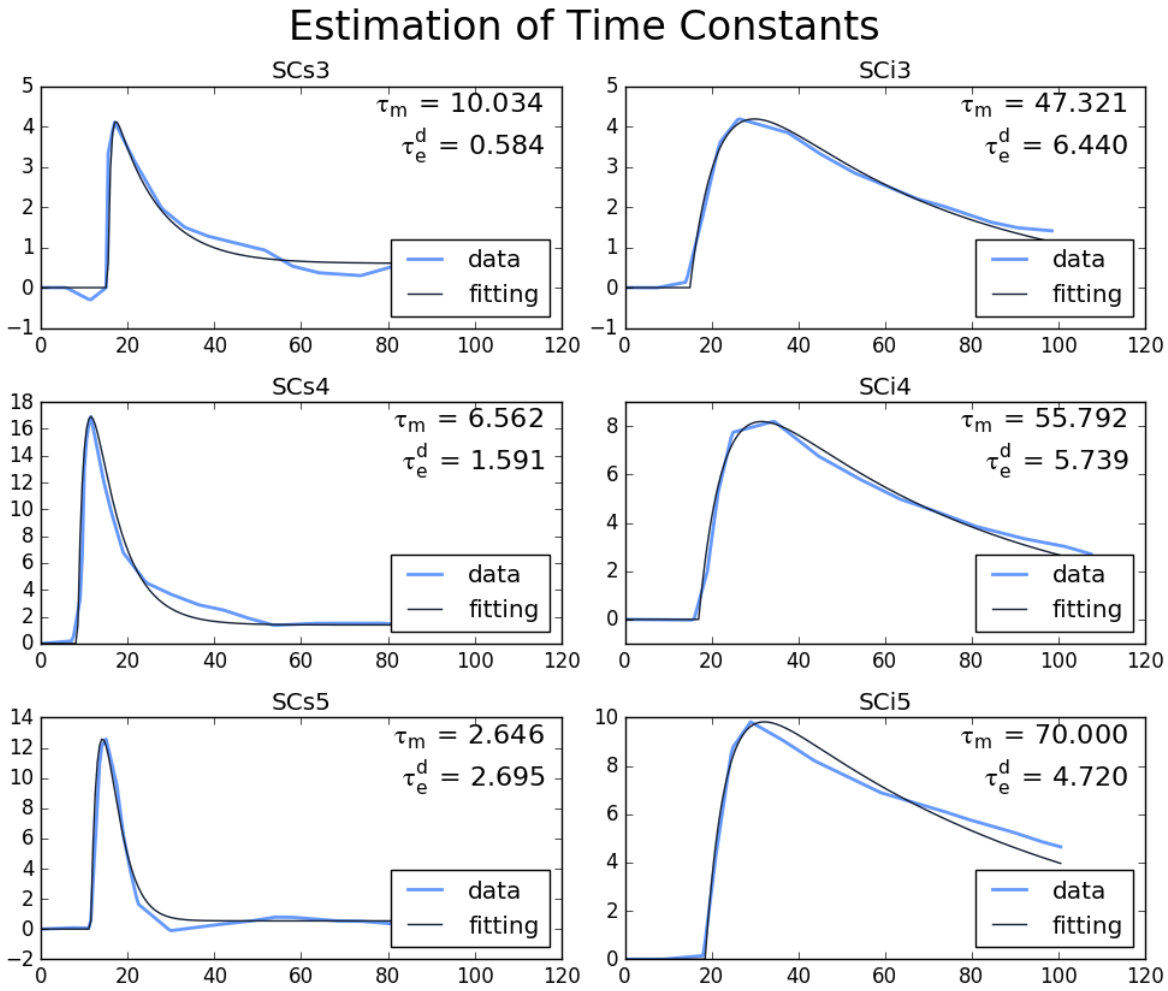

Figure 5-10: Estimation of the membrane potential decay time constant τ_m and of the synaptic decay time constant τ_e^d. *The data are from Phongphanphanee et al. (2014). We used their Figure 1C for the superficial layer of the SC (SCs) and their Figure 5C for the intermediate layer of the SC (SCi). From these figures, we used the curves 3, 4, and 5 with respect to the numbers displayed in each subplot title. The fitted model is a double exponential curve: τs corresponds to its rising constant while τm corresponds to its decay constant.*

6.3.2 Reproducing the Eleven-Pulse Voltage Clamp data

As shown in the right panel of **Figure 5-11**, the manual fitting of the SCi data was relatively simple using the unweighted sum model (Equation 12). Indeed, the extracted data presents very well defined synaptic pulses as if the recorded neuron had received 11 spikes from only one input neuron (see the saw teeth of blue and red curves). We estimated a slightly larger rising time constant for the excitation ($\tau_e^r = 1.5\ ms$, see EPSC) than for the inhibition ($\tau_i^r = 1\ ms$, see IPSC). Although it does help to obtain a better fit, this difference is not of great importance as to switch the values would give similar curves. More interestingly, we succeeded in reproducing the EPSC curve with $\tau_e^d = 5.6\ ms$ which is consistent with the previous section (see 6.3.1). And we needed longer time decay for the inhibition ($\tau_e^d =$

10.0 ms), which is not a surprising setting for neural field (longer inhibition gives more stability).

The only difficulty we faced is that τ_e^d and τ_i^d failed to explain the final decay when the stimulation is turned off (see **Figure 5-11**, after 80 ms). This is difficult to interpret; it could result from a mechanism that we have not yet considered. Whilst there is possibly an adaptation of the decay time constant, such a phenomenon would also have an impact on the first part of the curve.

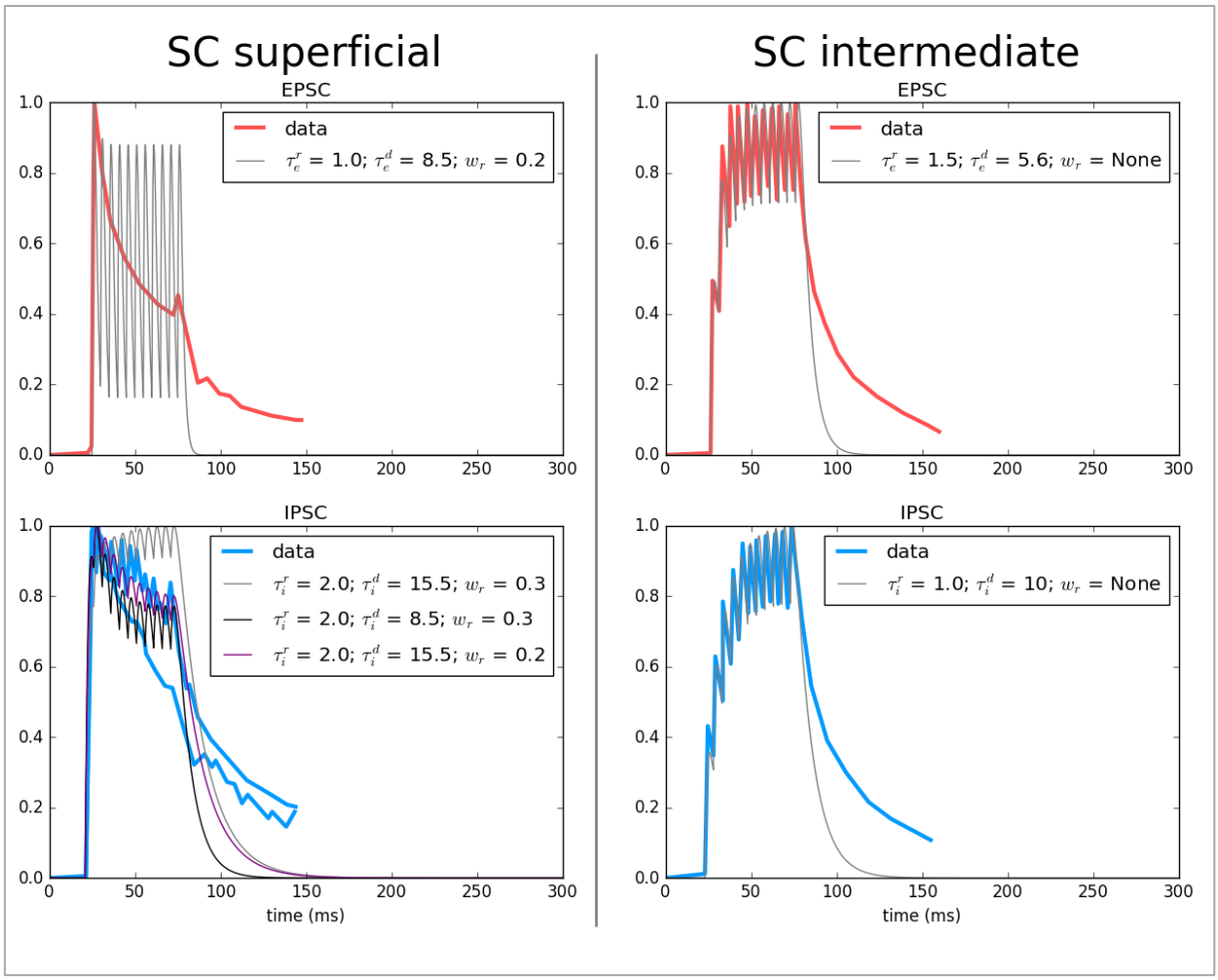

Figure 5-11: Manual Fit of the Synaptic Current Patterns observed in Phongphanphanee et al. (2014) in the superficial layer of the SC and in the intermediate layer of the SC. *The model was simply a sum of equal synaptic pulses (see Equations 12 and 13). The stereotypical synaptic pulse was defined by a double exponential function of rising constant τ_r and decay constant τ_d (similar to Equation 5), which are reported for the curves of each model (grey, purple, black curves). The sum of synaptic pulses was homogeneously weighted for the SCi models, but for the SCs models we needed to drastically decrease the weight of the synaptic pulses following the first pulse. The parameter w_r is the weight of the following pulses in proportion to the first; w_r corresponds to $W_{follower}$ in the main text. This parameter is reported as None in the SCi model as it was not used; however, it would be equivalent to use w_r = 1.*

As shown in the left side of **Figure 5-11**, the manual fit for the SCs was slightly more challenging. Indeed, the manual data extraction does not present very well defined synaptic

pulses and only provides a coarse pattern to replicate (see red and blue curves). In spite of this, the weighted sum model (Equation 13) worked rather well in reproducing the data. We estimated a slightly larger time rising for the inhibition ($\tau_i^r = 2\ ms$, see IPSC) than for the excitation ($\tau_e^r = 1.0\ ms$, see EPSC). We could explain the EPSC with an excitatory decay time $\tau_e^d = 8.5\ ms$ and a $W_{follower}$ = 0.2. This synaptic decay time is not in accord with what was observed in the previous section estimation ($\tau_e^d = 1.62 \pm 0.86$, see 6.3.1). Although the combination of τ_e^d and $W_{follower}$ allows some flexibility, we did not find any combination of $W_{follower}$ with $\tau_e^d = 1.6$ that could reproduce the data pattern.

Assuming $\tau_i^d > \tau_e^d$ to help the neural field to be stable and $W_{follower}$ being the same for inhibitory and excitatory synapses, we could match the pattern of IPSC with $\tau_i^d = 15.5\ ms$ and a $W_{follower}$ = 0.2 (see purple curve, bottom-left on **Figure 5-11**).

Importantly, the introduction of the variable $W_{follower}$ and the vagueness of the data make it difficult to find a unique optimal solution. The grey curve (in the bottom-left plot of **Figure 5-11**) shows that a slight change in $W_{follower}$ (increased to 0.3) is detrimental for the fitting but this change in $W_{follower}$ can be compensated by tweaking τ_i^d. Indeed, the black curve demonstrates that $\tau_i^d = 8.5\ ms$ and $W_{follower}$ = 0.3 provide a fitting that is qualitatively as good as $\tau_i^d = 15.5\ ms$ and a $W_{follower}$ = 0.2. Therefore, it would simply be arbitrary to choose one or the other solution. We chose to keep the solution $\tau_i^d = 15.5\ ms$ and a $W_{follower}$ = 0.2 for the sake of having more inhibition and having a consistent $W_{follower}$ between excitation and inhibition. Again, the estimated τ_e^d and τ_i^d failed to estimate the tail of the curves (after 80 ms).

Finally, we want to moderate/qualify the actual significance of our estimations. We are working with manually extracted data in which there is a part arbitrary choice and part manual imprecision while extracting the global pattern of Figure 7 in the work of Phongphanphanee et al (2014). To work on actual, noise free, and single neuron data would provide more constrained and thus more reliable estimations.

The lack of precision of the extracted data is, in part, why we used manual optimisation: while a human can optimize parameters to fit a global pattern, an algorithm would stick to the given data. However, as the reader may find it difficult to trust our manual fit, we show the results of an algorithmic optimization in **Figure 5-12**. To guide the algorithm, we set up similar constraints as the ones used for the manual fit: 1) $W_{follower}$ is fixed at 0.2 for SCs and at 1.0 for SCi; and 2) the points after 80 ms are ignored. One can appreciate how the results are close to what we manually estimated. Only the fit of the IPSP of the SCs diverges from

our manual fit and this is because the algorithm – ignoring the vagueness of the data -- tries to suppress the saw teeth of synaptic pulses to fit with the data curve.

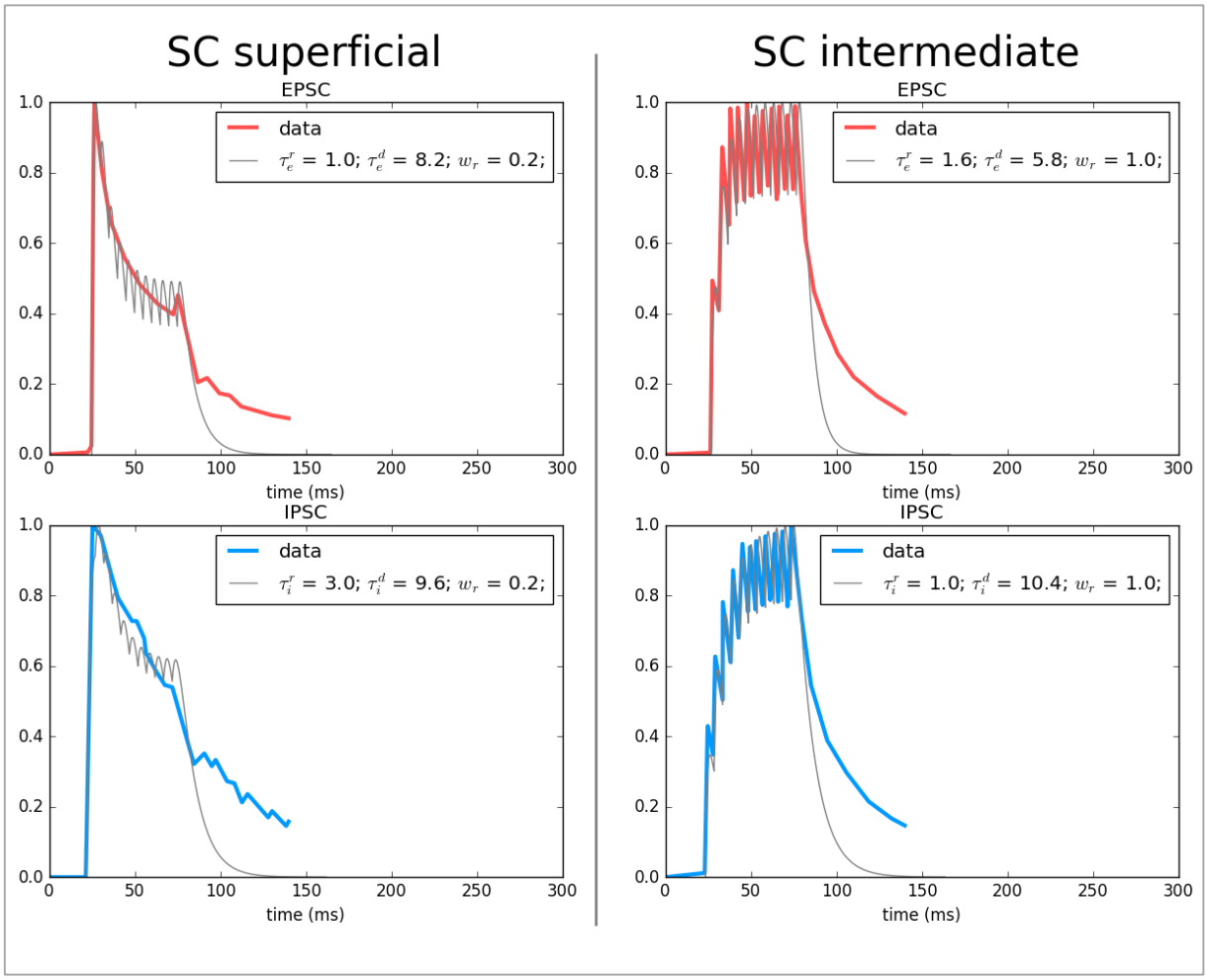

Figure 5-12: Automatic Fit of the Synaptic Current Patterns observed in Phongphanphanee et al. (2014) in the superficial layer of the SC and in the intermediate layer of the SC. *Same description as that given for* ***Figure 5-11****.*

6.3.3 Reproducing the Input Scale

The aim of this section is to estimate the membrane constant *Cm* and *gL* using the post-synaptic current (PSC) response to 11 pulses (Figure 4B and 6B in Phongphanphanee et al. (2014)) and the post-synaptic potential (PSP) response to 11 pulses (*their* Figure 1A and 5A).

First, we successfully implemented a spiking neuron model for the SCs neurons and the SCi neurons by gathering the parameters selected so far and using Equation 1. This model will give us a PSP for a given PSC according to a given *Cm* and *gL*. Note that, for the SCs model, Equation 1 was extended to incorporate the model of short term synaptic plasticity introduced by Tsodyks et al. (1998). It is clear that the spiking neuron models do produce

the same PSC responses as Equations 12 and 13 in the previous section (see **Figure 5-13** and **Figure 5-14**, to compare with **Figure 5-11**).

Second, we scaled the PSC responses. In this respect, the maximum current in response to 11 pulses was extracted from the figures 4B and 6B of Phongphanphanee et al. (2014). For the SCs, we estimated to 197 pA the maximum current of the excitatory PSCs and to 88 pA the maximum of the inhibitory one. For the SCi, we estimated to 81 pA the maximum of excitation current and to 83 pA the maximum of the inhibitory one (pA denotes picoAmpere). From these measures, we could estimate the inhibitory and excitatory weight of the stimulated neurons to the recorded neuron. We found that, for the SCs, we need the excitatory weight to be 3.8 nS (nanoSiemens) and the inhibitory weight to be 0.42 x 3.8 nS (see **Figure 5-13**, left side). This half-size inhibitory weight is what might be expected on the basis of the smaller IPSC amplitude (when compared with the excitation). For the SCi, we found that we need an excitatory weight of 1.1 nS and an inhibitory weight of 0.5 x 1.1 nS (see **Figure 5-14**, left side). Here the half-size inhibitory weight is unexpected as the EPSC and IPSC have the same maximum current response to 11 pulses. But as we used a decay time for the inhibition that was twice as long (see section 6.3.2; we selected $\tau_i^d = 15.5ms$ and $\tau_e^d = 8.5\ ms$), IPSCs need less weight to accumulate as rapidly as the EPSCs (at equal input frequency).

Finally, we measured the membrane potential shift caused by such PSCs on Figures 1C and 5C in Phongphanphanee et al. (2014). The maximum potential shift observed was 12.5 mV for the SCs and 24.4 mV for the SCi. -- Keeping *Cm/gL = 7 ms* for the SCs and *Cm/gL = 55 ms* for the SCi (as estimated in Section 6.3.1), we estimated that *Cm = 35 pF* and *gL = 5 nS* for the SCs model, and that *Cm=22 pF* and *gL=0.4 nS* for the SCi model (see **Figure 5-13** and **Figure 5-14**, right part). The estimation was made manually and without difficulty (see method section 6.2.6).

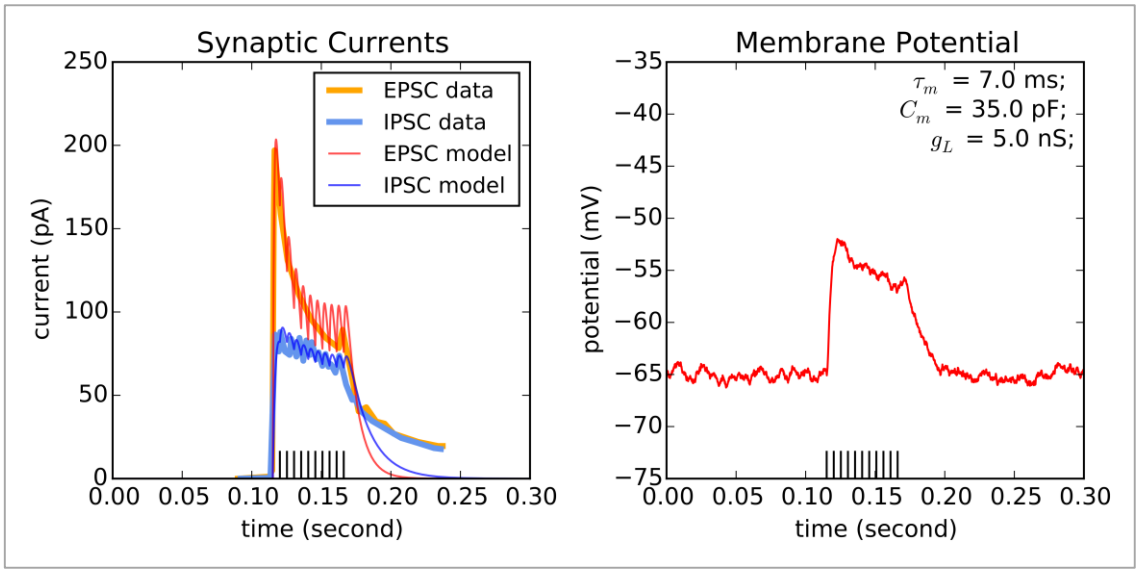

Figure 5-13: Simulation result of a spiking neuron model of the neurons in the superficial layer of the SC. *As opposed to Figure 5-11 and Figure 5-12, the synaptic currents plotted here come from an actual spiking neuron implementation (left side, red and blue thin curves). The membrane potential (right side, red curve) comes from the same spiking neuron model. The IPSC and EPSC data are the same as those shown in Figure 5-11. An input neuron was sending to the recorded neuron 11 spikes separated by 5 ms from time 0.11 to time 0.17 (vertical black lines).*

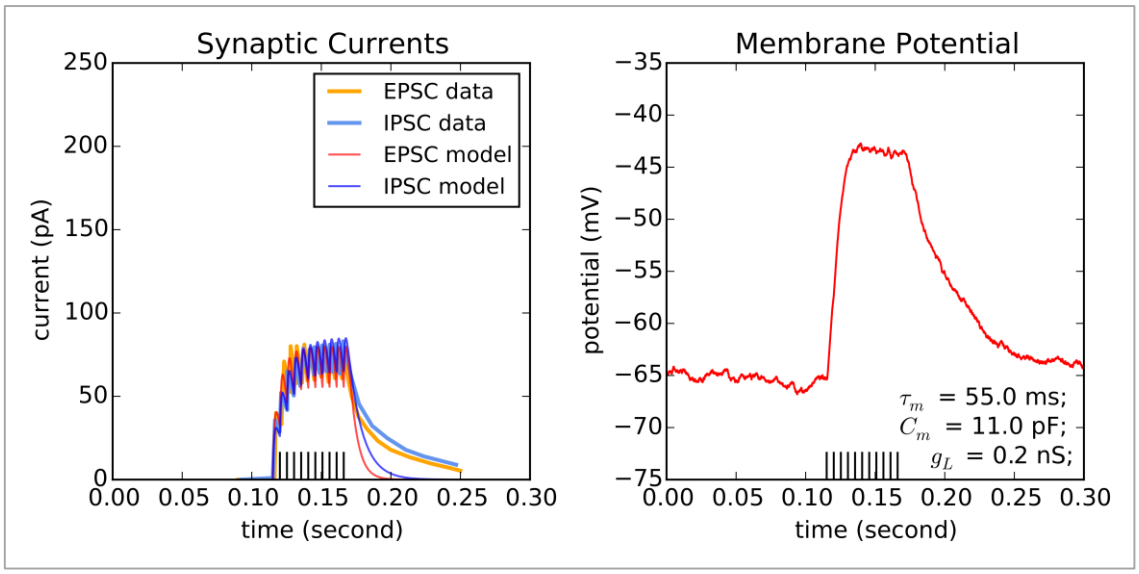

Figure 5-14: Simulation result of a spiking neuron model of the neurons in the intermediate layer of the SC. *Same description as that given for* ***Figure 5-13****.*

6.3.4 Fitting the f-I Curves reported by Saito and Isa (2003)

Figure 5-15 summarise the results of the manual estimation of parameters w_A and τA, which control the spike frequency adaptation. They can respectively be seen as the strength of auto-inhibition after each spike and the decay time constant of that auto-inhibition. To use spike frequency adaptation allows a substantial improvement in fitting the data of Saito and Isa (2003). With SCi neuron model, the average distance from the data becomes 14

times smaller, whilst with the SCs neuron model, the average distance from the data becomes 12.5 times smaller. Despite this significant improvement, we found it difficult to fit closely the data of Saito and Isa (2003) using only the spike frequency adaptation mechanism.

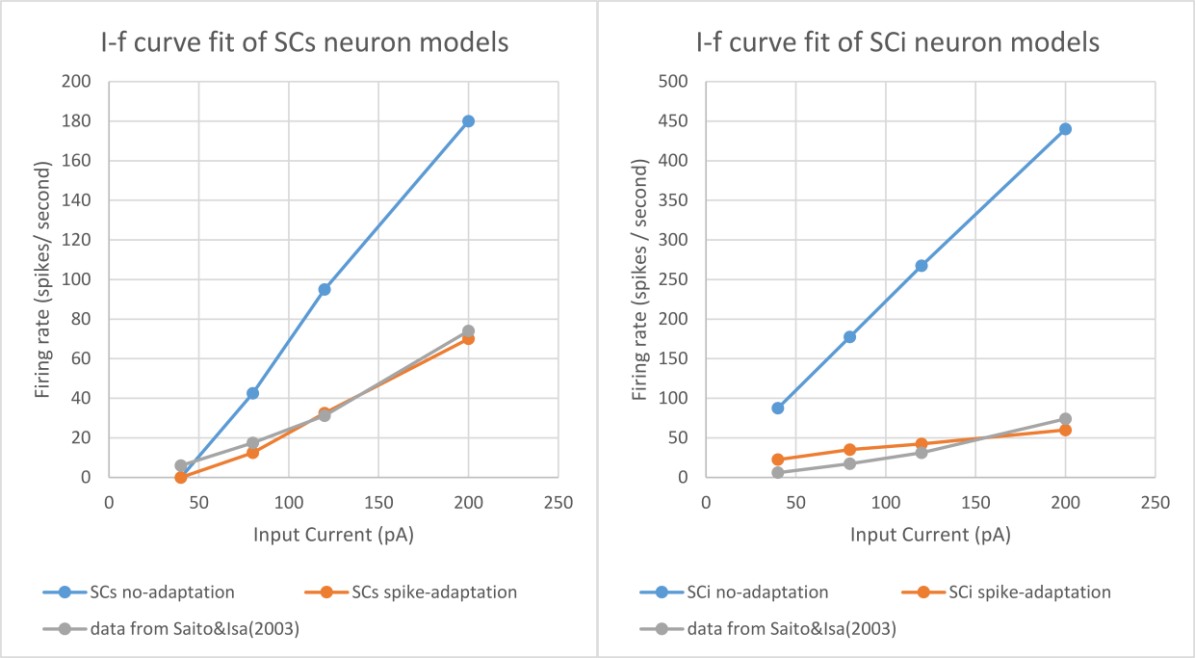

Figure 5-15: Improvement of the spiking neuron responses to step current due to spike-frequency adaptation. *The left and right plots describe the spike frequency response (or firing rate response) of the SCs and SCi neuron model to various current step inputs. The grey curve plots the data extracted from the Saito and Isa (2003) study, while the blue curves represent the performance of the neuron models without a spike frequency mechanism (w_{Adp} = 0). The orange curves represent the performance of the neuron models with a spike frequency mechanism (SCi: w_{Adp} = 9 nA, τA = 15 ms; SCs: w_{Adp} = 2 nA, τA = 35 ms).*

For instance, while f-I curves look completely linear in the study of Saito and Isa (2003), our neuron model produces non-linear f-I curves: a low current input does not cause the neuron to spike. We had to decrease the spiking threshold of the SCs neuron model to -50mV in order to obtain spikes for 80 pA current steps. Nevertheless, this change was not sufficient to obtain spikes with 40 pA current step. Finally, we considered zero spikes for 40 pA to be an acceptable fit. A discussion of this issue of fitting the data of Saito and Isa (2003) can also be found in Morén, Shibata and Doya (2010, Figure 2b, first point).

The fit with the SCi neuron model is 3.7 times less accurate than the fit made with the SCs neuron model (mean distance from data: 14.8 spikes/s against 4.0 spikes/s). It has been impossible to find a set of parameters that decreases the firing rate responses to low currents (40 pA, 80 pA) to values closer to the data while keeping firing rate responses to high currents (200pA) close to 70 spikes/second. In essence, manipulating w_A and τA did not allow us to easily control the slope and intercept of the f-I curves.

6.3.5 Summary of results:

This section essentially summarises the results from previous sections in one table.

Table 11: Summary of the parameters used to replicate the data from neurons of the superficial layer of the Superior Colliculus (SCs) and of the intermediate layer of the Superior Colliculus (SCi).

Symbol	Description	SCs model	SCi model
τ_m	Membrane decay time constant	7 ms	55 ms
C_m	Membrane capacitance	35 pF	11.0 pF
g_L	Membrane leak conductance	5 nS	0.2 nS
τ_e^r	Excitation rising time constant	1.0 ms	1.5 ms
τ_e^d	Excitation decay time constant	8.5 ms	5.6 ms
τ_i^r	Inhibition rising time constant	2.0 ms	1.0 ms
τ_e^r	Inhibition decay time constant	15.5 ms	10.0 ms
$V_{threshold}$	Potential threshold	-50 mV	-40 mV
V_{reset}	Reset potential	-80 mV	-80 mV
E_L	Leak Equilibrium (resting potential)	-65 mV	-65 mV
E_e	Excitation Equilibrium (Nernst Potential)	0 mV	0 mV
E_i	Inhibition Equilibrium (Nernst Potential)	-80 mV	-80 mV
E_A	Adaptation Equilibrium (Nernst Potential)	-80 mV	-80 mV
w_A	Weight of Spike Frequency Adaptation	2 nA	9 nA
τ_A	Spike Frequency Adaptation decay time constant	35 ms	15 ms
	Refractory period	1.6 ms	1.6 ms
	Gaussian White Noise variance	10 pA	2 pA

6.4 Discussion

We were able to model the membrane potential response to a pulse input without difficulty, and this provided us with an estimation of the membrane potential decay time as well as an estimation of the decay time of the excitatory synaptic current pulse.

The estimation of the synaptic pulse functions from the 11-pulse voltage-clamp data was relatively easy for the SCi. Interestingly, the excitatory synaptic decay time we found for the SCi with this method corresponded to the estimation made with the previous method. For the SCs, we needed a specific mechanism to explain the strong response to the first pulse and attenuated responses to the following pulses. We chose to explain this dynamic in terms of a short-term adaptation mechanism. Finally, we could not explain, neither for

the SCi or the SCs data, the speed of decay of synaptic current after the input pulses stopped. Indeed, the decay time constants that we needed to fit the curve during the input were different from the decay time constants needed to fit the decay of the curve after the offset of the input. It is difficult to interpret this inconsistency without knowing more about the network activity during the neurophysiology recording.

The scaling of the input from the 11 pulse voltage-clamp data and the estimation of the membrane potential parameters (Cm and gL) from the 11-pulse current-clamp was conducted without any difficulties. The spiking neuron models obtained are able to qualitatively reproduce the data used from Phongphanphanee et al. (2014).

Finally, we attempted to fit the f-I curves found for SCs and SCi neurons in Saito and Isa (2003) – i.e. they provide a curve of how neurons spike according to an input current (see **Figure 5-15**, grey curves). In order to decrease the f-I slope of the model (blue curves) to the range that is close to Saito and Isa (2003), we chose to add a spike frequency adaptation mechanism (orange curves). But even with this mechanism, it appears that to fit the f-I curves very closely is impossible – this limitation is more prominent for the SCi neuron data. One explanation is that integrate-and-fire types of neuron models have non-linear f-I curves. Indeed, this type of neuron produces approximately linear f-I curves with a positive x-intercept for strong current, but they do not emit any spike for a current below that x-intercept (Dayan & Abbott, 2001; their Chapter 5, p. 13) . On the other hand, the f-I curves of Saito and Isa (2003) report that biological neurons can emit spikes at very low firing for very low currents (**Figure 5-15**, grey curve) – i.e., the x-intercept is very low.

It is important to note that from Dayan & Abbot's equations, it is known that the slope and the x-intercept of the f-I curve can be controlled with the parameters Cm, gL, $V_{threshold}$, V_{reset} and E_L. In our work, Cm and gL were already estimated and fixed (see above) while $V_{threshold}$, V_{reset} and E_L could be manipulated. We did decrease the threshold of SCs neurons (compared to SCi neurons) to decrease the x-intercept (see section 6.3.4), but the only solution to obtain spikes for very low currents is to have $V_{threshold} \approx E_L$ (if $V_{threshold} \leq E_L$ the neuron goes spontaneously up to the threshold). We judged that this solution was not in accordance with intra-cellular recordings of the SC (R. Grantyn, Grantyn, & Schierwagen, 1983; Saito & Isa, 2003). Alternatively, more advanced adaptation mechanisms can also help to linearize the start of the f-I curves (Ermentrout, 1998). The addition of escape noise (stochastic threshold for spike) is also a good direction to explore in order to obtain spikes for small input currents.

Note also that in order to decrease the slope of the f-I curve -- and as an alternative to using a spike-frequency adaptation mechanism -- we could have increased the difference

between $V_{threshold}$ and V_{reset} while decreasing the difference between $V_{threshold}$ and E_L. This method can lead to $V_{threshold} \approx E_L$ that we judged unrealistic, as aforementioned. To justify further our choice of using a spike-frequency adaptation to control the f-I slope, it is important to note that this phenomenon is observed in the SC (R. Grantyn, Grantyn, & Schierwagen, 1983; Saito & Isa, 2003). Finally, it can be noted that f-I curves of Saito and Isa (2003) may be slightly convex: reproducing such a shape would require the introduction of additional currents (C. J. Wilson, Weyrick, Terman, Hallworth, & Bevan, 2004).

To conclude, our approach has generally been successful, sacrificing precision for simplicity and adding a mechanism only when it is needed. We were finally able to obtain one stereotype neuron model per SC layer and each replicates the general pattern of the data reported in Phongphanphanee et al. (2014) and in Saito and Isa (2003). The next step is to assess their behaviour when they implement a dynamic field network.

Chapter Six: General Discussion

1 Summary of the Thesis

This thesis aimed to contribute to a better understanding of the perception-to-action loop that defines the interactions between biological systems and their environment. Notably, this work attempted to characterize how spatial interactions occurring between endogenous signals (related to goals and expectations from the animal´s history) and exogenous (related to the environment) signals shape the decision of where-to-move-next. Importantly, this question marks an embodied approach to decision-making. In particular, we used the case of action selection for orienting responses, allowing us to use the visuo-oculomotor system and the Superior Colliculus (SC) as a biological model.

In the **General Introduction**, we highlighted the multitude of endogenous and exogenous signals converging to the SC – making the distinction between the superficial layers (SCs), that is, a visual treatment region, and the intermediate layers (SCi), that is a multimodal interface to the oculomotor system. We also highlighted the fact that biological systems such as the SCi blur the line between decision and execution (so that an embodied approach to biological decision processes is essential for its understanding). We argued that action selection is based on a mechanism transforming the overall activity on the SCi in eye movement as soon as this activity reaches a threshold. This mechanism means that: 1) biological systems can start to move, while internal decision processes selecting where-to-move did not reach a consensus; 2) action selection is still happening during action execution. As a consequence, the activity in the SCi could be deduced from the saccade properties.

In **Chapter 2**, pursuing our embodied approach to understanding the spatial interactions that shape decision processes, we implemented a 2D dynamic neural field of spiking neurons in order to infer what kinds of interactions between exogenous signals can be expected from the connection pattern that is found in the SCs -- and in several other brain regions of the visuo-oculomotor system. First, we observed that this connection pattern leads to suppression of too large stimuli. Second, when presenting stimuli simultaneously at different locations of the model map, that connection pattern yields to spatial deviations of the images of the stimuli. In the discussion and in the appendix, we addressed whether those interactions that we observed at a perceptive and/or retinotopic level can be detected at the actual behaviour level. In other words, we discussed how much the frontier between perception and action selection is permeable.

In **Chapter 3** - in contrast with the computational approach of Chapter 2 - we addressed the spatial interactions occurring in the SCi with an experimental paradigm. By exploiting

to our advantage the blurred line between action selection and action execution, we assessed a specific property of the saccades – i.e., the curvature in their trajectory –in order to reveal the presence of a signal modulating the activity of the SCi map. This procedure is routinely used in saccadic studies; our contribution was to detect a curvature caused by a spatiotopic signals – a result that invalidates recent models of the visuo-oculomotor system that explains saccadic curvatures in a retinotopic frame. In the discussion, we proposed improvements to these models in order to account for our results – in particular, we suggested an excitatory and spatiotopic update of the SCi.

In **Chapter 4**, we introduced a new way to assess the signals present in the SCi during a saccade: the bimodal GE. As opposed to the standard method using the curvature in trajectory, our method is simpler and more manageable as it is based on saccade endpoints. Furthermore, we introduced a simple theoretical model that explains the bimodal GE. Thus, given an experimental design that isolates a signal projecting to the SCi, our model allows us to interpret the modulation in bimodal GE directly as a modulation of the isolated signal. We used this method to trace the spatial influence of two different endogenous signals upon the SCi. Notably, we tested our method for the two main kinds of endogenous signals: history-related and goal-related signals.

Finally, in **Chapter 5**, we delved deeper into the embodiment of decision-making. We modelled the SCs and SCi based on neurophysiological data in order to explore how neural properties and connectivity affect the interactions of exogenous/endogenous stimuli – and ultimately the decision -- in those structures. Indeed, the SCs and SCi were recently reported to behave very differently when confronted with two electrical stimulations (Phongphanphanee et al., 2014). The former presents a winner-take-all dynamic whilst the later presents an accumulator dynamic. We assessed the conclusion of Phongphanphanee et al. that the properties and connectivity of the neurons - reported for each the SCs and the SCi -- could easily be linked to this difference in dynamic. We found that we could partially replicate the dynamic of the SCs, such as the transient response to step current, from their data. However, in order to create a winner-take-all dynamic, we needed to increase the strength of the inhibition and to annul the difference in delay between inhibition and excitation (as opposed to what was initially reported). In terms of the SCi, our model failed to replicate the dynamic reported by Phongphanphanee et al.(2014). We discussed how the single neuron model and the fitting method could be improved. We also pointed out that the assumption of neural homogeneity in the SCi/SCs could be a limitation in Phongphanphanee et al.'s approach. Finally, the model would require several improvements in order to directly link neural properties to behavioural decisions.

2 Toward an Implementation of Our Theoretical Framework

Our work has explored different aspects of the visuo-oculomotor system and it has also developed a theoretical framework to explain saccade curvatures caused by spatiotopic signals (Chapter 3), the bimodal Global Effect (Chapter 4) and also, to a lesser extent, the effect of auto-inhibition on the Global Effect (Chapter 2, Appendix A). A natural follow-up to our thesis is to build a model of the visuo-oculomotor system that could be used to implement the ideas that we have developed. Chapter 5 was an attempt to move in that direction. We will now review some of the points that will require particular attention when implementing our framework.

2.1 Read out of the SCi activity

One strong claim that was made in the General Introduction – and was used in particular in Chapter 2 (replication of Tandonnet et al.'s), Chapter 3 (Saccade Curvature) and Chapter 4 (Bimodal Global Effect) – is that the transformation of the activity of the SCi into an eye movement can be explained by way of a dynamic minivector summation model (summation theory). In fact, we postulated that this latter model was superior to a simple read-out of the winner-take-all position (WTA theory). Moreover, we claimed that the dynamic minivector summation model was equivalent to the saccadic vector-averaging model (averaging theory) when considering only the endpoints of the saccade.

In fact, it appears that such a claim is not reflecting the current opinion in the eye movement community, in which there are various standpoints. One view considers that the averaging theory and the summation theory are two opposite models (Gandhi & Katnani, 2011). These authors conclude their review with: "*Different methods are needed to better differentiate between the two models. One such approach may arise from microstimulation experiments that exploit the dependencies of saccade characteristics on stimulation parameters.*" (Gandhi & Katnani, 2011, p. 14). Another standpoint argues that the activity of the SCi (build up neurons) is better understood as a likelihood of saccade occurrence – introducing a Bayesian model of action selection (Kim & Basso, 2010). This standpoint does not consider the summation theory: it ranks the Bayesian model as having the best predictive power (with 82% of correct predictions), followed by the WTA model (71% of correct predictions) and finally the averaging theory (56% or 69% of correct predictions according to the implementation). In fact, the Bayesian approach to decision making has become popular for modelling motor planning and control in general, taking into account history and goal related information (Wolpert & Landy, 2012).

We believe that rather than distinguishing and differentiating the theories through the collection of experimental data, more attention should be given to demonstrating, at the analytic level, how similar those theories are, how they overlap with each other, and how they interlock/nest with each other. In short, more work is needed towards forming an integrative view.

2.2 Taking into account Reaction Times and Trajectory

Our work has focused on the spatial interactions between stimuli that shape action selection – notably the motor responses (which can consist of accuracy, trajectory, and landing position measures). Temporal interactions and reaction times[13] were addressed and used in our work[14] but they were not the focal point of our study. Considering endogenous/exogenous signals projecting on the SCi/motor map -- both the *temporal* and the *spatial* interactions of the projecting signals affect both the *reaction times* and the *motor responses*. In short, these four aspects are closely intertwined. Therefore, in order to obtain a general model of action selection in the visuo-oculomotor system, we would need to unify/cover all of these aspects. From this there is a logical direction: if we want to implement our theoretical framework, we will need to explore the temporal aspect/time course of Spatiotopic Deviation Away and the Bimodal Global Effect (Chapter 3 and 4). In addition, to cover all the aforementioned aspects, the model of Chapter 5 – or any other candidates -- would need a mechanism that generates both *eye trajectories* and *reaction times*. Here, we try to clarify the state of the literature regarding this matter.

Three groups of studies can be distinguished among those that have recently used dynamic neural fields (DNF) or population coding to model the visuo-oculomotor system. Our commitment to focus on spatial interactions and motor responses represents the opposite approach to the first group of studies (Bompas & Sumner, 2011; Marino et al., 2012; Satel et al., 2014; Satel, Wang, Trappenberg, & Klein, 2011; Trappenberg et al., 2001). This first group of studies was based on derivatives of Trappenberg et al. (2001)'s model, and focused on estimating only the reaction time of the eye movement responses with a simple activity threshold that the DNF needs to reach in order to trigger a saccade. These studies tend to ignore spatial interactions between signals by fixing the spatial configuration between

[13] i.e., the time spent between the onset of a stimulus and the onset of a motor response when that stimulus is assumed to have induced that motor response.

[14] In Chapter 2, a large section is reserved for the temporal dynamic of the membrane potential according to the size of the stimulated regions. In Chapter 3 (Saccade Curvature) we used stimulus duration and delays to modify their effect on the saccade deviation. In the appendix of Chapter 4, we proposed further analysis at individual level taking into account the reaction time in our theoretical model.

stimuli so that, sometimes their models could be reduced to few interconnected neuron/accumulator models. On the other hand, a second group of studies focused only on eye trajectories (velocity, trajectory, curvature, endpoint) and/or neuron responses (peak, duration, integral of the saccadic burst) while considering both spatial and temporal interactions between input signals (Arai & Keller, 2004; Arai et al., 1994; Morén et al., 2013; Quaia et al., 1999; Van Opstal & Goossens, 2008; Walton et al., 2005). In fact, the very popular model of Quaia et al. (1999) did report some reaction times/latencies of their model and notably failed to explain the expected change in latency after a collicular lesion. Finally, the third group of studies are those that tried to explain *both* reaction time and motor responses while taking into account *both* the temporal and spatial dynamic between signals (Kopecz & Schöner, 1995; Kruijne et al., 2014; Meeter et al., 2010; Z. Wang et al., 2012; Wilimzig et al., 2006). This last group of studies are based on two classes of model: derivatives of Meeter et al. (2010)'s model and derivatives of Kopecz and Schöner (1995)'s model (except Wang et al. (2012), which is a derivative of Trappenberg et al. (2001)'s model). However, Kopecz and Schöner (1995) and Trappenberg et al. (2001)'s classes of models often ignore eye trajectories – they only estimate the endpoint of saccades. Although the original work of Kopecz and Schöner was able to generate trajectory by using the dynamic minivector theory, this aspect was simplistic, with no actual feedback loop to explain saccade curvatures (Arai & Keller, 2004; Walton et al., 2005 for two different feedback systems).

Thus, the only model that has expressly attempted to explain both trajectories and reaction times is Meeter et al. (2010)'s model, and it failed to explain deviation away from a distractor. Rather, it was one of its derivatives -- Kruijne et al. (2014)'s model -- that invoked an additional mechanism to explain the deviation away. Unfortunately, as seen in Chapter 3, we refuted their model. In conclusion, it appears that the theoretical framework that we started to develop throughout this thesis – particularly if it is to be endowed with a temporal aspect -- has not yet been implemented in current models. Arai and Keller (2004)'s model -- although it did not address reaction times, and failed to replicate deviation away from distractor -- appears to us as an interesting alternative to Kruijne et al.(2014)'s model to explore. Notably, Arai and Keller used a minivector summation mechanism, and they insist on a relationship between SC/basal ganglia (this point will be taken up in Section 3.2). Finally, they revealed the need for an additional signal to explain saccade curvatures – one that may originate from the cerebellum or from other satellite structures (see Section 3.2).

3 Understanding the limits of the simplifications made in the Visuo-oculomotor frameworks

In our current work, we focused mainly on the SC and motor execution. We speculated on what behaviours could be explained when considering the patterns of activity and lateral connections in the SC and what activity of the SCi can be assessed from the motor response. In fact, the eye kinematic (trajectory/velocity) is tightly coupled to the activity in the SCi and this relationship is rather well understood (Goossens & Van Opstal, 2005; Port & Wurtz, 2003). On the other hand -- and from a modelling standpoint -- the reaction time is tightly coupled to the time point at which a model should start transforming the activity of the SCi into an eye movement. Therefore, this time point is of critical importance in defining the motor response; however, it remains poorly understood. There are several mechanisms that shaped the activity of the SCi, and the time at which that activity is transformed into eye movement. These mechanisms are either formed by neural populations in the SC, or by projections from either subcortical or cortical regions. In fact, the different structures working with the SCi are so tightly coupled with the SCi that current model of the SCi (Trappenberg et al., 2001) most likely comprise/compress/ summarise *implicitly* the dynamic of several structures into one DNF. Although simple models such as the one of Trappenberg et al. (2001) are successful in explaining some behaviours, we think that there are mechanisms that warrant attention and as such need to be considered explicitly. An integrative view of all these mechanisms is the key to our understanding of action selection and action execution.

3.1 On the Diversity of the neural population of the SC

One of the most exciting approaches for understanding the mechanisms of the SC is to break the assumption of one homogenous dynamic neural field to model the SCs or SCi.

3.1.1 Diversity of Neuro-transmitters and neuro-receptors

First, there is a neural diversity defined by neuro-receptors and neuro-transmitters. For instance, inhibitory and excitatory neurons do not share the same parameters and have different f-I curves (compare Endo, Yanagawa, Obata, & Isa, 2003 - Figure 3A with Saito & Isa, 2003 - Figure 4C). Both populations are driven by different mechanisms and get reached by different brain regions. For instance, it is known that GABAergic neurons – i.e. inhibitory -- in the SC emit spikes spontaneously (Saito & Isa, 2003 - Figure 3) and that they receive inhibitory connections from the Substantia Nigra (Kaneda, Isa, Yanagawa, & Isa, 2008).

Furthermore, it is known that there are two receptor types for excitatory neurons - the AMPA and the NMDA channel receptors (Saito & Isa, 2003). While AMPA receptors are very simple and readily fit with our neuron model, NMDA receptors would be a very interesting addition. These channels have two interesting properties: they have 1) a voltage dependence caused by a Mg2+ ions blocking the channel at low voltage and 2) they need both glutamate and glycine to open the channel (Ishii et al., 1993). The former mechanism may help neurons to emit bursts of spikes (Morén et al., 2010, 2013) while the latter is thought to help coincidence detection and synaptic plasticity (Seeburg et al., 2013). NMDA receptors have also been shown to control the size of the receptive fields in the SC, while not altering stimulus size tuning, in the hamster SC (Razak, 2003). Importantly, it has been proposed that the interplay between NMDA receptor neurons and GABAergic neurons plays an important role in explaining the bursting behaviour of the SCi and the gating of visual information to SCi (Morén et al., 2010, 2013; Saito & Isa, 2003). Thus, the simple addition of neurons with NMDA receptors in a model can offer many possibilities. Furthermore, to our knowledge, there is no work assessing the dynamic / presence of glycine – needed by NMDA receptors -- in the SCi.

3.1.2 A Broken Bridge between Functional and Anatomical Diversity?

Second, there is a neural diversity defined by the morphology of the neurons and their firing pattern (firing behaviour, neurophysiology). Several studies have reported different types of neurons inside the same SC functional layer. For instance, in the rat SCs, there are five major morphological categories: *marginal cells, horizontal cells, narrow field vertical cells, wide field vertical cells, and stellate cells* (Langer & Lund, 1974). In the cat SCs, two types of inhibitory neurons for a total of six type of neurons have been suggested (Mize, Spencer, & Sterling, 1982). On the side of the SCi, four different morphologies of efferent neurons, *the T, A, X, I,* have been reported and can be extended up to nine groups (Moschovakis & Karabelas, 1985; see also Moschovakis, Karabelas, & Highstein, 1988b for monkeys) . In the SCi, two functional types of neurons are commonly distinguished by extra-cellular recording methods: the visual related neurons and the saccade-related neurons (Mays & Sparks, 1980). In the saccade-related neurons, for instance, there were two subtypes – the *directional* or *vectorial* neurons – reported by Moschovakis, Karabelas and Highstein (1988a). Furthermore, the *vectorial and directional* neurons can be divided into *burst* and *build up* neurons (Munoz & Wurtz, 1995a) – although it is thought today that there is a continuum between the *burst* and *build up* types (Munoz, Dorris, Pare, & Everling, 2000; Quaia et al., 1999). Importantly, the build up and burst neurons are used as a common basis to build models of the SCi. However, extra-cellular recording made by neurophysiologists

in the SCi have *never* assured/guaranteed that the soma of the build up and burst neurons are in the SCi. Their recording electrode may record the axon of a neuron projecting to the SCi. Histological work combined with extra-cellular recording has already suggested that the so-called build up neurons have their soma in the mesencephalic reticular formation, while the burst neurons have their soma in the SCs (Moschovakis et al., 1988a). This kind of confusion may be detrimental for our understanding of action selection and it appears that work still needs to be done to understand the function of each aforementioned anatomical groups.

3.1.3 Structural heterogeneity and Conclusion

In the previous paragraphs, the presence of several neural populations in the SC is not entirely incompatible with the idea of using the framework of 2D homogenous DNFs as the basis for a model: several 2D homogeneous DNFs could be used to represent each population. However, such a trick may not always be applicable. For instance, when a slice is made orthogonal to the dorso-ventral axis (such a slice would represent the rostro-caudal and medio-lateral axis and so does 2D DNF) the rodent SCi presents a honeycomb/mosaic architecture that was first revealed by using a marker for acetylcholinesterase[15] (Chevalier & Mana, 2000). In this study, the honeycomb pattern consisted of approximately 100 rounded compartments throughout the entire SCi; regions with a strong density of acetylcholinesterase draw the boundaries of those compartments, i.e., they draw the *strands of a net*. Further investigations have shown that the afferent connections and the efferent neurons follow this honeycomb pattern (Mana & Chevalier, 2001a). The most striking result found by this team was the discovery of a three dimensional and complex architecture of the SCi (Mana & Chevalier, 2001b; their Figure 9 is particularly insightful). They also observed that the SNr was projecting preferentially into the region with acetylcholinesterase. We should emphasize that this work of Chevalier and Mana is not unique. Illing and Graybriel had demonstrated, in cats, that the SCi has a mosaic organisation shaped by the presence of acetylcholinesterase-rich patches and that the *Frontal cortex* and the *SNr* converge to those zones (Illing, 1996; Illing & Graybiel, 1985, 1986). The complex, three dimensional, compartmental organisation of afferent and efferent projections on the SCi was also studied in cats (John K. Harting & Van Lieshout, 1991; Michael F. Huerta & Harting, 1984) – Figure 1 of Huerta and Harting, 1984 is particularly insightful. This body of data casts serious doubts on how far the SCi can be simplified to multiple 2D homogenous DNFs. Unfortunately, it may have gone unnoticed

[15] Note that this enzyme basically neutralises acetylcholine that is a neurotransmitter. Most cortical structures used glutame and GABA for their projection to the SCi. Thus one question that can be raised is: which structure projects acetylcholine on the SC?

(no more than 30 citations for Chevalier and Mana, 2001; compared with 575 citations for the work of Munoz & Wurtz, 1995 that led to the build up/burst neuron segregation).

The quest for simplicity should not compromise the depth of our understanding. An important direction for modellers and neurophysiologists is to seek the limits of the simplifications we make. We need to build an integrative view of the neural diversity and architecture of the SC in order to reach a unified understanding of the SC. We saw in Chapter 5 that Neurophysiology began to develop new tools for population recording. Until recently, Neurophysiology was barely able to study different populations separately. However, new technologies such as the optogenetic technique[16] and genetically encoded indicators for voltage have opened a new avenue in this regard and these techniques have recently been applied to the study of the rodent SC (Feinberg & Meister, 2015; Stubblefield, Thompson, & Felsen, 2015). Interestingly, Feinberg and Meister (2015) found a columnar organisation of the neural/functional responses in the SCs of the mouse that is reminiscent of the anatomical work of Chevalier and Mana.

3.2 Subcortical mechanisms

In the framework of Trappenberg et al. (2001) and of Kopecz and Schöner (1995) the main source of endogenous signals on the motor planning map / action selection map was the cortical regions. In the theoretical framework adopted in the present thesis, we distinguished between goal-related and history-related endogenous signals and have extended the source of endogenous signals to subcortical regions such as the Locus Coeruleus (see Chapter 4). We review here some of the subcortical structures that are likely to be involved – those that are closely interconnected with the SC-- in defining action selection (from saccadic reaction times to saccade trajectories).

3.2.1 Central Mesencephalic Reticular Formation and Omnipause Neurons

A first mechanism that we will present involves the omnipause neurons (OPNs) in the midbrain pontine and the central mesencephalic reticular formation (cMRF). The OPNs inhibit tonically the brainstem burst generator to prevent saccades, therefore playing a gating role by releasing (or not) its inhibition. However, it is not clear which mechanism opens the gates. One possible suggestion is developed in the following account. First, it is important to note that a biological neuron by itself can implement a gating mechanism: for a range of too low input, one neuron can remain silent – i.e. it emits no spike (Gerstner & Kistler, 2002, fig. 2.5B, p. 38; Hodgkin & Huxley, 1952). It is known that the SCi sends *direct*

[16] i.e., specific cells are genetically modified so that they expressed a gene in the presence of a specific light

excitatory projections and *indirect* inhibitory projections to the OPNs (N. Wang et al., 2013). This indirect inhibition of the OPN passes through the cMRF. It is possible that relatively weak activity occurring in the SC does not succeed in activating the inhibitory neurons of the cMRF: instead weak activity excites directly the OPNs and prevents saccade. This is in concordance with studies reporting that some OPNs inherit the transient responses of the SC to visual stimulus (Boehnke & Munoz, 2008; Evinger et al., 1982). On the other hand, high activity in the SCi -- such as those created by the burst neurons -- would succeed in activating the inhibitory neurons of the cMRF, which in turn inhibits the OPNs, and leads to saccade initiation. It could be argued that such a mechanism is very close to the activity threshold/activity gating used in models of the SCi.

However, the story is not as straightforward as this. It should be made clear that the transient visually driven response can also be observed in electromyograms of the neck/shoulder muscles (Boehnke & Munoz, 2008). Thus, the notion of gating/threshold is blurred: although no movement can be recorded, *there is* a motor response to weak activity of the SCi. Furthermore, it is not entirely clear as to whether the inhibition from the cMRF could pause the OPN. Indeed, the projections of the cMRF to the OPN are primarily composed of GABA (N. Wang et al., 2013). There are both GABA-ergic and glycinergic terminals contacting the OPNs (Horn, Buttner-Ennever, Wahle, & Reichenberger, 1994). Only the glycinergic pathway appears to control directly the pause of OPNs (Kanda, Iwamoto, Yoshida, & Shimazu, 2007b) while the effect of GABA on OPNs has been linked to saccade velocity (Soetedjo et al., 2002). To our knowledge, the glycinergic brain regions projecting to the OPNs are unidentified. Nevertheless, the cMRF is known to contain glycinergic cell bodies (Rampon, Luppi, Fort, Peyron, & Jouvet, 1996). Furthermore, Wang et al. (2013) report that a third of projections of the cMRF onto OPNs may be non-GABA-ergic. Thus, the cMRF could possibly participate in pausing the OPN through as-yet-unspecified glycinergic projections. Alternatively, it could be worth investigating where the glycinergic neurons of the cMRF project – as these could provide the glycine needed to activate NMDA receptors in the SCi.

We should note that the cMRF also projects to the SCi forming a feedback circuit (Chen & May, 2000; Zhou, Warren, & May, 2008). This may be of particular importance when considering that cMRF is thought to be involved in coordinating head movement with eye movements and in the feedback control of the saccade (Waitzman, Pathmanathan, Presnell, Ayers, & Depalma, 2002; Waitzman, Silakov, DePalma-Bowles, & Ayers, 2000). Recently, the cMRF has been shown to project to nuclei that control the near triad – i.e., pupillary constriction, eye convergence, and accommodation (Bohlen, Warren, & May, 2015; May,

Warren, Bohlen, Barnerssoi, & Horn, 2015). In summary, a better characterization of the *roles* of cMRF and OPNs would help to better account for reaction times, trajectories, and general orienting responses in models.

3.2.2 Substantia Nigra pars reticulata

A second interesting mechanism involves the substantia nigra pars reticulata (SNr). This brain region tonically inhibits the SCi (Hikosaka & Wurtz, 1983, 1985), thus necessarily playing a gating role by releasing its inhibition to allow saccades. Interestingly, the SNr and the SCi share reciprocal and topographic connections (Peter Redgrave et al., 2010) and it has been proposed that this is this dynamic loop that creates a gating/threshold mechanism (Thurat, N'Guyen, & Girard, 2015; J. Zhang & Bogacz, 2008). Furthermore, as its projections are topographic, the SNr may release from inhibition only a region of the SC, participating in a type of winner-take-all dynamic while the disinhibited region of the SCi could be extensive enough to contain activity induced by "loser" inputs – the scenario that we considered in Chapter 4. However, the story is not so simple.

We shall note that SNr's inhibitory neurons send an equal amount of projections to the *inhibitory* and *excitatory* neurons of the SCi (Kaneda et al., 2008) and it projects bilaterally on the SCi (Basso & Liu, 2007; P. Liu & Basso, 2008). Furthermore, the SNr neurons also influence the build up neurons of the SCi that are known to have premotor activity. Taken together, these findings do not exactly point to a gating role for the SNr (P. Liu & Basso, 2008). In addition to this, SNr appears to have a different, if not greater, impact on memory guided saccades than on visually guided saccades (Basso & Liu, 2007; Bayer, Handel, & Glimcher, 2004). And as mentioned in the previous section, the SNr appears to send its projections preferentially to the regions of the SCi that contain acetylcholinesterase. Thus, it follows that the SNr may play a more advanced, and more subtle role than just a systematic blocking/unblocking of SCi motor commands (Shires, Joshi, & Basso, 2010). In fact, the SNr has been suggested to play an important role in general decision making (Bogacz & Gurney, 2007). Importantly, the SNr could bias its influence on the SCi map so that saccades toward highly rewarded positions are triggered more rapidly (Hikosaka, Nakamura, & Nakahara, 2006). This relates to the expectation-related signals that we assumed in our theoretical framework. In summary, we believe that the visuo-oculomotor system can only be poorly understood if we disregard the basal ganglia; however, most of the work to clarify its role and the complexity of its relationship with the SCi remains to be done.

3.2.3 Isthmic Nuclei

A third set of mechanisms that we believe to be important involves the isthmic nuclei (the name used in birds). A traditional view is that there are two main pathways to the SC/Optic Tectum: the GABA-ergic pathway and the cholinergic pathway that are formed respectively by the nucleus isthmi pars magnocellularis and the nucleus isthmi pars parvocellularis. In mammals, the GABA-ergic nucleus is named the lateral tegmental nucleus and it has been suggested to play a role in target selection/categorisation through an inhibition of inhibition (Mysore & Knudsen, 2012). On the other hand, the cholinergic nucleus in mammals is divided into two nuclei: the parabrachial and parabigeminal nucleus. The parabigeminal nucleus projects preferentially onto the SCs while the parabrachial region projects to the SCi. The parabrachial region is further divided into the pedunculopontine tegmental nucleus (PPTg) and the laterodorsal tegmental nucleus (LDTg). These cholinergic inputs to the SCi were suggested to control a gating mechanism (Kobayashi & Isa, 2002; Marín et al., 2007). Interestingly, the cholinergic input of the PPTg to the SCi overlaps with the input of the SNr (John K. Harting & Van Lieshout, 1991). Note that we mentioned earlier that the SNr and the Frontal cortex project to the SCi regions that are rich in acetylcholinesterase (Section 3.1.3, p. 6-10). Thus, there clearly appears to be a convergence of the SNr, Frontal Cortex, and PPTg projections onto those regions, and that there is an important, and as yet unspecified, mechanism underlying this convergence. More than the mere convergence of these three sources, it is the spatial organisation of this convergence on the SCi that is disconcerting/disturbing: in the honeycomb-like organisation of the SCi, the region of convergence draws the strands of the net that forms the honeycombs.

Further, it should be noted that the isthmic nuclei project also glycinergic afferents to the SC -- and that their spatial organisation differs from that of the GABA-ergic pathway (Hunt et al., 1977). To our knowledge, it has not received much attention, and again, in order to understand the NMDA mechanism in the SCi, we need to investigate all sources of glycine. Note also that the nucleus isthmic may be involved in creating winner-take-all / switch-like responses in the SC (Lai, Brandt, Luksch, & Wessel, 2011) and in representing a moving target trajectory (Ma, Cui, Lee, Anastasio, & Malpeli, 2013). Finally, the PPTg shares reciprocal connections with the SNr (Lavoie & Parent, 1994), the dorsal raphe and the Locus Coeruleus (Koyama & Kayama, 1993) -- which we introduced in Chapter 4 as source of expectation-related signal.

3.2.4 Contralateral Superior Colliculus and Conclusion

The last mechanism that we believe deserves attention involves the contralateral SC. Indeed, It has been shown that there are commissural inhibition and *excitation* between the two SCs. Interestingly, the excitatory projections are mirror-symmetric (Takahashi, Sugiuchi, Izawa, & Shinoda, 2005; Takahashi, Sugiuchi, & Shinoda, 2007). For instance, if the experimenter stimulates upward saccade regions of one SC, this will inhibit downward saccade regions of the contralateral SCi and this will also excite upward saccade regions of the contralateral SCi.

There is much more to say regarding the commissural connections, the isthmic nuclei, the SNr, the OPN and the cMRF, but our aim is not to give a complete picture of all these systems. Rather, our goal was to initiate interest for those mechanisms and encourage an integrative approach of the visuo-oculomotor system. There are possibly more mechanisms to consider (such as the cerebellum loop, Quaia et al., 1999), but we believe that the five aforementioned sets of mechanisms are of particular interest and deserve an advanced and integrated modelling effort. Understanding their interactions would help to clarify which simplifications we are making when using the current DNF models and more general decision-making models (see the next section). This is not a marginal viewpoint, since a review of the SC conducted by Jagadisan & Gandhi (2013) also highlights the role of the isthmic nuclei in action selection and an even more recent review of the SC by Wolf et al. (2015) reached very similar conclusions. In particular, they encourage research on the interactions of the neocortex, SNr, and PPTg with the SCi.

3.3 A note on some Cortical Structures Involved in Eye movements

It is clear that one important set of mechanisms to consider are those involving the cortical projections onto the SC, signals that have already been taken in account in the majority of visuo-oculomotor model frameworks. In our theoretical framework, we considered that the cortical projection to the SCi was representing top-down endogenous signals (as opposed to the subcortical endogenous signals). In Chapter 3, we introduced the Lateral Intraparietal region (LIP) as a candidate for sending excitatory spatiotopic update of stimulus position to the SCi neural population. In Chapter 4, we assessed a top-down/goal-related endogenous signal linked to the discrimination of a target among distractors. Perceptual decisions of this sort (target selection) have been linked to the Frontal Eye Field (FEF, Schall, 2002; Schall et al., 2011).

In fact, FEF and LIP have received a great deal of attention. LIP is famously linked to perceptual decision making during the random dot motion (RDM) paradigm where it is

thought to accumulate evidence of motion from visual area MT (middle temporal, V5), and to integrate the decision variable that defines the choice, its reaction time, and its certainty (Beck et al., 2008; Kiani & Shadlen, 2009; Shadlen & Newsome, 2001). FEF is famous in its importance in making saccade to memory-guided (Dias & Segraves, 1999) or goal-related targets such as in anti-saccade tasks (Guitton, Buchtel, & Douglas, 1985). FEF is also thought to play a role in perceptual decision making (Ding & Gold, 2011). Finally, LIP, and possibly to a lesser extent FEF, are considered as potential priority maps (Falkner, Krishna, & Goldberg, 2010; Ptak, 2012; Serences & Yantis, 2006). We will not give a complete overview of all the roles that have been attributed to FEF/LIP; what is important for our present purposes is that they have both been linked to a range of different aspects of action selection and decision making and it appears that there is no integrative model of LIP/FEF that accounts for all of these aspects. One reason for this could be the lack of integrative studies of LIP and FEF. It is important to note that most recording experiments focused on one task and selectively chose to record only the neurons that *were interesting for the study.* In fact, even without such a selection, several neurons are virtually invisible to the experimenter if they are not activated by the experimental paradigm. Therefore, when one team shows that LIP is involved in A, while another team shows that LIP is involved in B, it is impossible to know whether both teams are speaking about the same population of LIP. Fortunately, work has already begun on a more integrative approach that attempts to resolve the population dynamic of LIP and the heterogeneity of its population (Meister, Hennig, & Huk, 2013; Park, Meister, Huk, & Pillow, 2014; Premereur, Vanduffel, & Janssen, 2011). Note that the most recent study – Park et al., (2014) – is actually an application of the neural population fitting method from extra-cellular recording that we mentioned in the discussion of Chapter 5 (Pillow et al., 2008).

LIP and FEF have very similar patterns of activation to the SCs/SCi, with burst neurons, build up neurons, and visual neurons. Despite their common patterns of activity, when using specific paradigms such as a delay task, it can be revealed that SCi activity is more related to movement while LIP/FEF activity is more related to visual stimuli (Wurtz, Sommer, Paré, & Ferraina, 2001). In the same vein, the group of LIP neurons projecting to the FEF conveys rather visually-related information, while the separated group of LIP neurons projecting to the SC conveys rather motor-related information (Ferraina, Paré, & Wurtz, 2002). Interestingly, it has been suggested that the motor-related burst of activity in LIP/FEF only *reflects* the motor-related burst of activity initiated by the SC (J. Zhang & Bogacz, 2008). We believe that this idea of *activity reflection* is critical for our understanding of LIP/FEF – and possibly any brain structure. To record a motor signal in LIP does not necessarily mean that it is LIP that *generates* that signal, the LIP could be

merely *reflecting* the signal. Importantly, when recording decision making signals in LIP, it should be kept in mind that it may be only a reflection. However, although the notion of activity reflection is important, it is not black and white: the line between pure reflection and pure generation can be blurred and complex to draw. When inactivating the LIP, the velocity for visually triggered saccades remains intact while the velocity for memory guided saccades is decreased (Li, Mazzoni, & Andersen, 1999). Assuming that the saccadic velocity is an image of the saccadic burst (see also Van Opstal & Goossens, 2008), the former result is in line with Zhang and Bogacz's theory -- LIP only reflects the SC burst -- while the latter result indicates that the LIP *does* participate in generating the saccadic burst of memory-guided saccade. To complicate matters even further, during such inactivation of LIP, the latency of both visual and memory saccades is increased. This could be taken to imply that the LIP has, in *both cases*, a role to play in *initiating* the saccadic burst – even though it does not *generate* it for visual saccades.

To conclude, current understanding of the actual roles of LIP and FEF are only superficial. We believe that the notions of heterogeneity and reflection could provide a novel, deeper, understanding of these cortical inputs to the SCi and, in general, of any brain regions. Further, as a final comment, to our knowledge, the inferior temporal lobe – which projects to the SCi, as described in the General Introduction – has never been the target of intensive research for its role in saccadic movement. That represents an interesting future direction. Finally, our point in the previous sections was to encourage the understanding of the heterogeneity and complexity of the visuo-oculomotor system in order to *master* the simplifications of our current models.

4 Future Directions and Concluding remarks: toward a unification of Decision-Making models

4.1 The visuo-oculomotor system: a new general model of decision-making?

Within the framework of the present thesis, the decision of where-to-go is considered to be the result of spatial interactions between exogenous signals, goal-related signals, and expectation-related-signals. Furthermore, we have assumed that the decision of when-to-move is not systematically linked to the decision of where-to-move. Therefore, traces of this latter decision process can be extracted from the movement. Interestingly, the standard view in Psychology (i.e., all scientific fields studying the brain and its output) describes decision processes as an accumulation of evidence to thresholds that sanction the

decisions. For instance, the drift diffusion model (Ratcliff, 1978) -- the most famous and widely used model in Psychology – describes two-alternative choices with a decision variable that accumulates a noisy input that has a constant mean – i.e. the flux of evidence. A decision is taken if the accumulation variable reaches one of the two boundaries that represent each decision option. Thus, in this view of decision-making, there is only one exogenous signal with a strength that is noisy but has a constant mean. Furthermore, the strength of that exogenous signal has a biologically relevant polarity: e.g., to vary its strength would change the colour of the stimulus from red to green, or change its speed from left to right. Finally, in this view, the when-to-answer (that is analogous to when-to-move) corresponds systematically to what-to-answer (that is analogous to where-to-move) as both decisions share the same threshold. From that, the general models of Decision Making could possibly be reduced to a *very* particular case of what the visuo-oculomotor models of Decision Making can cover. This means that visuo-oculomotor models of Decision Making are *more general* than general Decision Making models. We believe that they have the potential to form the new general Decision Making framework. However, the label "visuo-oculomotor" makes them appear less general, and so we shall seek to apply our experience in modelling eye trajectories to any trajectory movements, including orienting responses, hand reaching, hand pointing -- possibly even to walking trajectory and to button-press movements if we can record precisely the pressure level over time.

We should also state that the other models used in general Decision Making -- such as leaky competing accumulator models (LCAC, Usher & McClelland, 2001), accumulator models (Vickers, 1970), or multi-hypothesis sequential probability ratio test models (MSPRT, Baum & Veeravalli, 1994) -- either follow a similar principle to that of the drift diffusion model or extend that principle to multiple alternatives. In fact, most two-alternative models, with the exception of the accumulator model, can be reduced to the drift diffusion model (Bogacz, Brown, Moehlis, Holmes, & Cohen, 2006; Ratcliff & Smith, 2004). This unifying approach of Bogacz et al. (2006) should be pursued to understand the interlocking between MSPRT, DNF and LCAC and other models that deal with multi-alternative decisions.

4.2 The need for a new general Decision Making framework?

But are the users of the standard Decision Making framework ready to change their habits and welcome a new and more complicated framework that would put the motor response at the core of decision-making? In the standard Decision Making framework, the interface input to communicate the decision is a button-press (left index finger / right index finger).

For monkeys, saccades either to the left or right are often used. In both cases, only the reaction times and the answer (left or right) are extracted for data analysis – this is because the Drift Diffusion model does not consider anything else. In such a context, where most tasks and inputs are tailored to the Drift Diffusion model, it would be impossible to fight years of inertia and introduce a new model. However a recent and self-motivated trend in Psychology is to use mouse tracking paradigms – which is easier to use than eye tracking or motion capture -- to replace the overexploited button-press paradigms (for review, see Freeman & Ambady, 2010; Freeman, Dale, & Farmer, 2011). Indeed, it has been shown that there is more information to extract from hand trajectories than from button press when concerned with the processes of decision making – particularly since the changes of mind and hesitations of the participant can be tracked (Hehman, Stolier, & Freeman, 2015; Resulaj, Kiani, Wolpert, & Shadlen, 2009). However, the current general Decision Making framework -- monopolised by the Drift Diffusion model -- does not offer any tools to model trajectories and so it offers no understanding of the new concepts yielded by the data. To fill the gap, there have been attempts to add new mechanisms over the Drift Diffusion model (Lepora & Pezzulo, 2015). Fortunately, the Dynamic Field Theory and the Visuo-oculomotor models have already a lot of experience in modelling trajectories, so the development of mouse tracking may be an excellent opportunity to introduce our models to broader audiences. This route could eventually encourage a theoretical unification between button press, eye movement and hand movement methods and yield a unification between general Decision Making models and the visuo-oculomotor model of Decision Making.

4.3 Concluding Remarks

In the General Introduction, we presented decisions as the outcomes of the interactions of a brained organism with its environment. The current environment provides exogenous signals to the brain of the animal while the current state of the brain is driving endogenous signals related to goals or expectations that have been formed from previous interactions with the environment – note that this view can be found elsewhere (Awh et al., 2012). Because the brain is a three dimensional structure, there should be spatial interactions between signals, and these might be influential when forming decisions. Using the visuo-oculomotor system as a biological model, our work has revealed some of the spatial interactions that can be expected between signals (Chapter 2), along with signals that had not previously been considered (Chapter 3 and 4), whilst giving rise to new tools and a conceptual framework to measure these interactions (Chapter 1, Chapter 4). Finally, this work has attempted to achieve a deeper understanding of these spatial interactions at a

neurophysiological level (Chapter 2 and 5). Ultimately, these journeys at both behavioural and neurophysiological levels led us to envisage the implementation of our conceptual framework, to seek the limits of its simplicity, and to consider its application to the theoretical and experimental study of decision making. Consequently, a number of new directions have emerged from this work and, we have also shown that the visuo-oculomotor system -- which is only a small subset of the brain -- reaches a level of complexity that can overwhelm a solitary researcher. We believe that the only way to capture and master such complexity is to begin integrating the different sources of knowledge into encyclopaedic models. Our work, we hope, will stimulate future research and promote a model-centric approach to Psychology.

References

Adams, F. (2010). Embodied cognition. *Phenomenology and the Cognitive Sciences*, *9*(4), 619–628.

Adamuk, E. (1872). Uber angeborene und erworbene Association von FC Donders. *Albrecht von Graefes Archiv Fur (klinische Und Experimentelle) Ophthalmologie*, *18*, 153–164.

Aitsebaomo, A. P., & Bedell, H. E. (2000). Saccadic and psychophysical discrimination of double targets. *Optometry & Vision Science*, *77*(6), 321–330.

Aizawa, H., & Wurtz, R. H. (1998). Reversible inactivation of monkey superior colliculus. I. Curvature of saccadic trajectory. *Journal of Neurophysiology*, *79*(4), 2082–2096.

Alexinsky, T., Aston-Jones, G., Rajkowski, J., & Revay, R. S. (1990). Physiological correlates of adaptive behavior in a visual discrimination task in monkeys. In *Society for Neuroscience Abstracts* (Vol. 16, p. b1).

Allman, J., Miezin, F., & McGuinness, E. (1985). Stimulus specific responses from beyond the classical receptive field: neurophysiological mechanisms for local-global comparisons in visual neurons. *Annual Review of Neuroscience*, *8*(1), 407–430.

Almeida, R., Barbosa, J., & Compte, A. (2015). Neural circuit basis of visuo-spatial working memory precision: a computational and behavioral study. *Journal of Neurophysiology*, *114*(3), 1806–1818. http://doi.org/10.1152/jn.00362.2015

Amari, S. (1977). Dynamics of pattern formation in lateral-inhibition type neural fields. *Biological Cybernetics*, *27*(2), 77–87.

Amlôt, R., Walker, R., Driver, J., & Spence, C. (2003). Multimodal visual–somatosensory integration in saccade generation. *Neuropsychologia*, *41*(1), 1–15.

Andersen, R. A., Asanuma, C., Essick, G., & Siegel, R. M. (1990). Corticocortical connections of anatomically and physiologically defined subdivisions within the inferior parietal lobule. *The Journal of Comparative Neurology*, *296*(1), 65–113. http://doi.org/10.1002/cne.902960106

Anderson, A. J., Yadav, H., & Carpenter, R. H. S. (2008). Directional Prediction by the Saccadic System. *Current Biology*, *18*(8), 614–618. http://doi.org/10.1016/j.cub.2008.03.057

Anderson, M. L. (2003). Embodied cognition: A field guide. *Artificial Intelligence*, *149*(1), 91–130.

Anderson, R. W., Keller, E. L., Gandhi, N. J., & Das, S. (1998). Two-dimensional saccade-related population activity in superior colliculus in monkey. *Journal of Neurophysiology*, *80*(2), 798–817.

Appell, P. P., & Behan, M. (1990). Sources of subcortical GABAergic projections to the superior colliculus in the cat. *Journal of Comparative Neurology*, *302*(1), 143–158.

Apter, J. T. (1946). Eye movements following strychninization of the superior colliculus of cats. *Journal of Neurophysiology*, *9*(2), 73–86.

Arai, K., & Keller, E. L. (2004). A model of the saccade-generating system that accounts for trajectory variations produced by competing visual stimuli. *Biological Cybernetics*, *92*(1), 21–37. http://doi.org/10.1007/s00422-004-0526-y

Arai, K., Keller, E. L., & Edelman, J. A. (1993). A spatio-temporal neural network model of saccade generation. In *Neural Networks, 1993., IEEE International Conference on* (pp. 70–74). Retrieved from http://ieeexplore.ieee.org/xpls/abs_all.jsp?arnumber=298529

Arai, K., Keller, E. L., & Edelman, J. A. (1994). Two-dimensional neural network model of the primate saccadic system. *Neural Networks*, *7*(6–7), 1115–1135. http://doi.org/10.1016/S0893-6080(05)80162-5

Arai, K., McPeek, R. M., & Keller, E. L. (2004). Properties of Saccadic Responses in Monkey When Multiple Competing Visual Stimuli Are Present. *Journal of Neurophysiology*, *91*(2), 890–900. http://doi.org/10.1152/jn.00818.2003

Arce, E. A., Bennett-Clarke, C. A., & Rhoades, R. W. (1994). Ultrastructural organization of the noradrenergic innervation of the superficial gray layer of the hamster's superior colliculus. *Synapse*, *18*(1), 46–54. http://doi.org/10.1002/syn.890180107

Aston-Jones, G., & Bloom, F. E. (1981). Activity of norepinephrine-containing locus coeruleus neurons in behaving rats anticipates fluctuations in the sleep-waking cycle. *The Journal of Neuroscience*, *1*(8), 876–886.

Aston-Jones, G., & Cohen, J. D. (2005). An integrative theory of locus coeruleus-norepinephrine function: adaptive gain and optimal performance. *Annu. Rev. Neurosci.*, *28*, 403–450.

Aston-Jones, G., Rajkowski, J., Kubiak, P., & Alexinsky, T. (1994). Locus coeruleus neurons in monkey are selectively activated by attended cues in a vigilance task. *The Journal of Neuroscience*, *14*(7), 4467–4480.

Awh, E., Belopolsky, A. V., & Theeuwes, J. (2012). Top-down versus bottom-up attentional control: a failed theoretical dichotomy. *Trends in Cognitive Sciences*, *16*(8), 437–443. http://doi.org/10.1016/j.tics.2012.06.010

Badel, L., Lefort, S., Berger, T. K., Petersen, C. C. H., Gerstner, W., & Richardson, M. J. E. (2008). Extracting non-linear integrate-and-fire models from experimental data using dynamic I–V curves. *Biological Cybernetics*, *99*(4-5), 361–370. http://doi.org/10.1007/s00422-008-0259-4

Badel, L., Lefort, S., Brette, R., Petersen, C. C. H., Gerstner, W., & Richardson, M. J. E. (2008). Dynamic I-V Curves Are Reliable Predictors of Naturalistic Pyramidal-Neuron Voltage Traces. *Journal of Neurophysiology*, *99*(2), 656–666. http://doi.org/10.1152/jn.01107.2007

Basso, M. A., & Liu, P. (2007). Context-Dependent Effects of Substantia Nigra Stimulation on Eye Movements. *Journal of Neurophysiology*, *97*(6), 4129–4142. http://doi.org/10.1152/jn.00094.2007

Basso, M. A., & Wurtz, R. H. (1998). Modulation of Neuronal Activity in Superior Colliculus by Changes in Target Probability. *The Journal of Neuroscience*, *18*(18), 7519–7534.

Basso, M. A., & Wurtz, R. H. (2002). Neuronal Activity in Substantia Nigra Pars Reticulata during Target Selection. *The Journal of Neuroscience*, *22*(5), 1883–1894.

Baum, C. W., & Veeravalli, V. V. (1994). A sequential procedure for multihypothesis testing. *Information Theory, IEEE Transactions on*, *40*(6). Retrieved from http://ieeexplore.ieee.org/xpls/abs_all.jsp?arnumber=340472

Bayer, H. M., Handel, A., & Glimcher, P. W. (2004). Eye position and memory saccade related responses in substantia nigra pars reticulata. *Experimental Brain Research*, *154*(4), 428–441.

Bays, P. M., & Husain, M. (2012). Active inhibition and memory promote exploration and search of natural scenes. *Journal of Vision*, *12*(8), 8–8. http://doi.org/10.1167/12.8.8

Beck, J. M., Ma, W. J., Kiani, R., Hanks, T., Churchland, A. K., Roitman, J., … Pouget, A. (2008). Probabilistic population codes for Bayesian decision making. *Neuron*, *60*(6), 1142–1152.

Behan, M., & Kime, N. M. (1996). Intrinsic circuitry in the deep layers of the cat superior colliculus. *Visual Neuroscience*, *13*(06), 1031–1042.

Bell, A. H., Everling, S., & Munoz, D. P. (2000). Influence of Stimulus Eccentricity and Direction on Characteristics of Pro- and Antisaccades in Non-Human Primates. *Journal of Neurophysiology*, *84*(5), 2595–2604.

Benda, J., & Herz, A. V. (2003). A universal model for spike-frequency adaptation. *Neural Computation*, *15*(11), 2523–2564.

Beurle, R. L. (1956). Properties of a mass of cells capable of regenerating pulses. *Philosophical Transactions of the Royal Society B: Biological Sciences*, *240*(669), 55–94.

Blatt, G. J., Andersen, R. A., & Stoner, G. R. (1990). Visual receptive field organization and cortico-cortical connections of the lateral intraparietal area (area LIP) in the macaque. *The Journal of Comparative Neurology*, *299*(4), 421–445. http://doi.org/10.1002/cne.902990404

Boch, R., Fischer, P. D. B., & Ramsperger, E. (1984). Express-saccades of the monkey: Reaction times versus intensity, size, duration, and eccentricity of their targets. *Experimental Brain Research*, *55*(2), 223–231. http://doi.org/10.1007/BF00237273

Boehnke, S. E., & Munoz, D. P. (2008). On the importance of the transient visual response in the superior colliculus. *Current Opinion in Neurobiology*, *18*(6), 544–551. http://doi.org/10.1016/j.conb.2008.11.004

Bogacz, R., Brown, E., Moehlis, J., Holmes, P., & Cohen, J. D. (2006). The physics of optimal decision making: a formal analysis of models of performance in two-alternative forced-choice tasks. *Psychological Review*, *113*(4), 700.

Bogacz, R., & Gurney, K. (2007). The basal ganglia and cortex implement optimal decision making between alternative actions. *Neural Computation*, *19*(2), 442–477.

Bohlen, M. O., Warren, S., & May, P. J. (2015). A central mesencephalic reticular formation projection to the supraoculomotor area in macaque monkeys. *Brain Structure and Function*, 1–21. http://doi.org/10.1007/s00429-015-1039-2

Bompas, A., & Sumner, P. (2011). Saccadic Inhibition Reveals the Timing of Automatic and Voluntary Signals in the Human Brain. *Journal of Neuroscience*, *31*(35), 12501–12512. http://doi.org/10.1523/JNEUROSCI.2234-11.2011

Bouret, S., & Richmond, B. J. (2009). Relation of Locus Coeruleus Neurons in Monkeys to Pavlovian and Operant Behaviors. *Journal of Neurophysiology*, *101*(2), 898–911. http://doi.org/10.1152/jn.91048.2008

Bozis, A., & Moschovakis, A. K. (1998). Neural network simulations of the primate oculomotor system III. An one-dimensional, one-directional model of the superior colliculus. *Biological Cybernetics*, *79*(3), 215–230.

Brette, R., & Gerstner, W. (2005). Adaptive exponential integrate-and-fire model as an effective description of neuronal activity. *Journal of Neurophysiology*, *94*(5), 3637–3642.

Bretzner, L., & Lindeberg, T. (1998). Feature tracking with automatic selection of spatial scales. *Computer Vision and Image Understanding*, *71*(3), 385–392.

Brown, J. W., Hanes, D. P., Schall, J. D., & Stuphorn, V. (2008). Relation of frontal eye field activity to saccade initiation during a countermanding task. *Experimental Brain Research*, *190*(2), 135–151.

Brown, S. D., & Heathcote, A. (2008). The simplest complete model of choice response time: Linear ballistic accumulation. *Cognitive Psychology*, *57*(3), 153–178.

Brunel, N., & van Rossum, M. C. (2007). Quantitative investigations of electrical nerve excitation treated as polarization. *Biological Cybernetics*, *97*(5), 341–349.

Butler, A. B., & Hodos, W. (2005). *Comparative Vertebrate Neuroanatomy: Evolution and Adaptation*. John Wiley & Sons.

Büttner-Ennever, J. A., & Büttner, U. (1978). A cell group associated with vertical eye movements in the rostral mesencephalic reticular formation of the monkey. *Brain Research*, *151*(1), 31–47.

Büttner-Ennever, J. A., Cohen, B., Pause, M., & Fries, W. (1988). Raphe nucleus of the pons containing omnipause neurons of the oculomotor system in the monkey, and its homologue in man. *Journal of Comparative Neurology*, *267*(3), 307–321.

Büttner-Ennever, J. A., & Henn, V. (1976). An autoradiographic study of the pathways from the pontine reticular formation involved in horizontal eye movements. *Brain Research*, *108*(1), 155–164.

Büttner-Ennever, J. A., Horn, A. K., Henn, V., & Cohen, B. (1999). Projections from the superior colliculus motor map to omnipause neurons in monkey. *Journal of Comparative Neurology*, *413*(1), 55–67.

Büttner, U., Büttner-Ennever, J. A., Henn, V., & others. (1977). Vertical eye movement related unit activity in the rostral mesencephalic reticular formation of the alert monkey. *Brain Research*, *130*(2), 239–252.

Cannon, S. C., & Robinson, D. A. (1987). Loss of the neural integrator of the oculomotor system from brain stem lesions in monkey. *Journal of Neurophysiology*, *57*(5), 1383–1409.

Casagrande, V. A., Harting, J. K., Hall, W. C., Diamond, I. T., & Martin, G. F. (1972). Superior Colliculus of the Tree Shrew: A Structural and Functional Subdivision into Superficial and Deep Layers. *Science*, *177*(4047), 444–447. http://doi.org/10.1126/science.177.4047.444

Casteau, S., & Vitu, F. (2012). On the effect of remote and proximal distractors on saccadic behavior: A challenge to neural-field models. *Journal of Vision*, *12*(12). http://doi.org/10.1167/12.12.14

Catania, K. C., & Remple, F. E. (2004). Tactile foveation in the star-nosed mole. *Brain, Behavior and Evolution*, *63*(1), 1–12.

Chen, B., & May, P. J. (2000). The feedback circuit connecting the superior colliculus and central mesencephalic reticular formation: a direct morphological demonstration. *Experimental Brain Research*, *131*(1), 10–21. http://doi.org/10.1007/s002219900280

Chevalier, G., & Mana, S. (2000). Honeycomb-like structure of the intermediate layers of the rat superior colliculus, with additional observations in several other mammals: AChE patterning. *Journal of Comparative Neurology*, *419*(2), 137–153.

Chou, I., Sommer, M. A., & Schiller, P. H. (1999). Express averaging saccades in monkeys. *Vision Research*, *39*(25), 4200–4216. http://doi.org/10.1016/S0042-6989(99)00133-9

Cohen, B., & Büttner-Ennever, J. A. (1984). Projections from the superior colliculus to a region of the central mesencephalic reticular formation (cMRF) associated with horizontal saccadic eye movements. *Experimental Brain Research*, *57*(1), 167–176.

Cohen, B., & Komatsuzaki, A. (1972). Eye movements induced by stimulation of the pontine reticular formation: evidence for integration in oculomotor pathways. *Experimental Neurology*, *36*(1), 101–117.

Cole, K. S., & Curtis, H. J. (1939). Electric impedance of the squid giant axon during activity. *The Journal of General Physiology*, *22*(5), 649–670.

Coren, S., & Hoenig, P. (1972). Effect of non-target stimuli upon length of voluntary saccades. *Perceptual and Motor Skills*, *34*(2), 499–508.

Cousineau, D. (2005). Confidence intervals in within-subject designs: A simpler solution to Loftus and Masson's method. *Tutorials in Quantitative Methods for Psychology*, *1*(1), 42–45.

Crish, S. D., Comer, C. M., Marasco, P. D., & Catania, K. C. (2003). Somatosensation in the superior colliculus of the star-nosed mole. *Journal of Comparative Neurology*, *464*(4), 415–425.

Curtis, H. J., & Cole, K. S. (1942). Membrane resting and action potentials from the squid giant axon. *Journal of Cellular and Comparative Physiology*, *19*(2), 135–144.

Dayan, P., & Abbott, L. F. (2001). *Theoretical neuroscience* (Vol. 806). Cambridge, MA: MIT Press. Retrieved from http://inis.jinr.ru/sl/Cs_Computer%20science/CsGn_Genetic,%20neural/Dayan%20P.,%20Abbott%20L.F.%20Theoretical%20neuroscience%20(2002)(432s).pdf.gz

Dean, P., Redgrave, P., & Westby, G. W. M. (1989). Event or emergency? Two response systems in the mammalian superior colliculus. *Trends in Neurosciences*, *12*(4), 137–147. http://doi.org/10.1016/0166-2236(89)90052-0

Derrington, A. M., & Lennie, P. (1984). Spatial and temporal contrast sensitivities of neurones in lateral geniculate nucleus of macaque. *The Journal of Physiology*, *357*, 219.

Deubel, H., Wolf, W., & Hauske, G. (1984). The evaluation of the oculomotor error signal. *Advances in Psychology*, *22*, 55–62.

Dias, E. C., & Segraves, M. A. (1999). Muscimol-Induced Inactivation of Monkey Frontal Eye Field: Effects on Visually and Memory-Guided Saccades. *Journal of Neurophysiology*, *81*(5), 2191–2214.

Ding, L., & Gold, J. I. (2011). Neural Correlates of Perceptual Decision Making before, during, and after Decision Commitment in Monkey Frontal Eye Field. *Cerebral Cortex*, bhr178. http://doi.org/10.1093/cercor/bhr178

Dominey, P. F., & Arbib, M. A. (1992). A cortico-subcortical model for generation of spatially accurate sequential saccades. *Cerebral Cortex*, *2*(2), 153–175.

Dorris, M. C., & Munoz, D. P. (1998). Saccadic Probability Influences Motor Preparation Signals and Time to Saccadic Initiation. *The Journal of Neuroscience*, *18*(17), 7015–7026.

Dorris, M. C., Olivier, E., & Munoz, D. P. (2007). Competitive Integration of Visual and Preparatory Signals in the Superior Colliculus during Saccadic Programming. *The Journal of Neuroscience*, *27*(19), 5053–5062. http://doi.org/10.1523/JNEUROSCI.4212-06.2007

Dorris, M. C., Paré, M., & Munoz, D. P. (1997). Neuronal Activity in Monkey Superior Colliculus Related to the Initiation of Saccadic Eye Movements. *The Journal of Neuroscience*, *17*(21), 8566–8579.

Drager, U. C., & Hubel, D. H. (1976). Topography of visual and somatosensory projections to mouse superior colliculus. *Journal of Neurophysiology*, *39*(1), 91–101.

Duhamel, J. R., Goldberg, M. E., Fitzgibbon, E. J., Sirigu, A., & Grafman, J. (1992). Saccadic dysmetria in a patient with a right frontoparietal lesion. The importance of corollary discharge for accurate spatial behaviour. *Brain: A Journal of Neurology*, *115 (Pt 5)*, 1387–1402.

du Lac, S., & Knudsen, E. I. (1990). Neural maps of head movement vector and speed in the optic tectum of the barn owl. *Journal of Neurophysiology*, *63*(1), 131–146.

Duzel, E., & Guitart-Masip, M. (2013). Not So Uncertain at Last: Locus Coeruleus and Decision Making. *Neuron*, *79*(1), 9–11. http://doi.org/10.1016/j.neuron.2013.06.023

Ebbesson, P. S. O. E. (1980). A visual thalamo-telencephalic pathway in a teleost fish (Holocentrus rufus). *Cell and Tissue Research*, *213*(3), 505–508. http://doi.org/10.1007/BF00237895

Edelman, J. A., & Keller, E. L. (1998). Dependence on Target Configuration of Express Saccade-Related Activity in the Primate Superior Colliculus. *Journal of Neurophysiology*, *80*(3), 1407–1426.

Edwards, M. D., White, A.-M., & Platt, B. (2002). Characterisation of rat superficial superior colliculus neurones: firing properties and sensitivity to GABA. *Neuroscience*, *110*(1), 93–104. http://doi.org/10.1016/S0306-4522(01)00558-9

Edwards, S. B., Ginsburgh, C. L., Henkel, C. K., & Stein, B. E. (1979). Sources of subcortical projections to the superior colliculus in the cat. *The Journal of Comparative Neurology*, *184*(2), 309–329. http://doi.org/10.1002/cne.901840207

Edwards, S. B., & Henkel, C. K. (1978). Superior colliculus connections with the extraocular motor nuclei in the cat. *The Journal of Comparative Neurology*, *179*(2), 451–467. http://doi.org/10.1002/cne.901790212

Ellard, C. G., & Goodale, M. A. (1986). The role of the predorsal bundle in head and body movements elicited by electrical stimulation of the superior colliculus in the Mongolian gerbil. *Experimental Brain Research*, *64*(3), 421–433.

Endo, T., Yanagawa, Y., Obata, K., & Isa, T. (2003). Characteristics of GABAergic neurons in the superficial superior colliculus in mice. *Neuroscience Letters*, *346*(1–2), 81–84. http://doi.org/10.1016/S0304-3940(03)00570-6

Erlhagen, W., & Bicho, E. (2006). The dynamic neural field approach to cognitive robotics. *Journal of Neural Engineering*, *3*(3), R36.

Ermentrout, B. (1998). Linearization of FI curves by adaptation. *Neural Computation*, *10*(7), 1721–1729.

Evinger, C., Kaneko, C. R., & Fuchs, A. F. (1982). Activity of omnipause neurons in alert cats during saccadic eye movements and visual stimuli. *Journal of Neurophysiology*, *47*(5), 827–844.

Ewert, J.-P. (1970). Neural Mechanisms of Prey-catching and Avoidance Behavior in the Toad <i>(Bufo bufo </i>L.). *Brain, Behavior and Evolution*, *3*(1-4), 36–56. http://doi.org/10.1159/000125462

Fecteau, J. H., & Munoz, D. P. (2006). Salience, relevance, and firing: a priority map for target selection. *Trends in Cognitive Sciences*, *10*(8), 382–390.

Feinberg, E. H., & Meister, M. (2015). Orientation columns in the mouse superior colliculus. *Nature*, *519*(7542), 229–232.

Fejtl, M., Stett, A., Nisch, W., Boven, K.-H., & Möller, A. (2006). On micro-electrode array revival: its development, sophistication of recording, and stimulation. In *Advances in Network Electrophysiology* (pp. 24–37). Springer. Retrieved from http://link.springer.com/content/pdf/10.1007/0-387-25858-2_2.pdf

Feldon, S., Feldon, P., & Kruger, L. (1970). Topography of the retinal projection upon the superior colliculus of the cat. *Vision Research*, *10*(2), 135–143.

Ferraina, S., Paré, M., & Wurtz, R. H. (2002). Comparison of cortico-cortical and cortico-collicular signals for the generation of saccadic eye movements. *Journal of Neurophysiology*, *87*(2), 845–858.

Ferrera, V. P., Nealey, T. A., & Maunsell, J. H. (1992). Mixed parvocellular and magnocellular geniculate signals in visual area V4. *Nature*, *358*(6389), 756–758.

Ferster, D., & Jagadeesh, B. (1992). EPSP-IPSP interactions in cat visual cortex studied with in vivo whole- cell patch recording. *The Journal of Neuroscience*, *12*(4), 1262–1274.

Findlay, J. M. (1982). Global visual processing for saccadic eye movements. *Vision Research*, *22*(8), 1033–1045.

Findlay, J. M., & Gilchrist, I. D. (1997). Spatial scale and saccade programming. *Perception*, *26*(9), 1159 – 1167. http://doi.org/10.1068/p261159

Findlay, J. M., & Walker, R. (1999). A model of saccade generation based on parallel processing and competitive inhibition. *Behavioral and Brain Sciences*, *22*(04), 661–674. http://doi.org/null

Finlay, B. L., Schneps, S. E., Wilson, K. G., & Schneider, G. E. (1978). Topography of visual and somatosensory projections to the superior colliculus of the golden hamster. *Brain Research*, *142*(2), 223–235.

Foote, S. L., Aston-Jones, G., & Bloom, F. E. (1980). Impulse activity of locus coeruleus neurons in awake rats and monkeys is a function of sensory stimulation and arousal. *Proceedings of the National Academy of Sciences*, *77*(5), 3033–3037.

Freeman, J., & Ambady, N. (2010). MouseTracker: Software for studying real-time mental processing using a computer mouse-tracking method. *Behavior Research Methods*, *42*(1), 226–241.

Freeman, J., Dale, R., & Farmer, T. (2011). Hand in motion reveals mind in motion. *Frontiers in Psychology*, *2*, 59.

Frens, M. A., & Van Opstal, A. J. (1998). Visual-auditory interactions modulate saccade-related activity in monkey superior colliculus. *Brain Research Bulletin*, *46*(3), 211–224.

Fries, W. (1984). Cortical projections to the superior colliculus in the macaque monkey: a retrograde study using horseradish peroxidase. *Journal of Comparative Neurology*, *230*(1), 55–76.

Fries, W. (1985). Inputs from motor and premotor cortex to the superior colliculus of the macaque monkey. *Behavioural Brain Research*, *18*(2), 95–105.

Fuchs, A. F., & Luschei, E. S. (1970). Firing patterns of abducens neurons of alert monkeys in relationship to horizontal eye movement. *Journal of Neurophysiology*, *33*(3), 382–392.

Gandhi, N. J., & Katnani, H. A. (2011). Motor Functions of the Superior Colliculus. *Annual Review of Neuroscience*, *34*, 205–231. http://doi.org/10.1146/annurev-neuro-061010-113728

Gandhi, N. J., & Keller, E. L. (1997). Spatial distribution and discharge characteristics of superior colliculus neurons antidromically activated from the omnipause region in monkey. *Journal of Neurophysiology*, *78*(4), 2221–2225.

Gerstner, W. (2001). What is different with spiking neurons? In *Plausible neural networks for biological modelling* (pp. 23–48). Springer. Retrieved from http://link.springer.com/chapter/10.1007/978-94-010-0674-3_2

Gerstner, W., & Kistler, W. M. (2002). *Spiking neuron models: Single neurons, populations, plasticity*. Cambridge university press. Retrieved from https://books.google.com/books?hl=en&lr=&id=Rs4oc7HfxIUC&oi=fnd&pg=PR11&dq=spiking+neuron+nonlinear+i-f+function&ots=2Qd-wZgQ_7&sig=RBmscekdapcnaAgMrioQH723KPY

Ghitani, N., Bayguinov, P. O., Vokoun, C. R., McMahon, S., Jackson, M. B., & Basso, M. A. (2014). Excitatory Synaptic Feedback from the Motor Layer to the Sensory Layers of the Superior Colliculus. *The Journal of Neuroscience*, *34*(20), 6822–6833. http://doi.org/10.1523/JNEUROSCI.3137-13.2014

Glimcher, P. W., & Sparks, D. L. (1993). Representation of averaging saccades in the superior colliculus of the monkey. *Experimental Brain Research*, *95*(3), 429–435.

Godijn, R., & Theeuwes, J. (2004). The relationship between inhibition of return and saccade trajectory deviations. *Journal of Experimental Psychology: Human Perception and Performance*, *30*(3), 538.

Goldberg, M. E., & Bruce, C. J. (1990). Primate frontal eye fields. III. Maintenance of a spatially accurate saccade signal. *Journal of Neurophysiology*, *64*(2), 489–508.

Goldberg, M. E., Colby, C. L., & Duhamel, J.-R. (1990). Representation of Visuomotor Space in the Parietal Lobe of the Monkey. *Cold Spring Harbor Symposia on Quantitative Biology*, *55*, 729–739. http://doi.org/10.1101/SQB.1990.055.01.068

Goldberg, M. E., & Wurtz, R. H. (1972). Activity of superior colliculus in behaving monkey. I. Visual receptive fields of single neurons. *J Neurophysiol*, *35*(4), 542–559.

Gold, J. I., & Shadlen, M. N. (2007). The Neural Basis of Decision Making. *Annual Review of Neuroscience*, *30*(1), 535–574. http://doi.org/10.1146/annurev.neuro.29.051605.113038

Goldstein, R. R., & Beck, M. R. (2013). The Effect of Distractor Presentation Frequency on Saccade Reaction Times & Curvature. *Trials*, *24*(3.735), 001.

Golomb, J. D., Chun, M. M., & Mazer, J. A. (2008). The Native Coordinate System of Spatial Attention Is Retinotopic. *The Journal of Neuroscience*, *28*(42), 10654–10662. http://doi.org/10.1523/JNEUROSCI.2525-08.2008

Goodale, M. A., & Milner, A. D. (1992). Separate visual pathways for perception and action. *Trends in Neurosciences*, *15*(1), 20–25. http://doi.org/10.1016/0166-2236(92)90344-8

Goodman, D., & Brette, R. (2008). Brian: a simulator for spiking neural networks in Python. *Frontiers in Neuroinformatics*, *2*. Retrieved from http://www.ncbi.nlm.nih.gov/pmc/articles/pmc2605403/

Goodman, D. F., & Brette, R. (2009). The brian simulator. *Frontiers in Neuroscience*, *3*(2), 192.

Goossens, H. H. L. M., & Van Opstal, A. J. (2005). Dynamic Ensemble Coding of Saccades in the Monkey Superior Colliculus. *Journal of Neurophysiology*, *95*(4), 2326–2341. http://doi.org/10.1152/jn.00889.2005

Graham, J. (1977). An autoradiographic study of the efferent connections of the superior colliculus in the cat. *The Journal of Comparative Neurology*, *173*(4), 629–654. http://doi.org/10.1002/cne.901730403

Grantyn, A., & Berthoz, A. (1985). Burst activity of identified tecto-reticulo-spinal neurons in the alert cat. *Experimental Brain Research*, *57*(2), 417–421. http://doi.org/10.1007/BF00236550

Grantyn, R., Grantyn, A., & Schierwagen, A. (1983). Passive membrane properties, afterpotentials and repetitive firing of superior colliculus neurons studied in the anesthetized cat. *Experimental Brain Research*, *50*(2-3), 377–391.

Graybiel, A. M. (1978). A satellite system of the superior colliculus: the parabigeminal nucleus and its projections to the superficial collicular layers. *Brain Research*, *145*(2), 365–374.

Gray, H. (1918). *Anatomy of the human body*. Lea & Febiger.

Griffith, J. S. (1963). A field theory of neural nets: I: Derivation of field equations. *The Bulletin of Mathematical Biophysics*, *25*(1), 111–120.

Griffith, J. S. (1965). A field theory of neural nets: II. Properties of the field equations. *The Bulletin of Mathematical Biophysics*, *27*(2), 187–195.

Gross, G. W. (1979). Simultaneous Single Unit Recording in vitro with a Photoetched Laser Deinsulated Gold Multimicroelectrode Surface. *IEEE Transactions on Biomedical Engineering*, *BME-26*(5), 273–279. http://doi.org/10.1109/TBME.1979.326402

Guitton, D., Buchtel, H. A., & Douglas, R. M. (1985). Frontal lobe lesions in man cause difficulties in suppressing reflexive glances and in generating goal-directed saccades. *Experimental Brain Research*, *58*(3), 455–472.

Hafed, Z. M., & Krauzlis, R. J. (2012). Similarity of superior colliculus involvement in microsaccade and saccade generation. *Journal of Neurophysiology*, *107*(7), 1904–1916.

Hai, A., Shappir, J., & Spira, M. E. (2010a). In-cell recordings by extracellular microelectrodes. *Nature Methods*, *7*(3), 200–202.

Hai, A., Shappir, J., & Spira, M. E. (2010b). Long-term, multisite, parallel, in-cell recording and stimulation by an array of extracellular microelectrodes. *Journal of Neurophysiology*, *104*(1), 559–568.

Hamill, O. P., Marty, A., Neher, E., Sakmann, B., & Sigworth, F. J. (1981). Improved patch-clamp techniques for high-resolution current recording from cells and cell-free membrane patches. *Pflügers Archiv*, *391*(2), 85–100.

Handel, A., & Glimcher, P. W. (1999). Quantitative Analysis of Substantia Nigra Pars Reticulata Activity During a Visually Guided Saccade Task. *Journal of Neurophysiology*, *82*(6), 3458–3475.

Hanes, D. P., & Schall, J. D. (1996). Neural control of voluntary movement initiation. *Science*, *274*(5286), 427–430.

Hanes, D. P., & Wurtz, R. H. (2001). Interaction of the Frontal Eye Field and Superior Colliculus for Saccade Generation. *Journal of Neurophysiology*, *85*(2), 804–815.

Harting, J. K. (1977). Descending pathways from the superior colliculus: An autoradiographic analysis in the rhesus monkey (Macaca mulatta). *The Journal of Comparative Neurology*, *173*(3), 583–612. http://doi.org/10.1002/cne.901730311

Harting, J. K., Hall, W. C., Diamond, I. T., & Martin, G. F. (1973). Anterograde degeneration study of the superior colliculus in Tupaia glis: Evidence for a subdivision between superficial and deep layers. *The Journal of Comparative Neurology*, *148*(3), 361–386. http://doi.org/10.1002/cne.901480305

Harting, J. K., & Van Lieshout, D. P. (1991). Spatial relationships of axons arising from the substantia nigra, spinal trigeminal nucleus, and pedunculopontine tegmental nucleus within the intermediate gray of the cat superior colliculus. *The Journal of Comparative Neurology*, *305*(4), 543–558. http://doi.org/10.1002/cne.903050403

Heeman, J., Theeuwes, J., & Van der Stigchel, S. (2014). The time course of top-down control on saccade averaging. *Vision Research*, *100*, 29–37. http://doi.org/10.1016/j.visres.2014.03.007

Hehman, E., Stolier, R. M., & Freeman, J. (2015). Advanced mouse-tracking analytic techniques for enhancing psychological science. *Group Processes & Intergroup Relations*, *18*(3), 384–401.

Heide, W., Blankenburg, M., Zimmermann, E., & Kömpf, D. (1995). Cortical control of double-step saccades: Implications for spatial orientation. *Annals of Neurology*, *38*(5), 739–748. http://doi.org/10.1002/ana.410380508

Hendry, S. H., & Reid, R. C. (2000). The koniocellular pathway in primate vision. *Annual Review of Neuroscience*, *23*(1), 127–153.

He, P., & Kowler, E. (1989). The role of location probability in the programming of saccades: Implications for ā€ center-of-gravityā€\= tendencies. *Vision Research*, *29*(9), 1165–1181.

Hepp, K., & Henn, V. (1983). Spatio-temporal recoding of rapid eye movement signals in the monkey paramedian pontine reticular formation (PPRF). *Experimental Brain Research*, *52*(1), 105–120. http://doi.org/10.1007/BF00237155

Hermens, F., Ghose, T., & Wagemans, J. (2013). Advance information modulates the global effect even without instruction on where to look. *Experimental Brain Research*, *226*(4), 639–648. http://doi.org/10.1007/s00221-013-3480-x

Hermens, F., Sumner, P., & Walker, R. (2010). Inhibition of masked primes as revealed by saccade curvature. *Vision Research*, *50*(1), 46–56. http://doi.org/10.1016/j.visres.2009.10.008

Herrero, L., Rodriguez, F., Salas, C., & Torres, B. (1998). Tail and eye movements evoked by electrical microstimulation of the optic tectum in goldfish. *Experimental Brain Research*, *120*(3), 291–305.

Hikosaka, O., Nakamura, K., & Nakahara, H. (2006). Basal Ganglia Orient Eyes to Reward. *Journal of Neurophysiology*, *95*(2), 567–584. http://doi.org/10.1152/jn.00458.2005

Hikosaka, O., & Wurtz, R. H. (1983). Visual and oculomotor functions of monkey substantia nigra pars reticulata. IV. Relation of substantia nigra to superior colliculus. *J Neurophysiol*, *49*(5), 1285–1301.

Hikosaka, O., & Wurtz, R. H. (1985). Modification of saccadic eye movements by GABA-related substances. II. Effects of muscimol in monkey substantia nigra pars reticulata. *Journal of Neurophysiology*, *53*(1), 292–308.

Hilchey, M. D., Klein, R. M., Satel, J., & Wang, Z. (2012). Oculomotor inhibition of return: How soon is it 'recoded' into spatiotopic coordinates? *Attention, Perception, & Psychophysics*, *74*(6), 1145–1153.

Hodgkin, A. L., & Huxley, A. F. (1952). A quantitative description of membrane current and its application to conduction and excitation in nerve. *The Journal of Physiology*, *117*(4), 500–544.

Hooge, I. T. C., & Frens, M. A. (2000). Inhibition of saccade return (ISR): spatio-temporal properties of saccade programming. *Vision Research*, *40*(24), 3415–3426.

Horn, A. K., Buttner-Ennever, J. A., Wahle, P., & Reichenberger, I. (1994). Neurotransmitter profile of saccadic omnipause neurons in nucleus raphe interpositus. *The Journal of Neuroscience*, *14*(4), 2032–2046.

Hubel, D. H., & Wiesel, T. N. (1968). Receptive fields and functional architecture of monkey striate cortex. *The Journal of Physiology*, *195*(1), 215–243.

Huerta, M. F. (1984). The mammalian superior colliculus: studies of its morphology and connections. *Comparative Neurology of the Optic Tectum*, 687–773.

Huerta, M. F., & Harting, J. K. (1984). Connectional organization of the superior colliculus. *Trends in Neurosciences*, *7*(8), 286–289. http://doi.org/10.1016/S0166-2236(84)80197-6

Hunter, J. D. (2007). Matplotlib: A 2D graphics environment. *Computing in Science & Engineering*, *9*(3), 0090–95.

Hunt, S. P., Streit, P., Künzle, H., & Cuénod, M. (1977). Characterization of the pigeon isthmo-tectal pathway by selective uptake and retrograde movement of radioactive compounds and by golgi-like horseradish peroxidase labeling. *Brain Research*, *129*(2), 197–212. http://doi.org/10.1016/0006-8993(77)90001-4

Hurley, L., Devilbiss, D., & Waterhouse, B. (2004). A matter of focus: monoaminergic modulation of stimulus coding in mammalian sensory networks. *Current Opinion in Neurobiology*, *14*(4), 488–495. http://doi.org/10.1016/j.conb.2004.06.007

Illing, R.-B. (1996). The mosaic architecture of the superior colliculus. *Progress in Brain Research*, *112*, 17–34.

Illing, R.-B., & Graybiel, A. M. (1985). Convergence of afferents from frontal cortex and substantia nigra onto acetylcholinesterase-rich patches of the cat's superior colliculus. *Neuroscience*, *14*(2), 455–482.

Illing, R.-B., & Graybiel, A. M. (1986). Complementary and non-matching afferent compartments in the cat's superior colliculus: innervation of the acetylcholinesterase-poor domain of the intermediate gray layer. *Neuroscience*, *18*(2), 373–394.

Indiveri, G., Chicca, E., & Douglas, R. J. (2009). Artificial Cognitive Systems: From VLSI Networks of Spiking Neurons to Neuromorphic Cognition. *Cognitive Computation*, *1*(2), 119–127. http://doi.org/10.1007/s12559-008-9003-6

Ipata, A. E., Gee, A. L., Goldberg, M. E., & Bisley, J. W. (2006). Activity in the Lateral Intraparietal Area Predicts the Goal and Latency of Saccades in a Free-Viewing Visual Search Task. *The Journal of Neuroscience*, *26*(14), 3656–3661. http://doi.org/10.1523/JNEUROSCI.5074-05.2006

Isa, T. (2002). Intrinsic processing in the mammalian superior colliculus. *Current Opinion in Neurobiology*, *12*(6), 668–677. http://doi.org/10.1016/S0959-4388(02)00387-2

Isa, T., Endo, T., & Saito, Y. (1998). The Visuo-Motor Pathway in the Local Circuit of the Rat Superior Colliculus. *The Journal of Neuroscience*, *18*(20), 8496–8504.

Isa, T., & Hall, W. C. (2009). Exploring the Superior Colliculus In Vitro. *Journal of Neurophysiology*, *102*(5), 2581–2593. http://doi.org/10.1152/jn.00498.2009

Ishii, T., Moriyoshi, K., Sugihara, H., Sakurada, K., Kadotani, H., Yokoi, M., … Masu, M. (1993). Molecular characterization of the family of the N-methyl-D-aspartate receptor subunits. *Journal of Biological Chemistry*, *268*(4), 2836–2843.

Izhikevich, E. M., & others. (2003). Simple model of spiking neurons. *IEEE Transactions on Neural Networks*, *14*(6), 1569–1572.

Jagadisan, U. K., & Gandhi, N. J. (2013). Neural mechanisms of target selection in the superior colliculus. *The New Visual Neurosciences (Chalupa LM, Werner JS, Eds), P in Press. Boston: MIT*. Retrieved from http://www.pitt.edu/~neg8/rajimages/pdf/TargetSelectionSC_JagadisanGandhi.pdf

Jantz, J. J., Watanabe, M., Everling, S., & Munoz, D. P. (2013). Threshold mechanism for saccade initiation in frontal eye field and superior colliculus. *Journal of Neurophysiology*, *109*(11), 2767–2780. http://doi.org/10.1152/jn.00611.2012

Jolivet, R., Lewis, T. J., & Gerstner, W. (2004). Generalized integrate-and-fire models of neuronal activity approximate spike trains of a detailed model to a high degree of accuracy. *Journal of Neurophysiology*, *92*(2), 959–976.

Jonikaitis, D., & Belopolsky, A. V. (2014). Target-Distractor Competition in the Oculomotor System Is Spatiotopic. *Journal of Neuroscience*, *34*(19), 6687–6691. http://doi.org/10.1523/JNEUROSCI.4453-13.2014

Jüttner, M., & Wolf, W. (1992). Occurrence of human express saccades depends on stimulus uncertainty and stimulus sequence. *Experimental Brain Research*, *89*(3), 678–681.

Kamogawa, H., Ohki, Y., Shimazu, H., Suzuki, I., & Yamashita, M. (1996). Inhibitory input to pause neurons from pontine burst neuron area in the cat. *Neuroscience Letters*, *203*(3), 163–166.

Kanda, T., Iwamoto, Y., Yoshida, K., & Shimazu, H. (2007a). Glycinergic inputs cause the pause of pontine omnipause neurons during saccades. *Neuroscience Letters*, *413*(1), 16–20. http://doi.org/10.1016/j.neulet.2006.11.024

Kanda, T., Iwamoto, Y., Yoshida, K., & Shimazu, H. (2007b). Glycinergic inputs cause the pause of pontine omnipause neurons during saccades. *Neuroscience Letters*, *413*(1), 16–20.

Kaneda, K., Isa, K., Yanagawa, Y., & Isa, T. (2008). Nigral Inhibition of GABAergic Neurons in Mouse Superior Colliculus. *The Journal of Neuroscience*, *28*(43), 11071–11078. http://doi.org/10.1523/JNEUROSCI.3263-08.2008

Kang, K., Shelley, M., & Sompolinsky, H. (2003). Mexican hats and pinwheels in visual cortex. *Proceedings of the National Academy of Sciences*, *100*(5), 2848–2853. http://doi.org/10.1073/pnas.0138051100

Kaplan, E., & Shapley, R. M. (1982). X and Y cells in the lateral geniculate nucleus of macaque monkeys. *The Journal of Physiology*, *330*(1), 125–143.

Kaplan, E., & Shapley, R. M. (1986). The primate retina contains two types of ganglion cells, with high and low contrast sensitivity. *Proceedings of the National Academy of Sciences*, *83*(8), 2755–2757.

Karnath, H.-O., Himmelbach, M., & Rorden, C. (2002). The subcortical anatomy of human spatial neglect: putamen, caudate nucleus and pulvinar. *Brain*, *125*(2), 350–360. http://doi.org/10.1093/brain/awf032

Katnani, H. A., & Gandhi, N. J. (2011). Order of operations for decoding superior colliculus activity for saccade generation. *Journal of Neurophysiology*, *106*(3), 1250–1259.

Katoh, Y. Y., Arai, R., & Benedek, G. (2000). Bifurcating projections from the cerebellar fastigial neurons to the thalamic suprageniculate nucleus and to the superior colliculus. *Brain Research*, *864*(2), 308–311.

Kiani, R., & Shadlen, M. N. (2009). Representation of Confidence Associated with a Decision by Neurons in the Parietal Cortex. *Science*, *324*(5928), 759–764. http://doi.org/10.1126/science.1169405

Kim, B., & Basso, M. A. (2010). A probabilistic strategy for understanding action selection. *The Journal of Neuroscience*, *30*(6), 2340–2355.

King, A. J. (1999). Sensory experience and the formation of a computational map of auditory space in the brain. *Bioessays*, *21*(11), 900–911.

Klein, R. M., & MacInnes, W. J. (1999). Inhibition of return is a foraging facilitator in visual search. *Psychological Science*, *10*(4), 346–352.

Kobayashi, Y., & Isa, T. (2002). Sensory-motor gating and cognitive control by the brainstem cholinergic system. *Neural Networks*, *15*(4), 731–741.

Koch, C., & Ullman, S. (1985). Shifts in selective visual attention: towards the underlying neural circuitry. In *Matters of intelligence* (pp. 115–141). Springer. Retrieved from http://link.springer.com/chapter/10.1007/978-94-009-3833-5_5

Kong, H., Akakin, H. C., & Sarma, S. E. (2013). A Generalized Laplacian of Gaussian Filter for Blob Detection and Its Applications. *IEEE Transactions on Cybernetics*, *43*(6), 1719–1733. http://doi.org/10.1109/TSMCB.2012.2228639

Kopecz, K. (1995). Saccadic reaction times in gap/overlap paradigms: a model based on integration of intentional and visual information on neural, dynamic fields. *Vision Research*, *35*(20), 2911–2925. http://doi.org/10.1016/0042-6989(95)00066-9

Kopecz, K., Engels, C., & Schöner, G. (1993). Dynamic Field Approach to Target Selection in Gaze Control. In S. Gielen & B. Kappen (Eds.), *ICANN '93* (pp. 96–101). Springer London. Retrieved from http://link.springer.com/chapter/10.1007/978-1-4471-2063-6_22

Kopecz, K., & Schöner, G. (1995). Saccadic motor planning by integrating visual information and pre-information on neural dynamic fields. *Biological Cybernetics*, *73*(1), 49–60. http://doi.org/10.1007/BF00199055

Koyama, Y., & Kayama, Y. (1993). Mutual interactions among cholinergic, noradrenergic and serotonergic neurons studied by ionophoresis of these transmitters in rat brainstem nuclei. *Neuroscience*, *55*(4), 1117–1126.

Kruijne, W., Van der Stigchel, S., & Meeter, M. (2014). A model of curved saccade trajectories: Spike rate adaptation in the brainstem as the cause of deviation away. *Brain and Cognition*, *85*, 259–270. http://doi.org/10.1016/j.bandc.2014.01.005

Kusunoki, M., & Goldberg, M. E. (2003). The time course of perisaccadic receptive field shifts in the lateral intraparietal area of the monkey. *Journal of Neurophysiology*, *89*(3), 1519–1527.

Lai, D., Brandt, S., Luksch, H., & Wessel, R. (2011). Recurrent Antitopographic Inhibition Mediates Competitive Stimulus Selection in an Attention Network. *Journal of Neurophysiology*, *105*(2), 793–805. http://doi.org/10.1152/jn.00673.2010

Langer, T. P., & Lund, R. D. (1974). The upper layers of the superior colliculus of the rat: A Golgi study. *The Journal of Comparative Neurology*, *158*(4), 405–435. http://doi.org/10.1002/cne.901580404

Lapicque, L. (1907). Recherches quantitatives sur l'excitation electrique des nerfs traitee comme une polarization. *J Physiol Pathol Gen*, *9*, 620–635.

Lavoie, B., & Parent, A. (1994). Pedunculopontine nucleus in the squirrel monkey: projections to the basal ganglia as revealed by anterograde tract-tracing methods. *Journal of Comparative Neurology*, *344*(2), 210–231.

Lazareva, O. F., Shimizu, T., & Wasserman, E. A. (2012). *How Animals See the World: Comparative Behavior, Biology, and Evolution of Vision*. OUP USA.

Lee, A. K., Manns, I. D., Sakmann, B., & Brecht, M. (2006). Whole-Cell Recordings in Freely Moving Rats. *Neuron*, *51*(4), 399–407. http://doi.org/10.1016/j.neuron.2006.07.004

Lee, C., Rohrer, W. H., & Sparks, D. L. (1988). Population coding of saccadic eye movements by neurons in the superior colliculus. *Nature*, *332*(6162), 357–360.

Lee, P., & Hall, W. C. (2006). An In Vitro Study of Horizontal Connections in the Intermediate Layer of the Superior Colliculus. *Journal of Neuroscience*, *26*(18), 4763–4768. http://doi.org/10.1523/JNEUROSCI.0724-06.2006

Lefèvre, P., & Galiana, H. L. (1992). Dynamic feedback to the superior colliculus in a neural network model of the gaze control system. *Neural Networks*, *5*(6), 871–890.

Leichnetz, G. R., Spencer, R. F., Hardy, S. G. P., & Astruc, J. (1981). The prefrontal corticotectal projection in the monkey; an anterograde and retrograde horseradish peroxidase study. *Neuroscience*, *6*(6), 1023–1041.

Lennie, P., & Movshon, J. A. (2005). Coding of color and form in the geniculostriate visual pathway (invited review). *JOSA A*, *22*(10), 2013–2033.

Lepora, N. F., & Pezzulo, G. (2015). Embodied choice: how action influences perceptual decision making. *PLoS Comput Biol*, *11*(4), e1004110.

Li, C.-S. R., Mazzoni, P., & Andersen, R. A. (1999). Effect of Reversible Inactivation of Macaque Lateral Intraparietal Area on Visual and Memory Saccades. *Journal of Neurophysiology*, *81*(4), 1827–1838.

Liu, C.-L., Tseng, P., Chiau, H.-Y., Liang, W.-K., Hung, D. L., Tzeng, O. J. L., … Juan, C.-H. (2011). The Location Probability Effects of Saccade Reaction Times Are Modulated in the Frontal Eye Fields but Not in the Supplementary Eye Field. *Cerebral Cortex*, *21*(6), 1416–1425. http://doi.org/10.1093/cercor/bhq222

Liu, P., & Basso, M. A. (2008). Substantia Nigra Stimulation Influences Monkey Superior Colliculus Neuronal Activity Bilaterally. *Journal of Neurophysiology*, *100*(2), 1098–1112. http://doi.org/10.1152/jn.01043.2007

Livingstone, M., & Hubel, D. (1988). Segregation of form, color, movement, and depth: anatomy, physiology, and perception. *Science*, *240*(4853), 740–749.

Lo, C.-C., Boucher, L., Paré, M., Schall, J. D., & Wang, X.-J. (2009). Proactive Inhibitory Control and Attractor Dynamics in Countermanding Action: A Spiking Neural Circuit Model. *The Journal of Neuroscience*, *29*(28), 9059–9071. http://doi.org/10.1523/JNEUROSCI.6164-08.2009

Lo, C.-C., & Wang, X.-J. (2006). Cortico–basal ganglia circuit mechanism for a decision threshold in reaction time tasks. *Nature Neuroscience*, *9*(7), 956–963. http://doi.org/10.1038/nn1722

Lock, T. M., Baizer, J. S., & Bender, D. B. (2003). Distribution of corticotectal cells in macaque. *Experimental Brain Research*, *151*(4), 455–470.

Lowe, D. G. (1999). Object recognition from local scale-invariant features. In *Computer vision, 1999. The proceedings of the seventh IEEE international conference on* (Vol. 2, pp. 1150–1157). Ieee. Retrieved from http://ieeexplore.ieee.org/xpls/abs_all.jsp?arnumber=790410

Ludwig, C. J., & Gilchrist, I. D. (2002). Measuring saccade curvature: A curve-fitting approach. *Behavior Research Methods, Instruments, & Computers*, *34*(4), 618–624.

Ludwig, C. J., & Gilchrist, I. D. (2003). Target similarity affects saccade curvature away from irrelevant onsets. *Experimental Brain Research*, *152*(1), 60–69.

Mana, S., & Chevalier, G. (2001a). Honeycomb-like structure of the intermediate layers of the rat superior colliculus: afferent and efferent connections. *Neuroscience*, *103*(3), 673–693. http://doi.org/10.1016/S0306-4522(01)00026-4

Mana, S., & Chevalier, G. (2001b). The fine organization of nigro-collicular channels with additional observations of their relationships with acetylcholinesterase in the rat. *Neuroscience*, *106*(2), 357–374. http://doi.org/10.1016/S0306-4522(01)00283-4

Ma, R., Cui, H., Lee, S.-H., Anastasio, T. J., & Malpeli, J. G. (2013). Predictive encoding of moving target trajectory by neurons in the parabigeminal nucleus. *Journal of Neurophysiology*, *109*(8), 2029–2043.

Margrie, T. W., Brecht, M., & Sakmann, B. (2002). In vivo, low-resistance, whole-cell recordings from neurons in the anaesthetized and awake mammalian brain. *Pflügers Archiv*, *444*(4), 491–498.

Marín, G., Salas, C., Sentis, E., Rojas, X., Letelier, J. C., & Mpodozis, J. (2007). A Cholinergic Gating Mechanism Controlled by Competitive Interactions in the Optic Tectum of the Pigeon. *The Journal of Neuroscience*, *27*(30), 8112–8121. http://doi.org/10.1523/JNEUROSCI.1420-07.2007

Marino, R. A., Levy, R., & Munoz, D. P. (2015). Linking express saccade occurance to stimulus properties and sensorimotor integration in the superior colliculus. *Journal of Neurophysiology*, *114*(2), 879–892.

Marino, R. A., Trappenberg, T. P., Dorris, M., & Munoz, D. P. (2012). Spatial interactions in the superior colliculus predict saccade behavior in a neural field model. *Journal of Cognitive Neuroscience*, *24*(2), 315–336.

Marmont, G. (1949). Studies on the axon membrane. I. A new method. *Journal of Cellular and Comparative Physiology*, *34*(3), 351–382.

Mathôt, S., & Theeuwes, J. (2010). Gradual remapping results in early retinotopic and late spatiotopic inhibition of return. *Psychological Science*, *21*(12), 1793–1798.

Maunsell, J. H., Nealey, T. A., & DePriest, D. D. (1990). Magnocellular and parvocellular contributions to responses in the middle temporal visual area (MT) of the macaque monkey. *The Journal of Neuroscience*, *10*(10), 3323–3334.

May, P. J., Warren, S., Bohlen, M. O., Barnerssoi, M., & Horn, A. K. E. (2015). A central mesencephalic reticular formation projection to the Edinger–Westphal nuclei. *Brain Structure and Function*, 1–17. http://doi.org/10.1007/s00429-015-1147-z

Mays, L. E., & Sparks, D. L. (1980). Dissociation of visual and saccade-related responses in superior colliculus neurons. *Journal of Neurophysiology*, *43*(1), 207–232.

McFarland, J. L., & Fuchs, A. F. (1992). Discharge patterns in nucleus prepositus hypoglossi and adjacent medial vestibular nucleus during horizontal eye movement in behaving macaques. *Journal of Neurophysiology*, *68*(1), 319–332.

McGraw, K. O., & Wong, S. P. (1992). A common language effect size statistic. *Psychological Bulletin*, *111*(2), 361.

McHaffie, J. G., & Stein, B. E. (1982). Eye movements evoked by electrical stimulation in the superior colliculus of rats and hamsters. *Brain Research*, *247*(2), 243–253.

McIlwain, J. T. (1982). Lateral spread of neural excitation during microstimulation in intermediate gray layer of cat's superior colliculus. *Journal of Neurophysiology*, *47*(2), 167–178.

McKinney, W. (2010). Data structures for statistical computing in Python. In *Proceedings of the 9th Python in Science Conference* (pp. 51–56). Retrieved from http://204.236.236.243/proceedings/scipy2010/pdfs/mckinney.pdf

McPeek, R. M. (2006). Incomplete Suppression of Distractor-Related Activity in the Frontal Eye Field Results in Curved Saccades. *Journal of Neurophysiology*, *96*(5), 2699–2711. http://doi.org/10.1152/jn.00564.2006

McPeek, R. M., Han, J. H., & Keller, E. L. (2003). Competition Between Saccade Goals in the Superior Colliculus Produces Saccade Curvature. *Journal of Neurophysiology*, *89*(5), 2577–2590. http://doi.org/10.1152/jn.00657.2002

McPeek, R. M., & Keller, E. L. (2002a). Saccade Target Selection in the Superior Colliculus During a Visual Search Task. *Journal of Neurophysiology*, *88*(4), 2019–2034.

McPeek, R. M., & Keller, E. L. (2002b). Superior colliculus activity related to concurrent processing of saccade goals in a visual search task. *Journal of Neurophysiology*, *87*(4), 1805–1815.

McSorley, E. (2006). Time Course of Oculomotor Inhibition Revealed by Saccade Trajectory Modulation. *Journal of Neurophysiology*, *96*(3), 1420–1424. http://doi.org/10.1152/jn.00315.2006

McSorley, E., Haggard, P., & Walker, R. (2004). Distractor modulation of saccade trajectories: spatial separation and symmetry effects. *Experimental Brain Research*, *155*(3), 320–333. http://doi.org/10.1007/s00221-003-1729-5

McSorley, E., Haggard, P., & Walker, R. (2009). The spatial and temporal shape of oculomotor inhibition. *Vision Research*, *49*(6), 608–614.

McSorley, E., & McCloy, R. (2009). Saccadic eye movements as an index of perceptual decision-making. *Experimental Brain Research*, *198*(4), 513–520. http://doi.org/10.1007/s00221-009-1952-9

Meeter, M., Stigchel, S. V. der, & Theeuwes, J. (2010). A competitive integration model of exogenous and endogenous eye movements. *Biological Cybernetics*, *102*(4), 271–291. http://doi.org/10.1007/s00422-010-0365-y

Mégardon, G., Tandonnet, C., Sumner, P., & Guillaume, A. (2015). Limitations of short range Mexican hat connection for driving target selection in a 2D neural field: activity suppression and deviation from input stimuli. *Frontiers in Computational Neuroscience*, 128. http://doi.org/10.3389/fncom.2015.00128

Meister, M. L. R., Hennig, J. A., & Huk, A. C. (2013). Signal Multiplexing and Single-Neuron Computations in Lateral Intraparietal Area During Decision-Making. *The Journal of Neuroscience*, *33*(6), 2254–2267. http://doi.org/10.1523/JNEUROSCI.2984-12.2013

Meredith, M. A., & Ramoa, A. S. (1998). Intrinsic circuitry of the superior colliculus: pharmacophysiological identification of horizontally oriented inhibitory interneurons. *Journal of Neurophysiology*, *79*(3), 1597–1602.

Meredith, M. A., & Stein, B. E. (1986). Visual, auditory, and somatosensory convergence on cells in superior colliculus results in multisensory integration. *Journal of Neurophysiology*, *56*(3), 640–662.

Merigan, W. H., & Maunsell, J. H. (1993). How parallel are the primate visual pathways? *Annual Review of Neuroscience*, *16*(1), 369–402.

Millner, S., Grübl, A., Meier, K., Schemmel, J., & Schwartz, M. (2010). A VLSI Implementation of the Adaptive Exponential Integrate-and-Fire Neuron Model (pp. 1642–1650). Presented at the Advances in Neural Information Processing Systems. Retrieved from http://machinelearning.wustl.edu/mlpapers/papers/NIPS2010_0425

Mishkin, M., Ungerleider, L. G., & Macko, K. A. (1983). Object vision and spatial vision: two cortical pathways. *Trends in Neurosciences*, *6*, 414–417.

Mize, R. R., Spencer, R. F., & Sterling, P. (1982). Two types of GABA-accumulating neurons in the superficial gray layer of the cat superior colliculus. *The Journal of Comparative Neurology*, *206*(2), 180–192. http://doi.org/10.1002/cne.902060207

Mooney, R. D., Bennett-Clarke, C., Chiaia, N. L., Sahibzada, N., & Rhoades, R. W. (1990). Organization and actions of the noradrenergic input to the hamster's superior colliculus. *The Journal of Comparative Neurology*, *292*(2), 214–230. http://doi.org/10.1002/cne.902920205

Morén, J., Shibata, T., & Doya, K. (2010). Toward a spiking-neuron model of the oculomotor system. In *From Animals to Animats 11* (pp. 104–113). Springer. Retrieved from http://link.springer.com/chapter/10.1007/978-3-642-15193-4_10

Morén, J., Shibata, T., & Doya, K. (2013). The Mechanism of Saccade Motor Pattern Generation Investigated by a Large-Scale Spiking Neuron Model of the Superior Colliculus. *PLoS ONE*, *8*(2), e57134. http://doi.org/10.1371/journal.pone.0057134

Moschovakis, A. K., & Karabelas, A. B. (1985). Observations on the somatodendritic morphology and axonal trajectory of intracellularly HRP-Labeled efferent neurons located in the deeper layers of the superior colliculus of the cat. *The Journal of Comparative Neurology*, *239*(3), 276–308. http://doi.org/10.1002/cne.902390304

Moschovakis, A. K., Karabelas, A. B., & Highstein, S. M. (1988a). Structure-function relationships in the primate superior colliculus. II. Morphological identity of presaccadic neurons. *Journal of Neurophysiology*, *60*(1), 263–302.

Moschovakis, A. K., Karabelas, A. B., & Highstein, S. M. (1988b). Structure-function relationships in the primate superior colliculus. I. Morphological classification of efferent neurons. *Journal of Neurophysiology*, *60*(1), 232–262.

Munoz, D. P., Dorris, M. C., Pare, M., & Everling, S. (2000). On your mark, get set: brainstem circuitry underlying saccadic initiation. *Canadian Journal of Physiology and Pharmacology*, *78*(11), 934–944.

Munoz, D. P., & Guitton, D. (1986). Presaccadic burst discharges of tecto-reticulo-spinal neurons in the alert head-free and -fixed cat. *Brain Research*, *398*(1), 185–190. http://doi.org/10.1016/0006-8993(86)91267-9

Munoz, D. P., & Guitton, D. (1991). Control of orienting gaze shifts by the tectoreticulospinal system in the head-free cat. II. Sustained discharges during motor preparation and fixation. *J Neurophysiol*, *66*(5), 1624–1641.

Munoz, D. P., & Istvan, P. J. (1998). Lateral inhibitory interactions in the intermediate layers of the monkey superior colliculus. *Journal of Neurophysiology*, *79*(3), 1193–1209.

Munoz, D. P., & Wurtz, R. H. (1993). Fixation cells in monkey superior colliculus. II. Reversible activation and deactivation. *Journal of Neurophysiology*, *70*(2), 576–589.

Munoz, D. P., & Wurtz, R. H. (1995a). Saccade-related activity in monkey superior colliculus. I. Characteristics of burst and buildup cells. *Journal of Neurophysiology*, *73*(6), 2313–2333.

Munoz, D. P., & Wurtz, R. H. (1995b). Saccade-related activity in monkey superior colliculus. II. Spread of activity during saccades. *Journal of Neurophysiology*, *73*(6), 2334–2348.

Mysore, S. P., Asadollahi, A., & Knudsen, E. I. (2011). Signaling of the strongest stimulus in the owl optic tectum. *The Journal of Neuroscience*, *31*(14), 5186–5196.

Mysore, S. P., & Knudsen, E. I. (2012). Reciprocal inhibition of inhibition: a circuit motif for flexible categorization in stimulus selection. *Neuron*, *73*(1), 193–205.

Neher, E., & Sakmann, B. (1976). Noise analysis of drug induced voltage clamp currents in denervated frog muscle fibres. *The Journal of Physiology*, *258*(3), 705.

Nicolelis, M. A. L. (2007). *Methods for Neural Ensemble Recordings, Second Edition*. CRC Press.

Northcutt, R. G. (2002). Understanding Vertebrate Brain Evolution. *Integrative and Comparative Biology*, *42*(4), 743–756. http://doi.org/10.1093/icb/42.4.743

Northmore, D. P. M., Levine, E. S., & Schneider, G. E. (1988). Behavior evoked by electrical stimulation of the hamster superior colliculus. *Experimental Brain Research*, *73*(3), 595–605.

Nyström, M., Hooge, I., & Holmqvist, K. (2013). Post-saccadic oscillations in eye movement data recorded with pupil-based eye trackers reflect motion of the pupil inside the iris. *Vision Research*, *92*, 59–66. http://doi.org/10.1016/j.visres.2013.09.009

Ottes, F. P., Van Gisbergen, J. A., & Eggermont, J. J. (1984). Metrics of saccade responses to visual double stimuli: two different modes. *Vision Research*, *24*(10), 1169–1179.

Ottes, F. P., Van Gisbergen, J. A., & Eggermont, J. J. (1985). Latency dependence of colour-based target vs nontarget discrimination by the saccadic system. *Vision Research*, *25*(6), 849–862.

Ottes, F. P., Van Gisbergen, J. A., & Eggermont, J. J. (1986). Visuomotor fields of the superior colliculus: a quantitative model. *Vision Research*, *26*(6), 857–873.

Özen, G., Helms, M. C., & Hall, W. C. (2004). The intracollicular neuronal network. *The Superior Colliculus: New Approaches for Studying Sensorimotor Integration. CRC Press, Boca Raton, FL*, 147–158.

Paré, D., & Collins, D. R. (2000). Neuronal Correlates of Fear in the Lateral Amygdala: Multiple Extracellular Recordings in Conscious Cats. *The Journal of Neuroscience*, *20*(7), 2701–2710.

Paré, M., & Guitton, D. (1994). The fixation area of the cat superior colliculus: effects of electrical stimulation and direct connection with brainstem omnipause neurons. *Experimental Brain Research*, *101*(1), 109–122.

Paré, M., & Hanes, D. P. (2003). Controlled movement processing: superior colliculus activity associated with countermanded saccades. *The Journal of Neuroscience*, *23*(16), 6480–6489.

Paré, M., & Wurtz, R. H. (1997). Monkey posterior parietal cortex neurons antidromically activated from superior colliculus. *Journal of Neurophysiology*, *78*(6), 3493–3497.

Park, I. M., Meister, M. L. R., Huk, A. C., & Pillow, J. W. (2014). Encoding and decoding in parietal cortex during sensorimotor decision-making. *Nature Neuroscience*, *17*(10), 1395–1403. http://doi.org/10.1038/nn.3800

Perez, F., & Granger, B. E. (2007). IPython: A System for Interactive Scientific Computing. *Computing in Science & Engineering*, *9*(3), 21–29. http://doi.org/10.1109/MCSE.2007.53

Person, R. I., Andrezik, J. A., Dormer, K. J., & Foreman, R. D. (1986). Fastigial nucleus projections in the midbrain and thalamus in dogs. *Neuroscience*, *18*(1), 105–120. http://doi.org/10.1016/0306-4522(86)90182-X

Pertzov, Y., Zohary, E., & Avidan, G. (2010). Rapid formation of spatiotopic representations as revealed by inhibition of return. *The Journal of Neuroscience*, *30*(26), 8882–8887.

Peterka, D. S., Takahashi, H., & Yuste, R. (2011). Imaging voltage in neurons. *Neuron*, *69*(1), 9–21. http://doi.org/10.1016/j.neuron.2010.12.010

Phongphanphanee, P., Kaneda, K., & Isa, T. (2008). Spatiotemporal Profiles of Field Potentials in Mouse Superior Colliculus Analyzed by Multichannel Recording. *The Journal of Neuroscience*, *28*(37), 9309–9318. http://doi.org/10.1523/JNEUROSCI.1905-08.2008

Phongphanphanee, P., Marino, R. A., Kaneda, K., Yanagawa, Y., Munoz, D. P. ., & Isa, T. (2014). Distinct local circuit properties of the superficial and intermediate layers of the rodent superior colliculus. *European Journal of Neuroscience*, *40*(2), 2329–2343. http://doi.org/10.1111/ejn.12579

Pillow, J. W., Shlens, J., Paninski, L., Sher, A., Litke, A. M., Chichilnisky, E. J., & Simoncelli, E. P. (2008). Spatio-temporal correlations and visual signalling in a complete neuronal population. *Nature*, *454*(7207), 995–999.

Ploner, C. J., Ostendorf, F., & Dick, S. (2004). Target Size Modulates Saccadic Eye Movements in Humans. *Behavioral Neuroscience*, *118*(1), 237–242. http://doi.org/10.1037/0735-7044.118.1.237

Port, N. L., & Wurtz, R. H. (2003). Sequential Activity of Simultaneously Recorded Neurons in the Superior Colliculus During Curved Saccades. *Journal of Neurophysiology*, *90*(3), 1887–1903. http://doi.org/10.1152/jn.01151.2002

Posner, M. I., & Cohen, Y. (1984). Components of visual orienting. *Attention and Performance X: Control of Language Processes*, *32*, 531–556.

Premereur, E., Vanduffel, W., & Janssen, P. (2011). Functional Heterogeneity of Macaque Lateral Intraparietal Neurons. *The Journal of Neuroscience*, *31*(34), 12307–12317. http://doi.org/10.1523/JNEUROSCI.2241-11.2011

Preuschoff, K., 't Hart, B. M., & Einhauser, W. (2011). Pupil Dilation Signals Surprise: Evidence for Noradrenaline's Role in Decision Making. *Frontiers in Neuroscience*, *5*. http://doi.org/10.3389/fnins.2011.00115

Privitera, C. M., Renninger, L. W., Carney, T., Klein, S., & Aguilar, M. (2010). Pupil dilation during visual target detection. *Journal of Vision*, *10*(10), 3. http://doi.org/10.1167/10.10.3

Purcell, B. A., Heitz, R. P., Cohen, J. Y., Schall, J. D., Logan, G. D., & Palmeri, T. J. (2010). Neurally Constrained Modeling of Perceptual Decision Making. *Psychological Review*, *117*(4), 1113–1143. http://doi.org/10.1037/a0020311

Quaia, C., Aizawa, H., Optican, L. M., & Wurtz, R. H. (1998). Reversible inactivation of monkey superior colliculus. II. Maps of saccadic deficits. *Journal of Neurophysiology*, *79*(4), 2097–2110.

Quaia, C., Lefèvre, P., & Optican, L. M. (1999). Model of the Control of Saccades by Superior Colliculus and Cerebellum. *Journal of Neurophysiology*, *82*(2), 999–1018.

Quaia, C., & Optican, L. M. (1998). Commutative saccadic generator is sufficient to control a 3-D ocular plant with pulleys. *Journal of Neurophysiology*, *79*(6), 3197–3215.

Raftery, A. E. (1995). Bayesian model selection in social research. *Sociological Methodology*, *25*, 111–164.

Rampon, C., Luppi, P. H., Fort, P., Peyron, C., & Jouvet, M. (1996). Distribution of glycine-immunoreactive cell bodies and fibers in the rat brain. *Neuroscience*, *75*(3), 737–755. http://doi.org/10.1016/0306-4522(96)00278-3

Ratcliff, R. (1978). A theory of memory retrieval. *Psychological Review*, *85*(2), 59–108.

Ratcliff, R., & McKoon, G. (2008). The Diffusion Decision Model: Theory and Data for Two-Choice Decision Tasks. *Neural Computation*, *20*(4), 873–922. http://doi.org/10.1162/neco.2008.12-06-420

Ratcliff, R., & Rouder, J. N. (1998). Modeling response times for two-choice decisions. *Psychological Science*, *9*(5), 347–356.

Ratcliff, R., & Smith, P. L. (2004). A Comparison of Sequential Sampling Models for Two-Choice Reaction Time. *Psychological Review*, *111*(2), 333–367. http://doi.org/10.1037/0033-295X.111.2.333

Raybourn, M. S., & Keller, E. L. (1977). Colliculoreticular organization in primate oculomotor system. *Journal of Neurophysiology*, *40*(4), 861–878.

Razak, K. A. (2003). NMDA Receptor Blockade in the Superior Colliculus Increases Receptive Field Size Without Altering Velocity and Size Tuning. *Journal of Neurophysiology*, *90*(1), 110–119. http://doi.org/10.1152/jn.01029.2002

Redgrave, P., Coizet, V., Comoli, E., McHaffie, J. G., Leriche, M., Vautrelle, N., … Overton, P. (2010). Interactions between the Midbrain Superior Colliculus and the Basal Ganglia. *Frontiers in Neuroanatomy*, *4*. http://doi.org/10.3389/fnana.2010.00132

Redgrave, P., Marrow, L., & Dean, P. (1992). Topographical organization of the nigrotectal projection in rat: evidence for segregated channels. *Neuroscience*, *50*(3), 571–595.

Reiner, A., Medina, L., & Veenman, C. L. (1998). Structural and functional evolution of the basal ganglia in vertebrates. *Brain Research Reviews*, *28*(3), 235–285. http://doi.org/10.1016/S0165-0173(98)00016-2

Resulaj, A., Kiani, R., Wolpert, D. M., & Shadlen, M. N. (2009). Changes of mind in decision-making. *Nature*, *461*(7261), 263–266. http://doi.org/10.1038/nature08275

Richter, M., Sandamirskaya, Y., & Schoner, G. (2012). A robotic architecture for action selection and behavioral organization inspired by human cognition. In *2012 IEEE/RSJ International Conference on Intelligent Robots and Systems (IROS)* (pp. 2457–2464). http://doi.org/10.1109/IROS.2012.6386153

Rivaud, S., Müri, R. M., Gaymard, B., Vermersch, A. I., & Pierrot-Deseilligny, C. (1994). Eye movement disorders after frontal eye field lesions in humans. *Experimental Brain Research*, *102*(1), 110–120. http://doi.org/10.1007/BF00232443

Robinson, D. A. (1970). Oculomotor unit behavior in the monkey. *Journal of Neurophysiology*, *33*(3), 393–403.

Robinson, D. A. (1972). Eye movements evoked by collicular stimulation in the alert monkey. *Vision Research*, *12*(11), 1795–1808.

Robinson, D. A. (1975). Oculomotor control signals. *Basic Mechanisms of Ocular Motility and Their Clinical Implications*, *24*, 337–374.

Robinson, J. T., Jorgolli, M., Shalek, A. K., Yoon, M.-H., Gertner, R. S., & Park, H. (2012). Vertical nanowire electrode arrays as a scalable platform for intracellular interfacing to neuronal circuits. *Nature Nanotechnology*, *7*(3), 180–184.

Rodgers, C. K., Munoz, D. P., Scott, S. H., & Paré, M. (2006). Discharge properties of monkey tectoreticular neurons. *Journal of Neurophysiology*, *95*(6), 3502–3511.

Rossant, C., Goodman, D. F. M., Fontaine, B., Platkiewicz, J., Magnusson, A. K., & Brette, R. (2011). Fitting neuron models to spike trains. *Frontiers in Neuroscience*, *5*, 9. http://doi.org/10.3389/fnins.2011.00009

Rossant, C., Goodman, D. F. M., Platkiewicz, J., & Brette, R. (2010). Automatic Fitting of Spiking Neuron Models to Electrophysiological Recordings. *Frontiers in Neuroinformatics*, *4*. http://doi.org/10.3389/neuro.11.002.2010

Rouder, J. N., & Morey, R. D. (2012). Default Bayes factors for model selection in regression. *Multivariate Behavioral Research*, *47*(6), 877–903.

Rouder, J. N., Morey, R. D., Speckman, P. L., & Province, J. M. (2012). Default Bayes factors for ANOVA designs. *Journal of Mathematical Psychology*, *56*(5), 356–374.

Rousche, P. J., & Normann, R. A. (1998). Chronic recording capability of the Utah Intracortical Electrode Array in cat sensory cortex. *Journal of Neuroscience Methods*, *82*(1), 1–15. http://doi.org/10.1016/S0165-0270(98)00031-4

Sachdev, R. N., Krause, M. R., & Mazer, J. A. (2012). Surround suppression and sparse coding in visual and barrel cortices. *Frontiers in Neural Circuits*, *6*. Retrieved from http://www.ncbi.nlm.nih.gov/pmc/articles/PMC3389675/

Sailer, U., Eggert, T., Ditterich, J., & Straube, A. (2002). Global effect of a nearby distractor on targeting eye and hand movements. *Journal of Experimental Psychology: Human Perception and Performance*, *28*(6), 1432.

Saint-Cyr, J. A., Ungerleider, L. G., & Desimone, R. (1990). Organization of visual cortical inputs to the striatum and subsequent outputs to the pallido-nigral complex in the monkey. *The Journal of Comparative Neurology*, *298*(2), 129–156. http://doi.org/10.1002/cne.902980202

Saitoh, K., Ménard, A., & Grillner, S. (2007). Tectal Control of Locomotion, Steering, and Eye Movements in Lamprey. *Journal of Neurophysiology*, *97*(4), 3093–3108. http://doi.org/10.1152/jn.00639.2006

Saito, Y., & Isa, T. (2003). Local Excitatory Network and NMDA Receptor Activation Generate a Synchronous and Bursting Command from the Superior Colliculus. *The Journal of Neuroscience*, *23*(13), 5854–5864.

Saito, Y., & Isa, T. (2005). Organization of Interlaminar Interactions in the Rat Superior Colliculus. *Journal of Neurophysiology*, *93*(5), 2898–2907. http://doi.org/10.1152/jn.01051.2004

Sandamirskaya, Y. (2014). Dynamic neural fields as a step toward cognitive neuromorphic architectures. *Frontiers in Neuroscience*, *7*. http://doi.org/10.3389/fnins.2013.00276

Sandamirskaya, Y., Zibner, S. K., Schneegans, S., & Schöner, G. (2013). Using dynamic field theory to extend the embodiment stance toward higher cognition. *New Ideas in Psychology*, *31*(3), 322–339.

Satel, J., Fard, F. S., Wang, Z., Trappenberg, T. P., & others. (2014). Simulating oculomotor inhibition of return with a two-dimensional dynamic neural field model of the superior colliculus. *Australian Journal of Intelligent Information Processing Systems*, *14*(1). Retrieved from https://www.researchgate.net/profile/Jason_Satel/publication/267990591_Simulating_oculomotor_inhibition_of_return_with_a_two-dimensional_dynamic_neural_field_model_of_the_superior_colliculus/links/550624b80cf24cee3a051f00.pdf

Satel, J., Wang, Z., Trappenberg, T. P., & Klein, R. M. (2011). Modeling inhibition of return as short-term depression of early sensory input to the superior colliculus. *Vision Research*, *51*(9), 987–996. http://doi.org/10.1016/j.visres.2011.02.013

Sawatari, A., & Callaway, E. M. (1996). Convergence of magno-and parvocellular pathways in layer 4B of macaque primary visual cortex. *Nature*, *380*(6573), 442–446.

Sceniak, M. P., Ringach, D. L., Hawken, M. J., & Shapley, R. (1999). Contrast's effect on spatial summation by macaque V1 neurons. *Nature Neuroscience*, *2*(8), 733–739.

Schall, J. D. (2002). The neural selection and control of saccades by the frontal eye field. *Philosophical Transactions of the Royal Society of London. Series B: Biological Sciences*, *357*(1424), 1073–1082.

Schall, J. D., & Hanes, D. P. (1993). Neural basis of saccade target selection in frontal eye field during visual search. *Nature*, *366*(6454), 467–469.

Schall, J. D., Hanes, D. P., Thompson, K. G., & King, D. J. (1995). Saccade target selection in frontal eye field of macaque. I. Visual and premovement activation. *The Journal of Neuroscience*, *15*(10), 6905–6918.

Schall, J. D., Purcell, B. A., Heitz, R. P., Logan, G. D., & Palmeri, T. J. (2011). Neural mechanisms of saccade target selection: gated accumulator model of the visual-motor cascade: Gated accumulator for visuomotor cascade. *European Journal of Neuroscience*, *33*(11), 1991–2002. http://doi.org/10.1111/j.1460-9568.2011.07715.x

Schiller, P. H. (1970). The discharge characteristics of single units in the oculomotor and abducens nuclei of the unanesthetized monkey. *Experimental Brain Research*, *10*(4), 347–362.

Schiller, P. H., & Chou, I. -ha. (1998). The effects of frontal eye field and dorsomedial frontal cortex lesions on visually guided eye movements. *Nature Neuroscience*, *1*(3), 248–253. http://doi.org/10.1038/693

Schiller, P. H., & Sandell, J. H. (1983). Interactions between visually and electrically elicited saccades before and after superior colliculus and frontal eye field ablations in the rhesus monkey. *Experimental Brain Research*, *49*(3), 381–392.

Schiller, P. H., & Stryker, M. (1972). Single-unit recording and stimulation in superior colliculus of the alert rhesus monkey. *Journal of Neurophysiology*, *35*(6), 915–924.

Schiller, P. H., True, S. D., & Conway, J. L. (1980). Deficits in eye movements following frontal eye-field and superior colliculus ablations. *Journal of Neurophysiology*, *44*(6), 1175–1189.

Schneegans, S., Spencer, J. P., Schöner, G., Hwang, S., & Hollingworth, A. (2014). Dynamic interactions between visual working memory and saccade target selection. *Journal of Vision*, *14*(11), 9.

Schneider, G. E. (1969). Two visual systems. *Science*. Retrieved from http://psycnet.apa.org/psycinfo/1971-00255-001

Schöner, G., Spencer, J., Group DFT Research, & others. (2015). *Dynamic Thinking: A Primer on Dynamic Field Theory*. Oxford University Press. Retrieved from https://books.google.com/books?hl=en&lr=&id=WiexCgAAQBAJ&oi=fnd&pg=PP1&dq=Dynamic+Thinking:+A+Primer+on+Dynamic+Field+Theory&ots=yyR-WVwcXP&sig=NTjHP8W6ZnxwRDka2ekf8k1ZL8A

Schwabe, L., Obermayer, K., Angelucci, A., & Bressloff, P. C. (2006). The Role of Feedback in Shaping the Extra-Classical Receptive Field of Cortical Neurons: A Recurrent Network Model. *The Journal of Neuroscience*, *26*(36), 9117–9129. http://doi.org/10.1523/JNEUROSCI.1253-06.2006

Scudder, C. A. (1988). A new local feedback model of the saccadic burst generator. *Journal of Neurophysiology*, *59*(5), 1455–1475.

Scudder, C. A., Kaneko, C. R., & Fuchs, A. F. (2002). The brainstem burst generator for saccadic eye movements. *Experimental Brain Research*, *142*(4), 439–462.

Seeburg, P. H., Burnashev, N., Kohr, G., Kuner, T., Sprengel, R., & Monyer, H. (2013). The NMDA receptor channel: molecular design of a coincidence detector. *Recent Prog Horm Res*, *50*, 19–34.

Serences, J. T., & Yantis, S. (2006). Selective visual attention and perceptual coherence. *Trends in Cognitive Sciences*, *10*(1), 38–45.

Series, P., Lorenceau, J., & Frégnac, Y. (2003). The 'silent' surround of V1 receptive fields: theory and experiments. *Journal of Physiology-Paris*, *97*(4), 453–474.

Shadlen, M. N., & Newsome, W. T. (1998). The variable discharge of cortical neurons: implications for connectivity, computation, and information coding. *The Journal of Neuroscience*, *18*(10), 3870–3896.

Shadlen, M. N., & Newsome, W. T. (2001). Neural basis of a perceptual decision in the parietal cortex (area LIP) of the rhesus monkey. *Journal of Neurophysiology*, *86*(4), 1916–1936.

Shipp, S. (2004). The brain circuitry of attention. *Trends in Cognitive Sciences*, *8*(5), 223–230. http://doi.org/10.1016/j.tics.2004.03.004

Shires, J., Joshi, S., & Basso, M. A. (2010). Shedding new light on the role of the basal ganglia-superior colliculus pathway in eye movements. *Current Opinion in Neurobiology*, *20*(6), 717–725. http://doi.org/10.1016/j.conb.2010.08.008

Shouval, H. Z., Bear, M. F., & Cooper, L. N. (2002). A unified model of NMDA receptor-dependent bidirectional synaptic plasticity. *Proceedings of the National Academy of Sciences*, *99*(16), 10831–10836. http://doi.org/10.1073/pnas.152343099

Sincich, L. C., & Horton, J. C. (2005). THE CIRCUITRY OF V1 AND V2: Integration of Color, Form, and Motion. *Annual Review of Neuroscience*, *28*(1), 303–326. http://doi.org/10.1146/annurev.neuro.28.061604.135731

Smith, T. J., & Henderson, J. M. (2009). Facilitation of return during scene viewing. *Visual Cognition*, *17*(6-7), 1083–1108. http://doi.org/10.1080/13506280802678557

Smith, T. J., & Henderson, J. M. (2011). Does oculomotor inhibition of return influence fixation probability during scene search? *Attention, Perception, & Psychophysics*, *73*(8), 2384–2398. http://doi.org/10.3758/s13414-011-0191-x

Soetedjo, R., Kaneko, C. R. S., & Fuchs, A. F. (2002). Evidence That the Superior Colliculus Participates in the Feedback Control of Saccadic Eye Movements. *Journal of Neurophysiology*, *87*(2), 679–695.

Sogo, H., & Takeda, Y. (2006). Effect of previously fixated locations on saccade trajectory during free visual search. *Vision Research*, *46*(22), 3831–3844. http://doi.org/10.1016/j.visres.2006.07.003

Sommer, M. A., & Wurtz, R. H. (2000). Composition and topographic organization of signals sent from the frontal eye field to the superior colliculus. *Journal of Neurophysiology*, *83*(4), 1979–2001.

Sparks, D. L. (2002). The brainstem control of saccadic eye movements. *Nature Reviews Neuroscience*, *3*(12), 952–964.

Sparks, D. L., & Hartwich-Young, R. (1989). The deep layers of the superior colliculus. *Rev Oculomot Res*, *3*, 213–255.

Sparks, D. L., Holland, R., & Guthrie, B. L. (1976). Size and distribution of movement fields in the monkey superior colliculus. *Brain Research*, *113*(1), 21–34. http://doi.org/10.1016/0006-8993(76)90003-2

Sparks, D. L., & Mays, L. E. (1990). Signal transformations required for the generation of saccadic eye movements. *Annual Review of Neuroscience*, *13*(1), 309–336.

Spencer, J. P., Perone, S., & Johnson, J. S. (2009). The dynamic field theory and embodied cognitive dynamics. *Toward a Unified Theory of Development: Connectionism and Dynamic Systems Theory Re-Considered*, 86–118.

Spira, M. E., & Hai, A. (2013). Multi-electrode array technologies for neuroscience and cardiology. *Nature Nanotechnology*, *8*(2), 83–94. http://doi.org/10.1038/nnano.2012.265

Spratling, M. W. (2010). Predictive Coding as a Model of Response Properties in Cortical Area V1. *The Journal of Neuroscience*, *30*(9), 3531–3543. http://doi.org/10.1523/JNEUROSCI.4911-09.2010

Stevens, C. F., & Wang, Y. (1995). Facilitation and depression at single central synapses. *Neuron*, *14*(4), 795–802. http://doi.org/10.1016/0896-6273(95)90223-6

Strassman, A., Evinger, C., McCrea, R. A., Baker, R. G., & Highstein, S. M. (1987). Anatomy and physiology of intracellularly labelled omnipause neurons in the cat and squirrel monkey. *Experimental Brain Research*, *67*(2), 436–440. http://doi.org/10.1007/BF00248565

Stubblefield, E. A., Thompson, J. A., & Felsen, G. (2015). Optogenetic cholinergic modulation of the mouse superior colliculus in vivo. *Journal of Neurophysiology*, *114*(2), 978–988. http://doi.org/10.1152/jn.00917.2014

Sumner, P. (2006). Inhibition versus attentional momentum in cortical and collicular mechanisms of IOR. *Cognitive Neuropsychology*, *23*(7), 1035–1048.

Sumner, P. (2007). Negative and positive masked-priming–implications for motor inhibition. *Advances in Cognitive Psychology*, *3*(1-2), 317.

Sumner, P., Nachev, P., Castor-Perry, S., Isenman, H., & Kennard, C. (2006). Which visual pathways cause fixation-related inhibition? *Journal of Neurophysiology*, *95*(3), 1527–1536.

Sumner, P., Nachev, P., Morris, P., Peters, A. M., Jackson, S. R., Kennard, C., & Husain, M. (2007). Human Medial Frontal Cortex Mediates Unconscious Inhibition of Voluntary Action. *Neuron*, *54*(5), 697–711. http://doi.org/10.1016/j.neuron.2007.05.016

Sumner, P., Nachev, P., Vora, N., Husain, M., & Kennard, C. (2004). Distinct Cortical and Collicular Mechanisms of Inhibition of Return Revealed with S Cone Stimuli. *Current Biology*, *14*(24), 2259–2263. http://doi.org/10.1016/j.cub.2004.12.021

Takahashi, M., Sugiuchi, Y., Izawa, Y., & Shinoda, Y. (2005). Commissural Excitation and Inhibition by the Superior Colliculus in Tectoreticular Neurons Projecting to Omnipause Neuron and Inhibitory Burst Neuron Regions. *Journal of Neurophysiology*, *94*(3), 1707–1726. http://doi.org/10.1152/jn.00347.2005

Takahashi, M., Sugiuchi, Y., & Shinoda, Y. (2007). Commissural Mirror-Symmetric Excitation and Reciprocal Inhibition Between the Two Superior Colliculi and Their Roles in Vertical and Horizontal Eye Movements. *Journal of Neurophysiology*, *98*(5), 2664–2682. http://doi.org/10.1152/jn.00696.2007

Taketani, M., & Baudry, M. (2006). Advances in network electrophysiology. *US: Springer*. Retrieved from http://link.springer.com/content/pdf/10.1007/b136263.pdf

Tandonnet, C., Massendari, D., & Vitu, F. (2012). When larger visual distractors become less disruptive: Behavioral evidence for lateral inhibition in saccade generation. *Journal of Vision*, *12*(4), 2. http://doi.org/10.1167/12.4.2

Tandonnet, C., & Vitu, F. (2013). Stimulus properties and saccade metrics: When local features are more critical than global features. *Behavioral Neuroscience*, *127*(1), 121.

Tan, H., Mooney, R. D., & Rhoades, R. W. (1999). Effects of norepinephrine upon superficial layer neurons in the superior colliculus of the hamster: in vitro studies. *Visual Neuroscience*, *16*(3), 557–570.

Taouali, W., Goffart, L., Alexandre, F., & Rougier, N. P. (2015). A parsimonious computational model of visual target position encoding in the superior colliculus. *Biological Cybernetics*, *109*(4-5), 549–559.

Thomas, C. A., Springer, P. A., Loeb, G. E., Berwald-Netter, Y., & Okun, L. M. (1972). A miniature microelectrode array to monitor the bioelectric activity of cultured cells. *Experimental Cell Research*, *74*(1), 61–66.

Thomas, N. W. D., & Paré, M. (2007). Temporal Processing of Saccade Targets in Parietal Cortex Area LIP During Visual Search. *Journal of Neurophysiology*, *97*(1), 942–947. http://doi.org/10.1152/jn.00413.2006

Thurat, C., N'Guyen, S., & Girard, B. (2015). Biomimetic race model of the loop between the superior colliculus and the basal ganglia: Subcortical selection of saccade targets. *Neural Networks*, *67*, 54–73. http://doi.org/10.1016/j.neunet.2015.02.004

Tigges, J., & Tigges, M. (1981). Distribution of retinofugal and corticofugal axon terminals in the superior colliculus of squirrel monkey. *Investigative Ophthalmology & Visual Science*, *20*(2), 149–158.

Trappenberg, T. P., Dorris, M. C., Munoz, D. P., & Klein, R. M. (2001). A model of saccade initiation based on the competitive integration of exogenous and endogenous signals in the superior colliculus. *Journal of Cognitive Neuroscience*, *13*(2), 256–271.

Tsodyks, M., Pawelzik, K., & Markram, H. (1998). Neural networks with dynamic synapses. *Neural Computation*, *10*(4), 821–835.

Tweed, D. B., & Vilis, T. (1990). The superior colliculus and spatiotemporal translation in the saccadic system. *Neural Networks*, *3*(1), 75–86. http://doi.org/10.1016/0893-6080(90)90046-N

Umeno, M. M., & Goldberg, M. E. (1997). Spatial processing in the monkey frontal eye field. I. Predictive visual responses. *Journal of Neurophysiology*, *78*(3), 1373–1383.

Ungerleider, L. G., & Haxby, J. V. (1994). 'What'and 'where'in the human brain. *Current Opinion in Neurobiology*, *4*(2), 157–165.

Van der Stigchel, S. (2010). Recent advances in the study of saccade trajectory deviations. *Vision Research*, *50*(17), 1619–1627.

Van der Stigchel, S., Heeman, J., & Nijboer, T. C. W. (2012). Averaging is not everything: The saccade global effect weakens with increasing stimulus size. *Vision Research*, *62*, 108–115. http://doi.org/10.1016/j.visres.2012.04.003

Van der Stigchel, S., Meeter, M., & Theeuwes, J. (2007). The spatial coding of the inhibition evoked by distractors. *Vision Research*, *47*(2), 210–218. http://doi.org/10.1016/j.visres.2006.11.001

Van der Stigchel, S., & Nijboer, T. C. W. (2013). How global is the global effect? The spatial characteristics of saccade averaging. *Vision Research*, *84*, 6–15. http://doi.org/10.1016/j.visres.2013.03.006

Van der Stigchel, S., Vries, J. P., Bethlehem, R., & Theeuwes, J. (2011). A global effect of capture saccades. *Experimental Brain Research*, *210*(1), 57–65. http://doi.org/10.1007/s00221-011-2602-6

Vanegas, H. (1984). *Comparative neurology of the optic tectum*. Plenum Pub Corp.

Van Gisbergen, J. A. M., Van Opstal, A. J., & Tax, A. A. M. (1987). Collicular ensemble coding of saccades based on vector summation. *Neuroscience*, *21*(2), 541–555.

Vankov, A., Hervé-Minvielle, A., & Sara, S. J. (1995). Response to Novelty and its Rapid Habituation in Locus Coeruleus Neurons of the Freely Exploring Rat. *European Journal of Neuroscience*, *7*(6), 1180–1187. http://doi.org/10.1111/j.1460-9568.1995.tb01108.x

Van Opstal, A. J., & Goossens, H. H. L. M. (2008). Linear ensemble-coding in midbrain superior colliculus specifies the saccade kinematics. *Biological Cybernetics*, *98*(6), 561–577. http://doi.org/10.1007/s00422-008-0219-z

Van Opstal, A. J., & Van Gisbergen, J. A. M. (1989). A nonlinear model for collicular spatial interactions underlying the metrical properties of electrically elicited saccades. *Biological Cybernetics*, *60*(3), 171–183.

Vargha, A., & Delaney, H. D. (2000). A critique and improvement of the CL common language effect size statistics of McGraw and Wong. *Journal of Educational and Behavioral Statistics*, *25*(2), 101–132.

Vidyasagar, T. R., Kulikowski, J. J., Lipnicki, D. M., & Dreher, B. (2002). Convergence of parvocellular and magnocellular information channels in the primary visual cortex of the macaque. *European Journal of Neuroscience*, *16*(5), 945–956.

Vokoun, C. R., Huang, X., Jackson, M. B., & Basso, M. A. (2014). Response normalization in the superficial layers of the superior colliculus as a possible mechanism for saccadic averaging. *The Journal of Neuroscience: The Official Journal of the Society for Neuroscience*, *34*(23), 7976–7987. http://doi.org/10.1523/JNEUROSCI.3022-13.2014

Waitzman, D. M., Pathmanathan, J., Presnell, R., Ayers, A., & Depalma, S. (2002). Contribution of the Superior Colliculus and the Mesencephalic Reticular Formation to Gaze Control. *Annals of the New York Academy of Sciences*, *956*(1), 111–129. http://doi.org/10.1111/j.1749-6632.2002.tb02813.x

Waitzman, D. M., Silakov, V. L., DePalma-Bowles, S., & Ayers, A. S. (2000). Effects of reversible inactivation of the primate mesencephalic reticular formation. I. Hypermetric goal-directed saccades. *Journal of Neurophysiology*, *83*(4), 2260–2284.

Walker, M. F., Fitzgibbon, E. J., & Goldberg, M. E. (1995). Neurons in the monkey superior colliculus predict the visual result of impending saccadic eye movements. *Journal of Neurophysiology*, *73*(5), 1988–2003.

Walker, R., Deubel, H., Schneider, W. X., & Findlay, J. M. (1997). Effect of remote distractors on saccade programming: evidence for an extended fixation zone. *Journal of Neurophysiology*, *78*(2), 1108–1119.

Walker, R., McSorley, E., & Haggard, P. (2006). The control of saccade trajectories: Direction of curvature depends on prior knowledge of target location and saccade latency. *Perception & Psychophysics*, *68*(1), 129–138.

Wallace, M. T., Meredith, M. A., & Stein, B. E. (1993). Converging influences from visual, auditory, and somatosensory cortices onto output neurons of the superior colliculus. *Journal of Neurophysiology*, *69*(6), 1797–1809.

Wallace, M. T., Wilkinson, L. K., & Stein, B. E. (1996). Representation and integration of multiple sensory inputs in primate superior colliculus. *Journal of Neurophysiology*, *76*(2), 1246–1266.

Walton, M. M. G., Sparks, D. L., & Gandhi, N. J. (2005). Simulations of Saccade Curvature by Models That Place Superior Colliculus Upstream From the Local Feedback Loop. *Journal of Neurophysiology*, *93*(4), 2354–2358. http://doi.org/10.1152/jn.01199.2004

Walt, S. van der, Colbert, S. C., & Varoquaux, G. (2011). The NumPy Array: A Structure for Efficient Numerical Computation. *Computing in Science & Engineering*, *13*(2), 22–30. http://doi.org/10.1109/MCSE.2011.37

Wang, L., Sarnaik, R., Rangarajan, K., Liu, X., & Cang, J. (2010). Visual Receptive Field Properties of Neurons in the Superficial Superior Colliculus of the Mouse. *The Journal of Neuroscience :*

The Official Journal of the Society for Neuroscience, *30*(49), 16573–16584. http://doi.org/10.1523/JNEUROSCI.3305-10.2010

Wang, N., Perkins, E., Zhou, L., Warren, S., & May, P. J. (2013). Anatomical Evidence that the Superior Colliculus Controls Saccades through Central Mesencephalic Reticular Formation Gating of Omnipause Neuron Activity. *The Journal of Neuroscience*, *33*(41), 16285–16296. http://doi.org/10.1523/JNEUROSCI.2726-11.2013

Wang, X.-J. (2002). Probabilistic decision making by slow reverberation in cortical circuits. *Neuron*, *36*(5), 955–968.

Wang, Z., Kruijne, W., & Theeuwes, J. (2012). Lateral interactions in the superior colliculus produce saccade deviation in a neural field model. *Vision Research*, *62*, 66–74. http://doi.org/10.1016/j.visres.2012.03.024

Wang, Z., Satel, J., Trappenberg, T. P., & Klein, R. M. (2011). Aftereffects of saccades explored in a dynamic neural field model of the superior colliculus. *Journal of Eye Movement Research*, *4*(2), 1–16.

Wang, Z., & Theeuwes, J. (2014). Distractor Evoked Deviations of Saccade Trajectory Are Modulated by Fixation Activity in the Superior Colliculus: Computational and Behavioral Evidence. *PLoS ONE*, *9*(12), e116382. http://doi.org/10.1371/journal.pone.0116382

Wardak, C., Olivier, E., & Duhamel, J.-R. (2002). Saccadic Target Selection Deficits after Lateral Intraparietal Area Inactivation in Monkeys. *The Journal of Neuroscience*, *22*(22), 9877–9884.

Webster, M. J., Bachevalier, J., & Ungerleider, L. G. (1994). Connections of Inferior Temporal Areas TEO and TE with Parietal and Frontal Cortex in Macaque Monkeys. *Cerebral Cortex*, *4*(5), 470–483. http://doi.org/10.1093/cercor/4.5.470

Weller, R. E., & Kaas, J. H. (1989). Parameters affecting the loss of ganglion cells of the retina following ablations of striate cortex in primates. *Visual Neuroscience*, *3*(04), 327–349. http://doi.org/10.1017/S0952523800005514

White, B. J., & Munoz, D. P. (2011). The superior colliculus. *Lateral*, *3*(5), 4.

White, B. J., Theeuwes, J., & Munoz, D. P. (2012). Interaction between visual-and goal-related neuronal signals on the trajectories of saccadic eye movements. *Journal of Cognitive Neuroscience*, *24*(3), 707–717.

Wilimzig, C., Schneider, S., & Schöner, G. (2006). The time course of saccadic decision making: Dynamic field theory. *Neural Networks*, *19*(8), 1059–1074. http://doi.org/10.1016/j.neunet.2006.03.003

Wilson, C. J., Weyrick, A., Terman, D., Hallworth, N. E., & Bevan, M. D. (2004). A model of reverse spike frequency adaptation and repetitive firing of subthalamic nucleus neurons. *Journal of Neurophysiology*, *91*(5), 1963–1980.

Wilson, H. R., & Cowan, J. D. (1972). Excitatory and Inhibitory Interactions in Localized Populations of Model Neurons. *Biophysical Journal*, *12*(1), 1–24. http://doi.org/10.1016/S0006-3495(72)86068-5

Wilson, H. R., & Cowan, J. D. (1973). A mathematical theory of the functional dynamics of cortical and thalamic nervous tissue. *Kybernetik*, *13*(2), 55–80.

Wise, K. D., & Angell, J. B. (1975). A low-capacitance multielectrode probe for use in extracellular neurophysiology. *Biomedical Engineering, IEEE Transactions on*, (3), 212–219.

Wolf, A. B., Lintz, M. J., Costabile, J. D., Thompson, J. A., Stubblefield, E. A., & Felsen, G. (2015). An integrative role for the superior colliculus in selecting targets for movements. *Journal of Neurophysiology*, *114*(4), 2118–2131. http://doi.org/10.1152/jn.00262.2015

Wolpert, D. M., & Landy, M. S. (2012). Motor control is decision-making. *Current Opinion in Neurobiology*, *22*(6), 996–1003. http://doi.org/10.1016/j.conb.2012.05.003

Wurtz, R. H., Sommer, M. A., Paré, M., & Ferraina, S. (2001). Signal transformations from cerebral cortex to superior colliculus for the generation of saccades. *Vision Research*, *41*(25), 3399–3412.

Young, J. Z. (1936). Structure of nerve fibres and synapses in some invertebrates. In *Cold Spring Harbor Symposia on Quantitative Biology* (Vol. 4, pp. 1–6). Cold Spring Harbor Laboratory Press. Retrieved from http://symposium.cshlp.org/content/4/1.extract

Zeng, C., Li, Y., & Li, C. (2011). Center–surround interaction with adaptive inhibition: A computational model for contour detection. *NeuroImage*, *55*(1), 49–66. http://doi.org/10.1016/j.neuroimage.2010.11.067

Zhang, J., & Bogacz, R. (2008). Superior colliculus and basal ganglia control the saccadic response in motion discrimination tasks. In *Advances in Cognitive Neurodynamics ICCN 2007* (pp. 475–479). Springer. Retrieved from http://link.springer.com/chapter/10.1007/978-1-4020-8387-7_82

Zhang, Y., Mooney, R. D., & Rhoades, R. W. (1999). Effects of norepinephrine on the activity of visual neurons in the superior colliculus of the hamster. *Visual Neuroscience*, *16*(03), 541–555.

Zhou, L., Warren, S., & May, P. J. (2008). The feedback circuit connecting the central mesencephalic reticular formation and the superior colliculus in the macaque monkey: tectal connections. *Experimental Brain Research*, *189*(4), 485–496.

Zihl, J., & Cramon, D. V. (1979). The contribution of the 'second' visual system to directed visual attention in man. *Brain*, *102*(4), 835–856. http://doi.org/10.1093/brain/102.4.835